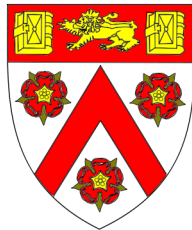


Double Parton Scattering in Proton-Proton Collisions

Jonathan Richard Gaunt

Trinity College



A dissertation submitted to the University of Cambridge
for the degree of Doctor of Philosophy
July 2012

Double Parton Scattering in Proton-Proton Collisions

Jonathan Richard Gaunt

Abstract

Double hard parton-parton interactions are expected to occur frequently in proton-proton (p-p) collisions at the LHC. They can give rise to significant backgrounds to certain rare single scattering (SPS) signals, and are an interesting signal process in their own right. In this thesis, we discuss the theoretical description of the double parton scattering (DPS) cross section in the context of Quantum ChromoDynamics (QCD).

After an overview of QCD and an introduction to DPS in Chapter 1, we describe in Chapter 2 a framework for calculating the p-p DPS cross section introduced by Snigirev *et al.*, in which this cross section is expressed in terms of double PDFs $D_p^{ij}(x_1, x_2, Q_A^2, Q_B^2)$ (dPDFs). We show that the equal-scale dPDFs are subject to momentum and number sum rule constraints, and use these in the construction of an explicit set of leading order (LO) equal-scale dPDFs (the ‘GS09’ dPDFs). The leptonic same-sign WW DPS signal obtained using GS09 dPDFs is compared with that obtained using simple factorised forms, and the prospects of observing this signal taking into account SPS backgrounds are analysed.

We discuss two ways in which the dPDF framework for describing p-p DPS is deficient in Chapter 3. We discuss interference and correlated parton effects in flavour, spin, colour, and parton type, which are ignored by the dPDF framework. We then study DPS-type graphs in which the parton pairs from both protons have arisen from a perturbative $1 \rightarrow 2$ branching, derive an expression for the part of such graphs associated with the particles arising from the $1 \rightarrow 2$ branchings being almost on-shell, and use this to demonstrate that the treatment of these graphs by the the dPDF framework is unsatisfactory.

In Chapter 4, we study DPS-type graphs in which the parton pair from only one proton has arisen from a perturbative $1 \rightarrow 2$ branching. We discover that such graphs contribute to the LO p-p DPS cross section, and that crosstalk between partons in the ‘nonperturbatively generated’ pair is allowed provided that it occurs at a lower scale than that of the perturbative $1 \rightarrow 2$ branching in the other proton. The result of this analysis is combined with that of the previous chapter to propose a formula for the LO total DPS cross section, and our proposal is compared with those from other authors. We finish in Chapter 5 with some conclusions and suggestions for further work.

Declaration

This dissertation is the result of my own work and includes nothing which is the outcome of work done in collaboration except where specifically indicated in the text. It has not been submitted for another qualification to this or any other university.

The introductory chapter, Chapter 1, is a review of important results in QCD and single scattering theory, and an introduction to double parton scattering theory. The content of this chapter is not original, and is mainly drawn from [9, 10, 15, 20, 36, 53]. Chapter 2 is based on original research work performed in collaboration with James Stirling [46], and Steve Kom, Anna Kulesza and James Stirling [47]. Section 3.2 in Chapter 3 is based on section 2 of the conference proceedings [82], which in turn is a pedagogical summary of work contained in the papers [33, 36, 37, 83, 84]. Section 3.3 in Chapter 3 is based on original research work performed in collaboration with James Stirling [81]. Finally, Chapter 4 is based on my original research work [125].

This thesis does not exceed the 60,000 word limit prescribed by the Degree Committee for Physics and Chemistry.

Jonathan Richard Gaunt

Acknowledgements

I would like to begin by thanking my supervisor, Professor James Stirling, for accepting me as a student, providing me with an exciting thesis topic to work on, and for all of his guidance and encouragement over the years. Whenever I have been stuck on a research problem, he has always been available with invaluable suggestions to surmount the problem, and encouragement that the problem can be solved. It has been a pleasure and a privilege to work with him. I also enjoyed working with Steve Kom and Anna Kulesza, with whom I collaborated for one paper.

My interest in high energy physics was fostered during a literature review and summer project with Deirdre Black, and during a Part III project with Bryan Webber. Deirdre and Bryan expanded my understanding of high energy physics considerably, as well as inspiring me to do a PhD in the subject, and I am grateful to them both. I would also like to acknowledge interesting lecture courses by Chris Lester, David Ward, Mark Thomson, David Tong, and Hugh Osborn.

During my PhD, I have been supported financially by the Science and Technologies Facilities Council, and then by a Trinity College Senior Rouse Ball Studentship for the final six months. I have also received funds from the Trinity College Rouse Ball/Eddington Research Fund which allowed me to attend the RADCOR 2011 conference in India.

For interesting discussions, both about physics and about other subjects, I would like to thank various members of the HEP theory group, both past and present: Deirdre Black, Lucian Harland-Lang, Steve Kom, Andreas Papaefstathiou, Are Raklev, Clara Salas, Marco Sampaio, Edwin Stansfield, Eleni Vryonidou, and Bryan Webber. Many thanks must also go to Tomas Kasemets for proofreading the thesis.

Last, but by no means least, I would like to thank my family – my parents Stephen and Mary, my brother Alex and his fiancée Beth, and my sister Steph. All of them have supported me in their own important way over the years, and I would not have made it to this stage without every one of them.

Contents

1	Partons in the Proton	1
1.1	Introduction	1
1.2	Deep Inelastic Scattering and the Parton Model	4
1.3	Quantum ChromoDynamics and Scaling Violations	12
1.3.1	Renormalisation and the running of the strong coupling constant . .	16
1.3.2	Quark Masses	23
1.3.3	Scaling Violations in QCD	24
1.4	Introduction to Double Parton Scattering	35
2	Double PDFs and Double Parton Scattering	45
2.1	Introduction	45
2.2	Double PDFs and the Double DGLAP equation	47
2.3	The Double Parton Sum Rules and the Initial Distributions	56
2.3.1	The Double Parton Sum Rules	56
2.3.2	Use of the Double Parton Sum Rules to improve the Input Distributions	58
2.4	Numerical Solution of the Double DGLAP Equation	71
2.4.1	The dDGLAP Evolution Program	72
2.4.2	Flavour Number Schemes	73
2.4.3	Accuracy of the Program	74
2.5	Properties of the dPDFs	75
2.6	Effects of using GS09 dPDFs on same-sign WW DPS signal	83
2.7	Summary	89
3	Flaws in the double PDF Framework	93
3.1	Introduction	93
3.2	Interference and Correlation Effects in DPS	94
3.2.1	Why are Interference and Correlation Effects Allowed for DPS? . .	94
3.2.2	Sudakov Suppression of Colour Interference Distributions	97
3.2.3	Conclusions	102
3.3	Double Parton Scattering Singularity in One-Loop Integrals	103
3.3.1	Introduction	103
3.3.2	Singularities in the Crossed Box	107

3.3.3	Physical Investigation of the Crossed Box	115
3.3.4	DPS singularity in Loops with More Than Four Legs	131
3.3.5	Conclusions	134
4	The Double Parton Scattering Cross Section	137
4.1	Introduction	137
4.2	‘Two versus One’ Contributions to the DPS Cross Section	139
4.3	Crosstalk between Ladders in the 2v1 Contribution	153
4.4	Total Cross Section for Double Parton Scattering	162
4.5	Conclusions	166
5	Conclusions	169
A	Conventions and Notation	173
B	Numerical techniques for evaluating dDGLAP integrals	177
C	Sum Rules using light cone wavefunction representations	181
C.1	Momentum sum rule	183
C.2	Number sum rule	184

Chapter 1

Partons in the Proton

1.1 Introduction

The subject of the microscopic substructure of matter has fascinated mankind for many years. Documented discussion of this topic goes back to the ancient Greeks and Indians, although this earlier discussion was of a philosophical nature rather than being based on empirical evidence. It was in these early discussions that the notion that matter might be built out of discrete and indivisible units – labelled ‘atoms’ by the ancient Greek philosopher Democritus – had its genesis.

Scientific developments in the subjects really began in the 17th and 18th century with the development of the modern science of chemistry. In 1789 Antoine Lavoisier wrote the *Traité Élémentaire de Chimie*, in which he presented the observation that mass was preserved in chemical reactions (law of conservation of mass), and introduced the concept of an element as a substance that could not be further broken down using chemical means. This was followed by the proposal in 1805 by John Dalton that all elements were composed of indivisible units of a single, unique type (which he labelled as atoms after Democritus), and that these atoms could join together to form chemical compounds. Among the predictions of this theory was the law of multiple proportions, and the validation of this prediction by experiment lent strong support to the theory (the law states that if two elements can react to form more than one compound, then the ratio of masses of the first element reacting with a fixed mass of the second element to form the two compounds is a small whole number, or the reciprocal of one). Dalton’s work is considered to be the origin of the modern atomic theory.

For a period it was believed that Dalton’s atoms might truly be the fundamental

building blocks of nature. However, in 1897 J J Thomson discovered the electron in his studies of cathode rays, and concluded that they were a component of atoms, implying that atoms cannot be fundamental. Thomson proposed a model of atoms – later referred to as the ‘plum pudding model’ – in which the negatively charged electrons were impregnated in a diffuse cloud of matter with positive charge (positively charged matter must exist inside the atom to balance the negative charge of the electrons and hold them together). This model was overturned by the experimental work of Hans Geiger and Ernest Marsden under the direction of Ernest Rutherford. They directed alpha particles generated by the radioactive decay of radium onto a thin sheet of gold foil and measured the frequency with which particles were scattered at different angles. The prediction from Thomson’s model was that all of the particles would be deflected very little as they passed through the diffuse charge distribution of the gold atoms. In fact what Geiger and Marsden observed was that although a large proportion of alpha particles were deflected by small angles, a few were deflected by large angles of greater than 90 degrees. This led Rutherford to conclude in 1911 that the plum pudding model was incorrect, and that the positive charge of the atom must be concentrated in a very small volume (the nucleus) to explain the data.

In the following years the constituents of the nucleus were gradually established. Antonius van den Broek suggested in 1911 that the number of charges in the nucleus was equal to the atomic number (position in the periodic table) of that nucleus. The results of Henry Moseley’s experiments in x-ray spectroscopy of elements, interpreted using the quantum model of Niels Bohr, provided support for this proposal. In 1917 Rutherford transmuted nitrogen into oxygen by bombarding it with alpha particles, releasing hydrogen nuclei in the process. He concluded from this that hydrogen nuclei were a constituent of nitrogen (and other) nuclei and were the particle carrying the electric charge of the nucleus, naming them protons. Rutherford also hypothesised (in 1921) that a further type of electrically uncharged particle existed in the nucleus that would somehow compensate for the electrical repulsion between the protons. The existence of this particle, now named the neutron, was confirmed experimentally in 1932 by James Chadwick using a nuclear reaction between alpha particles and beryllium that produces neutrons. This finding explained an earlier observation that atoms with different masses, but with the same chemical properties (indicating the same element) appeared to exist (with the simple explanation being that the atoms only differ in neutron number, which does not affect chemical properties).

Given that the atom is not fundamental but is composed of a nucleus and electrons, and that the nucleus is not fundamental but is composed of protons and neutrons, the question arises as to whether protons and neutrons (and a large number of similarly-interacting particles all collectively known as hadrons) themselves are fundamental, or whether there is further substructure in these objects. A suggestion of hadron substructure could be found in the quark model for hadrons that was proposed by Murray Gell-Mann [1] and George Zweig [2, 3] in 1964, although quarks were introduced in this model as part of an ordering scheme for hadrons, and it was a subject of debate at the time as to whether the quarks were real or merely abstract mathematical entities. Elastic scattering of electrons from the proton had established that protons were not point-like, which was suggestive of substructure but not, of course, conclusive. The definitive answer to this question was provided by the deep inelastic scattering (DIS) experiments performed at the Stanford Linear Accelerator Centre (SLAC) in the 1960s, in which electrons were fired at a proton target (the proton being an obvious choice for a hadron target due to its ubiquity and stability).

In the next section, I demonstrate that the results from SLAC were consistent with the so-called ‘Parton Model’ picture of Feynman, in which the proton is composed of a large number of point-like constituents (‘partons’) that can be viewed as approximately free particles over the short timescale of the DIS process. The ‘partons’ involved in the DIS process were the quarks and antiquarks of Gell-Mann and Zweig. Given that free quarks and antiquarks are not observed in nature, it must be the case that the so-called ‘strong force’ binding these objects is weak at short distances and timescales, but strong and confining at larger distances and timescales, such that quarks and antiquarks are bound together into hadrons. In section 1.3 I introduce the quantum field theory of the strong force, Quantum ChromoDynamics (QCD), that has the property that it is weaker at shorter distances but stronger and larger ones, and is believed to be confining (although it has not yet been conclusively proven that QCD has this property). I also show that the full QCD theory implies gradual (logarithmic) deviations from the predictions of the parton model. These were later observed at the electron-positron collider HERA, and are built in to modern fits of the ‘parton distribution functions’ that dictate the collinear momentum distributions of partons in the proton (subsequently we will refer to these as single PDFs, or sPDFs).

The QCD-improved parton model can be readily applied to predict the rates of hard interactions (i.e. interactions involving a large momentum or short distance scale) in

proton-proton collisions, if one assumes that a single parton-parton interaction is the dominant mechanism that can give rise to the products of the interaction – as we shall see, this is normally a valid assumption. Many predictions for hard event rates at the Large Hadron Collider in Geneva rely on this framework. However, given that each proton is composed of many partons, the possibility exists that a given set of hard interaction products in a proton-proton collision might have been produced via two (or more) independent hard scatterings, with the double scattering mechanism being most probable. Double parton scattering (DPS) processes can form an important background to certain Higgs and new physics signals at the LHC. In addition to this, DPS is an interesting signal process in its own right, as it gives us further insight into the substructure of the proton – in particular, it reveals information on the correlation between partons in the proton. In section 1.4, I present a basic introduction of DPS that mainly draws on parton model intuition, but which nevertheless highlights some important qualitative features of the process and shows that there is a region of phase space within which one might hope to measure DPS. Proper treatment of the phenomenon using perturbative QCD has received rather little attention until recent years, with only one group proposing a ‘hard scattering’ factorisation framework for describing DPS that supposedly incorporates perturbative QCD corrections [4–6]. In the remainder of this thesis we will introduce this framework and explore the issue of the description of DPS using perturbative QCD in more detail. Note that we outline the conventions used in this thesis in Appendix A.

1.2 Deep Inelastic Scattering and the Parton Model

The strategy employed by the SLAC experimentalists to probe the internal structure of the proton was rather similar in spirit to the approach used by Rutherford and collaborators to determine the internal structure of the atom. Just as in the Rutherford scattering experiment, a charged particle (in this case, an electron) was fired at the target material, and the virtual photon exchanged between the charged particle and the target probed the charge distribution in the target particles. However, to probe the structure of the proton much higher energies are needed than to probe the atom – to be precise, the four-momentum of the exchange photon q must have a larger magnitude $\sqrt{|q^2|}$, as, roughly speaking, the resolving wavelength of the virtual photon is inversely proportional to this magnitude (by the de Broglie relation).

The DIS process is illustrated in figure 1.1, in which the four-momenta relevant to the

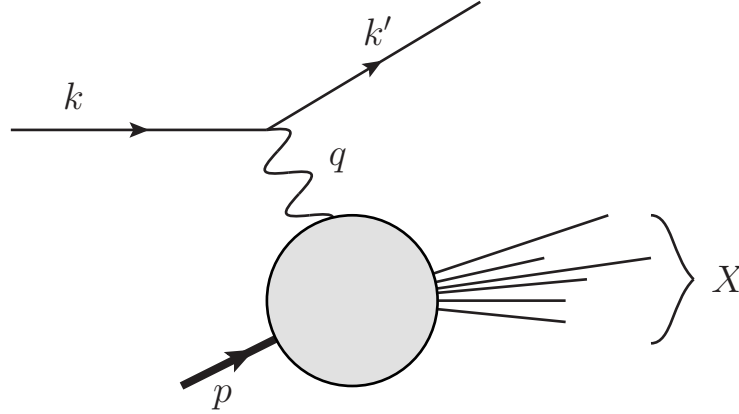


Figure 1.1: Kinematics of the DIS process.

process are also labelled. We take the incoming proton and electron to be unpolarised. At the momentum transfers required to probe the internal structure of the proton, the scattering process causes the breakup of the proton into a collection of hadrons collectively referred to as ‘X’, with $M_X^2 \gg m_p^2$ – hence the adjective ‘inelastic’ in the name of the process. We will assume in the following discussion that the interaction between the electron and the proton is dominated by single photon exchange – this was certainly valid at SLAC given the small coupling constant α of Quantum ElectroDynamics (QED) and the fact that momentum transfers accessible in the early experiments were much less than the mass of the Z boson. At higher momentum transfers (such as were achieved at the electron-proton collider HERA) one needs to include the effects of Z boson exchange and $Z\gamma$ interference, but this is straightforwardly done and we do not need to concern ourselves with it in the present discussion.

The important kinematic invariants relevant to the DIS process $e^-(k) + p(p) \rightarrow e^-(k') + X$ are defined as follows:

$$Q^2 \equiv -q^2 \quad x \equiv \frac{Q^2}{2p \cdot q} \quad y \equiv \frac{q \cdot p}{k \cdot p} \quad (1.1)$$

Using only the information that the electron interacts with the hadron via a single photon (and Lorentz invariance), we can write down the following expression for the cross section of the process:

$$d\sigma = \frac{4\alpha^2}{s} \frac{d^3\vec{k}'}{2|\vec{k}'|Q^4} L^{\mu\nu}(k, q) W_{\mu\nu}(p, q) \quad (1.2)$$

where $s = (p + k)^2$, and \vec{k}' is the 3-momentum of the outgoing electron with 4-momentum k' .

The two tensors $L^{\mu\nu}$ and $W^{\mu\nu}$ describe the coupling of the photon to the electron and hadronic system respectively. Assuming that the electron behaves as a fundamental point-like particle (as is found to be the case at all energy/distance scales probed so far), the leptonic tensor $L^{\mu\nu}$ may be straightforwardly calculated explicitly using the rules of QED:

$$L^{\mu\nu} = \frac{1}{2} \text{Tr}[\not{k} \gamma^\mu \not{k}' \gamma^\nu] \quad (1.3)$$

where $\not{k} \equiv k_\mu \gamma^\mu$, and the γ^μ are the gamma matrices (our conventions for which can be found in Appendix A).

A few statements can be made about the hadronic tensor even without knowing the details of the internal dynamics of the proton. The tensor $W_{\mu\nu}$ must be Lorentz covariant. For unpolarised scattering, it must satisfy $W^{\mu\nu} = W^{\nu\mu}$, $W^{\mu\nu} = W^{\mu\nu*}$ to a good approximation. These properties are associated with the fact that the interactions inside the proton are predominantly strong ones and the probe is a photon, and both the strong and electromagnetic interactions are invariant under parity and time reversal transformations. Finally, conservation of the electromagnetic current imposes $q_\mu W^{\mu\nu} = 0$.

Given these constraints, we find that $W_{\mu\nu}$ must be a sum of only two possible tensor structures, each multiplied by a scalar function of the Lorentz invariants x and Q^2 (these are known as the structure functions of the proton):

$$\begin{aligned} W_{\mu\nu} = & - \left(g_{\mu\nu} - \frac{q_\mu q_\nu}{q^2} \right) F_1(x, Q^2) \\ & + \left(p_\mu + \frac{q_\mu}{2x} \right) \left(p_\nu + \frac{q_\nu}{2x} \right) \frac{1}{p \cdot q} F_2(x, Q^2) \end{aligned} \quad (1.4)$$

Inserting (1.3) and (1.4) into (1.2), we arrive at the following expression for the DIS differential cross section (for $Q^2 \gg m_p^2$):

$$\frac{d^2\sigma}{dx dQ^2} = \frac{4\pi\alpha^2}{Q^4} \left[(1-y) \frac{F_2(x, Q^2)}{x} + y^2 F_1(x, Q^2) \right] \quad (1.5)$$

The SLAC experiments of the late 1960s measured the differential DIS cross section for a range of incident electron energies and scattering angles, using (1.5) to extract the structure functions $F_1(x, Q^2)$ and $F_2(x, Q^2)$. The experimenters observed two very important features in their data. First, they found that the structure functions did not

appear to vary with Q^2 at fixed x for $Q^2 \gtrsim m_p^2$. Second, they discovered that the structure functions were not independent, but instead appeared to obey the relation $F_2(x, Q^2) = 2xF_1(x, Q^2)$ (the Callan-Gross relation [7]).

These features in the data are explained if the proton is considered as being composed of a number of electromagnetically charged fermionic point-like constituents, that only interact over time and length scales of the order of the hadronic radius $\sim 1/m_p$ (in the rest frame of the proton). This is the ‘parton model’ picture of the proton introduced by Feynman [8]. We will now show how the parton model picture of the proton gives rise to the features observed in the SLAC data, where our discussion will to a large extent follow that in [9, 10].

Let us use the light cone coordinate system described in Appendix A. In this coordinate system, we write a 4-vector A as (A^+, A^-, A^1, A^2) where the components of this vector are related to the conventional components A^0, A^1, A^2 and A^3 according to:

$$A^\pm = \frac{1}{\sqrt{2}}(A^0 \pm A^3) \quad (1.6)$$

We choose a frame in which the momenta of the proton and exchanged photon are both large and the proton momentum is zero along the transverse directions:

$$q = \frac{1}{\sqrt{2}}(-Q, Q, \mathbf{0}) \quad p = \frac{1}{\sqrt{2}}\left(\frac{Q}{x}, \frac{xm_p^2}{Q}, \mathbf{0}\right) \quad (1.7)$$

In this frame the proton has been highly boosted from its rest frame along the positive z axis with a speed β given by $\sqrt{1+\beta}/\sqrt{1-\beta} = Q/(xm_p)$ which is $\sim Q/m_p$ if x is not too small compared to 1¹. We recall that the parton model stipulates that the interaction points between the parton constituents of the proton are separated by space-time distances of order $1/m_p$ in the proton rest frame. The large boost of the proton in the frame considered means that the interaction points are stretched out in the x^+ direction and compressed in the x^- direction, such that Δx^+ and Δx^- between interaction points are of the order of $\sim 1/m_p \times Q/m_p = Q/m_p^2$ and $\sim 1/m_p \times m_p/Q = 1/Q$ respectively.

The large virtuality of the exchange photon means its existence is confined to a small space-time region – in particular, it can only travel over a distance of order $1/Q$ in the x^+ direction, which can be considered as the ‘time’ direction relevant to the highly boosted hadron. Since the separation between interaction points in the x^+ direction Q/m_p^2 is very

¹Note that if x is small then one does need to take account of the factors of x , and the picture changes somewhat dramatically. However we shall not concern ourselves with this eventuality here.

much longer than the x^+ distance travelled by the photon $1/Q$ in the kinematic region we are considering ($Q^2 \gg m_p^2$), the photon sees the proton as being composed of a number of non-interacting free point partons, with definite momenta.

It is clear that if the interactions between the partons in the rest frame of the proton occur over space-time scales of order $1/m_p$, then the energies and momenta of the partons in the proton rest frame are restricted to values of order m_p . Following the boost, the plus momentum component of each parton is of order Q , the minus component is of order m_p^2/Q , and the transverse components are unchanged and of order m_p – that is, all of the momentum components of a parton i are negligible in the frame considered apart from the plus component p_i^+ . We can consider the ‘free partons’ seen by the photon as being collinear to the proton, and will specify the momentum of a parton i using the ‘momentum fraction’ variable $\xi_i = p_i^+/p^+$.

We can make a rough estimate of the probability that the exchange photon will encounter a parton during its lifetime as follows. The largest possible transverse area that can be explored by the exchange photon during its lifetime will be of order $1/Q^2$. Assuming that there is a reasonably small number of partons filling the proton disc of transverse radius $\sim 1/m_p$, the probability of an interaction will then be $\sim m_p^2/Q^2$ which is small. An important consequence of this is that the probability of the photon interacting with $n > 1$ partons is suppressed and can be neglected, being of order $(m_p^2/Q^2)^n$. At very small x it turns out that there is an enormous number of partons in the proton so this picture has to be modified – we shall not concern ourselves with this detail here.

When, on rare occasions, the photon does interact with a single parton and is absorbed by it, the parton acquires large momentum components in directions other than the plus direction and is ejected from the proton. The ejected parton must interact with the remnant partons to form the collection of hadrons ‘X’, since we do not observe free partons experimentally. However, in the parton model these interactions occur over time and distance scales that are large compared to the photon-parton interaction, and so do not interfere with this process.

Bearing all of this in mind, we see that the DIS cross section in the parton model can be calculated by calculating the cross section for an electron to scatter off a single parton i with momentum given by $(\xi_i p^+, 0, 0, 0)$, convolving this result with the number distribution to find a parton i with momentum fraction ξ_i in the proton $D_p^i(\xi_i)$ (this is the ‘sPDF’ that we discussed in section 1.1), and then summing over charged parton types. The shape of the sPDF is determined by the strong long-distance interactions that bind

partons together in the proton, and therefore cannot be calculated in perturbation theory. However, measurements of e^-p DIS allow one to extract a particular linear combination of sPDFs (see below), whilst DIS processes with other probes and targets are sensitive to other linear combinations of sPDFs (e.g. e^-d , νN , $\bar{\nu}N$, where d is deuterium and N is a heavy nucleus) – so by combining these measurements the sPDFs can be extracted experimentally.

The double differential cross section for the electron to scatter off a fermionic point-like parton i with charge e_i and momentum fraction ξ_i is straightforwardly calculated to be:

$$\frac{d^2\sigma_i}{dx dQ^2}(\xi_i) = \frac{4\pi\alpha^2}{Q^4} [1 + (1-y)^2] \frac{1}{2} e_i^2 \delta(x - \xi_i) \quad (1.8)$$

Note the equivalence between the kinematic variable x and the momentum fraction of the scattered parton ξ_i in this formula. Convoluting (1.8) with the sPDF, we obtain the hadron-level cross section:

$$\begin{aligned} \frac{d^2\sigma}{dx dQ^2} &= \sum_i \int_0^1 d\xi_i \frac{d^2\sigma_i}{dx dQ^2}(\xi_i) D_p^i(\xi_i) \\ &= \frac{4\pi\alpha^2}{Q^4} [1 + (1-y)^2] \frac{1}{2} \sum_i e_i^2 D_p^i(x) \end{aligned} \quad (1.9)$$

Here and in the rest of this section, the sum runs over all electromagnetically charged fermionic partons in the proton (this includes antipartons). Comparing (1.9) and (1.5), we can finally extract the parton model predictions for F_1 and F_2 :

$$F_2(x, Q^2) = 2xF_1(x, Q^2) = x \sum_i e_i^2 D_p^i(x) \quad (1.10)$$

As anticipated, the parton model successfully reproduces the important features observed in the SLAC data – namely the scaling of the structure functions for $Q^2 \gg m_p^2$ and fixed finite x , and the Callan-Gross relation between the structure functions. The fact that the Callan-Gross relation is obeyed by the parton model is related to the fact that the charged proton constituents are spin 1/2 fermions in the parton model – if the partons had a different spin then the relationship between F_1 and F_2 would be different (for scalar partons one finds $F_1(x, Q^2) = 0 \times F_2(x, Q^2)$ for example). The agreement between the parton model predictions and the SLAC data is direct evidence for point-like, spin 1/2 substructure in the proton. If the electric charge had been uniformly distributed

in the proton, then wide-angle scattering of electrons in DIS would have been rare and the structure functions would have died off rapidly with Q^2 , which is not observed.

By combining data from e^-p and e^-n scattering (the latter of which has to be extracted from data on e^-d scattering owing to the instability of the neutron in vacuum), and using isospin symmetry to relate the sPDFs in the neutron to those in the proton, one can get a value for the quantity $\sum_i \int_0^1 \xi d\xi D_p^i(\xi)$, where the sum here is only over the electromagnetically charged fermionic partons. This is the total momentum fraction of the proton carried by these partons, which should have the value of 1 if there are no other constituents in the proton. The value obtained experimentally is ~ 0.5 , which indicates that about half of the proton's momentum is carried by some electrically uncharged constituents. These are the gluons, which are the force-carrying bosons responsible for binding the fermionic partons (the quarks and antiquarks) together in the proton. We shall discuss these particles in more detail in section 1.3.

Shortly after the parton model was introduced to explain the features of the SLAC DIS data, it was used to make cross section predictions for other scattering processes involving hadrons. A classic example process that was studied is the Drell-Yan process $h_1(p_1) + h_2(p_2) \rightarrow l^+(p_3) + l^-(p_4) + X$, in which two hadrons h_1 and h_2 collide to produce a lepton pair l^+l^- with a large invariant mass amongst the interaction products [11].

Let us introduce the following kinematic invariants for this process:

$$s \equiv (p_1 + p_2)^2 \quad M^2 \equiv (p_3 + p_4)^2 \quad \tau \equiv M^2/s \quad (1.11)$$

In the parton model the most likely fundamental interaction producing the lepton pair for $M^2 \ll M_Z^2$ is the following annihilation interaction involving a single electromagnetically charged parton i and its antiparton \bar{i} , one of which comes from h_1 and the other of which comes from h_2 :

$$i + \bar{i} \rightarrow \gamma^* \rightarrow l^+ + l^- \quad (1.12)$$

where γ^* denotes a virtual photon.

If $M^2 \gg m_p^2$ such that the space-time extent of the Drell-Yan interaction (1.12) is small compared to the space-time separation of partonic interactions inside each hadron in the centre of mass frame of the collision, and τ is not too small such that the momentum fractions of the colliding partons are not too small, then the prediction of the parton

model for the Drell-Yan cross section is the following:

$$\begin{aligned} \left. \frac{d\sigma}{dM^2} \right|_{h_1 h_2 \rightarrow l^+ l^- + X} (s, M^2) &= \sum_i \int_0^1 d\xi_1 d\xi_2 D_{h_1}^i(\xi_1) D_{h_2}^{\bar{i}}(\xi_2) \\ &\times \left. \frac{d\hat{\sigma}}{dM^2} \right|_{i\bar{i} \rightarrow l^+ l^-} (\hat{s} = \xi_1 \xi_2 s, M^2) \end{aligned} \quad (1.13)$$

It is worthwhile emphasising the sPDFs in this formula are the same sPDFs that appear in the cross section formula for DIS. We can calculate the parton-level cross section in this expression straightforwardly using the QED Feynman rules:

$$\left. \frac{d\hat{\sigma}}{dM^2} \right|_{i\bar{i} \rightarrow l^+ l^-} (\hat{s}, M^2) = \frac{4\pi\alpha^2}{3M^2 N_c} e_i^2 \delta(\hat{s} - M^2) \quad (1.14)$$

Note the presence of a factor $1/N_c = 1/3$ in this formula - this is due to the fact that the fermionic partons (quarks and antiquarks) carry a quantum number known as colour (this is related to the strong force that binds the partons together – see the next section), and the parton and antiparton must combine in a colourless state (i.e. colour plus anticolour) to produce the colourless photon. With N_c colours, this only happens in 1 out of N_c collisions assuming all colours are equally likely (which is the case in QCD given that the parent hadron states are colourless and that all colour degrees of freedom are treated equally in QCD) – hence the factor $1/N_c$. Inserting (1.14) into (1.13):

$$\begin{aligned} M^4 \frac{d\sigma}{dM^2} \Big|_{h_1 h_2 \rightarrow l^+ l^- + X} &= \frac{4\pi\alpha^2}{3N_c} \tau \int_0^1 d\xi_1 d\xi_2 \sum_i e_i^2 D_{h_1}^i(\xi_1) D_{h_2}^{\bar{i}}(\xi_2) \\ &\times \delta(\xi_1 \xi_2 - \tau) \end{aligned} \quad (1.15)$$

One sees that a prediction of the parton model is that $M^4 d\sigma/dM^2$ should exhibit scaling with τ – i.e. that $M^4 d\sigma/dM^2$ should depend on M^2 and s only via the quotient $\tau = M^2/s$. In fact, if one is equipped with values for the sPDFs $D_{h_1}^i(\xi)$, $D_{h_2}^{\bar{i}}(\xi)$ extracted from DIS measurements, then one can use (1.15) to make very detailed parton model predictions for Drell-Yan cross sections (and differential cross sections). The predictions of the parton model were found to be obeyed fairly well by the experimental data, although the overall normalisation was underestimated by a factor of approximately 2, and the mean transverse momentum of leptons was found to be larger than predicted [12] (hinting that adjustments to the parton model picture, described in the next section, were required).

The parton model of the internal dynamics of the proton was successful in describing

the important features of the DIS and Drell-Yan data, but it was just a model, not based on any rigorous field-theoretic description of the proton constituents and their interactions. It did however give some guidance as to what features should be contained in the full quantum theory of the partons and their interactions – namely, it should give rise to a force between partons that is small for small space-time scales but increases as the separation between partons in space-time is increased. This required property is known as *asymptotic freedom*. It was discovered in 1973 by Gross, Politzer and Wilczek [13, 14] that there exists a class of theories that are asymptotically free – these are the $SU(N)$ non-Abelian gauge theories. In the next section I will discuss the quantum field theory of the strong interactions, Quantum ChromoDynamics, which is an $SU(N)$ non-Abelian gauge theory with $N = 3$.

1.3 Quantum ChromoDynamics and Scaling Violations

In this section I will provide a brief description of Quantum ChromoDynamics (QCD), our quantum field theoretic description of the fermionic constituents of hadrons and the ‘strong interaction’ between them. We will see that the theory is asymptotically free – i.e. possesses a coupling constant that falls with increasing momentum scale, or decreasing distance scale, as is required from the successes of the parton model. However, we will also find that the theory predicts logarithmic scaling violations from the parton model predictions. We aim here for a practical and pedagogical introduction to these features, and refer the reader to [15, 16] for more detailed discussion and rigorous derivations.

As mentioned in the previous section, QCD is a non-Abelian $SU(3)$ gauge field theory for Dirac spinors. The quantum Lagrangian density of the theory, from which the Feynman rules are derived, is composed from three parts:

$$\mathcal{L}_{QCD} = \mathcal{L}_{\text{classical}} + \mathcal{L}_{\text{gauge-fixing}} + \mathcal{L}_{\text{ghost}} \quad (1.16)$$

The expression for the classical Lagrangian density is:

$$\mathcal{L}_{\text{classical}} = -\frac{1}{4}F_{\alpha\beta}^A F^{A\alpha\beta} + \sum_{i=1}^{N_f} \bar{\psi}_i^a (i\not{D}_{ab} - m_i\delta_{ab})\psi_i^b \quad (1.17)$$

Two different types of field are contained in this term. There are N_f spinor fields q_i

with masses m_i , corresponding to N_f spin 1/2 particles and antiparticles, and one vector field A corresponding to a spin 1 particle (contained within the factors $F_{\alpha\beta}$ and \not{D} of (1.17) that we shall give explicit expressions for below). The spin 1/2 particles are the quarks and antiquarks of Gell-Mann and Zweig, that may be identified with the electromagnetically charged fermionic partons of the previous section. In the Standard Model (our current theory of subatomic particles and their interactions, that includes QCD as a part of it), the number of quark flavours $N_f = 6$ (the six flavours written in order of increasing mass are referred to as up, down, strange, charm, bottom, and top, or u, d, s, c, b, t). The spin 1 boson is known as the gluon, and mediates the strong force between the quarks and antiquarks (we also saw in the last section that gluons are electrically uncharged particles that carry $\sim 50\%$ of the collinear momentum of the proton).

Aside from carrying an electromagnetic (in fact, more generally, an electroweak) charge, the quarks and antiquarks carry a further quantum number or charge associated with the strong force, known as colour. There are $N = 3$ possible colours for each quark (red, green or blue) – hence each spinor field q_i has a colour index a that can run between 1 and 3. Since gluons are emitted (and absorbed) by quarks and antiquarks, they must have both a colour and an anticolour index to ensure conservation of colour in the interaction. Naively this would give $N^2 = 9$ colour possibilities for the gluons. However, one of these corresponds to a colour singlet (uncoloured) gluon, which would be able to escape the proton due to its lack of strong colour charge and give rise to a long range component of the strong force. This is not observed – therefore there are $N^2 - 1 = 8$ colour possibilities for the gluon², and the colour index A on the gluon field A (and e.g. the field strength tensor $F_{\alpha\beta}$ in (1.17)) runs from 1 to 8.

The explicit form of the gluon field strength tensor $F_{\alpha\beta}^A$ is:

$$F_{\alpha\beta}^A = \partial_\alpha A_\beta^A - \partial_\beta A_\alpha^A + g_s f^{ABC} A_\alpha^B A_\beta^C \quad (1.18)$$

The presence of a ‘two gluon’ term in the field strength tensor is a characteristic feature of non-Abelian theories. This term gives rise to interactions between gluons when inserted into $\mathcal{L}_{\text{classical}}$, and these gluon self-interactions are key to the asymptotically free nature of the theory. The quantity g_s is the coupling constant of QCD – instead of this

²In the language of group theory, the situation with nine gluons would correspond to QCD being a U(3) gauge theory, whilst the physically realised situation with eight gluons corresponds to QCD being an SU(3) theory. The U(3) group has one more ‘group generator’ than the SU(3) group, which commutes with all the other generators and corresponds to the colour singlet unconfined gluon in the discussion above.

we will often use α_s , defined to be $g_s^2/(4\pi)$. The structure constants $f^{ABC} \equiv iT_{BC}^A$ are a set of constant colour matrices that dictate the colour structure of interactions between gluons.

The operator \not{D} in (1.17) $\equiv D_\mu \gamma^\mu$, where the covariant derivative D_μ acting on the quark fields is:

$$(D_\alpha)_{ab} = \partial_\alpha \delta_{ab} - ig_s t_{ab}^C A_\alpha^C \quad (1.19)$$

The constant matrix t_{ab}^C dictates the colour structure of the interactions between gluons and quarks. Explicit representations for the t_{ab}^C and f^{ABC} matrices do exist – however, the use of these in practical calculations is cumbersome. Instead, one makes use of the following relations, true for a general $SU(N)$ theory, to perform the colour part of an amplitude calculation:

$$t_{ab}^A t_{ba}^B = T_R \delta^{AB} \quad (1.20)$$

$$t_{ab}^A t_{cd}^A = \frac{1}{2} \left(\delta_{ad} \delta_{bc} - \frac{1}{N} \delta_{ab} \delta_{cd} \right) \quad (1.21)$$

$$T_{AB}^C T_{BA}^D = f^{ABC} f^{ABD} = C_A \delta^{CD} \quad (1.22)$$

where:

$$T_R = \frac{1}{2} \quad C_A = N \quad (1.23)$$

and $N = 3$ for QCD.

By construction, $\mathcal{L}_{\text{classical}}$ is invariant under the following simultaneous transformation of the quark and gluon fields, with $\theta^A(x)$ a set of eight arbitrary real, smooth functions of space-time:

$$q_a(x) \rightarrow q'_a(x) = [\exp(it^A \theta^A(x))]_{ab} q_b(x) = [U(x)]_{ab} q_b(x) \quad (1.24)$$

$$t^A A_\alpha^A \rightarrow t^A A_\alpha'^A = U(x) t^A A_\alpha^A U^{-1}(x) + \frac{i}{g_s} U(x) (\partial_\alpha U^{-1}(x)) \quad (1.25)$$

This is an $SU(3)$ gauge transformation, and the matrices t_{ab}^A are also known as the fundamental generators of the $SU(3)$ group (the matrices T_{AB}^C are known as the adjoint generators of this group). This property of the $\mathcal{L}_{\text{classical}}$ is vital in ensuring that the theory of QCD is well-defined (or more specifically, renormalisable – see later). However, it does also mean that if one naively tries to use the classical Lagrangian on its own to calculate

QCD Green's functions, one gets ill-defined and divergent results. At the level of the Feynman rules, this problem appears as an ill-defined gluon propagator – the piece of $\mathcal{L}_{\text{classical}}$ quadratic in A cannot be inverted.

The source of the problem is in the integration over all field configurations in the path integral formula for the Green's function. This includes an integration over multiple field configurations (in fact an infinite number of field configurations) that are related by a gauge transformation, and correspond to the same physics (due to the invariance of the Lagrangian under the gauge transformation). Each physically-distinct field configuration is included an infinite number of times in the Green's function integral, and it is therefore no surprise that the results of the calculation are ill-defined.

To obtain sensible results from the Green's function computations, a delta functional $\delta[F(A)]$ needs to be inserted into the integrations over field configurations in the Green's function expressions, where the function $F(A)$ should be chosen such that only one field configuration from each gauge orbit is included in the integration (this is known as 'fixing the gauge'). Alternatively one can achieve the same result using an integration over a family of delta functions – for example, one can make the following replacement in the functional integrations:

$$\delta[F(A)] \rightarrow \int d[f] \delta[F(A) - f] e^{-\frac{i}{2\xi} \int d^4x f(x) f(x)} \quad (1.26)$$

It turns out that if the gauge fixing is performed according to (1.26) then the gauge fixing piece can be written as extra contribution to the Lagrangian, $\mathcal{L}_{\text{gauge-fixing}}$:

$$\mathcal{L}_{\text{gauge-fixing}} = -\frac{1}{2\lambda} [F(A)]^2 \quad (1.27)$$

In the limit $\lambda \rightarrow 0$ the condition $F(A(x))^A = 0$ is enforced.

Accompanying the gauge-fixing term in the Lagrangian, one needs to include a further 'ghost' term involving an unphysical complex scalar field c obeying Fermi statistics:

$$\mathcal{L}_{\text{ghost}} = -\bar{c}^A F'(A)^\mu \{D_\mu\}^{AB} c^B \quad (1.28)$$

The ghost field c must carry the same colour charges as the gluon (i.e. it is charged

under the adjoint of $SU(3)$), and the covariant derivative acting on such fields is:

$$(D_\alpha)^{AB} = \partial_\alpha \delta^{AB} - ig_s T_{AB}^C A_\alpha^C \quad (1.29)$$

We can give an idea of why the term (1.28) must be included using a simple example. Say one had the integral $\int f(x)dx$ and one wanted to extract the value of $f(x)$ at the value of x satisfying $g(x) = 0$, x^* , from the integral. Then if one inserted the delta function $\delta(g(x))$ into the integral then one would not quite obtain the desired result – one would obtain $f(x^*)/g'(x^*)$ rather than $f(x^*)$. Thus, to obtain the desired result one has to insert $g'(x^*)\delta(g(x))$ into the integral instead. The ghost term is the analogue of the factor $g'(x^*)$ in the simple example, translated into functional space and then put into the form of a contribution to the Lagrangian. In Feynman diagrams ghost particles perform the role of cancelling out the effects of unphysical scalar and longitudinal gluon polarisations inside loops.

Two popular choices for the gauge fixing function $F(A)$ are the covariant and axial gauge choices:

$$\text{Covariant Gauge: } F(A) = \partial_\alpha A^\alpha \quad (1.30)$$

$$\text{Axial Gauge: } F(A) = n_\alpha A^\alpha, n \text{ constant.} \quad (1.31)$$

Feynman rules corresponding to the two gauge classes are presented in Table (1.1). The choice of axial gauge possesses the advantage that ghosts decouple from the theory (this is manifest in the pure axial gauge for which $\lambda = 0$). However the price that one has to pay for this is the appearance of unpleasant $n \cdot p$ factors in the gluon propagator denominators (which is related to the violation of Lorentz covariance by the gauge fixing term).

1.3.1 Renormalisation and the running of the strong coupling constant

If one takes either the axial or covariant gauge Feynman rules of Table (1.1) and uses them to compute Green's functions, then one runs into trouble as soon as one attempts to calculate graphs containing a loop (or more than one loop). For certain loop graphs, the integral over loop momentum in the graph gives rise to a divergent contribution associated with large momentum in the loop. Considering the space-time picture of the

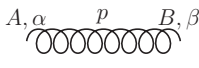
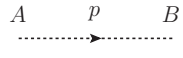
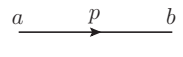
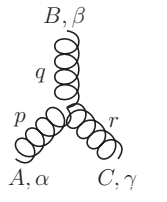
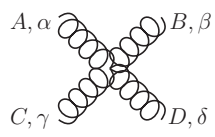
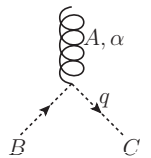
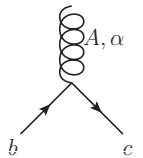
	Covariant Gauge	Axial Gauge
	$\delta^{AB} \frac{i}{p^2 + i\varepsilon} [-g^{\alpha\beta} + (1 - \lambda) \frac{p^\alpha p^\beta}{p^2 + i\varepsilon}]$	$\delta^{AB} \frac{i}{p^2 + i\varepsilon} [-g^{\alpha\beta} + \frac{n^\alpha p^\beta + p^\alpha n^\beta}{n \cdot p} - \frac{(n^2 + \lambda p^2) p^\alpha p^\beta}{(n \cdot p)^2}]$
	$\delta^{AB} \frac{i}{p^2 + i\varepsilon}$	$\delta^{AB} \frac{1}{n \cdot p}$
	$\delta^{ab} \frac{i}{\not{p} - m + i\varepsilon}$	
	$g_s f^{ABC} [(p - q)^\gamma g^{\alpha\beta} + (q - r)^\alpha g^{\beta\gamma} + (r - p)^\beta g^{\gamma\alpha}]$	
	$-ig_s^2 f^{XAC} f^{XBD} [g^{\alpha\beta} g^{\gamma\delta} - g^{\alpha\delta} g^{\gamma\beta}]$ $-ig_s^2 f^{XAD} f^{XBC} [g^{\alpha\beta} g^{\gamma\delta} - g^{\alpha\gamma} g^{\delta\beta}]$ $-ig_s^2 f^{XAB} f^{XCD} [g^{\alpha\gamma} g^{\beta\delta} - g^{\alpha\delta} g^{\gamma\beta}]$	
	$-g_s f^{ABC} q^\alpha$	$-ig_s f^{ABC} n^\alpha$
	$ig_s (t^A)_{cb} \gamma^\alpha$	

Table 1.1: Feynman rules for QCD in covariant and axial gauges.

graph, the divergent contribution is associated with the loop shrinking into a single space-time point, such that the loop resembles a vertex. This indicates a strategy for handling the infinities in which the large momentum parts of loops are absorbed into redefinitions of the appropriate coupling constants and fields. The ‘bare’ coupling constants and fields with which we started in (1.16) would then have to be infinite in order to absorb the infinite loop contribution and give a finite result – but this is perfectly acceptable since these are just parameters of the theory which do not have any direct physical manifestation.

For this strategy to work, it is necessary that the loops with divergences should have the same external leg structure as the vertices of the theory. Furthermore, there are subtleties at the two loop level and above with regard to subdivergences – i.e. divergences related to some of the momenta in the loops becoming large whilst the others remain finite. Nevertheless, it is possible to show that all of the divergent large momentum/small distance behaviour in QCD can be absorbed into redefinitions of coupling constants and fields. This procedure is referred to as renormalisation, and QCD is said to be renormalisable (there are a number of other renormalisable theories – e.g. QED, the Standard Model). It is important to note that the coupling constant remains universal between all of the QCD vertices in Table (1.1) even after renormalisation – this is a consequence of the gauge invariance of the theory.

The procedure of renormalisation requires the introduction of a scale μ_R above which one regards momenta as ‘large’ and absorbs them into coupling constants or fields. The coupling constants and fields then become functions of μ_R . Let us see how this works for the case of a more simple field theory than QCD – massless scalar ϕ^4 theory in four dimensions. The Lagrangian for this theory, written in terms of the ‘bare’ fields and coupling constants (i.e. the basic parameters of the theory, with no loop divergences absorbed into them), is $\mathcal{L} = \frac{1}{2}(\partial_\mu \phi_0)^2 - \frac{\lambda_0}{4!} \phi_0^4$ (in fact there’s also a mass term $-\frac{1}{2}m_0 \phi_0^2$, where the bare mass m_0 has to be precisely chosen to ensure the renormalised mass m is equal to zero – but we’ll largely skirt this issue in what follows). We’ll also only focus on the momentum-space four-point Green’s function in this theory, $G^{(4)}(p_1, \dots, p_4)$. The tree-level and one-loop diagrams contributing to $G^{(4)}$ are:

$$G^{(4)} = \begin{array}{c} \text{Diagram 1: Tree-level exchange} \\ \text{Diagram 2: One-loop bubble} \\ \text{Diagram 3: One-loop box} \\ \text{Diagram 4: One-loop triangle} \end{array} + \mathcal{O}(\lambda_0^3) \quad (1.32)$$

In (1.32) we've omitted the one-loop propagator corrections in the external legs – at one loop these are entirely cancelled using the divergent parts of m_0 required to set $m = 0$, and we do not need to consider them further.

The value of $G^{(4)}$ at one loop may be computed using the Feynman rules in Appendix A.1 of [17]:

$$G^{(4)} = [-i\lambda_0 + (-i\lambda_0)^2(iV(s) + iV(t) + iV(u))] \cdot \prod_{i=1..4} \frac{i}{p_i^2 + i\epsilon} + \mathcal{O}(\lambda_0^3) \quad (1.33)$$

where:

$$V(p^2) = \int \frac{d^4k}{(2\pi)^4} \frac{i}{(k^2 + i\epsilon)((k+p)^2 + i\epsilon)} \quad (1.34)$$

Each one-loop integral V contributing to $G^{(4)}$ is divergent. We must regulate these integrals in order to be able to manipulate them in any sort of meaningful way. The most crude way would be to cut off the momentum integrals at some (large) scale Λ_{UV} (which one would eventually hope to send to infinity after the renormalisation process). However, we shall instead regulate them by deforming the spacetime dimension from 4 to $d = 4 - \epsilon$ (this is known as dimensional regularisation). The divergences in the loop integrals then manifest themselves as poles in ϵ . Dimensional regularisation has the advantage that it preserves the Lorentz invariance of loop integrals (and also preserves gauge invariance for QCD and other gauge theories).

Now we perform the renormalisation procedure – i.e. absorb the small-distance one-loop divergences in the four-point function into the coupling constant λ of the theory. We split the (infinite) bare coupling λ_0 into a (finite) renormalised coupling λ and an (infinite) ‘counterterm’ $\delta\lambda$:

$$\lambda_0 = \mu^\epsilon(\lambda + \delta\lambda) \quad (1.35)$$

We have premultiplied the right hand side of (1.35) by μ^ϵ , where μ is a quantity with the dimensions of energy. This is done to ensure that the renormalised coupling λ remains dimensionless even for $d \neq 4$. The quantity μ in dimensional regularisation is essentially the analogue of the cutoff Λ_{UV} in the crude cutoff regularisation scheme.

Inserting (1.35) into (1.33) and requiring that $G^{(4)}$ and λ be finite, we see that $\delta\lambda$ at lowest order must be equal to minus the divergent parts of the one-loop integrals (i.e. the parts proportional to $1/\epsilon$) – possibly also with a finite part added on (with the choice

of finite part determining the so-called renormalisation scheme). Rearranging (1.35), we obtain:

$$\lambda = \lambda_0 \mu^{-\varepsilon} - \delta_\lambda \quad (1.36)$$

The renormalised coupling contains the bare coupling plus the divergent parts of the one-loop integrals (plus additional finite parts), as we stated above.

In any renormalisation scheme, one has to specify a renormalisation scale μ_R at which the divergences are absorbed into the renormalised coupling λ (in some schemes, such as the ones we will discuss here, the scale is clear, whilst in other schemes, such as the on-shell renormalisation scheme, the scale involved is less explicit). Let us first consider a simple renormalisation scheme in which we require that $G^{(4)} = -i\lambda\mu^\varepsilon$ when all of the invariants $(p_1 + p_2)^2$, $(p_2 + p_3)^2$, and $(p_1 + p_4)^2$ are spacelike and of order $-M^2$. In this scheme the renormalisation scale is M , and at one-loop order we must have:

$$\begin{aligned} \delta_{\lambda, MOM} &= (-i\lambda)^2 \cdot 3V(-M^2)\mu^\varepsilon = \frac{3\lambda^2\mu^\varepsilon}{2(4\pi)^{d/2}} \int_0^1 dx \frac{\Gamma(\frac{\varepsilon}{2})}{(x(1-x)M^2)^{\varepsilon/2}} \\ &= \frac{3\lambda^2}{2(4\pi)^2} \left[\frac{2}{\varepsilon} - \log\left(\frac{M^2}{\mu^2}\right) + \text{finite} \right] \end{aligned} \quad (1.37)$$

where the finite terms do not depend on M . Even though the bare coupling λ_0 does not depend on M , the renormalised coupling λ does due to (1.36) and the fact that δ_λ depends on M . It is worth noting that λ does not depend on the regularisation scale μ , which may now be sent to infinity.

An alternative renormalisation scheme is the modified minimal subtraction scheme, or \overline{MS} scheme. In this scheme the counterterms are pure ε poles, except for a special factor S_ε for each loop. The factor S_ε is defined according to:

$$S_\varepsilon = \frac{(4\pi)^{\varepsilon/2}}{\Gamma(1 - \varepsilon/2)} \quad (1.38)$$

So δ_λ at one-loop order in the \overline{MS} scheme is:

$$\delta_{\lambda, \overline{MS}} = \frac{3\lambda^2 S_\varepsilon}{2(4\pi)^2} \frac{2}{\varepsilon} \quad (1.39)$$

Comparing (1.37) with (1.39), we observe that the \overline{MS} scheme corresponds to using the scale μ as the renormalisation scale. It is straightforward to verify using (1.36) and (1.39) that λ depends on μ in the \overline{MS} renormalisation scheme, even though λ_0 does not.

The \overline{MS} scheme is a popular renormalisation scheme in contemporary particle physics calculations.

Let us now return to our discussion of renormalisation focussing on the QCD Lagrangian (1.16). The renormalisation scale μ_R is not a parameter of the original Lagrangian (1.16) – therefore any physical observable cannot depend on it and in an all-order calculation we could set it to any arbitrary value to perform the calculation. However, in practice we are restricted to calculations of $\mathcal{O}(\alpha_s^n)$, with n a small finite number – then there remains a dependence on μ_R of $\mathcal{O}(\alpha_s^{n+1})$. In this case what is the optimum choice for μ_R ? Consider a dimensionless physical observable R which depends on a single energy scale Q , and for the moment let us set quark masses m_i to zero for simplicity. Then R can only be a function of $\alpha_s(\mu_R^2)$ and Q^2/μ_R^2 :

$$R = R(Q^2/\mu_R^2, \alpha_s(\mu_R^2)) \quad (1.40)$$

If one picks $\mu_R^2 \sim Q^2$, then the coefficients of the perturbation expansion of R in $\alpha_s(Q^2)$ can only be of order 1, as is required for a sensible expansion. On the other hand, if μ_R^2 is very different from Q^2 then large ratios of Q^2/μ_R^2 appear in the coefficients of the perturbation expansion (in QCD, they appear inside large logarithms), which effectively ruin the perturbation expansion in $\alpha_s(\mu_R^2)$. The large logarithms are associated with the sudden appearance of quantum fluctuations with momenta in between Q^2 and μ_R^2 in loop calculations, which have not been smoothly absorbed into the coupling constants. For a calculation of a physical quantity with scale Q , then, the appropriate value of the coupling constant (and other Lagrangian quantities) to use is the renormalised value at scale Q .

The way that α_s changes (‘runs’) with scale μ_R is determined by the beta function $\beta(\alpha_s)$:

$$\beta(\alpha_s) \equiv \mu_R^2 \frac{\partial \alpha_s}{\partial \mu_R^2} \quad (1.41)$$

This can be calculated to $\mathcal{O}(\alpha_s^{n+1})$ from a calculation of the physical quantity R to order (α_s^n) by using the fact that this quantity does not depend on μ_R to this order:

$$\mu_R^2 \frac{dR}{d\mu_R^2} = \left\{ \mu_R^2 \frac{\partial}{\partial \mu_R^2} + \beta(\alpha_s) \frac{\partial}{\partial \alpha_s} \right\} R = 0 \implies \beta(\alpha_s) = -\frac{\mu_R^2 \partial R / \partial \mu_R^2}{\partial R / \partial \alpha_s} \quad (1.42)$$

The leading contribution to the beta function is well-known:

$$\beta(\alpha_s) = -b\alpha_s^2 + O(\alpha_s^3) \quad (1.43)$$

$$b \equiv \frac{11C_A - 4T_R N_f}{12\pi} = \frac{33 - 2N_f}{12\pi} \quad (1.44)$$

In the Standard Model $N_f = 6$, b is positive, and $\beta(\alpha_s)$ is negative. Thus $\alpha_s(Q)$ decreases with increasing Q , and QCD has the required property that it is asymptotically free. This fundamental feature of QCD is a result of the fact that gluons themselves carry colour charge and couple to other gluons. This gives rise to an antiscreening effect around a QCD colour charge due to gluon pair fluctuations in the vacuum, which turns out to completely overwhelm the screening effect due to fermion-antifermion pair fluctuations (note that in QED there is only the latter effect, so its β function slowly increases with scale). Note that higher order corrections to the β function change the precise running of α_s , but not the qualitative picture.

The equation (1.43) can be solved to give an explicit LO expression for the running of α_s :

$$\alpha_s(\mu_R^2) = \frac{\alpha_s(\mu_{R0}^2)}{1 + \alpha_s(\mu_{R0}^2)b \ln(\mu_R^2/\mu_{R0}^2)} \quad (1.45)$$

$$= \frac{1}{b \ln(\mu_R^2/\Lambda_{QCD}^2)} \quad (1.46)$$

where $\alpha_s(\mu_{R0}^2)$ is the running coupling at some reference scale μ_{R0}^2 (the value of $\alpha_s(\mu_{R0}^2)$ must be determined experimentally), whilst Λ_{QCD}^2 is defined according to:

$$\Lambda_{QCD}^2 = \mu_{R0}^2 \exp\left(-\frac{1}{b\alpha_s(\mu_{R0}^2)}\right) \quad (1.47)$$

and is in fact independent of μ_{R0} . Λ_{QCD}^2 here is the scale at which the perturbative one-loop coupling constant diverges – note, however, the true coupling constant will not exhibit such extreme behaviour as we cannot trust perturbation theory in this region. Rather, this scale should be thought of as the scale at which nonperturbative effects become important. Somewhat unsurprisingly, Λ_{QCD} is found experimentally to have a value of $\sim 1\text{GeV}$, similar to the typical mass scale for a hadron.

1.3.2 Quark Masses

So far we have paid little attention to the issue of quark masses in QCD. The bare masses m_i in any quantum field theory are similar to the coupling constants in that they are just parameters that require renormalisation, giving rise to finite running masses $m_i(\mu_R^2)$. If one has a theory in which single particles can be isolated (e.g. QED), then one can introduce the concept of a physical mass, which is calculated as the position of the pole in the renormalised two-point Green's function of that particle. However, it is not such a useful concept for the confined quarks of QCD – in this case it is sensible to retain the description in terms of running quark masses. Calculations show that the variation of quark masses with μ_R is a slow logarithmic decrease. Therefore as Q of a hard process becomes large, the corresponding running mass of the quarks $m_i(\mu_R)$ becomes negligible compared to Q , and one can treat the quarks as massless particles (for a quark i , Q is large if it is much larger than the ‘typical’ mass of that quark). Even at $Q = 1\text{GeV}$ (which is essentially the smallest scale at which one can make perturbative calculations), the up and down quarks only have masses of a few MeV , and the strange quark has a mass of a hundred or so MeV – thus, to a good approximation, one can take these quarks to be massless in perturbative calculations. On the other hand, the masses of the heavier charm, bottom, and top quarks have to be taken account of explicitly in calculations.

For a heavy quark with (pole) mass $M_Q \gg \Lambda_{QCD}$, there exists the possibility that the perturbative scale Q at which we would like to calculate the observable R is much less than M_Q . At such scales one would intuitively expect the effects of internal loops of the heavy quark to be suppressed by Q^2/M_Q^2 , and the heavy quarks to ‘decouple’ from the theory. This decoupling is not manifest if one naively applies the ‘standard’ \overline{MS} scheme to renormalise QCD – therefore this scheme is not ideal for performing QCD computations when there is a heavy quark mass $\gg Q$. Instead, it is preferable to use the Collins, Wilczek and Zee (CWZ) scheme [18], which does satisfy manifest decoupling for the heavy quarks. Computation of the observable $R(Q^2)$ in this scheme proceeds as follows. The full set of six quarks is partitioned into a set of ‘active’ quarks (with masses smaller than Q) and ‘inactive’ quarks (with masses greater than Q). In graphs contributing to R containing only active quarks, normal \overline{MS} counterterms are used. However, zero-momentum subtractions are applied to the graphs containing at least one internal line for an inactive quark. It is clear that this scheme is in fact a composite scheme, consisting of subschemes that are applied at different values of Q . Matching conditions must be satisfied at the switching points between subschemes (the heavy quark masses), such

that they give identical physical predictions in the matching region. At LO in the CWZ scheme α_s runs according to (1.41) with N_f set to the number of active flavours, and the LO matching condition for this quantity is that it should be continuous at the quark mass switching points.

1.3.3 Scaling Violations in QCD

Let us now revisit the issue of deep inelastic scattering (DIS) of a lepton l from a hadron h and see to what extent the full QCD theory reproduces the features of the naive parton model. In fact one can tell straight away that there are going to be deviations just from looking at the behaviour of $\alpha_s(Q^2)$ in QCD. The coupling constant decreases to zero as Q becomes large, as also occurs for the ‘strong coupling’ in the parton model – however, the decrease with Q is slow (logarithmic), and the value of $\alpha_s(Q^2)$ is appreciable even at values of $Q^2 \gg m_p^2$. This is in contrast to the behaviour of the coupling constant in the parton model, which is dramatically cut off at momentum scales larger than m_p . In QCD we therefore expect some contribution from strong interaction effects at all length scales between $1/m_p$ and $1/Q$, contrary to the predictions of the parton model.

We can see this more explicitly in the context of DIS by considering the lowest order strong corrections to the F_2 structure function of an individual quark parton q_i (where we set the ξ of this parton to 1 for the moment). The value of this quantity $\hat{F}_2(x)$ prior to strong corrections may be extracted from (1.8) with ξ set to 1 and is:

$$\hat{F}_2(x) = e_{q_i}^2 \delta(1 - x) \quad (1.48)$$

In figure 1.2 we catalogue the complete set of lowest order strong corrections to $\hat{F}_2(x)$ using a cut diagram notation. In this notation, a contribution to the cross section $|\mathcal{M}|^2$ from a particular diagram in the amplitude \mathcal{M} and a particular diagram in the conjugate amplitude \mathcal{M}^* is written as a single diagram with a dashed line running vertically through the middle (the ‘cut’). On the left hand side of the cut is written the diagram from the amplitude, with the initial state on the left, whilst the diagram from the conjugate amplitude is written on the right hand side of the cut, with the initial state on the right. The final states from the diagrams in the amplitude and conjugate are ‘sewn together’ at the cut. Note that the diagrams in figure 1.2, with the particles crossing the cut being put on shell, can also be considered as contributions to the imaginary part of the amplitude for the forward process $q\gamma^* \rightarrow q\gamma^*$, according to the optical theorem (see, for example,

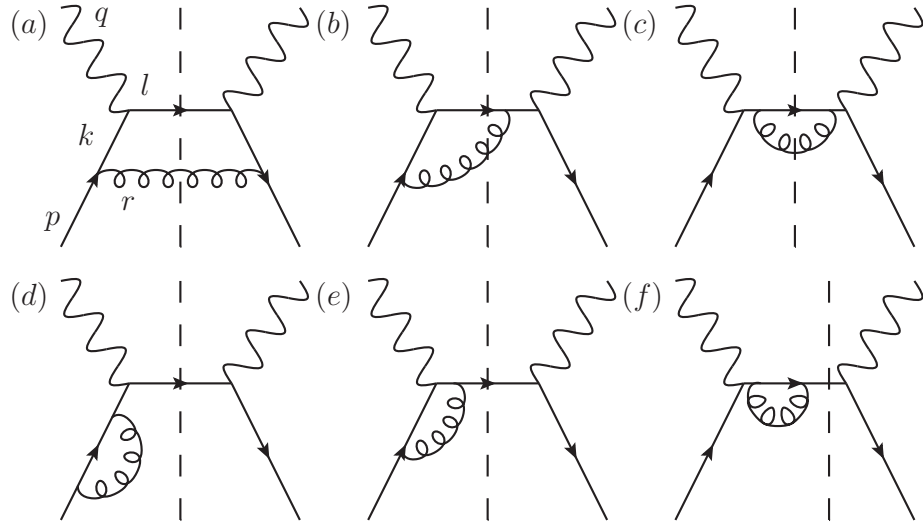


Figure 1.2: Graphs contributing to the quark DIS cross section at $O(\alpha_s)$. The full set of graphs contributing to this quantity is comprised from the set above plus the hermitian conjugate graphs of (b), (d), (e) and (f). Graphs (a)-(c) are real emission graphs, whilst (d)-(f) are virtual corrections. Note that graphs (d) and (f) involve 1PI loop corrections on an external leg – therefore these graphs have to be handled using the method of Lehmann, Symanzik and Zimmerman (LSZ). This tells us that for the correction on external leg i we should multiply the amplitude by a factor of $Z_i^{1/2}$, where Z_i is the residue of the pole of the propagator for particle i (for more detail concerning the LSZ formula, please see [17, 19]).

section 7.3 of [17]).

For the parton model predictions to be fully realised, the graphs in figure 1.2 would all have to be dominated by momenta and virtualities on the order of m_p – then we could safely absorb the contributions from all of these graphs into scale-independent parton distributions.

We begin with the computation of the important ‘ladder’ graph figure 1.2(a). The calculation will be performed in light-cone gauge, which is a particular choice of axial gauge in which the condition $A^+ = 0$ is imposed. Guided by the parton model predictions, we will evaluate the matrix element in the limit in which k_\perp^2 and k^2 of the virtual quark in the graph is small (i.e. $\ll Q^2$). We’ll also take the quark participating in the interaction to be massless, for simplicity. Under these approximations diagram (a) gives the following contribution to the parton-level DIS cross section [20]:

$$\frac{d^2\sigma}{dx dQ^2}|_{qe \rightarrow eq, a} = \int_0^1 dz \int^{Q^2} \frac{dk_\perp^2}{k_\perp^2} \frac{\alpha_s}{2\pi} C_F \left[\frac{1+z^2}{1-z} \right] \frac{d^2\sigma}{dx dQ^2}|_{qe \rightarrow eq}(z) \quad (1.49)$$

The quantity z in this expression is the light-cone momentum fraction of the initial ‘parent’ quark carried by the virtual ‘daughter’ quark, and the virtuality of the virtual quark is connected to the transverse momentum by:

$$k^2 = -k_\perp^2/(1-z) \quad (1.50)$$

We see in (1.49) that the transverse momentum and virtuality of the quark produced by the QCD splitting are not in fact restricted to small values – instead there is a broad logarithmic integral over transverse momentum (or virtuality) all the way up to Q^2 . Note that the integral over k_T is formally divergent at the infrared end – this is a divergence associated with the quark and gluon becoming collinear, and would be regulated by the quark mass for the case of a heavy quark. We will see how this is dealt with shortly, but for the time being will simply introduce a regulator κ^2 such that the k_\perp integral gives $\log(Q^2/\kappa^2)$.

A further important point to make is that since k_T is not restricted to small values, the expression (1.49) which is derived under this approximation is not the full story – there is a further (finite) contribution from figure 1.2(a) associated with momenta of order Q . Computing the exact expressions for all of the graphs in figure 1.2, adding them together, and then extracting the $\mathcal{O}(\alpha_s)$ correction to $\hat{F}_2^{qi}(x, Q^2)$ from the result, one obtains the

following expression for $\hat{F}_2^{q_i}(x, Q^2)$ to $\mathcal{O}(\alpha_s)$:

$$\hat{F}_2^{q_i}(x, Q^2) = e_{q_i}^2 x \left[\delta(1-x) + \frac{\alpha_s}{2\pi} \left(P_{qq}(x) \ln \left(\frac{Q^2}{\kappa^2} \right) + C(x) \right) + \dots \right] \quad (1.51)$$

$C(x)$ is a finite function and $P_{qq}(x)$ is defined as follows:

$$P_{qq}(x) = C_F \left[\frac{1+x^2}{(1-x)_+} + \frac{3}{2} \delta(1-x) \right] \quad (1.52)$$

where the function $1/(1-x)_+$ is defined to be equal to $1/(1-x)$ for $x < 1$, but has a singularity at $x = 1$ such that its integral with any smooth function $f(x)$ gives:

$$\int_0^1 dx \frac{f(x)}{(1-x)_+} = \int_0^1 dx \frac{f(x) - f(1)}{1-x} \quad (1.53)$$

In the axial gauge, only the real emission diagram figure 1.2(a) and the virtual diagrams 1.2(d) contain logarithmic integrations over a broad range of transverse momentum and the associated $\ln(Q^2/\kappa^2)$ factors. In the remaining diagrams the transverse momentum/virtuality integrations are actually dominated by values close to Q^2 , such that these diagrams only give small perturbative corrections to $\hat{F}_2^{q_i}$.

Since QCD effects are not restricted to small transverse momenta $< m_p$ as in the parton model but instead occur over a broad range of transverse momenta, one cannot bundle all of the effects of QCD into parton distributions that are invariant in Q^2 and universally applicable for hard scales $> \Lambda_{QCD}$, and calculate DIS cross sections using these parton distributions and free quark cross sections. Instead, we are forced to introduce an arbitrary scale μ_F , absorbing QCD effects with transverse momenta $< \mu_F$ into the parton distribution, which therefore becomes a function of μ_F , and leaving the remainder as a correction to the parton-level cross section. This factorisation procedure in which small momentum fluctuations are absorbed into the parton distributions is strongly analogous to the renormalisation procedure in which high momentum fluctuations are absorbed into the coupling constants of the theory.

Let us give a very rough demonstration of how the factorisation procedure is put into practice. The structure function of the proton including strong corrections is calculated by convolving the parton-level structure function of (1.51) with some ‘bare’ parton

distributions $D_{h,0}^{q_i}$:

$$F_2(x, Q^2) = \sum_{q, \bar{q}} \int d\xi \hat{F}_2^{q_i} \left(\frac{x}{\xi}, Q^2 \right) D_{h,0}^{q_i}(\xi) \quad (1.54)$$

$$= x \sum_{q, \bar{q}} e_{q_i}^2 \left[D_{h,0}^{q_i}(x) + \frac{\alpha_s}{2\pi} \int_x^1 \frac{d\xi}{\xi} D_{h,0}^{q_i}(\xi) \left\{ P_{qq} \left(\frac{x}{\xi} \right) \ln \left(\frac{Q^2}{\kappa^2} \right) + C \left(\frac{x}{\xi} \right) \right\} + \dots \right]$$

We define a ‘renormalised’ parton distribution $D_h^{q_i}(x, \mu_F^2)$ that absorbs the parts of the QCD splittings with transverse momenta $< \mu_F$:

$$D_h^{q_i}(x, \mu_F^2) = D_{h,0}^{q_i}(x) + \frac{\alpha_s}{2\pi} \int_x^1 \frac{d\xi}{\xi} D_{h,0}^{q_i}(\xi) \left\{ P_{qq} \left(\frac{x}{\xi} \right) \ln \left(\frac{\mu_F^2}{\kappa^2} \right) + C' \left(\frac{x}{\xi} \right) \right\} + \dots \quad (1.55)$$

For this to be finite, the bare quark distributions must be infinite – but this is not a problem (just as it was not a problem that the bare coupling constants of QCD are infinite) since the bare quark distributions are not measurable. If this notion is uncomfortable, one can alternatively consider obtaining the proton structure function by convolution of \hat{F}^{q_i} with the PDFs of the parton model, which are supposed to include the effects of strong interactions with transverse momenta $< \Lambda_{QCD}$. In this case the logarithmic integration in \hat{F}^{q_i} should be cut-off at transverse momenta of order m_p to prevent double counting between \hat{F}^{q_i} and the PDFs, and the PDF redefinition (1.55) becomes a relation between finite quantities.

When introducing the ‘renormalised’ PDF, we have the freedom to absorb any amount of the finite correction C into its definition – in (1.55) the finite part that is absorbed is denoted as C' . The choice of finite part to be absorbed into $D_h^{q_i}(x, \mu_F^2)$ defines the so-called factorisation scheme (this is analogous to the renormalisation scheme for UV divergences). Popular choices for the factorisation scheme include the \overline{MS} scheme, and the DIS scheme, in which the finite parts absorbed into the PDFs are chosen to ensure the relation $F_2(x, Q^2) = x \sum_i e_i^2 D_p^i(x, Q^2)$ holds to all orders in perturbation theory.

Rewriting F_2 in terms of the renormalised PDF, we obtain:

$$F_2(x, Q^2) = x \sum_{q, \bar{q}} e_{q_i}^2 \int_0^1 \frac{d\xi}{\xi} D_h^{q_i}(x, \mu_F^2) \left\{ \delta \left(1 - \frac{x}{\xi} \right) + \frac{\alpha_s}{2\pi} \left[P_{qq} \left(\frac{x}{\xi} \right) \ln \left(\frac{Q^2}{\mu_F^2} \right) + (C - C') \left(\frac{x}{\xi} \right) + \dots \right] \right\} \quad (1.56)$$

$$= x \sum_{q, \bar{q}} e_{q_i}^2 \int_0^1 \frac{d\xi}{\xi} D_h^{q_i}(x, Q^2) \left\{ \delta \left(1 - \frac{x}{\xi} \right) + \frac{\alpha_s}{2\pi} \left[(C - C') \left(\frac{x}{\xi} \right) + \dots \right] \right\}$$

where in the second line of (1.56) we have set $\mu_F = Q$. We see that in (leading order) QCD we recover a formula for F_2 that resembles the parton model result, but is modified from it in two respects. First, and perhaps most important, the parton distributions now depend logarithmically on Q , resulting in logarithmic scaling violations in F_2 – these have been observed in experiment. Second, the parton model \hat{F}_2 in the formula is supplemented by QCD perturbative corrections.

The precise expression for the scale dependence of the parton distributions $D_h^{q_i}$ can be deduced by differentiating the first line of (1.56) and noting that F_2 as a physical quantity cannot depend on μ_F (the procedure is similar to that used to obtain β in (1.42)). The result is:

$$\mu_F^2 \frac{\partial D_h^{q_i}(x, \mu_F^2)}{d\mu_F^2} = \frac{\alpha_s(\mu_F^2)}{2\pi} \int_x^1 \frac{d\xi}{\xi} D_h^{q_i} \left(\frac{x}{\xi}, \mu_F^2 \right) P_{qq}(\xi) \quad (1.57)$$

The argument of α_s has been set to μ_F^2 here – we do not justify this choice here, only remark that more rigorous treatments indicate that this is the appropriate choice for μ_R^2 in α_s [15, 21, 22]. This is (an incomplete leading order form of) the celebrated Dokshitzer-Gribov-Lipatov-Altarelli-Parisi (DGLAP) equation. It resums multiple emission of gluons from the quark line, in the kinematic regime in which successive emissions are strongly ordered in transverse momentum. This region corresponds to the largest number of logarithms arising from the integration over transverse momentum (one per power of α_s).

In the last paragraph we stated that equation (1.57) is incomplete. That is because (1.57) only sums up the leading logarithmic contributions from a single type of QCD splitting process – emission of a gluon from a quark line. There are other QCD branching processes that can also contribute at the leading logarithmic level – quark-antiquark, or gluon pair production from a gluon, or gluon production from a quark (with the accompanying quark being emitted rather than going on to the DIS process). Including all of these effects, the DGLAP equation becomes a matrix equation involving the gluon distribution D_h^g :

$$\mu_F^2 \frac{\partial}{\partial \mu_F^2} \begin{pmatrix} D_h^{q_i}(x, \mu_F^2) \\ D_h^g(x, \mu_F^2) \end{pmatrix} = \frac{\alpha_s(\mu_F^2)}{2\pi} \sum_j \int_x^1 \frac{d\xi}{\xi} \begin{pmatrix} P_{q_i q_j}(\frac{x}{\xi}) & P_{q_i g}(\frac{x}{\xi}) \\ P_{g q_j}(\frac{x}{\xi}) & P_{g g}(\frac{x}{\xi}) \end{pmatrix} \begin{pmatrix} D_h^{q_j}(\xi, \mu_F^2) \\ D_h^g(\xi, \mu_F^2) \end{pmatrix} \quad (1.58)$$

In (1.58) the indices i and j run over all quark flavours, as well as all antiquark flavours. The leading order splitting functions P_{ij} in (1.58) are straightforward to calculate, and are well-known:

$$P_{q_i q_j}(x) = \delta_{ij} C_F \left[\frac{1+x^2}{1-x} \right]_+ \quad (1.59)$$

$$P_{q_i g}(x) = T_R [x^2 + (1-x)^2] \quad (1.60)$$

$$P_{g q_i}(x) = C_F \left[\frac{1+(1-x)^2}{x} \right] \quad (1.61)$$

$$P_{gg}(x) = 2C_A \left[\frac{x}{(1-x)_+} + \frac{1-x}{x} + x(1-x) \right] \\ + \delta(1-x) \frac{11C_A - 4n_f T_R}{6} \quad (1.62)$$

Equation (1.58) is a coupled set of integro-differential equations. The structure of this set of equations can be simplified by using PDFs that describe the distributions of the following linear combinations of partons:

$$\begin{aligned} V_i &= q_i^- & T_3 &= u^+ - d^+ \\ T_8 &= u^+ + d^+ - 2s^+ & T_{15} &= u^+ + d^+ + s^+ - 3c^+ \\ T_{24} &= u^+ + d^+ + s^+ + c^+ - 4b^+ & T_{35} &= u^+ + d^+ + s^+ + c^+ + b^+ - 5t^+ \\ \Sigma &= \sum_i q_i^+ \end{aligned} \quad (1.63)$$

where:

$$q_i^\pm = q_i \pm \bar{q}_i \quad (1.64)$$

We shall refer to this basis for the parton indices in the DGLAP equation as the ‘evolution basis’, referring to the basis in which the parton indices in the DGLAP equation are q_i, \bar{q}_i and g as the ‘human basis’. In the evolution basis only the evolution of the Σ and g distributions are coupled, whilst all of the V_i and T_i distributions evolve according to (1.57) at leading order. The DGLAP evolution equations are simplified in the basis (1.63) due to the flavour structure and symmetries of the QCD interaction. For example, the evolution of the combination T_3 is simple because, for scales much larger than the u and d mass (which in practice means all perturbative scales), the u and d quark appear identical from the point of view of the QCD interactions (as do the \bar{u} and \bar{d} antiquarks) – this is isospin symmetry.

The V_i distribution describes the net number of quarks minus antiquarks of flavour i in the proton, and is subject to the following ‘number’ sum rule:

$$\int_0^1 dx D_h^{V_i}(x, Q^2) = N_i \quad (1.65)$$

N_i is a finite number describing the number of ‘valence’ i quarks in the hadron (for the proton, $N_u = 2$, $N_d = 1$, and $N_i = 0$ for $i \neq u, d$). Owing to the fact that the quarks and gluons must carry all of the momentum of the proton, the Σ and g distributions are subject to the following ‘momentum’ sum rule:

$$\int_0^1 dx x (D_h^\Sigma(x, Q^2) + D_h^g(x, Q^2)) = 1 \quad (1.66)$$

There exist formal operator representations of the quark and gluon PDFs [15, 16], which for a proton target read:

$$D_p^q(\xi) = \frac{1}{2\pi} \int dw^- e^{-iP^+ w^- \xi} \langle P | \bar{\psi}_{qa}(w) \mathcal{G}_{ab}(w, 0) \frac{\gamma^+}{2} \psi_{qb}(0) | P \rangle_c |_{w^+=0, \mathbf{w}=0} \quad (1.67)$$

$$D_p^g(\xi) = \frac{1}{2\pi\xi P^+} \sum_{i=1}^2 \int dw^- e^{-iP^+ w^- \xi} \langle P | F_A^{+i}(w) \mathcal{G}_{AB}(w, 0) F^{+i}(0)_B | P \rangle_c |_{w^+=0, \mathbf{w}=0} \quad (1.68)$$

In these formulae, $\psi_{qb}(z)$ is the quark field operator with colour index b evaluated at space-time position z , and $F_A^{\alpha\beta}(z)$ is the gluon field strength operator (see (1.18)) with colour index A evaluated at z . The plus and minus components of a four vector are defined in (1.6), and $\mathbf{w} \equiv (w^1, w^2)$. The ‘c’ subscript at the end of each definition implies that we only consider the contribution from this matrix element where the quark or gluon fields are connected to the proton state $|P\rangle$. In (1.67) and (1.68) the Wilson line factors \mathcal{G} are given by:

$$\mathcal{G}(w^-, 0) = P \left\{ \exp \left(-ig_s \int_0^{w^-} dy^- A^{+A}(y^-) t_r^A \right) \right\} \quad (1.69)$$

where the t_r^A matrices are the fundamental colour matrices t^A in (1.67) and the adjoint colour matrices T^A in (1.68). In the light-cone gauge $A^+ = 0$, the Wilson line factors reduce to simple delta functions δ_{ab} or δ_{AB} .

In fact, the parton distributions defined by (1.67) and (1.68) are not the same as those appearing in the formula for F_2 . The former quantities, when defined using bare coupling

constants and fields, are the *bare* PDFs (one should note that these bare PDFs are not quite the same as those introduced in (1.54) – see section 9.11 of [15]). The bare PDFs are divergent, and require renormalisation. The renormalisation process introduces a scale into the PDFs that is precisely the factorisation scale μ_F . It is the renormalised PDFs $D_p^i(\xi, Q^2)$ that then appear in the formula for F_2 .

In the preceding paragraphs we have argued that the structure function F_2 for deep inelastic scattering can be factorised into parton distributions and ‘hard’ parton-level coefficient functions \hat{F}_2 :

$$F_2^{(lh)}(x, Q^2) = \sum_i \int_0^1 \frac{d\xi}{\xi} D_h^i(\xi, \mu_F^2) \hat{F}_2^{(li)}(x/\xi, Q^2/\mu_F^2, \alpha_s) \quad (1.70)$$

where here (and from henceforth) the sum is over all parton types (quarks, antiquarks, and gluons).

In this argument we have restricted ourselves to the leading order in QCD (really, the leading order in transverse momentum logarithms, or LLA). It is possible to show in a rigorous way that F_2 (and indeed all other structure functions, and the full DIS cross section) can still be factorised into parton distributions and hard coefficient functions at any order in QCD, up to corrections that are suppressed by a power of Λ_{QCD}^2/Q^2 [15]. At the n th order in α_s , the general form (1.58) of the DGLAP equation continues to hold, but the splitting functions contain extra terms proportional to α_s , α_s^2 , etc. up to α_s^n . At NLO and above, the form of the splitting functions depends on the factorisation scheme. The splitting functions are known to $\mathcal{O}(\alpha_s^2)$ – i.e. NNLO³ – in the most widely used factorisation schemes (i.e. the \overline{MS} and DIS schemes).

The property of all-order factorisation up to corrections of $\mathcal{O}(\Lambda_{QCD}^2/Q^2)$ that is enjoyed by the DIS cross section turns out to carry over to the Drell-Yan cross section, and indeed many other inclusive hard-scattering processes in hadron-hadron collisions. The all-order QCD cross section for a hard scattering process with associated scale Q^2 producing final

³Note that these statements are made under our convention in which we pull a factor of α_s out of the splitting function and write it explicitly on the right hand side of the DGLAP equation, as in (1.58). Under a convention in which this factor of α_s is retained in the splitting function, NNLO corresponds to including terms up to $\mathcal{O}(\alpha_s^3)$ in the splitting function.

state A to occur in the collision of hadrons h_1 and h_2 is:

$$\begin{aligned} \sigma_A(s) = \sum_{ij} \int_0^1 d\xi_1 d\xi_2 D_{h_1}^i(\xi_1, \mu_F^2) D_{h_2}^j(\xi_2, \mu_F^2) \\ \times \hat{\sigma}_{ij \rightarrow A}(\hat{s} = \xi_1 \xi_2 s, Q^2/\mu_F^2, \alpha_s) + \mathcal{O}(\Lambda_{QCD}^2/Q^2) \end{aligned} \quad (1.71)$$

Factorisation for the process $h_1 h_2 \rightarrow A + X$ does not follow trivially from factorisation for DIS – in the Drell-Yan process, exchange of soft gluons between the incident hadrons prior to the hard interaction could change the distributions of partons in the hadrons and destroy the simple parton-model type picture. Classical arguments (see e.g. section 7.2 of [23]) indicate that such effects only cause factorisation to be broken at order Λ_{QCD}^4/s^2 , and factorisation for the Drell-Yan process has been proven explicitly at leading order in the power corrections [15, 24]. Note that just as in the case of the DIS cross section, the predictions of QCD for the Drell-Yan cross section differ from those of the parton model (1.13) only by logarithmic scaling violations and perturbative corrections. These corrections to the parton model picture can be quite important – for example, the use of NLO QCD parton distributions and parton-level cross sections rather than parton model ones results in a Drell-Yan cross section that is roughly a factor of 2 larger (for fixed target energies and masses), in agreement with the data.

The parton distributions appearing in (1.71) are precisely the same as those appearing in (1.70) – that is, the parton distributions are universal. We cannot calculate these objects using perturbation theory due to the fact that the parton distributions include large distance nonperturbative physics. However the universality of the parton distributions means that we can collect data from various scattering processes involving protons, and use this together with the factorised cross sections for the processes and the DGLAP equation (1.58) to *fit* the proton PDFs at some particular scale Q_0 . These ‘input scale’ PDFs can then be used together with (1.58) and factorised cross sections to make cross section predictions for processes of a different type (e.g. Higgs production cross section at the LHC), or predictions at a different scale.

In practice, groups performing PDF fits provide grids of PDF values covering a range of x and Q , obtained by evolving their fitted inputs using the DGLAP equation, along with some interpolation code. In figure 1.3 are plotted the NLO PDFs of Martin, Stirling, Thorne and Watt (MSTW) obtained from a global fit of data in 2008. The PDFs are plotted at two values of Q^2 – 10 GeV^2 and 10^4 GeV^2 . An important point to make is that the number of partons at small x values is very large (one can see that all of the

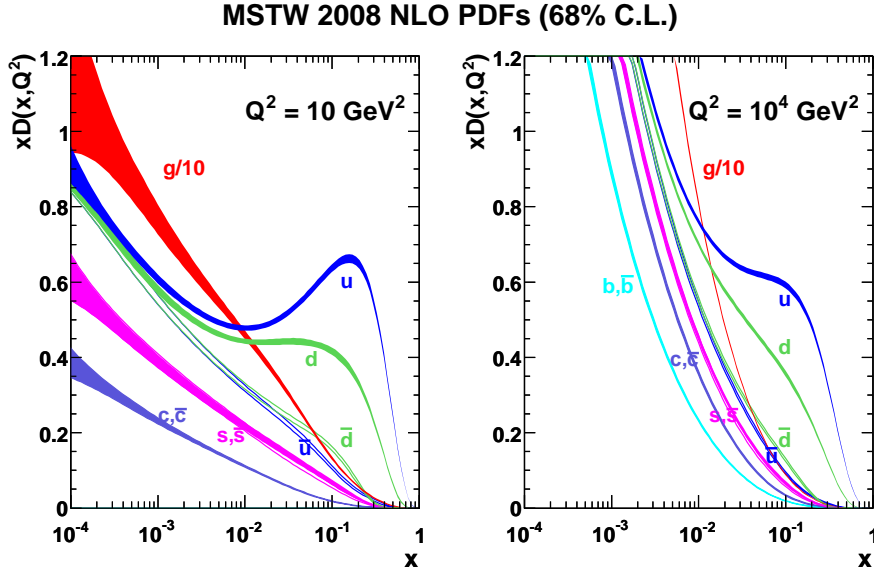


Figure 1.3: The MSTW2008 NLO PDFs at $Q^2 = 10 \text{ GeV}^2$ and $Q^2 = 10^4 \text{ GeV}^2$. Plot taken from the MSTW HepForge page [25].

distributions in figure 1.3 diverge more strongly than $\sim x^{-1}$ at low x , such that the number of partons of any type in the proton is formally infinite).

Note that in figure 1.3 there are b, \bar{b} distributions in the right plot with $Q^2 > M_b^2$ but not in the left plot with $Q^2 < M_b^2$. In treating the effects of a heavy quark i in hadronic scattering processes there are two extremes of possibility. One could restrict the heavy quark to appear only in hard parton-level cross sections (this is the fixed flavour number scheme, or FFNS)– this works well for $Q^2 \sim M_i^2$ since it takes full account of the mass of the quark, but starts to break down for $Q^2 \gg M_i^2$ due to the appearance of large collinear logarithms $\log(Q^2/M_i^2)$. Alternatively, one could simply include the quark as a massless parton for scales $> M_i^2$ (this is the zero mass variable flavour number scheme, or ZM-VFNS) – this resums the logs of Q^2/M_i^2 and so works well for $Q^2 \gg M_i^2$, but gives poor predictions for $Q^2 \sim M_i^2$ since the mass of the quark is essentially neglected. In modern treatments (such as MSTW 2008), general mass flavour schemes (GM-VFNS) are used, that combine the advantages of both methods and allow accurate predictions to be made over the full range of Q . The prescription for parton distributions in a GM-VFNS is the same as that for the ZM-VFNS, and up to NLO is very simple – the PDF for the heavy quark is evolved from zero at $\mu_F^2 = M_i^2$, and the rest of the parton distributions are continuous at this scale.

1.4 Introduction to Double Parton Scattering

The form of (1.71) indicates that the leading power cross section for the hard final state A to be produced in the collision of hadrons h_1 and h_2 is associated with the interaction of a single parton from h_1 with a single parton from h_2 (i.e. a single parton scattering, or SPS, process). The total cross section for A to be produced via n independent parton-parton scatterings is suppressed by a factor of $(\Lambda_{QCD}^2/Q^2)^{n-1}$ with respect to the SPS cross section, for similar reasons to those we gave in Section 1.2 to explain why the interaction of the photon in DIS with n partons in the proton is suppressed by $(\Lambda_{QCD}^2/Q^2)^{n-1}$ with respect to the single interaction probability.

Nevertheless, given that the proton is a composite object, multiple hard parton-parton scattering can occur in a single proton-proton collision – we focus in this section (and in this thesis) on the case of double hard parton-parton scattering (DPS) as the most probable multiple hard scattering process. One expects the importance of double scattering relative to single scattering for a final state AB with a given hard scale Q^2 to grow with collider energy s . This is because as s grows with fixed Q^2 , the protons are probed at lower x where the populations of partons are larger, and the probability of a double parton-parton interaction in the collision of the more densely populated proton discs increases. Thus double parton scattering is more important at the Large Hadron Collider (a proton-proton collider) currently taking data at CERN in Geneva than at any previous hadron collider. Although formally suppressed by (Λ_{QCD}^2/Q^2) , double scattering can compete with single scattering if the parton-level cross section to produce AB via single scattering is suppressed by small or multiple coupling constants, whilst the coupling constants in the DPS parton-level mechanism for producing AB are not so small. Therefore DPS can be an important background to rare SPS processes, including those associated with Higgs production or new physics [26–31]. Furthermore, we present a simplified argument in this section that suggests that for any final state AB that can be produced via DPS, there is a region of final state phase space inside which the DPS contribution is comparable with the SPS contribution. This means that there is scope to make measurements of DPS in multiple processes at the LHC, extracting in the process novel information regarding the correlations between partons in the proton.

Assuming only that the hard processes A and B in a DPS process can be factorised, we can write the cross section for the DPS process producing final state AB in very general

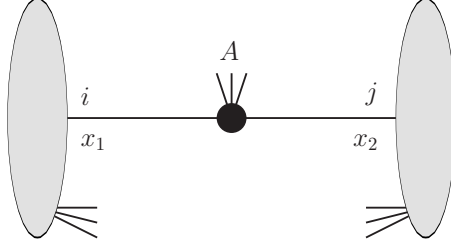
terms as follows:

$$\begin{aligned} \sigma_{(A,B)}^D(s) = & \frac{m}{2} \sum_{i,j,k,l} \int \prod_{a=1}^4 dx_a \hat{\sigma}_{ik \rightarrow A}(\hat{s} = x_1 x_3 s) \hat{\sigma}_{jl \rightarrow B}(\hat{s} = x_2 x_4 s) \\ & \times \int d^2 \mathbf{b} \Gamma_{ij}(x_1, x_2, \mathbf{b}; Q_A^2, Q_B^2) \Gamma_{kl}(x_3, x_4, \mathbf{b}; Q_A^2, Q_B^2) \end{aligned} \quad (1.72)$$

The cross section formula is somewhat similar to that used for single parton scattering (SPS), except that two parton-level cross sections $\hat{\sigma}$ appear, and the PDF factors are two-parton generalised PDFs Γ (2pGPDs) rather than single PDFs. The 2pGPD $\Gamma_{ij}(x_1, x_2, \mathbf{b}; Q_A^2, Q_B^2)$ may be loosely interpreted as the inclusive probability distribution to find partons i, j with longitudinal momentum fractions x_1, x_2 at scale Q_A^2, Q_B^2 in the proton, with the two partons being separated by a transverse displacement \mathbf{b} . The quantity m is a symmetry factor that equals 1 if $A = B$ and 2 otherwise. It is important to note that in this formula the two 2pGPDs are integrated over a common parton pair transverse separation \mathbf{b} – the transverse separation must clearly be identical in both protons in order that two pairs of partons meet in two separate hard interactions A and B. The DPS cross section cannot naturally be written in terms of PDFs that are each fully integrated over their parton impact parameter arguments, as is the case for the SPS cross section. Pictorial representations of the double and single parton scattering formulae, (1.72) and leading power part of (1.71), are given in figure (1.4).

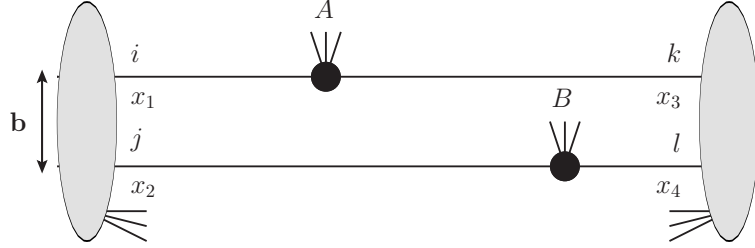
Clearly the DPS process involving two distinct hard scatterings is not the only power suppressed process that can contribute to the cross section for the production of the final state AB . The four partons from the two protons could interact via a single hard process in both amplitude and conjugate. We shall refer to these processes as (4-parton)² processes since they probe two 4-parton matrix elements (we have four partons in each hadronic matrix element because there are two in the amplitude and two in the conjugate amplitude – note also that the parton fields in each matrix element are all evaluated at the same transverse position). Alternatively one could conceive of (2-parton) \times (4-parton) processes giving rise to AB (such as processes in which one parton from the first proton interacts with two partons from the other proton, in a single hard interaction in both amplitude and conjugate). There are also (3-parton) \times (3-parton) processes (these include the interference between DPS and SPS). If any of these processes are only power suppressed to the same extent that DPS is (i.e. by (Λ_{QCD}^2/Q^2)) then they should also be included in (1.72). This is because, at the cross section level, we cannot distinguish

SPS :



$$\sigma_A^S(s) = D_p^i(x_1) \otimes \sigma_{ij \rightarrow A}(\hat{s} = x_1 x_2 s) \otimes D_p^j(x_2)$$

DPS :



$$\sigma_{(A,B)}^D(s) = \Gamma_{ij}(x_1, x_2, \mathbf{b}) \otimes \sigma_{ik \rightarrow A}(\hat{s} = x_1 x_3 s) \otimes \sigma_{jl \rightarrow B}(\hat{s} = x_2 x_4 s) \otimes \Gamma_{kl}(x_3, x_4, \mathbf{b})$$

Figure 1.4: Schematic representations of Single and Double Parton Scattering in a proton-proton collision. The grey blobs are protons.

between the DPS process producing AB and other processes suppressed by (Λ_{QCD}^2/Q^2) – we should just include them all together in (1.72) as the lowest order power correction to $\sigma_{AB}(s)$. The $(4\text{-parton})^2$ process is suppressed by (Λ_{QCD}^4/Q^4) , so we can ignore it in (1.72). Also 3-parton matrix elements vanish for an unpolarised hadron [32, 33], so we do not need to worry about the $(3\text{-parton}) \times (3\text{-parton})$ processes. On the other hand, the $(2\text{-parton}) \times (4\text{-parton})$ processes are only power suppressed by (Λ_{QCD}^2/Q^2) , so should really be included in (1.72). We will return to this issue in Chapter 4.

In (1.72) we wrote the DPS cross section in terms of a mixed longitudinal momentum and transverse displacement representation for the 2pGPDs. However, it is also possible to write the cross section in terms of ‘ \mathbf{r} -space’ 2pGPDs that are a function of momentum arguments only [34–37]:

$$\begin{aligned} \sigma_{(A,B)}^D(s) = \frac{m}{2} \sum_{i,j,k,l} \int \prod_{a=1}^4 dx_a \hat{\sigma}_{ik \rightarrow A}(\hat{s} = x_1 x_3 s) \hat{\sigma}_{jl \rightarrow B}(\hat{s} = x_2 x_4 s) \\ \times \int \frac{d^2 \mathbf{r}}{(2\pi)^2} \Gamma_{ij}(x_1, x_2, \mathbf{r}; Q_A^2, Q_B^2) \Gamma_{kl}(x_3, x_4, -\mathbf{r}; Q_A^2, Q_B^2) \end{aligned} \quad (1.73)$$

The transverse momentum argument \mathbf{r} that appears in the 2pGPDs and is integrated

over in (1.73) is the transverse momentum imbalance of any one of the partons i, j, k, l between the amplitude contributing to the DPS cross section and the conjugate. In DPS, because two partons from each proton participate in independent hard interactions, we can have contributions from interference processes in transverse momentum space. Processes in which transverse momentum \mathbf{r} is transferred between partons from the same proton in going from amplitude to conjugate are permitted, provided that a transfer in the other direction occurs in the other proton. Only when equal and opposite momentum transfers occur in the two protons do all of the final state particles have the same momentum in amplitude and conjugate, as is required. A diagrammatic depiction of the transverse momentum structure of equation (1.73) is given in figure (1.5), that shows the transverse momentum interference between amplitude and conjugate.

The transverse momentum imbalance \mathbf{r} is the Fourier conjugate variable to the parton pair separation \mathbf{b} , such that the \mathbf{b} - and \mathbf{r} -space 2pGPDs are related by:

$$\Gamma_{ij}(x_1, x_2, \mathbf{r}) = \int d^2\mathbf{b} e^{i\mathbf{b}\cdot\mathbf{r}} \Gamma_{ij}(x_1, x_2, \mathbf{b}) \quad (1.74)$$

The DPS cross section involves a new nonperturbative object $\Gamma_{ij}(x_1, x_2, \mathbf{b})$ (or $\Gamma_{ij}(x_1, x_2, \mathbf{r})$) that so far has been constrained little by experiment. Therefore in past studies of DPS phenomenologists have applied a number of approximations to the 2pGPD, based on rough intuitive arguments, that relate the 2pGPD to the measured single PDFs and allow numerical predictions of DPS cross sections to be made. The first of these is to assume that $\Gamma_{ij}(x_1, x_2, \mathbf{b})$ can be approximately factorised into a product of a longitudinal and transverse pieces. The transverse piece is modelled as a smooth function with a width of the order of the radius of the proton, and is typically taken to be flavour and scale independent:

$$\Gamma_{ij}(x_1, x_2, \mathbf{b}; Q_A^2, Q_B^2) \simeq D_p^{ij}(x_1, x_2; Q_A^2, Q_B^2) F(\mathbf{b}) \quad (1.75)$$

This assumption is made to simplify the expression for the DPS cross section. If one introduces a quantity σ_{eff} (that has the dimensions of a cross section) via $\sigma_{eff} \equiv 1/[\int F(\mathbf{b})^2 d^2\mathbf{b}]$, then upon applying (1.75) one finds that one may write $\sigma_{(A,B)}^D$ entirely in terms of the longitudinal piece and σ_{eff} :

$$\begin{aligned} \sigma_{(A,B)}^D(s) = & \frac{m}{2} \frac{1}{\sigma_{eff}} \sum_{i,j,k,l} \int \prod_{a=1}^4 dx_a D_p^{ij}(x_1, x_2; Q_A^2, Q_B^2) D_p^{kl}(x_3, x_4; Q_A^2, Q_B^2) \\ & \times \hat{\sigma}_{ik \rightarrow A}(\hat{s} = x_1 x_3 s) \hat{\sigma}_{jl \rightarrow B}(\hat{s} = x_2 x_4 s) \end{aligned} \quad (1.76)$$

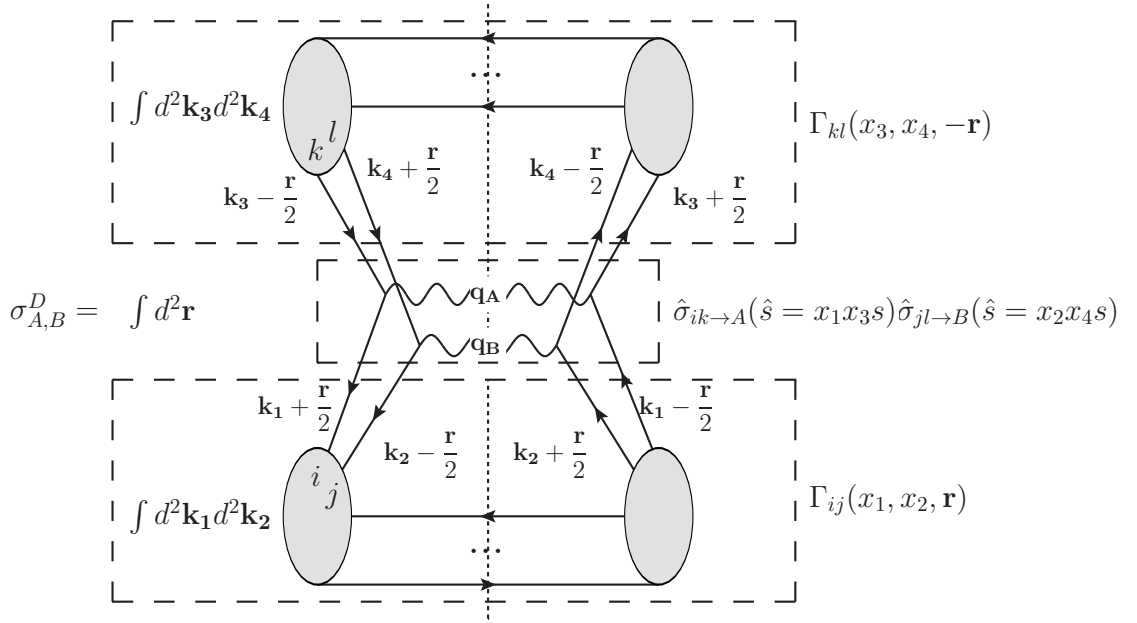


Figure 1.5: Transverse momentum integration structure in the DPS cross section formula (1.73). The part of the graph to the left of the cut (horizontal dashed line) corresponds to the amplitude, whilst that to the right corresponds to the amplitude conjugate. The integrals over the transverse momenta of i and j averaged between amplitude and conjugate, \mathbf{k}_1 and \mathbf{k}_2 , are contained in the definition of $\Gamma_{ij}(x_1, x_2, \mathbf{r})$. Similarly, the integrals over the average transverse momenta of k and l , \mathbf{k}_3 and \mathbf{k}_4 are contained within the definition of $\Gamma_{kl}(x_3, x_4, -\mathbf{r})$.

From the viewpoint of the naive parton model, a transverse profile which is essentially flat up to distance scales of the order of the proton radius, as in (1.76), appears reasonable. However, in Chapter 3 we shall see that in QCD the assumption (1.76) is a step too far.

The second approximation that is applied is to ignore correlations in x between the two partons and write $D_p^{ij}(x_1, x_2; Q_A^2, Q_B^2)$ as a product of two single PDFs:

$$D_p^{ij}(x_1, x_2; Q_A^2, Q_B^2) \simeq D_p^i(x_1; Q_A^2) D_p^j(x_2; Q_B^2) \quad (1.77)$$

It is argued that this is approximately valid at small x since there is a large population of partons at such x values that has arisen as a result of a large number of parton splittings – therefore it is likely that an individual pair of partons picked from this population will only be linked via a huge splitting chain that extends back to a much lower scale and higher x , and washes out any correlations in x between the partons. However, it is clear even from elementary considerations that (1.77) must be violated on some level. The relation (1.77) fails to take account of the fact that finding a quark of given flavour reduces the chances of finding another with the same flavour (this effect should be particularly important for the ‘valence’ quark distributions, since the number of such quarks is finite and small). It also fails to take proper account of the fact that $D_p^{ij}(x_1, x_2; Q_A^2, Q_B^2)$ should approach zero as one nears the kinematic limit $x_1 + x_2 = 1$ due to phase space effects (typically a crude cut-off or suppression factor is included on the right hand side of (1.77) to take account of this in an approximate way)⁴.

Inserting (1.77) into (1.76), one obtains a simple formula for $\sigma_{(A,B)}^D(s)$:

$$\sigma_{(A,B)}^D(s) = \frac{m}{2} \frac{\sigma_A^S(s) \sigma_B^S(s)}{\sigma_{eff}} \quad (1.78)$$

With the DPS cross section reduced to the form (1.78) numerical predictions of DPS cross sections are straightforward. One simply calculates two single scattering cross sections (using (1.71) and explicit forms for the PDFs from one of the fitting collaborations), multiplies them together, and divides them by a value for σ_{eff} . The value of σ_{eff} used should be of order R_p^2 , and in practice one uses an experimentally determined value extracted from the analysis of the DPS contribution to a particular process (e.g. the D0 collaboration obtained $\sigma_{eff} = 15.1$ mb from an analysis of DPS in $\gamma + 3j$ production [38], and the CDF collaboration obtained $\sigma_{eff} = 14.5$ mb from an analysis of the same pro-

⁴In more formal terms, the relation (1.77) fails to satisfy number and momentum sum rule constraints, the form of which we will write down in section 2.3.

cess [39, 40]).

There is some suggestion from the experimental analysis of the DPS contribution to $\gamma + 3$ jet production by the CDF collaboration that the approximation (1.77) may be approximately valid for sea partons at moderately small x . They investigated the x dependence of σ_{eff} , and found none over the x ranges accessible to them ($0.01 - 0.40$ for the subprocess producing $\gamma + j$, and $0.002 - 0.20$ for the subprocess producing $2j$) [40].

Even though (1.78) is only approximate, it exhibits some of the important qualitative features of DPS mentioned at the beginning of this section. From (1.78) we can see explicitly that DPS cross sections grow faster than SPS cross sections as s is increased at fixed Q^2 , since in (1.78) σ^D is proportional to the square of SPS cross sections. Further we see explicitly from (1.78) that the total DPS cross section is power suppressed with respect to the single cross section. Examination of (1.71) reveals that SPS cross sections go like $1/Q^2$ – then, using (1.78) and noting $1/\sigma_{eff}$ is $\mathcal{O}(\Lambda_{QCD}^2)$, we see:

$$\frac{\sigma^D}{\sigma^S} \propto \frac{\Lambda_{QCD}^2}{Q^2} \quad (1.79)$$

Although DPS is a power correction to SPS in terms of the total cross section, the fact that it comprises two independent hard scatterings rather than one means that it will populate the final state phase space in a different way to SPS, and this raises the possibility of a region of final state phase space in which the DPS contribution is comparable to the SPS contribution. To identify the relevant region let us consider the most naive description of the two processes using the parton model. In this model the transverse momentum of the partons participating in the hard interactions is restricted to values of order Λ_{QCD} . Then, all of the DPS events producing AB are concentrated in the region of final state phase space with $|\mathbf{q}_A|, |\mathbf{q}_B| \lesssim \Lambda_{QCD}$. On the other hand, in SPS events producing AB , only $|\mathbf{q}_A + \mathbf{q}_B|$ is restricted to values $\lesssim \Lambda_{QCD}$, and one expects that \mathbf{q}_A or \mathbf{q}_B , as the transverse momentum of a subset of particles produced in the hard scattering of scale Q , can range up to Q . If one considers the cross section for AB to be produced with $|\mathbf{q}_A|, |\mathbf{q}_B| \lesssim \Lambda_{QCD}$, then the parton model predicts that the DPS contribution will be $\sim \Lambda_{QCD}^2/Q^4$ (i.e. the full contribution), whilst the SPS contribution will be $\sim 1/Q^2 \times \Lambda_{QCD}^2/Q^2 \sim \Lambda_{QCD}^2/Q^4$ – that is, the two contributions are comparable in this region of small $|\mathbf{q}_A|, |\mathbf{q}_B|$.

One would of course expect there to be important corrections to this picture when including full QCD effects. For example, if the process under consideration was same

sign WW production, where the DPS contribution involves two independent $q\bar{q} \rightarrow W$ processes, then one would expect the \mathbf{q}_A and \mathbf{q}_B distributions for the DPS process to be peaked at a few GeV rather than close to zero due the effects of soft gluons in QCD [27]. However, there is still the general expectation that DPS events will be concentrated at small $\mathbf{q}_A^2, \mathbf{q}_B^2$ values $\ll Q_A^2, Q_B^2$ even in full QCD. In this region the DPS signal will be significant compared to the SPS background, and thus can potentially be measured experimentally. Every experimental extraction of DPS so far has used the fact that DPS events are concentrated at small $\mathbf{q}_A^2, \mathbf{q}_B^2 \ll Q_A^2, Q_B^2$ in order to extract the DPS signal – the AFS measurement of DPS in the $4j$ final state [41], the UA2 measurement of DPS in the $4j$ final state [42], the CDF measurements of DPS in the $4j$ [43] and $\gamma + 3j$ [39, 40] final state, the D0 measurement of DPS in the $\gamma + 3j$ final state [38], and most recently the ATLAS measurement of DPS in the $W + 2j$ final state [44].

In this brief introduction to DPS we have presented a naive treatment of the phenomenon based on intuitive arguments and approximations, that is nevertheless the treatment used in many phenomenological studies of DPS. An interesting and experimentally relevant question is how and to what extent the simple picture of this section is modified by perturbative QCD corrections. This subject forms the focus of the remainder of this thesis.

Note that in this thesis we will mainly focus on the description of the total cross section for DPS. Since the experimental extraction of DPS relies on the fact that the DPS cross section differential in the transverse momenta of A and B , \mathbf{q}_A and \mathbf{q}_B , is strongly peaked at small \mathbf{q}_A and \mathbf{q}_B , it is perhaps the DPS cross section differential in \mathbf{q}_A and \mathbf{q}_B rather than the total cross section that is more relevant for making experimentally testable predictions [34–37]. In the region of $\mathbf{q}_A, \mathbf{q}_B$ of interest (i.e. $\mathbf{q}_A^2, \mathbf{q}_B^2 \ll Q_A^2, Q_B^2$) this quantity is described in terms of transverse momentum dependent 2pGPDs (TMD 2pGPDs), rather than the collinear 2pGPDs appearing in (1.72), (1.73). On the other hand, it is expected that for $\Lambda^2 \ll \mathbf{q}_A^2, \mathbf{q}_B^2 \ll Q_A^2, Q_B^2$ the TMD 2pGPD should be expressible in terms of the collinear 2pGPD and a perturbatively calculable piece [36, 37]. In that case there is a ‘collinear part’ of the differential cross section whose structure closely resembles the total cross section formula (1.72), (1.73). Knowledge of how the total DPS cross section is to be treated should be helpful in establishing the correct way to treat this collinear part. It is with this ultimate purpose in mind that we continue to discuss only the total cross section for DPS in the remainder of the thesis.

In this thesis we attempt to describe DPS using a ‘hard scattering factorisation’ type

framework. This framework requires a large virtuality or momentum transfer in both of the scattering processes, but is valid in the full range of parton momentum transfers, with corrections suppressed by powers of Λ/Q . There is a complementary approach, based on the high energy limit and using BFKL methods – see for example [45]. The validity of the BFKL approach is restricted to the small x regime.

Chapter 2

Double PDFs and Double Parton Scattering

This chapter is based on the original research papers [46] and [47]. The work for the first of these was performed in collaboration with James Stirling, and the work for the second was performed in collaboration with Steve Kom, Anna Kulesza, and James Stirling.

2.1 Introduction

In the sequence of papers [4–6] a QCD framework for describing the proton-proton DPS cross section for the case in which the two hard scales are equal $Q_A = Q_B \equiv Q$ is proposed. This framework is a ‘hard scattering factorisation’ framework, since the cross section is written as a convolution of parton distributions and parton-level cross sections, as in (1.72). The starting point in the formulation of this framework is the assumption that the 2pGPD can, to a reasonably good approximation, be factorised into longitudinal and transverse pieces as in (1.75) [6]. Then, if we choose to normalise $F(\mathbf{b})$ according to $\int d^2\mathbf{b}F(\mathbf{b}) = 1$, we can identify the factorised longitudinal piece of the 2pGPD with the integral of the 2pGPD over \mathbf{b} . We shall refer to the latter quantity as the double parton distribution function, or dPDF. The equation dictating the leading order QCD scaling violations of the dPDF with the two scales set equal is derived in [5, 6] – we shall henceforth refer to this equation as the double DGLAP, or dDGLAP equation. In the framework of [4–6] (which we shall refer to as the ‘dPDF framework’, for obvious reasons), the LO DPS cross section with $Q_A = Q_B \equiv Q$ is calculated using the formula (1.76) with $Q_A = Q_B \equiv Q$, with the dPDFs $D_p^{ij}(x_1, x_2; Q^2, Q^2) \equiv D_p^{ij}(x_1, x_2; Q^2)$ in this formula

evolving according to the dDGLAP equation.

An important prediction of the dDGLAP equation is that, even if the dPDFs were to factorise into products of sPDFs at some scale Q_0 , then at *any* different scale the dPDFs would no longer be equal to a product of sPDFs. That is, evolution according to the dDGLAP equation induces correlations in x fraction between partons, and the dPDF framework predicts deviations from the naive formulae (1.77) and (1.78). Explicit numerical solutions of the LO ‘double DGLAP’ (dDGLAP) equation based on factorised inputs at $Q_0^2 \sim 1 \text{ GeV}^2$ suggest that the deviations may be significant, with deviations on the order of 10 – 30% at $x_1 = x_2 \sim 0.1, Q^2 \sim 10^4 \text{ GeV}^2$ [48, 49].

In this chapter, we document the development of an explicit set of LO equal scale dPDFs – the GS09 dPDFs – that can be used to make detailed numerical investigations of the deviations from (1.77) and (1.78) in the context of the dPDF framework. We begin by showing that the dPDFs must satisfy certain valence number and momentum sum rule constraints analogous to (1.65) and (1.66) for the sPDFs. These are used as a guide to construct ‘improved’ $Q = 1 \text{ GeV}$ input dPDFs starting with naive products of MSTW2008LO sPDFs at that scale as the basis (note that at $Q = 1 \text{ GeV}$ factorised products of sPDFs are not likely to be a very accurate approximation to the true dPDFs – on the other hand we are essentially forced to start with products of sPDFs in the construction of the input dPDFs, owing to the lack of any experimental or nonperturbative input). By including the sum rule constraints we ensure that the important momentum and valence number effects discussed in the paragraph below (1.77) are included in our dPDFs. The low scale inputs are then dDGLAP evolved to higher scales using a numerical algorithm we have written. The end result of this process is a set of LO dPDF grids covering the ranges $10^{-6} < x_1 < 1, 10^{-6} < x_2 < 1, 1 < Q^2 < 10^9 \text{ GeV}^2$, and all possibilities for the parton indices i and j . These grids, in addition to a simple interpolation subroutine designed to extract from the grids a dPDF value at a given x_1, x_2 and Q , can be found at Ref. [50].

Having constructed the GS09 dPDFs, we compare them with simple factorised forms, both directly and in terms of their respective predictions for the DPS contribution to same sign WW production, where both W bosons decay leptonically. We choose same sign WW as an interesting example process to study because it has traditionally been regarded as a rather clean channel to use to measure DPS, the ‘direct’ $WWjj$ SPS background having a low rate and containing two additional jets, which distinguish this background and allow one to cut it away (note that for same sign Ws , there is no ‘simple’ $q\bar{q}' \rightarrow WW$ production mechanism, as is allowed for opposite sign Ws , because the final state has

charge ± 2 and the initial state cannot possibly have this charge). In the discussion of the same sign WW process, we summarise some of the important findings of [47] with regard to SPS backgrounds to the process. In particular, we point out that there are additional SPS backgrounds that have not been previously considered (arising from other electroweak gauge boson pairs in the final state and heavy flavour), list the basic cuts introduced in [47] to minimise the impact of the backgrounds, and present results for the signal and background after cuts. We discuss the possibility of experimentally measuring the distinguishing features of the GS09 DPS signal in the presence of the backgrounds.

This chapter is organised as follows. We begin with a brief review of dPDFs and the dDGLAP equation in Section 2.2. The dPDF sum rules are introduced and discussed in Section 2.3, where we also explain how we have used these rules to construct input dPDFs at $Q_0 = 1$ GeV corresponding to the MSTW2008LO sPDF inputs. In Section 2.4, the numerical procedure designed to evolve the input distributions to higher scales using the LO dDGLAP equation and generate the GS09 grids is discussed in detail. Section 2.5 examines the ways in which our GS09 dPDFs differ from those obtained using previous approaches. The same-sign WW DPS signal obtained using GS09 is compared with that obtained using factorised forms in Section 2.6, and the SPS backgrounds to this process are discussed. Finally, we conclude with a summary of the chapter in Section 2.7.

2.2 Double PDFs and the Double DGLAP equation

The dPDF $D_p^{ij}(x_1, x_2; Q_A^2, Q_B^2)$ is defined to be the integral of the corresponding 2pGPD $\Gamma_{ij}(x_1, x_2, \mathbf{b}; Q_A^2, Q_B^2)$ over \mathbf{b} , with all UV divergences associated with the first parton regulated at scale Q_A^2 , and all those associated with the second parton regulated at scale Q_B^2 . The bare two quark dPDF (i.e. prior to renormalisation) has the following operator representation:

$$\begin{aligned}
D_{p(0)}^{q_1 q_2}(\xi_1, \xi_2) = & \langle P | 2p^+ \int \sum_{i=1}^2 \frac{dz_i^-}{2\pi} e^{i\xi_i z_i^- p^+} dy^- d^2 \mathbf{y} \\
& \times \bar{\psi}_{q_2, a(0)}(y - \tfrac{1}{2}z_2) \mathcal{G}_{ab}(y - \tfrac{1}{2}z_2, y + \tfrac{1}{2}z_2) \tfrac{1}{2} \gamma^+ \psi_{q_2, b(0)}(y + \tfrac{1}{2}z_2) \\
& \times \bar{\psi}_{q_1, c(0)}(-\tfrac{1}{2}z_1) \mathcal{G}_{cd}(-\tfrac{1}{2}z_1, \tfrac{1}{2}z_2) \tfrac{1}{2} \gamma^+ \psi_{q_1, d(0)}(\tfrac{1}{2}z_1) | P \rangle_c \Big|_{z_i^+ = y^+ = 0, \mathbf{z}_i = 0} \quad (2.1)
\end{aligned}$$

The bare quark-gluon and gluon-gluon dPDFs can be obtained from this expression by replacing an appropriate number of quark bilinears by the gluon bilinear $\frac{1}{\xi_i p^+} F_{A(0)}^{+j} \mathcal{G}_{AB} F_{B(0)}^{+j}$,

where the gluon bilinear should have the same position four-vector arguments as the replaced quark bilinear, and the index i should be the same as that found in the position arguments.

In this chapter we predominantly focus on the equal-scale dPDF, which is the dPDF with Q_A^2 and Q_B^2 both set to the common value of Q^2 . This is primarily for reasons of simplicity, although there are several processes at the LHC that directly probe the equal-scale dPDFs under the dPDF framework (for example the same sign WW DPS process studied in section 2.6). In the equal-scale dPDF all UV divergences in the bare quantity are subtracted at the single scale Q^2 . For convenience, we shall henceforth in this chapter use the term ‘dPDF’ to mean equal-scale dPDF, and where we need to refer to the more general object $D_p^{ij}(x_1, x_2; Q_A^2, Q_B^2)$, we will call this the ‘unequal scale dPDF’. We will discuss how the unequal scale dPDFs should be calculated at the end of this section.

The double DGLAP, or dDGLAP equation, is a renormalisation group equation dictating the change of the dPDFs $D_p^{ij}(x_1, x_2; Q^2)$ with the hard scale Q^2 . It is analogous to the (single) DGLAP (sDGLAP) equation (1.58) for sPDFs. The dDGLAP equation has been derived to leading order (really leading logarithmic order, or LLA) in [4, 5]. Just as in the case of the sDGLAP equation, the leading order dDGLAP equation resums leading powers of $[\alpha_s \log(Q^2)]^n$ generated by parton branching processes strongly ordered in k_T .

Introducing the variable $t \equiv \log(Q^2)$, the LLA form of the dDGLAP equation is [4, 5]:

$$\begin{aligned} \frac{dD_p^{j_1 j_2}(x_1, x_2; t)}{dt} = & \frac{\alpha_s(t)}{2\pi} \left[\sum_{j'_1} \int_{x_1}^{1-x_2} \frac{dx'_1}{x'_1} D_p^{j'_1 j_2}(x'_1, x_2; t) P_{j'_1 \rightarrow j_1} \left(\frac{x_1}{x'_1} \right) \right. \\ & + \sum_{j'_2} \int_{x_2}^{1-x_1} \frac{dx'_2}{x'_2} D_p^{j_1 j'_2}(x_1, x'_2; t) P_{j'_2 \rightarrow j_2} \left(\frac{x_2}{x'_2} \right) \\ & \left. + \sum_{j'} D_p^{j'}(x_1 + x_2; t) \frac{1}{x_1 + x_2} P_{j' \rightarrow j_1 j_2} \left(\frac{x_1}{x_1 + x_2} \right) \right] \quad (2.2) \end{aligned}$$

Recall that the argument t in the above is the factorisation scale (which in practical calculations is typically set equal to the characteristic hard scale of the subprocesses). The renormalisation scale has been set equal to the factorisation scale to obtain this equation (as is conventional in a leading order analysis).

In addition to the dPDFs and sPDFs $D_p^j(x; t)$, the equation (2.2) contains two different types of splitting functions. The first are the well-known splitting functions $P_{i \rightarrow j}(x)$, whose leading order forms are given in (1.59). At this order, the function $P_{i \rightarrow j}(x)$ may be

interpreted as the probability of a parton i splitting to give a parton j with a fraction x of the longitudinal momentum of the parent parton and a transverse momentum squared much smaller than Q^2 (where $t \equiv \ln(Q^2)$) [51]. The second, the $P_{i \rightarrow jk}(x)$, are new. They may be interpreted at LO as the probability of a parton i splitting to give the two partons j and k , the first of which has a fraction x of the linear momentum of the parent parton, the second of which has the remainder of the linear momentum $1 - x$, and both of which have transverse momentum squared much less than Q^2 . We shall refer to the splitting function $P_{i \rightarrow j}(x)$ as the $1 \rightarrow 1$ splitting function and the novel splitting function $P_{i \rightarrow jk}(x)$ as the $1 \rightarrow 2$ splitting function, for obvious reasons.

The splitting functions $P_{i \rightarrow i}(x)$ each possess a large negative contribution at $x = 1$ (these are contained within the ‘plus prescription’ functions together with explicit delta functions in the definitions). This contribution is included to take account of the fact that splittings of the parton i into other partons with lower momentum act to reduce the population of partons with the original momentum. At the level of Feynman diagrams, the contributions at $x = 1$ result from virtual gluon radiation diagrams in axial gauge.

On the other hand, the $1 \rightarrow 2$ splitting functions do not contain such contributions. This is to be expected as a virtual process is clearly not able to achieve the $1 \rightarrow 2$ splitting $i \rightarrow jk$. At LO, the function $P_{i \rightarrow jk}(x)$ is related to the ‘real splitting’ part¹ of the normal splitting functions $P_{i \rightarrow j}^R(x)$ according to²:

$$P_{i \rightarrow j}^R(x) = \sum_k P_{i \rightarrow jk}(x) \quad (2.5)$$

A further simplification to (2.5) is possible at LO. Due to the fact that QCD only allows

¹The functions $P_{i \rightarrow j}^R(x)$ are obtained from the functions $P_{i \rightarrow j}(x)$ by dropping the terms proportional to $\delta(1 - x)$. This includes removing plus prescription + signs where they appear.

²One might expect that (2.5) could be generalised to higher orders. Say that we expand the ‘all-order’ $1 \rightarrow 2$ splitting function in terms of powers of α_s :

$$P_{i \rightarrow jk}(x_1, x_2) = \delta(1 - x_1 - x_2) P_{i \rightarrow jk}^{(0)}(x_1) + \frac{\alpha_s}{2\pi} P_{i \rightarrow jk}^{(1)}(x_1, x_2) + \dots \quad (2.3)$$

This splitting function has two x arguments, since at NLO and above j and k do not necessarily share all of the momentum of i , so specifying the momentum fraction of j does not fix that of k (one consequence of this is that the form of the final term on the right hand side of (2.2) has to be modified at NLO and above). Then one might expect that the generalisation of (2.5) to higher orders is:

$$P_{i \rightarrow j}^{(n)}(x_1) = \sum_k \int_0^{1-x_1} dx_2 P_{i \rightarrow jk}^{(n)}(x_1, x_2) \quad (2.4)$$

However, (2.4) does not hold beyond leading order. This is because on the left hand side of this

certain types of three particle vertices (i.e. triple gluon vertices and ‘gluon emission from a quark’ type vertices), the LO $P_{i \rightarrow jk}(x)$ is only nonzero for a small number of $\{i, j, k\}$ combinations. In fact, given i and j , there exists at most one choice for k which makes $P_{i \rightarrow jk}(x)$ nonzero. We shall denote this special value of k by $\kappa(i, j)$. For example, $\kappa(i, j)$ is g when $i = q_i, j = q_i$, and \bar{q}_i when $i = g, j = q_i$.

Given this fact, we note that (2.5) must contain at most only one term on the right hand side, and we may write:

$$P_{i \rightarrow j}^R(x) = P_{i \rightarrow j\kappa(i, j)}(x) \quad (2.6)$$

In (2.6), we have extended the definition of $\kappa(i, j)$ to cases where there exists no choice for k to make $P_{i \rightarrow jk}(x)$ nonzero. In these cases, $\kappa(i, j)$ can be chosen to be any parton, as both the right and left hand sides are zero for any choice.

Equation (2.6) effectively defines $P_{i \rightarrow jk}$ for all cases in which it is nonzero. At LO then, we may construct the following definition for $P_{i \rightarrow jk}$:

$$P_{i \rightarrow jk}(x) = \begin{cases} P_{i \rightarrow j}^R(x) & \text{if } k = \kappa(i, j) \\ 0 & \text{otherwise} \end{cases} \quad (2.7)$$

One can interpret the terms on the right-hand side of (2.2) using the parton branching picture.³ Consider the inclusive probability of finding a pair of partons in the proton with flavours j_1 and j_2 and longitudinal momentum fractions between x_1 and $x_1 + \delta x_1$ and x_2 and $x_2 + \delta x_2$ respectively at scale t , $D_p^{j_1 j_2}(x_1, x_2; t) \delta x_1 \delta x_2$. When t is increased to $t + \Delta t$, there are two main types of process that can contribute to the change in this quantity. First, there are ‘independent branching processes’. In these, one starts off with a pair of partons, one of which has the appropriate x and flavour, and the other of which splits, either giving rise to the other parton of the appropriate x and flavour, or removing it. Second, there is a ‘single parton feed’ process. In this, one starts off with a single parton

equation, all of the partons that accompany j and are implicitly summed over are timelike, whereas on the right hand side, one of the partons that accompanies j and is summed over is spacelike (i.e. parton k). This is important at NLO and above and leads to discrepancies between the right and left hand sides of (2.4). For the same reasons, one cannot obtain the $1 \rightarrow 2$ splitting functions at NLO by taking the calculation of the $1 \rightarrow 1$ NLO splitting functions and ‘undoing’ one of the x integrations, or by equating them to the analogous quantities that appear in the evolution of the fracture functions (the latter approach is advocated in [52]).

³We use similar arguments as are used in Section 5.2 of [53] to explain the terms on the right hand side of the sDGLAP equation.

with momentum fraction $x_1 + x_2$, and this splits into a pair with the appropriate x values and flavours.

There are four ‘independent branching’ splitting processes. Two of these involve splittings from higher-momentum partons, and give rise to $j_1 j_2$ pairs with the correct momentum (i.e. act to increase $D_p^{j_1 j_2}(x_1, x_2; t)$). The other two involve splittings within the $j_1 j_2$ pair, and reduce the number of $j_1 j_2$ pairs with the correct momentum (i.e. act to reduce $D_p^{j_1 j_2}(x_1, x_2; t)$). The four processes are depicted in figure (2.1). It is clear from the figure that the four processes correspond to the first two sets of terms on the right hand side of (2.2), with the ‘real emission’ parts of these terms corresponding to the branching processes increasing $D_p^{j_1 j_2}(x_1, x_2; t)$, and the ‘virtual correction’ parts of the terms corresponding to the branching processes decreasing $D_p^{j_1 j_2}(x_1, x_2; t)$. We have added suitable labels to figure (2.1) to bring out this correspondence.

There is only one ‘single parton feed’ process, which we have drawn in figure 2.2. This process always acts to increase $D_p^{j_1 j_2}(x_1, x_2; t)$, and corresponds to the final set of terms on the right hand side of (2.2). We see that this set of terms contains sPDFs because it corresponds to a diagram in which a *single* parton splits to give the pair $j_1 j_2$. Also, there are no integrals in these terms because of the property of LO QCD that a single splitting can only give rise to two partons. Thus the single parton that splits is essentially restricted to have momentum exactly equal to $x_1 + x_2$. We shall hereafter refer to the last set of terms on the right hand side of (2.2) as the ‘sPDF feed’ terms, for obvious reasons.

It is interesting to consider the generalisation of (2.2) to higher orders. It should be reasonably clear from our ‘parton branching’ picture of the dDGLAP equation that at $N^n\text{LO}$ ($n \geq 1$), the independent branching terms have the same structure, with the only alteration being the replacement of the LO $1 \rightarrow 1$ splitting functions with their $N^n\text{LO}$ generalisations. On the other hand, at $N^n\text{LO}$ the $1 \rightarrow 2$ splitting functions become functions of two variables, and the structure of the ‘sPDF feed’ term has to be modified such that it includes an integral over the momentum of the parent parton:

$$\left. \frac{dD_p^{j_1 j_2}(x_1, x_2; t)}{dt} \right|_{\text{sPDF feed}} = \sum_{j'} \int_{x_1+x_2}^1 \frac{dx'}{x'^2} D_p^{j'}(x'; t) P_{j' \rightarrow j_1 j_2} \left(\frac{x_1}{x'}, \frac{x_2}{x'} \right) \quad (2.8)$$

The reason for this is that an $\mathcal{O}(\alpha_s^{n+1})$, $n \geq 1$ splitting vertex can produce more than two partons. At $N^n\text{LO}$ it will no longer be the case that the momentum of the second daughter parton is entirely fixed by the momentum of the first parton and that of the parent, and we need two x arguments in $P_{j' \rightarrow j_1 j_2}$. The expansion of the more general

$$\Delta_{indep} \left[D_h^{j_1 j_2} (x_1, x_2; t) \delta x_1 \delta x_2 \right]$$

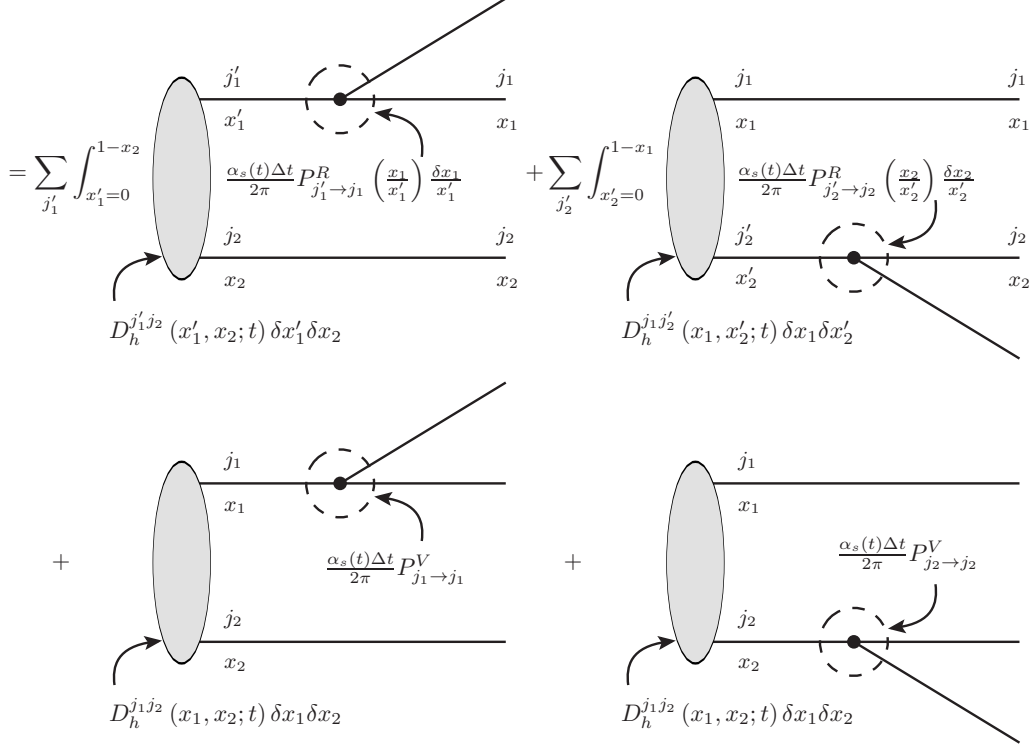


Figure 2.1: Independent branching processes leading to changes in the dPDF when the scale is increased from t to $t + \Delta t$. $P_{i \rightarrow j}^R(x)$ is the ‘real splitting’ part of the splitting function $P_{i \rightarrow j}(x)$ – i.e. the splitting function minus the terms proportional to $\delta(1 - x)$. $P_{j \rightarrow j}^V$ is equal to the sum of the coefficients of the $\delta(1 - x)$ terms in the splitting function $P_{j \rightarrow j}(x)$ (including $\delta(1 - x)$ terms contained within plus prescription functions).

$$\Delta_{feed} \left[D_h^{j_1 j_2} (x_1, x_2; t) \delta x_1 \delta x_2 \right]$$

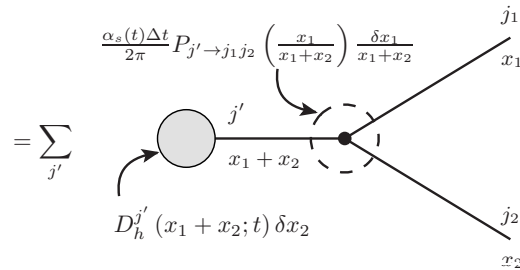


Figure 2.2: Single parton feed process leading to changes in the dPDF when the scale is increased from t to $t + \Delta t$.

function $P_{i \rightarrow jk}(x_1, x_2)$ in terms of powers of α_s reads as follows:

$$P_{i \rightarrow jk}(x_1, x_2) = \delta(1 - x_1 - x_2)P_{i \rightarrow jk}^{(0)}(x_1) + \frac{\alpha_s}{2\pi}P_{i \rightarrow jk}^{(1)}(x_1, x_2) + \dots \quad (2.9)$$

It is worth pointing out that the higher-order coefficients in this expansion cannot be obtained trivially from the higher-order coefficients of the $1 \rightarrow 1$ splitting function $P_{i \rightarrow j}(x)$ as in the LO case.

A solution to (2.2) in terms of sPDFs is obtained in [4, 54], and presented for the first time in x -space in [6]. Let us introduce the ‘natural’ evolution variable τ defined in terms of t according to:

$$\begin{aligned} \tau &= \int_{t_0}^t dt' \frac{\alpha_s(t')}{2\pi} \\ &= \frac{1}{2\pi b} \ln \left[\frac{t - \ln(\Lambda_{QCD}^2)}{t_0 - \ln(\Lambda_{QCD}^2)} \right] \text{ at LO} \end{aligned} \quad (2.10)$$

In terms of the variable τ , the solution to the dDGLAP equation reads:

$$\begin{aligned} D_p^{j_1 j_2}(x_1, x_2; \tau) &= D_{h(corr)}^{j_1 j_2}(x_1, x_2; \tau) \\ &+ \sum_{j'_1 j'_2} \int_{x_1}^{1-x_2} \frac{dz_1}{z_1} \int_{x_2}^{1-z_1} \frac{dz_2}{z_2} D_p^{j'_1 j'_2}(z_1, z_2; \tau=0) \\ &\times D_{j'_1}^{j_1} \left(\frac{x_1}{z_1}; \tau \right) D_{j'_2}^{j_2} \left(\frac{x_2}{z_2}; \tau \right) \end{aligned} \quad (2.11)$$

where:

$$\begin{aligned} D_{p(corr)}^{j_1 j_2}(x_1, x_2; \tau) &= \sum_{j'_1 j'_2} \int_0^\tau d\tau' \int_{x_1}^{1-x_2} \frac{dz_1}{z_1} \int_{x_2}^{1-z_1} \frac{dz_2}{z_2} D_p^{j'_1 j'_2}(z_1 + z_2; \tau') \\ &\times \frac{1}{z_1 + z_2} P_{j' \rightarrow j'_1 j'_2} \left(\frac{z_1}{z_1 + z_2} \right) D_{j'_1}^{j_1} \left(\frac{x_1}{z_1}; \tau, \tau' \right) D_{j'_2}^{j_2} \left(\frac{x_2}{z_2}; \tau, \tau' \right) \end{aligned} \quad (2.12)$$

The Green’s functions $D_i^j(x; \tau, \tau')$ are defined such that they satisfy the initial conditions $D_i^j(x; \tau', \tau') = \delta_{ij}\delta(1-x)$ and change with τ according to the sDGLAP equation:

$$\frac{dD_i^j(x; \tau, \tau')}{d\tau} = \sum_{j'} \int_x^1 \frac{dz}{z} D_i^{j'}(z; \tau, \tau') P_{j' \rightarrow j}(x/z) \quad (2.13)$$

In effect, the function $D_i^j(x; \tau, \tau')$ gives the inclusive probability that one finds a parton j with longitudinal momentum fraction x at scale τ inside an object that looks like a pure i parton at the scale τ' .

A pictorial representation of the solution (2.11) in terms of parton branching is given in Fig. 2.3. One observes the need to specify some initial conditions $D_p^{j_1 j_2}(x_1, x_2; \tau = 0)$ to obtain the distributions at higher scale, which is a direct reflection of the fact that the dDGLAP equation can only predict changes in the distributions with τ .

The depiction of dDGLAP evolution as in Fig. 2.3 leads us to make a suggestion as to how one might calculate the unequal scale double PDFs, $D_p^{ij}(x_1, x_2; \tau_1, \tau_2)$ (indeed, one might argue that it is the only plausible option). The arguments τ_1 and τ_2 in this distribution correspond to the factorisation scales for parton i and j respectively. Consider the analogous figure to Fig. 2.3 for these distributions. It seems likely that this figure would be the same, except with τ_1 replacing τ on the ‘upper legs’ of the diagrams, τ_2 replacing τ on the ‘lower legs’ of the diagrams, and the upper limit of the τ' integration replaced by $\min(\tau_1, \tau_2)$. If this ansatz is correct, the double distributions $D_p^{ij}(x_1, x_2; \tau_1, \tau_2)$ with (say) $\tau_1 < \tau_2$ should be calculated by taking the dPDFs with $\tau = \tau_1$, and then performing sDGLAP evolution at each x_1 from τ_1 to τ_2 in the x_2 variable. The upper limit in the sDGLAP evolution at given x_1 should be $1 - x_1$.

$$\begin{aligned}
& D_h^{j_1 j_2}(x_1, x_2; \tau) \delta x_1 \delta x_2 \\
&= \sum_{j', j'_1, j'_2} \int_{\tau'=0}^{\tau} \int_{z_1=x_1}^{1-x_2} \int_{z_2=x_2}^{1-z_1} \Delta \tau P_{j' \rightarrow j'_1 j'_2} \left(\frac{z_1}{z_1+z_2} \right) \frac{\delta z_1}{z_1+z_2} \\
&\quad \times \left[D_h^{j'_1} \left(\frac{x_1}{z_1}; \tau - \tau' \right) \frac{\delta x_1}{z_1} \right. \\
&\quad \left. D_h^{j'_2} \left(\frac{x_2}{z_2}; \tau - \tau' \right) \frac{\delta x_2}{z_2} \right] \\
&\quad + \sum_{j'_1, j'_2} \int_{z_1=x_1}^{1-x_2} \int_{z_2=x_2}^{1-z_1} D_h^{j'_1 j'_2}(z_1, z_2; 0) \delta z_1 \delta z_2 \\
&\quad \times \left[D_h^{j'_1} \left(\frac{x_1}{z_1}; \tau \right) \frac{\delta x_1}{z_1} \right. \\
&\quad \left. D_h^{j'_2} \left(\frac{x_2}{z_2}; \tau \right) \frac{\delta x_2}{z_2} \right]
\end{aligned}$$

Figure 2.3: A schematic representation of the solution of the dDGLAP equation (2.11) in terms of the parton branching picture.

2.3 The Double Parton Sum Rules and the Initial Distributions

2.3.1 The Double Parton Sum Rules

It is well known that the sPDFs satisfy two types of sum rule, (1.65) and (1.66), which represent the fact that both valence quark number and momentum should be conserved under evolution. One might wonder whether corresponding rules exist for the dPDFs. In Appendix C we give an all-order proof that the dPDFs satisfy the following constraints at all scales:

Momentum Sum Rule:

Let M be the momentum fraction carried by the proton ($= 1$). Then:

$$\sum_{j_1} \int_0^{1-x_2} dx_1 x_1 D_p^{j_1 j_2}(x_1, x_2; t) = (M - x_2) D_p^{j_2}(x_2; t) \quad (2.14)$$

Number Sum Rule:

Let $j_{1v} \equiv j_1 - \bar{j}_1$ ($j_1 \neq g$), and $N_{j_{1v}}$ be the number of ‘valence’ j_1 quarks in the proton. Then:

$$\int_0^{1-x_2} dx_1 D_p^{j_{1v} j_2}(x_1, x_2; t) = \begin{cases} N_{j_{1v}} D_p^{j_2}(x_2; t) & \text{when } j_2 \neq j_1 \text{ or } \bar{j}_1 \\ (N_{j_{1v}} - 1) D_p^{j_2}(x_2; t) & \text{when } j_2 = j_1 \\ (N_{j_{1v}} + 1) D_p^{j_2}(x_2; t) & \text{when } j_2 = \bar{j}_1 \end{cases} \quad (2.15)$$

The only nontrivial inputs to this proof are the following relations, which must be obeyed by the splitting functions in order that the number and momentum integrals are conserved for the sPDFs:

$$\sum_j \int_0^1 dx_1 x_1 P_{j' \rightarrow j}(x_1) = 0; \quad \int_0^1 dx_1 P_{j' \rightarrow j_v}(x_1) = 0 \quad (2.16)$$

Given that the dPDFs must obey the constraints (2.14) and (2.15) at all scales, the dDGLAP equation must have the property that it preserves the equalities (2.14) and (2.15) if they hold at the initial scale t_0 . We have also proved this less general statement, but we do not present the proof here, since it is straightforward and rather lengthy.

By appropriately combining equations (2.14) and (2.15) with the sPDF momentum and number sum rules, one can construct integrals over both arguments of the dPDFs which give conserved quantities such as M or N_{j_v} (or products of these quantities). Examples of such integrals are given below:

$$\sum_{j_1 j_2} \int_0^1 dx_2 \int_0^{1-x_2} dx_1 \frac{x_1 x_2}{M - x_2} D_p^{j_1 j_2}(x_1, x_2; t) = M = 1 \quad (2.17)$$

$$\int_0^1 dx_2 \int_0^{1-x_2} dx_1 \frac{D_p^{j_{1v} j_1}(x_1, x_2; t)}{N_{j_{1v}} - 1} - \frac{D_p^{j_{1v} \bar{j}_1}(x_1, x_2; t)}{N_{j_{1v}} + 1} = N_{j_{1v}} \quad (2.18)$$

These relations are preserved under dDGLAP evolution. By contrast, integrals such as $\sum_{j_1 j_2} \int_0^1 dx_2 \int_0^{1-x_2} dx_1 x_1 x_2 D_p^{j_1 j_2}(x_1, x_2; t)$ and $\int_0^1 dx_2 \int_0^{1-x_2} dx_1 D_p^{j_{1v} j_{1v}}(x_1, x_2; t)$, which one might naively think should give conserved momenta or valence quark numbers, are not conserved by dDGLAP evolution and so do not correspond to such physical quantities.

An appealing interpretation of (2.14) and (2.15) exists in terms of probability theory (although such a picture has in no way been used to obtain these relations). The dPDF sum rules are analogous to the result in probability theory that for two continuous random variables X and Y , the probability density functions relating to X and Y must satisfy ⁴:

$$\int dx x^a f(X = x \cap Y = y) = E(X^a | Y = y) f(Y = y) \quad (2.19)$$

The integral is performed over all values that X can take given that $Y = y$, and $E(X^a | Y = y)$ is the expectation value of X^a given that Y has value y . All of the prefactors on the right hand sides of Eqns. (2.14) and (2.15) are essentially conditional expectations as in (2.19). The $(1 - x_2)$ factor on the right hand side of (2.14) is the conditional expectation value for the momentum of all of the other partons in the proton given that one has found a parton of longitudinal momentum fraction x_2 . The $(N_{j_{1v}} - 1)$ factor for the $j_2 = j_1$ case of (2.15) is the conditional expectation for the number of j_1 partons minus the number of \bar{j}_1 partons elsewhere in the proton, given that one has found a parton of flavour j_1 . The prefactors for the other number sum rule cases may be

⁴One should bear in mind that the correspondence between (2.19) and (2.14)/(2.15) is not completely straightforward, as the parton density functions are not really simple probabilities. Rather, they may be better interpreted as number distributions. This results in, for example, the sPDFs being normalised to the number of partons of the given type in the proton rather than 1. Of course an analogous relation to (2.19) exists for such distributions.

interpreted as conditional expectation values using similar logic.

It is notable that the complete set of dPDF sum rules, (2.14) and (2.15), do not appear anywhere in the extant literature, although similar sum rules have been derived for the two-particle fragmentation functions in [55]. An early paper on the subject, [56] (see also [57]), introduces some ‘constraints’ resembling the number sum rules, which are used as an aid in constructing some simple model dPDFs. However, the constraints are only imposed for two specific dPDF cases, and the paper does not make any explicit statement about the general form of the number sum rule. In particular, they do not describe the subtleties of the number sum rule with regard to the different possible proportionality constants on the right hand side of (2.15).

In some sense, the dPDF sum rules are more restrictive than their sPDF counterparts. The sPDF sum rules state that the quantities $M \equiv \sum_i \int_0^1 dx x D_p^i(x; t)$ and $N_{i_v} \equiv \int_0^1 dx D_p^{i_v}(x; t)$ are conserved under evolution whatever their initial values, and we make the physical choices $M = 1, N_{u_v} = 2, N_{d_v} = 1$ for the proton. On the other hand, Eqns. (2.14) and (2.15) are only preserved under evolution if they hold at the starting scale. This is linked to the fact that one initially has the freedom in the sum rules to specify the momentum/parton composition of the hadron M and N_{i_v} (although $M \neq 1$ is not very physical). However, once these have been specified in the sPDF sector, the structure of the multiparton sum rules is effectively fixed.

The restrictive nature of the dPDF sum rules can be used to place nontrivial constraints on the input distributions that are physically allowable in the dDGLAP equation. Given that the dPDF sum rules should hold at the starting scale, we can use the constraints provided by the rules to improve on the factorised inputs previously used at the starting scale $Q_0^2 \sim 1 \text{ GeV}^2$. This is discussed in the next section.

2.3.2 Use of the Double Parton Sum Rules to improve the Input Distributions

As was mentioned in Section 1.4, it is a common assumption that the input double distributions should be equal to the product of the relevant sPDFs at low x_1 and x_2 . The logic behind this is that there exist large populations of partons of all active flavour types and x values at low x . Given these large populations, we would expect the extraction of a parton with a given flavour type j_1 and small longitudinal momentum x_1 not to have a strong effect on the probability of finding another parton of flavour j_2 (where j_2 can be equal to j_1) and small longitudinal momentum x_2 . This leads to a joint probability

dPDF Type	Relevant Sum Rules
Valence-Valence	Number (involved in two rules)
Valence-Sum	Number + Momentum
Valence-Tensor	Number
Tensor-Tensor	None
Tensor-Sum	Momentum
Sum-Sum	Momentum (involved in two rules)

Table 2.1: The different dPDF classes under the ‘double evolution’ representation of the dPDFs, and the types of sum rules each is engaged in.

distribution which can be expressed as a product of single distributions at low x_1, x_2 .

This factorisation assumption appears to be backed up by the available CDF and D0 data, as mentioned in section 1.4. Consequently, we would like our improved input dPDFs to maintain a factorised form for low x_1, x_2 , whilst now obeying the sum rules (2.14) and (2.15). The first question to be addressed in this section is whether this is in fact possible for all the dPDFs, i.e. whether the sum rules are compatible with factorisation at low x_1, x_2 in all cases.

To help answer this question, we introduce the ‘double evolution’ representation for the dPDFs. In this representation, the well-known {singlet,gluon,valence,tensor} / $\{\Sigma, g, V_i, T_i\}$ combinations (defined in equation (1.63)) are used as the flavour basis for both parton indices in the dPDF. The relationship between this basis and the ‘double human’ basis in which both parton indices i, j are one of g, u, \bar{u} etc. can be clarified using an example:

$$\begin{aligned}
D_p^{T_3 u_v} &= D_p^{(u+\bar{u}-d-\bar{d})(u-\bar{u})} \\
&= D_p^{uu} + D_p^{\bar{u}u} - D_p^{du} - D_p^{\bar{d}u} - D_p^{u\bar{u}} - D_p^{\bar{u}\bar{u}} + D_p^{d\bar{u}} + D_p^{\bar{d}\bar{u}}
\end{aligned} \tag{2.20}$$

The longitudinal momentum arguments of each term in this equation are the same. The use of the ‘double evolution’ representation has the advantage that it splits the dPDFs into six sets, each of which must satisfy different combinations of the sum rules. We refer to the singlet and gluon combinations as the ‘sum’ combinations (as they describe the sum of quark and gluon contributions respectively). Since $\sum j = \Sigma + g$, any dPDF with a ‘sum’ flavour index will be involved in a momentum sum rule, whilst any dPDF with a ‘valence’ flavour index will be involved in a number sum rule. Those dPDFs where each of the indices are one out of the ‘sum’ and ‘valence’ combinations will be involved in two sum rules.

The six sets of dPDFs along with the combinations of sum rules each is involved in are given in Table 2.1. We do not write out the explicit forms of the sum rules under the double evolution basis in this table. To obtain each rule, one must first construct the appropriate integral (i.e. $\int dx_1 x_1 [D_p^{\Sigma k}(x_1, x_2) + D_p^{gk}(x_1, x_2)]$ for a momentum sum rule or $\int dx_1 x_1 D_p^{i_v k}(x_1, x_2)$ for a number sum rule, where k can be any double evolution basis index). The sum rule is then obtained by expanding each dPDF in the integral in terms of human basis dPDFs (as in (2.20)), followed by the use of equations (2.14) and (2.15). We illustrate this procedure for the case of the $u_v T_3$ number sum rule:

$$\begin{aligned}
\int_0^{1-x_1} dx_2 D_p^{T_3 u_v}(x_1, x_2) &= \int_0^{1-x_1} dx_2 \left[D_p^{u u_v}(x_1, x_2) + D_p^{\bar{u} u_v}(x_1, x_2) \right. \\
&\quad \left. - D_p^{d u_v}(x_1, x_2) - D_p^{\bar{d} u_v}(x_1, x_2) \right] \\
&= (N_{u_v} - 1) D_p^u(x_1) + (N_{u_v} + 1) D_p^{\bar{u}}(x_1) \\
&\quad - N_{u_v} D_p^d(x_1) - N_{u_v} D_p^{\bar{d}}(x_1) \\
&= N_{u_v} D_p^{T_3}(x_1) - D_p^{u_v}(x_1)
\end{aligned} \tag{2.21}$$

If one investigates the classes of dPDF and their respective sum rules, one finds that in most cases dPDFs which satisfy the sum rules and are approximately equal to the product of single distributions at low x_1 and x_2 are allowed. There is however a type of dPDF for which these two requirements cannot be simultaneously satisfied – the dPDF with two of the same valence combinations as its flavour indices (e.g. $D_p^{u_v u_v}$).

The number sum rule that this type of dPDF must satisfy reads:

$$\int_0^{1-x_2} dx_1 D_p^{j_v j_v}(x_1, x_2; t_0) = N_{j_v} D_p^{j_v}(x_2; t_0) - D_p^{j_v \bar{j}}(x_2; t_0) \tag{2.22}$$

Consider this equation for small x_2 . Assuming no pathological behaviour of the function $D_p^{j_v j_v}(x_1, x_2; t_0)$ near the kinematical bound $x_1 + x_2 = 1$, the integral on the left hand side of (2.22) is dominated by contributions from the small x_1 region where $D_p^{j_v j_v}(x_1, x_2; t_0)$ is largest. A factorised form for $D_p^{j_v j_v}(x_1, x_2; t_0)$ at small x_1, x_2 would then result in the left hand side behaving like $x_2^{-a_v}$ (where x^{-a_v} is the small x behaviour of a typical valence sPDF).

On the other hand, the right hand side of (2.22) is dominated by the $-D_p^{j_v \bar{j}}(x_2; t_0)$ term. This is due to the fact that this term receives contributions from the sea, and sea sPDFs diverge faster than valence sPDFs at low x . We expect $-D_p^{j_v \bar{j}}(x_2)$ to behave like

$-x_2^{-a_s}$ (where a typical sea sPDF behaves like x^{-a_s} at low x). The right hand side then behaves very differently⁵ from the left hand side, and it is impossible to satisfy the sum rule (2.22) using a dPDF that factorises at low x_1, x_2 .

We conclude that we must abandon the possibility of factorisation into a product of sPDFs at low x_1, x_2 for the $D_p^{j_v j_v}(x_1, x_2; t_0)$. The fundamental origin of the second term on the right hand side of (2.22) which precludes the possibility of a factorised form for $D_p^{j_v j_v}(x_1, x_2; t_0)$ is of course in number effects. By ‘number effects’ we mean the fact that finding a parton of a given type alters the probability of finding a further parton of the same type, due to the fact that the number of that parton has decreased.

The CDF and D0 results are not in contradiction with the above conclusion, since in these experiments the vast majority of double parton scatterings observed would have been initiated by gluons and sea quarks. The dPDFs relevant to these partons are able to have factorised forms at low x_1, x_2 .

At first glance, it might appear that the statement of the inadequacy of factorised forms as applied to the valence-valence distributions has already been made, in [57]. However, our statement and the one in [57] are really very different things. In [57], the authors argue that one should not use a factorised form for the valence-valence dPDFs at *large* x_1, x_2 . The reasoning behind this is that the inaccuracies of the factorised ansatz at large x_1, x_2 due to the fact that it neglects momentum conservation effects are most strongly noticed in the valence-valence dPDFs, which are dominant at large x_1, x_2 . Whilst we agree with their conclusions, we further propose that the factorised forms should not be used to describe equal flavour valence-valence dPDFs at *small* x_1, x_2 , a point that is missed in [57] and elsewhere.

Bearing in mind the points made above, we proceed to discuss how some input distributions approximately obeying the sum rules might be obtained. One might initially wonder whether it is possible to develop a framework for constructing dPDFs out of combinations of sPDFs that does not make reference to any specific choices for the input sPDFs (e.g. MSTW, CTEQ). Instead, it would make intelligent use of the sum rules the sPDFs have to satisfy to ensure the dPDF sum rules were satisfied. However, we were not able to find a framework of this kind, even to construct dPDFs that only satisfy one of the two types of sum rules.

Our discussion must therefore be based around some specific set of input sPDFs. For

⁵Regge theory arguments, for example, would suggest $a_v \simeq \frac{1}{2}$ and $a_s \simeq 1$, and ‘modern’ global fit sPDFs show a similar trend.

the purposes of producing the most accurate set of dPDFs we can, it would seem sensible to use the inputs from the most recent LO fit by one of the PDF fitting collaborations. We have chosen to use a set which almost exactly corresponds to the MSTW2008 LO inputs (equations 6-12 and the first column of table 4 in [58], with $Q_0 = 1$ GeV and $\alpha_s(Q_0) = 0.68183$). The only differences between our inputs and those of [58] are that we have set the initial s_v distribution to zero, and have added the following terms to the \bar{d} distribution:

$$-148.103388x^3(1-x)^{10.8801} + 500x^4(1-x)^{10.8801} \quad (2.23)$$

These modifications have been made in order to fix the problem that the MSTW2008 LO \bar{s} and \bar{d} input distributions go slightly negative in some region of x . Even though strictly speaking these LO sPDFs should never go negative, the deviations below zero observed in the MSTW2008 LO \bar{s} and \bar{d} inputs are perhaps tolerable in single scattering calculations due to their small size ($\bar{s}, \bar{d} > -0.0005$). However, we must insist on using sPDFs which are strictly non-negative when expressed in the ‘human’ flavour basis⁶ to build our input dPDFs. We can explain why this has to be the case by considering the dPDFs in the ‘double human’ basis in which at least one flavour index corresponds to an sPDF which goes negative. Like all LO dPDFs in the ‘double human’ basis, they cannot go negative (due to their interpretation as a probability). If we use a pseudo-factorised prescription to construct the dPDFs, then these dPDFs will go very seriously negative where the sPDF in one direction takes small negative values, and the sPDF in the other becomes large and positive. We therefore require strictly non-negative input sPDFs.

We can identify two key features that we would like to build in to our set of input dPDFs. These are the following:

1. The dPDFs should be suppressed below factorised values near the kinematical bound (i.e. the line $x_1 + x_2 = 1$) due to phase space considerations.
2. Terms should be added/subtracted from certain dPDFs to take account of number effects.

Let us begin by discussing how the first requirement might be incorporated. In the early papers [56, 57, 59, 60], a common $(1 - x_1 - x_2)$ suppression factor multiplying all of the dPDFs was advocated. This was motivated by arguments based on the recombination model of [61], or the Kuti-Weisskopf model of [62]. More recently [49], it has

⁶The ‘human’ flavour basis is the one in which the parton index $i = g, u, \bar{u}$, etc.

been suggested that a higher power of $(1 - x_1 - x_2)$, such as $(1 - x_1 - x_2)^2$, might be appropriate. With the benefit of knowledge of the sum rules, we can see that neither of these alternatives is entirely satisfactory. To illustrate this, let us just consider the momentum sum rule for the moment (which is the relevant rule with regards to phase space considerations), and let us consider the two lines $x_1 = 0$ and $x_2 = 0$. Along these lines, all momentum sum rules are perfectly satisfied using factorised dPDFs, whilst dPDFs including a $(1 - x_1 - x_2)$ or $(1 - x_1 - x_2)^2$ factor violate the sum rules badly.

Thus a $(1 - x_1 - x_2)^n$ factor alone multiplying all of the dPDFs suppresses the functions rather too severely near the lines $x_1 = 0$ and $x_2 = 0$, and it would seem that a phase space factor which approached 1 near these lines would be more desirable. We can actually make sense of this from an intuitive point of view. The phase space suppression factor is inserted to take account of the fact that finding a parton with $x = x_1$ reduces the probability of finding another parton with $x = x_2$ if $x_1 + x_2$ is close to 1. One would expect a much smaller reduction if x_1 were small and x_2 were large than if both x_1 and x_2 were large, even if the sum of x_1 and x_2 was the same in both cases. Indeed, one would anticipate that the reduction should tend to zero as x_1 (or x_2) tended to zero – that is, the phase space factor should approach 1 as one approaches the lines $x_1 = 0$ and $x_2 = 0$.

Here, we continue to follow the tradition set by previous papers in that we have attempted to apply a universal phase space factor to all of the dPDFs. Use of a (positive) universal phase space factor has the advantage that it is guaranteed to produce positive double human basis dPDFs. However, instead of using $(1 - x_1 - x_2)^n$ alone, we tried the following as a ‘first guess’ for the phase space factor ρ , motivated by the above discussion:

$$\rho(x_1, x_2) = (1 - x_1 - x_2)^n (1 - x_1)^{-n} (1 - x_2)^{-n} \quad (2.24)$$

Following the more recent work by Korotkikh and Snigirev [49], we choose n to be 2. This choice of phase space factor gave dPDFs which satisfied the momentum sum rules reasonably well. In the left panel of Fig. 2.4, we plot the ‘sum rule ratio’ with this phase space factor for the particular example of the $(\Sigma + g)g$ momentum sum rule – the sum rule ratios for the other momentum sum rules exhibit very similar behaviour. The sum rule ratio for a particular sum rule and set of dPDFs is defined as the sum rule integral calculated using the dPDFs divided by the sPDF quantity it should be equal to. It is a function of an x variable, and measures how well the dPDFs satisfy the given sum rule – the closer the ratio is to 1 over the full x range, the better the dPDFs satisfy the sum

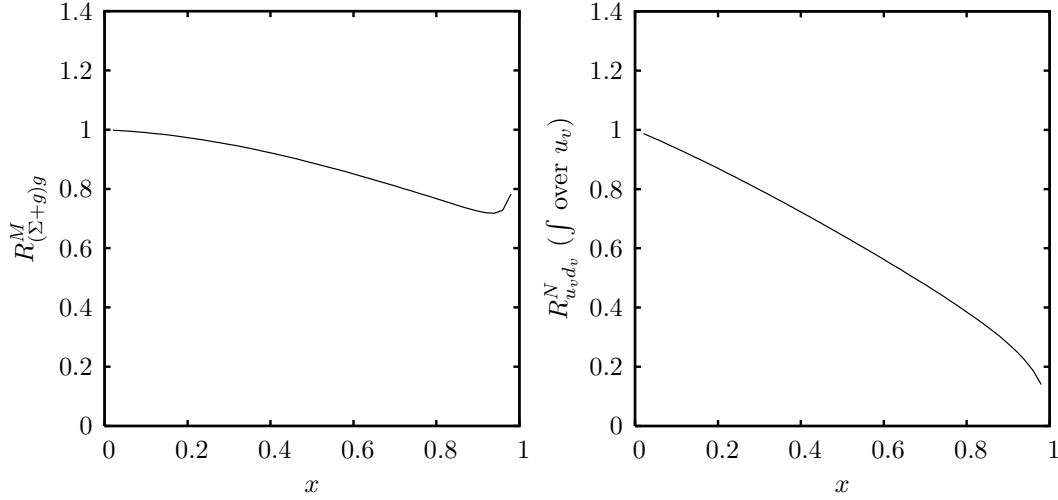


Figure 2.4: Sum rule ratios for the $(\Sigma+g)g$ momentum and $u_v d_v$ (integrating over u_v) number sum rules, when the phase space factor is as given in (2.24) with $n = 2$.

rule⁷.

On the other hand, the dPDF number sum rules are not particularly well satisfied by this prescription (this is illustrated in the right panel of Fig. 2.4). This is true even for those dPDFs which are involved in a number sum rule but which are not affected by number effects – e.g. $u_v d_v$. For these dPDFs, the phase space factor alone should be sufficient to cause the dPDFs to satisfy the relevant number sum rules – thus our first guess is not fully satisfactory. We have discovered that a slight adjustment to the form (2.24) resolves this problem. Let us allow the phase space factor to depend on the parton indices i, j on the dPDF such that (prior to adjustments relating to point 2 above) the input dPDFs are constructed according to:

$$D_p^{ij}(x_1, x_2; t_0) = D_p^i(x_1; t_0) D_p^j(x_2; t_0) \rho^{ij}(x_1, x_2) \quad (2.25)$$

We now define $\rho^{ij}(x_1, x_2)$ as follows:

$$\rho^{ij}(x_1, x_2) = (1 - x_1 - x_2)^2 (1 - x_1)^{-2-\alpha(j)} (1 - x_2)^{-2-\alpha(i)} \quad (2.26)$$

⁷Bear in mind that this quantity may not be the best measure of how well a dPDF satisfies a given sum rule when the sPDF quantity in the sum rule becomes very small or passes through zero. We will see some examples of this in what follows, and will provide additional commentary in these cases.

where:

$$\alpha(i) = \begin{cases} 0 & \text{if } i \text{ is a sea parton} \\ 0.5 & \text{if } i \text{ is a valence parton} \end{cases} \quad (2.27)$$

If either i and/or j contain both valence and sea contributions, then one should construct the dPDF by taking the factorised product, splitting it into sets of terms corresponding to valence-valence, valence-sea, sea-sea, etc., and then applying the appropriate phase space factor to each set of terms. The value $\alpha(i) = 0.5$ for i a valence parton was obtained by a crude trial and error fitting procedure – there was no physical motivation behind our choice of $\alpha(i) = 0.5$ for i valence. Note that the phase space factor is no longer universal, but is nearly so – it turns out that this prescription is guaranteed to produce positive human basis dPDFs provided all the valence sPDFs are positive, which is the case for the set we have chosen.

With the choice (2.26), the dPDFs involved in number sum rules but which are not affected by number effects satisfy their sum rules to a much better degree. It also turns out that once we have included terms to take account of number effects (described shortly), insertion of phase space factors according to (2.26) into dPDFs affected by these effects similarly improves the degree to which these dPDFs satisfy their number sum rules. In addition, the momentum sum rules are much better satisfied when one uses (2.26) rather than (2.24). Illustration of some of these points for some representative dPDF cases, as well as an exposition of the extent to which we satisfy the sum rules with this choice of phase space factor, is given in Fig. 2.5.

Having found a satisfactory phase space factor, we proceed to discuss how the second required feature in the list above – namely the incorporation of number effects – might be achieved in our input dPDFs. We have seen that number effects are particularly important for equal flavour valence-valence dPDFs, and we shall outline how suitable inputs for this particular type of dPDF may be constructed shortly. However, number effects can in principle have an impact on any other dPDF for which the same parton type appears in both parton indices. Since there are only a finite number of valence up and down quarks in the proton (as opposed to an infinite number of sea quarks and gluons), one might anticipate number effects relating to these valence quarks to be most important. We now discuss how these effects can be included in dPDFs which ‘contain’ an up and/or a down valence combination in both of their parton indices (e.g. u_+u_+ , d_+d_+ , where $i_+ \equiv i + \bar{i}$).

An example of such a distribution would be the u_+u_+ distribution, since $u_+u_+ =$

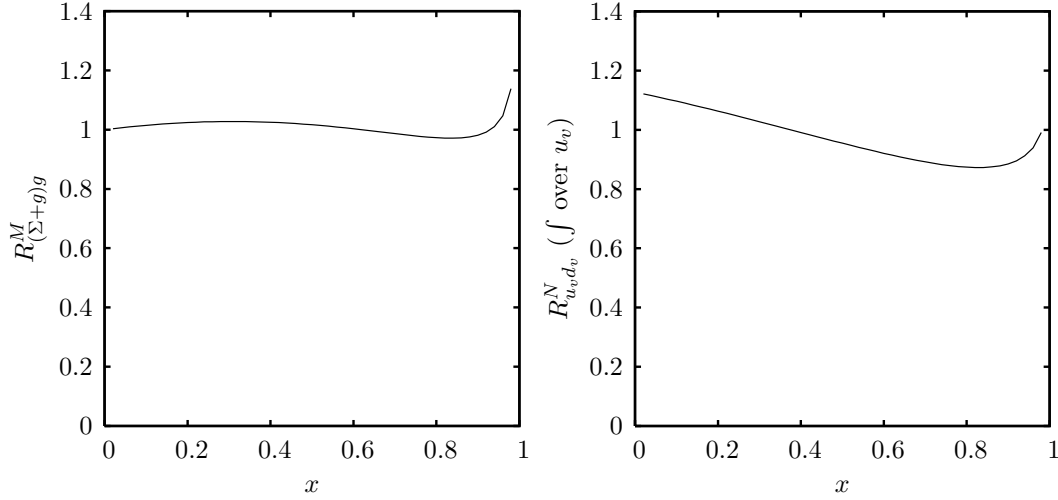


Figure 2.5: The same sum rule ratios as in Fig. 2.4, but this time plotted with the phase space factor as in (2.26).

$(u_v + 2u_s)(u_v + 2u_s)$, where $u_s = \bar{u}$. Consider the ways in which one can pick two up flavour partons (either quarks or antiquarks) from the proton. Either one can pick two sea partons, or one can pick a sea parton and a valence quark (in either order), or one can pick two valence quarks – these possibilities of course correspond to the different terms in the expansion of $(u_v + 2u_s)(u_v + 2u_s)$. Factorised terms multiplied by phase space factors are reasonable for all possibilities apart from the two valence option, where it would seem important to take account of the fact that removing a valence up halves the probability to find another. At a crude level we can incorporate this fact by using a term which is equal to half of the naive ‘factorised \times phase space factor’ guess for the valence-valence term. We can think of this adjustment in another way, and say that we incorporate number effects in the u_+u_+ distribution by subtracting the following term from our initial ‘factorised \times phase space factor’ construct:

$$\frac{1}{2} D_p^{u_v}(x_1; t_0) D_p^{u_v}(x_2; t_0) \rho^{u_v u_v}(x_1, x_2) \quad (2.28)$$

Generalising this argument, we observe that a dPDF which contains n times the up valence–up valence combination in its parton indices must have n times the term (2.28) subtracted from it to take account of number effects. Similarly, a distribution which contains n times the down valence–down valence combination in its parton indices must have n times $D_p^{d_v}(x_1; t_0) D_p^{d_v}(x_2; t_0) \rho^{d_v d_v}(x_1, x_2)$ subtracted from it. Note in this case that we must remove the naive $d_v d_v$ term entirely because there is no chance of finding two

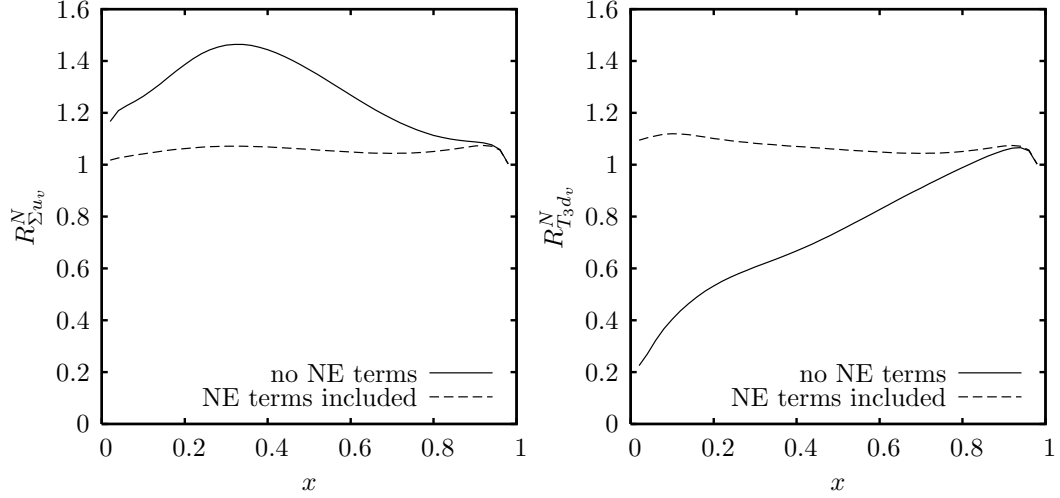


Figure 2.6: The effect of adding number effect (NE) terms on the sum rule ratios for the $u_v \Sigma$ and $d_v T_3$ number sum rules.

valence down quarks in the proton⁸. Fig. 2.6 shows how inclusion of the number effect terms improves the extent to which dPDFs satisfy number sum rules, for a few sample cases.

We now turn our attention to the construction of some equal flavour valence-valence dPDFs approximately satisfying the sum rules. The flavours we must be concerned about here are up, down, *and strange*. Note that the $s_v s_v$ distribution is not zero with the given set of input sPDFs, even though the s_v sPDF is zero. The sum rule for this dPDF reads:

$$\int_0^{1-x_2} dx_1 D_p^{s_v s_v}(x_1, x_2; t_0) = -D_p^{s+}(x_2; t_0) \quad (2.29)$$

Since the MSTW 2008LO s_+ input is nonzero, the right hand side of (2.29) is nonzero, and consequently the $s_v s_v$ dPDF cannot be zero. We can explain why the $s_v s_v$ distribution should be nonzero by expanding the combination into double human basis pairs – $s_v s_v = ss - s\bar{s} - \bar{s}s + \bar{s}\bar{s}$. We expect the probability to find an $s\bar{s}$ pair to be higher than that to find an ss or $\bar{s}\bar{s}$ pair due to number effects. Given that one has found a strange (antistrange)

⁸Clearly, this construction makes use of the number of each type of valence quark in the proton (i.e. two up, one down). One could in principle test this construction more extensively by applying it to a neutron target (with one down and two up valence quarks), and seeing if gave appropriate DPS cross section predictions for hadronic scattering processes involving neutrons. There are experimental complications in performing such tests, one of which is that free neutrons are not stable – typically one uses a deuteron (neutron + proton) to provide a neutron, and either neglects the effect of nuclear shadowing, nucleon off-shellness, Fermi motion and binding, and nuclear pions, or attempts to model these in some way (see e.g. [63] and references therein).

in the proton, the probability to find a further strange (antistrange) is reduced, whilst that to find an antistrange (strange) in addition remains the same.

In order to construct satisfactory distributions for these three flavour types, we imagine that there exists a scale $\tilde{t} < t_0$ at which only the three valence quarks in the proton may be resolved, and all sea distributions are zero. The sea distributions at t_0 are then generated dynamically by DGLAP evolution between \tilde{t} and t_0 . This idea has previously been put forward in [64–68], in which it was investigated whether the possibility exists to fit deep inelastic scattering data using only u_v and d_v inputs at a fitted low scale \tilde{t} . As it turns out, one cannot achieve a fully satisfactory fit of data using this approach, as is admitted in [69]. However, since we shall only use this idea very loosely in what follows, this point is not of great concern to us.

At the scale \tilde{t} , the only equal flavour valence-valence dPDF which can be nonzero is the $u_v u_v$ distribution, as there is no possibility of finding two down or strange partons (be they quarks or antiquarks) at this scale. A suitable ansatz for the $u_v u_v$ at \tilde{t} is a product of u_v sPDFs multiplied by a phase space factor $\tilde{\rho}$ appropriate at the scale, and divided by two to take account of valence-valence number effects:

$$D_p^{u_v u_v}(x_1, x_2; \tilde{t}) = \frac{1}{2} D_p^{u_v}(x_1; \tilde{t}) D_p^{u_v}(x_2; \tilde{t}) \tilde{\rho}^{u_v u_v}(x_1, x_2) \quad (2.30)$$

One can straightforwardly verify that the above forms for the equal flavour valence-valence dPDFs are consistent with the number sum rules at this scale. Now let us consider how the dPDFs change as we evolve from \tilde{t} to t_0 under (2.2). The first two sets of terms on the RHS of (2.2) will mainly serve to take (2.30) into its equivalent at t_0 (and leave the other equal flavour valence-valence distributions zero). However, the final set of ‘sPDF feed’ terms results in an extra contribution appearing in each equal flavour valence-valence dPDF. Only the $-j\bar{j} - \bar{j}j$ component of an equal flavour valence-valence combination receives nonzero sPDF feed contributions during evolution ($g \rightarrow j\bar{j}$ contributions). Therefore, the sPDF feed for an equal flavour valence-valence dPDF is the following:

$$-2 \frac{\alpha_s(t)}{2\pi} D_p^g(x_1 + x_2; t) \frac{1}{x_1 + x_2} P_{qg} \left(\frac{x_1}{x_1 + x_2} \right) \quad (2.31)$$

The splitting function P_{qg} is not a very strong function of its argument (only varying between $\frac{1}{2}$ and $\frac{1}{4}$). This means that, roughly speaking, we can take the sPDF feed term for the equal flavour valence-valence distributions as being a function of $(x_1 + x_2)$. If we then ignore the subsequent effect of the first two sets of terms on the RHS of (2.2) on the

sPDF feed contributions, then we expect the sum total sPDF feed contribution to each valence-valence dPDF at t_0 to be a function of $(x_1 + x_2)$ only:

$$D_p^{j_v j_v}(x_1, x_2; t_0) = \frac{N_{j_v} - 1}{N_{j_v}} D_p^{j_v}(x_1; t_0) D_p^{j_v}(x_2; t_0) \rho^{j_v j_v}(x_1, x_2) - 2g^{j\bar{j}}(x_1 + x_2; t_0) \quad (2.32)$$

We shall refer to the function $g^{j\bar{j}}(x_1 + x_2; t_0)$ as the $j\bar{j}$ correlation term, as it represents the ‘nonfactorised’ part of the $j\bar{j}$ (or $\bar{j}j$) distribution which is built up from correlation-inducing sPDF feed contributions. How should we decide on the form of this function for a particular choice for the flavour j ? We can answer this question by using the number sum rule that (2.32) must satisfy, which we shall write here as:

$$\int_0^{1-x_2} dx_1 D_p^{j_v j_v}(x_1, x_2; t_0) = (N_{j_v} - 1) D_p^{j_v}(x_2; t_0) - 2D_p^{\bar{j}}(x_2; t_0) \quad (2.33)$$

The first term on the RHS of (2.32) integrates to give approximately the first term on the RHS of (2.33). The $-2g^{j\bar{j}}(x_1 + x_2; t_0)$ must therefore integrate to give the second term on the RHS of this equation:

$$-2 \int_0^{1-x_2} dx_1 g^{j\bar{j}}(x_1 + x_2; t_0) = -2D_p^{\bar{j}}(x_2; t_0) \quad (2.34)$$

This is an integral equation with a unique solution, and it is straightforward to show that the solution is the following:

$$g^{j\bar{j}}(x; t_0) = -\frac{\partial D_p^{\bar{j}}(x; t_0)}{\partial x} \quad (2.35)$$

Our proposed form for the input equal flavour valence-valence distributions is therefore (2.32) with $g^{j\bar{j}}$ given by (2.35). Clearly the $d_v d_v$ and $s_v s_v$ number sum rules will be perfectly satisfied using this form. Fig. 2.7 shows how well the $u_v u_v$ sum rule is satisfied.

Unfortunately, with this choice for the equal flavour valence-valence dPDFs, the $\bar{u}\bar{u}$, $\bar{d}\bar{d}$, ss and $\bar{s}\bar{s}$ dPDFs all go negative. Naively, one might view this as arising because the forms we have used for the equal flavour valence-valence dPDFs are in some way unsatisfactory. However, instead we observe that it occurs because we have omitted an important term in our above treatment of the $j_+ j_+$ distributions. Since these distributions contain the parton combination $j\bar{j} + \bar{j}j$ that also appears in the $j_v j_v$ distribution with the opposite sign, the $j_+ j_+$ receive the same sPDF feed contributions as the $j_v j_v$ during

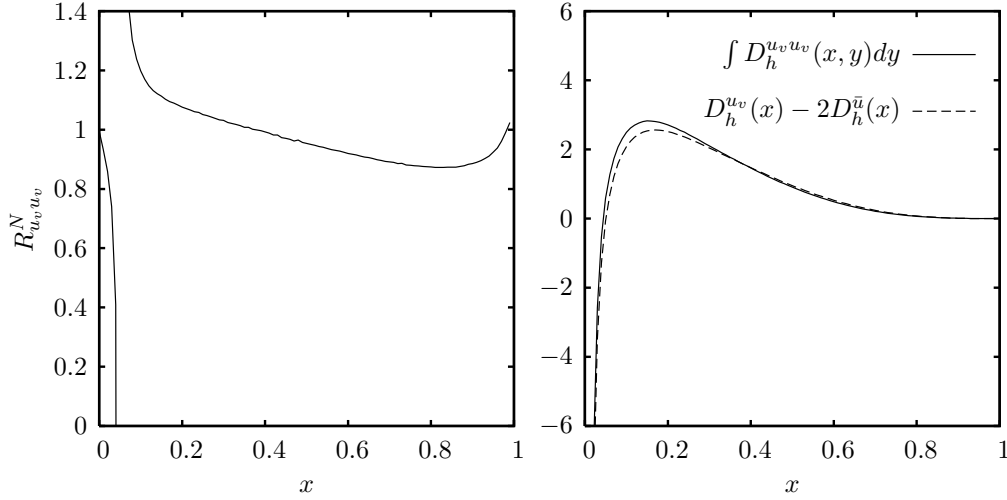


Figure 2.7: *Left panel:* The sum rule ratio for the $u_v u_v$ number sum rule when $D_p^{u_v u_v}$ is constructed according to (2.32) and (2.35). The ratio is close to 1 over most of the range of x , except near $x = 0.05$ where it diverges violently. This appears to indicate that the sum rule is being badly violated near $x = 0.05$. *Right panel:* The $u_v u_v$ sum rule integral plotted against the sPDF quantity it should be equal to. This plot reveals that the divergence in the sum rule ratio is caused by the integral curve slightly missing a zero in the sPDF quantity, and is not serious in practice.

evolution, but with the opposite sign. Thus for consistency each $j_+ j_+$ distribution should have an extra term added onto it equal to *plus* $2g^{\bar{j}\bar{j}}(x_1 + x_2; t_0)$. With this alteration, all double human basis dPDFs are again positive, and we see little adverse effect on the extent to which the sum rules involving $j_+ j_+$ distributions are satisfied.

Having now completed our description of how we constructed some suitable input dPDFs, we conclude our discussion with a short summary of how well the dPDFs satisfy the complete set of sum rules. In the context of the double human basis, the sum rule ratios are all within 25% of 1 for $x \lesssim 0.8$. Above this value, the sum rules are not obeyed so well – however the values of the PDFs are tiny at these x values, so large/small sum rule ratio values at these x values are not in practice too great a problem. In the double evolution basis the story is the same, barring trivial divergences due to the sum rule integral slightly missing a zero in the sPDF quantity it should be equal to. The one exception to this is the case of the $T_3(\Sigma + g)$ momentum sum rule. The sum rule ratio for this sum rule, plotted in the left panel of Fig. 2.8, plunges to 0.65 around $x = 0.02$. This possibly looks worse than it is – if one plots both the integral and the sPDF quantity it should be equal to (right panel of Fig. 2.8), then one notices that the dip in the sum rule ratio is due to the integral slightly overestimating a dip in the sPDF quantity in a region

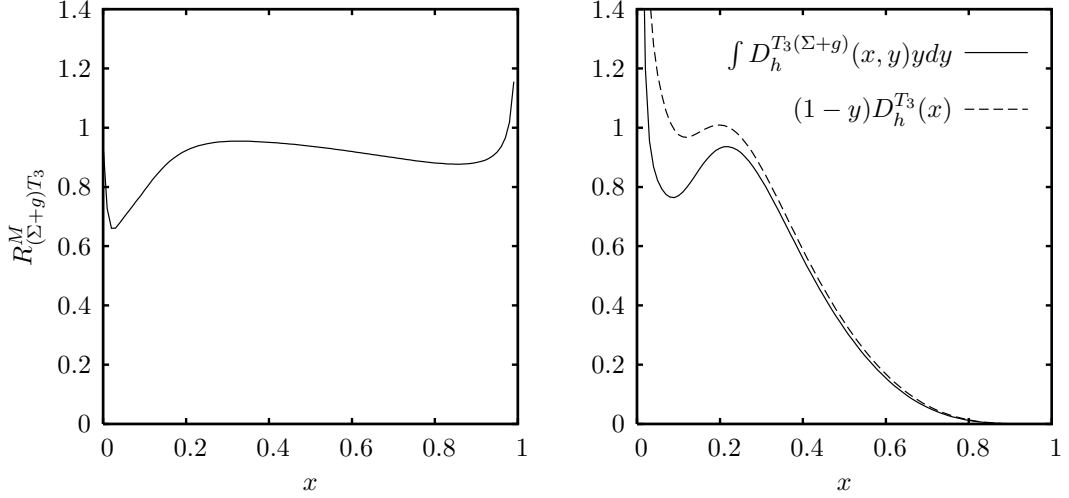


Figure 2.8: *Left panel:* The sum rule ratio for the $(\Sigma+g)T_3$ momentum sum rule, plotted using the fully constructed set of input dPDFs. *Right panel:* The $(\Sigma+g)T_3$ momentum sum rule integral plotted against the sPDF quantity it should be equal to.

where the sPDF quantity is rather small. Furthermore, it is unlikely that the particular combination $T_3(\Sigma+g)$ will be directly accessed by any scattering processes at the LHC. Consequently we are prepared to accept the large deviation from 1 in the $T_3(\Sigma+g)$ sum rule ratio.

2.4 Numerical Solution of the Double DGLAP Equation

There exist several options for the broad numerical method to use to integrate the dDGLAP equations. One could choose to adapt either the direct x space or Mellin transform methods which are commonly used to numerically integrate the sDGLAP equation (see, for example, [70,71] for routines using the x space method for solution of the sDGLAP equation, and [72] for a routine using the Mellin transform method). Alternatively, one could develop a numerical method based on the explicit solution of the dDGLAP equation in terms of sPDFs (2.11). This is the approach that has been preferred in the previous numerical treatments of the subject [48, 49]. Here we adopt an x space method. This has the advantages that it is conceptually simple, is flexible enough to take the inputs described in Section 2.3.2 with no problems, and is competitive in efficiency with the other methods in the context of the dDGLAP equation. It also has the advantage over

the ‘explicit solution’ method in that the $D_i^j(x; t)$ Green’s functions, which are difficult to calculate numerically to a sufficient degree of accuracy, do not feature.

2.4.1 The dDGLAP Evolution Program

Our program solves the dDGLAP equation (2.2) directly using a grid in x_1, x_2 and t . We choose the spacing of the grid points in t to be linear – this is the ‘natural’ choice, and it is adopted in a number of sDGLAP x -space routines (e.g. [70, 71]). In the x_1 and x_2 directions, the points are taken to be evenly spaced in the variable $u = \ln(\frac{x}{1-x})$, with equal numbers of points in the x_1 and x_2 directions (600 for the grids of [50]). This gives a spacing uniform in $\ln(x)$ in the small x regions and directions in which the dPDF is diverging rapidly, and a linear spacing in larger x regions and directions in which the variation of the dPDF is slower. The boundary of the grid in (x_1, x_2) space is defined by the lines $x_1 = x_{\min}$, $x_2 = x_{\min}$, $x_1 = 1 - x_{\min}$, $x_2 = 1 - x_{\min}$, and $x_1 + x_2 = 1$ (the kinematical boundary), with a default $x_{\min} = 10^{-6}$. The methods we use for the numerical integration of the first two terms on the right hand side of the dDGLAP equations are described in Appendix B.

The final set of terms in the dDGLAP equation (the ‘sPDF feed’ terms) are obtained at a given t by numerically evolving the sDGLAP equations contemporaneously with the dDGLAP equations. The grid used for the sDGLAP evolution is similar to that used for the dDGLAP evolution. The only difference is that it extends in just one x direction, between x_{\min} and $(1 - x_{\min})$. For consistency, the sPDF inputs used are the MSTW2008LO inputs.

Given the structure of the dDGLAP equation, the dDGLAP evolution routine requires the values of the sPDFs at x values of the form $x_i + x_j$, where x_i and x_j are two x values on the uniform in $\ln(x/(1-x))$ grid. With the grid used, it is clear that $x_i + x_j$ does not also lie on the grid, so interpolation has to be used to obtain the sPDF values required. Away from the edges of the sPDF x -grid, natural cubic spline interpolation based on the sPDF values at the nearest four grid points is used, whilst linear interpolation is used at the edges.

The program uses the ‘double evolution’ basis introduced in Section 2.3 as its internal basis for the evolution of the dPDFs. Use of this basis for the evolution is advantageous because the dDGLAP equations become in some sense ‘minimally coupled’ in this basis. Out of the 91 equations, 66 are rendered diagonal at LO using this basis (i.e. rate of change of D_p^{ij} with t is given only by the two integral terms involving D_p^{ij} , with no nonzero sPDF

feed terms). The remaining equations have very few terms on the RHS (two terms in each integral term plus one sPDF feed term). The use of this basis makes the coding in of the dDGLAP equations manageable.

Stepwise evolution in t is carried out by a fourth-order Runge-Kutta method. The evolution begins at a scale t_0 equal to that at which the input distributions are defined ($Q_0^2 = 1 \text{ GeV}^2$ with the MSTW2008LO inputs). The final scale obtained in the evolution t_f and the number of Runge-Kutta steps used to reach this scale N_t may be specified by the user. To produce the grids of [50], 120 points were used in the t direction.

2.4.2 Flavour Number Schemes

Our program has the potential to perform the evolution using either a fixed or variable flavour number scheme (see section 1.3.3), with n_f fixed at 3, 4, 5 or 6 in the FFNS, or potentially varying from $3 \rightarrow 6$ in the VFNS. The scheme can be determined by the user via the variables LGMCSQ, LGMBQS and LGMTSQ which are equal to the thresholds in t at which the charm, bottom and top flavours become active respectively. For a FFNS of given n_f , LGMCSQ, LGMBQS and LGMTSQ should be set appropriately either above t_0 or below t_f (e.g. for a FFNS with $n_f = 5$, set LGMCSQ $< t_0$, LGMBQS $< t_0$ and LGMTSQ $> t_f$). For a VFNS, at least one of LGMCSQ, LGMBQS and LGMTSQ must lie in between t_0 and t_f . It should be noted that to produce the grids of [50], the program was run under a VFNS with n_f varying between 3 and 5. The variables LGMCSQ and LGMBQS were set according to the values of m_c and m_b preferred by MSTW – 1.40 GeV and 4.75 GeV respectively.

Prior to the evolution, the program compares LGMCSQ, LGMBQS and LGMTSQ with t_0 and t_f . Depending on the results of this, it splits the full evolution from t_0 and t_f into up to four intervals, each with a different value of n_f . The total number of integration steps in t , N_t , is divided up amongst these intervals roughly in proportion to the interval sizes in t .

In each interval, the strong coupling constant t is calculated according to the LO analytic form:

$$\alpha_S(t) = \frac{\alpha_S(t')}{1 + \alpha_S(t')b(t - t')}; \quad b \equiv \frac{33 - 2n_f}{12\pi}. \quad (2.36)$$

The quantity t' corresponds to the value of t at the beginning of the interval. In the first interval, the boundary value of the strong coupling constant, $\alpha_S(t')$, is taken to be the initial value specified by the user $\alpha_S(t_0)$. In later intervals it is chosen to ensure continuity

in α_S , which as we mentioned in section 1.3.2 is the appropriate matching condition at LO.

2.4.3 Accuracy of the Program

We wish to get a rough estimate of the error in the dPDF values at Q introduced by numerical evolution with N_x points in each x direction, and N_t points in the t direction. To do this, one might propose doing an evolution with twice as many points in each direction, and then taking the error in the original dPDFs at Q as being the absolute difference between the dPDF values produced by the two evolutions. Unfortunately, we cannot perform this procedure for the values of N_x and N_t used to produce the grids in [50] (600 and 120). This is because doubling the number of x points in this case causes the program to require far more RAM than a typical modern machine can provide. Instead, we show here that the accuracy of the program is reasonable even when N_x and N_t take on the smaller values of 150 and 10 respectively – we then know that the accuracy of the procedure with $N_x = 600$ and $N_t = 120$ should be very good.

We perform the error estimation evolution from $Q_0 = 1$ GeV to $Q_f = 100$ GeV. In Fig. 2.9, the fractional error in the distribution D_p^{gg} along the sample line $x_1 = x_2 = x$ as calculated by the above method is plotted. That is, we plot:

$$\varepsilon(x; Q_f) \equiv \frac{|D_h^{gg}(x, x, Q_f)_{N_x=150, N_t=10} - D_h^{gg}(x, x, Q_f)_{N_x=300, N_t=20}|}{D_h^{gg}(x, x, Q_f)_{N_x=300, N_t=20}}. \quad (2.37)$$

We choose to look at D_p^{gg} because this is one of the dPDFs which should be calculated least accurately by an evolution routine. As expected, the error increases as one approaches the kinematical bound due to the fact that fewer x points are used in the evolution integrations for the dPDF values closer to the bound. We see that the error is small in the crucial small x region – less than 1% for $x \lesssim 0.3$, and less than 6% for $x \lesssim 0.4$. The error becomes large as one approaches $x = 0.5$, but since this region is not likely to be important in applications at the LHC (which probes $x_1, x_2 \lesssim 0.1$), this is not a major problem. The graph indicates that even with $N_x = 150$ and $N_t = 10$ the numerical evolution to LHC scales introduces errors which are less than 1% for $x_1 < 0.3, x_2 < 0.3$, and less than 6% for $x_1 < 0.4, x_2 < 0.4$.

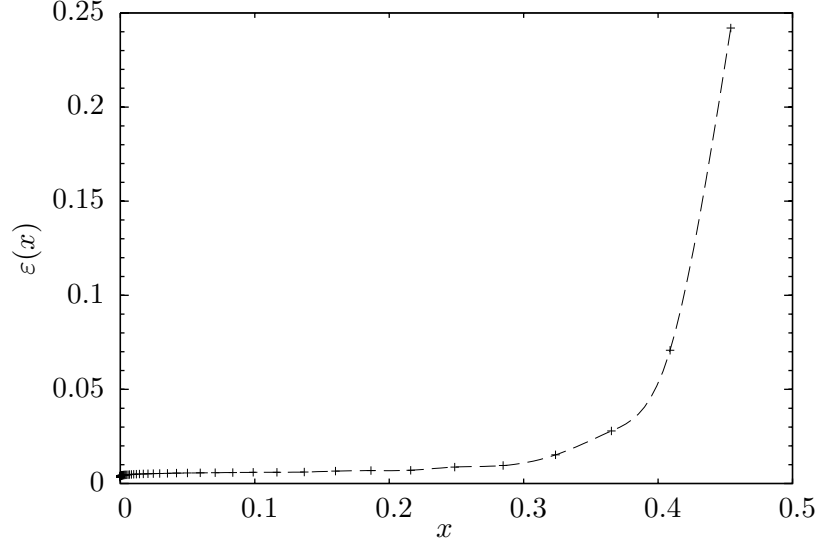


Figure 2.9: An estimation of the numerical error when one performs an evolution from $Q = 1$ GeV to $Q = 100$ GeV using a grid with 150 points in each x direction, and 10 in the t . The error values plotted are those in the gg dPDF along the line $x_1 = x_2 = x$.

2.5 Properties of the dPDFs

We have seen that there are two ways to improve on using simple products of sPDFs as the dPDFs at the (high) scale Q . First, one can use dDGLAP evolution to obtain the dPDFs at Q , with a reasonable choice of dPDFs at a low scale Q_0 used as the starting point for the evolution. Second, one can use improved inputs at the low scale Q_0 , which take account of momentum and number effects. In this section, we describe and illustrate the extent to which introducing these improvements changes the dPDFs at the scale Q .

The large number of dPDFs precludes the possibility of discussing them all. Instead, we choose to focus on a small number of parton pairings which should be important in double scattering processes at the LHC, and which in some sense might be considered to form a representative set. These are the uu , $u\bar{u}$, ug and gg pairings. Note that we have a dPDF for which our input form contains a valence number effect term in this set (the uu), and a distribution for which our input contains a $j\bar{j}$ correlation term (the $u\bar{u}$). Furthermore, we see that the set covers all types of sPDF feed term that can appear in LO dDGLAP evolution.

For the purposes of making concrete comparisons between different methods of obtaining the dPDFs at a high scale Q , we also need to make a specific choice for Q . Except where otherwise stated, we make the reasonable choice $Q = 100$ GeV ($\sim M_W, M_Z$, for

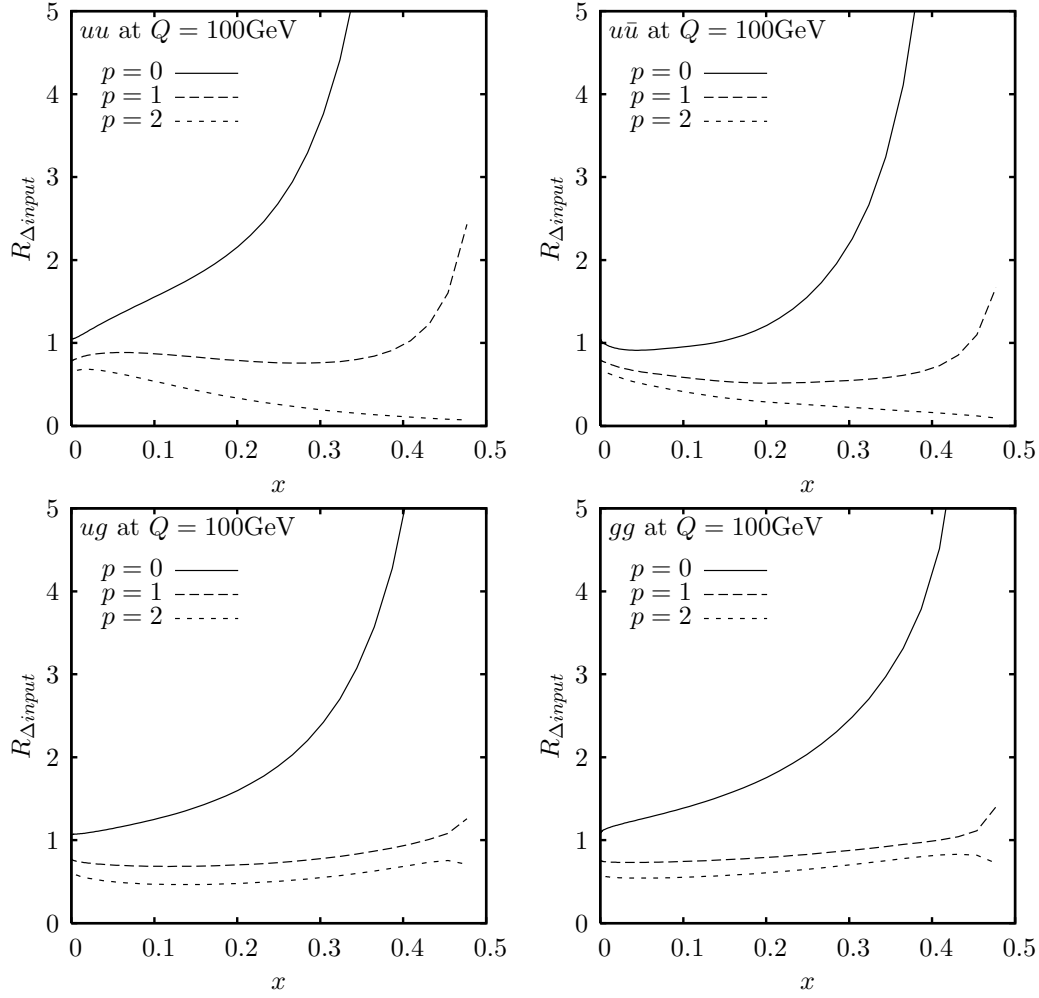


Figure 2.10: Plots of the ratio $R_{\Delta input}^{ij}$ defined in equation (2.38) for $Q = 100$ GeV, $p = 0, 1$ and 2 , and the parton combinations ij discussed in the text.

example). At the scale Q , we only look at the dPDF values along the line $x_1 = x_2$ – this allows us to produce easily readable 2D plots.

The main novel component of the work discussed so far in this Chapter is the introduction of the improved input dPDFs of Section 2.3.2. Consequently, the first question we should like to answer is how use of the improved inputs in the dDGLAP equation, as opposed to naive ‘factorised $\times (1 - x_1 - x_2)^p$ ’ inputs, affects the dPDFs at the scale Q . To this end, we have plotted the following ratio for our sample dPDFs in Fig. 2.10:

$$R_{\Delta input}^{ij}(x; Q) \equiv \frac{D_p^{ij}(x, x; Q) \big|_{\text{input } D_p^{ij}(x_1, x_2; Q_0) = D_p^i(x_1; Q_0) D_p^j(x_2; Q_0) (1 - x_1 - x_2)^p}}{D_p^{ij}(x, x; Q) \big|_{\text{input } D_p^{ij}(x_1, x_2; Q_0) = \text{our improved inputs}}} \quad (2.38)$$

We have made plots for each of the common traditional choices for $p = 0, 1$ and 2 . One immediately notices in Fig. 2.10 that all of the ratio curves deviate significantly from 1. This shows that the precise choice of inputs at the low scale has an important impact on the high scale dPDFs, and demonstrates the inadequacy of the traditional naive input forms. We see that multiplying factorised inputs by a phase space factor of $(1 - x_1 - x_2)$ or $(1 - x_1 - x_2)^2$ gives high scale dPDFs which are generally too small for small (x_1, x_2) . This is expected – we have seen that $(1 - x_1 - x_2)$ or $(1 - x_1 - x_2)^2$ phase space factors suppress the inputs too much in the high x_1 , low x_2 and high x_2 , low x_1 regions. Since these regions directly feed the small x_1, x_2 region, this directly translates into a deficiency in the high scale dPDFs in the small x_1, x_2 region. Conversely, we see that not using a phase factor in the inputs results in high scale dPDFs which are generally too large. This is because in this scenario the inputs are too large near the kinematic bound, and this excess propagates down to smaller x_1, x_2 values during evolution.

It is interesting to note that, contrary to the previous general statement, the $p = 0$ ratio for the $u\bar{u}$ dPDF actually dips below unity between $x = 0.005$ and $x = 0.15$. Furthermore, we see that the $p = 0$ uu ratio rises above the corresponding ratios for the other flavour combinations. The origin of each of these features is in the extra terms we included in our improved inputs to take account of valence number effects or $j\bar{j}$ correlations, which do not appear in the naive inputs. The inclusion of a positive $j\bar{j}$ correlation term in the $u\bar{u}$ distribution causes our $u\bar{u}$ dPDF to be larger at the high scale than it would be if the correlation term were absent. Since our dPDFs appear on the denominator of $R_{\Delta input}^{ij}$, this manifests itself as a reduction in our $p = 0$ $u\bar{u}$ ratio. Conversely, the subtraction of a valence number effect term from our uu input results in a reduction of our uu dPDF at Q , which increases the uu ratio.

For $p = 1$ and 2 , we observe that the uu ratio is still larger than the others for small x . However, the $u\bar{u}$ ratio is now very slightly larger than the ug and gg ratios at small x values. This is because the ug and gg high scale distributions at small x are more sensitive to the form of the input distributions near the kinematic boundary than the $u\bar{u}$. This is a simple consequence of the fact that gluon type evolution causes a faster cascade of PDFs to low x values than u or \bar{u} type evolution. The reduction in the ug and gg ratios at small x relative to the $u\bar{u}$ due to the change in p overcomes the small effect of including the $j\bar{j}$ correlation term in our $u\bar{u}$.

The contributions of the $j\bar{j}$ correlation and valence number effect terms to the high scale ($Q = 100$ GeV) double human basis dPDFs are most cleanly observed at $x \sim 0.05$,

and are on the order of 10% in this x region. For smaller x , the contributions from the extra terms are swamped by sea-sea contributions to the dPDF, whilst at larger x , phase space effects become dominant.

Aside from looking at the effect of using different inputs on the dPDFs at scale Q , we can also ask to what extent correlations introduced by dDGLAP evolution affect the dPDFs at Q . There are essentially two types of correlations that the dDGLAP equation introduces – correlations due to the requirement of momentum conservation, and more interesting correlations generated by the sPDF feed terms. Here, we choose to look specifically at the effect of the latter.

In order to do this, we evolved our improved input dPDFs up to the scales $Q = 10$ GeV, $Q = 100$ GeV, and $Q = 1000$ GeV, both with the sPDF feed terms included in the evolution, and also with these terms set to zero. For each final scale and parton pairing in our selected set, the following ratio was then plotted:

$$R_{\text{no feed}}^{ij}(x; Q) \equiv \frac{D_p^{ij}(x, x; Q) \mid_{\text{our improved inputs, no sPDF feed}}}{D_p^{ij}(x, x; Q) \mid_{\text{our improved inputs}}} \quad (2.39)$$

We plot the results using a logarithmic x scale in Fig. 2.11⁹. The effect of the sPDF terms is small but non-negligible, being at roughly the 10% level for $x < 10^{-2}$ in all of the dPDFs considered, and increasing with Q .

We observe that the ratios for all of the given flavour combinations look very similar for x from 10^{-6} to 10^{-4} . The reason for this is that the small x shape of the distributions considered is very strongly determined by the (either direct or indirect) feeding of these distributions by the gg distribution. If the gg dPDF loses its sPDF feed and is reduced by a certain percentage at small x , the connection of the other dPDFs to the gg will result in these dPDFs being reduced by a similar amount. This explanation can be verified by investigating what happens if we remove all of the sPDF terms except for the gg feed. In this case the ratios for all of the considered dPDFs are much closer to 1 for $10^{-6} < x < 10^{-4}$, suggesting that the subtraction of the gg sPDF feed is the dominant factor determining the shapes of the plots in Fig. 2.11 for small x .

For larger x , the deviation of the uu ratio from 1 remains small, and tends to 0 as x approaches its maximum of 0.5. This is expected since there is no direct sPDF feed term in the evolution of the uu dPDF. The $u\bar{u}$ ratio also seems to tend to 1 as $x \rightarrow 0.5$, albeit

⁹In this figure, and in figures 2.12 and 2.14, we make plots down to $x = 10^{-6}$. Although it is interesting to look at our LO dPDFs at very small x , we should mention that we do not expect the leading order approximation to produce very accurate dPDFs in this region.

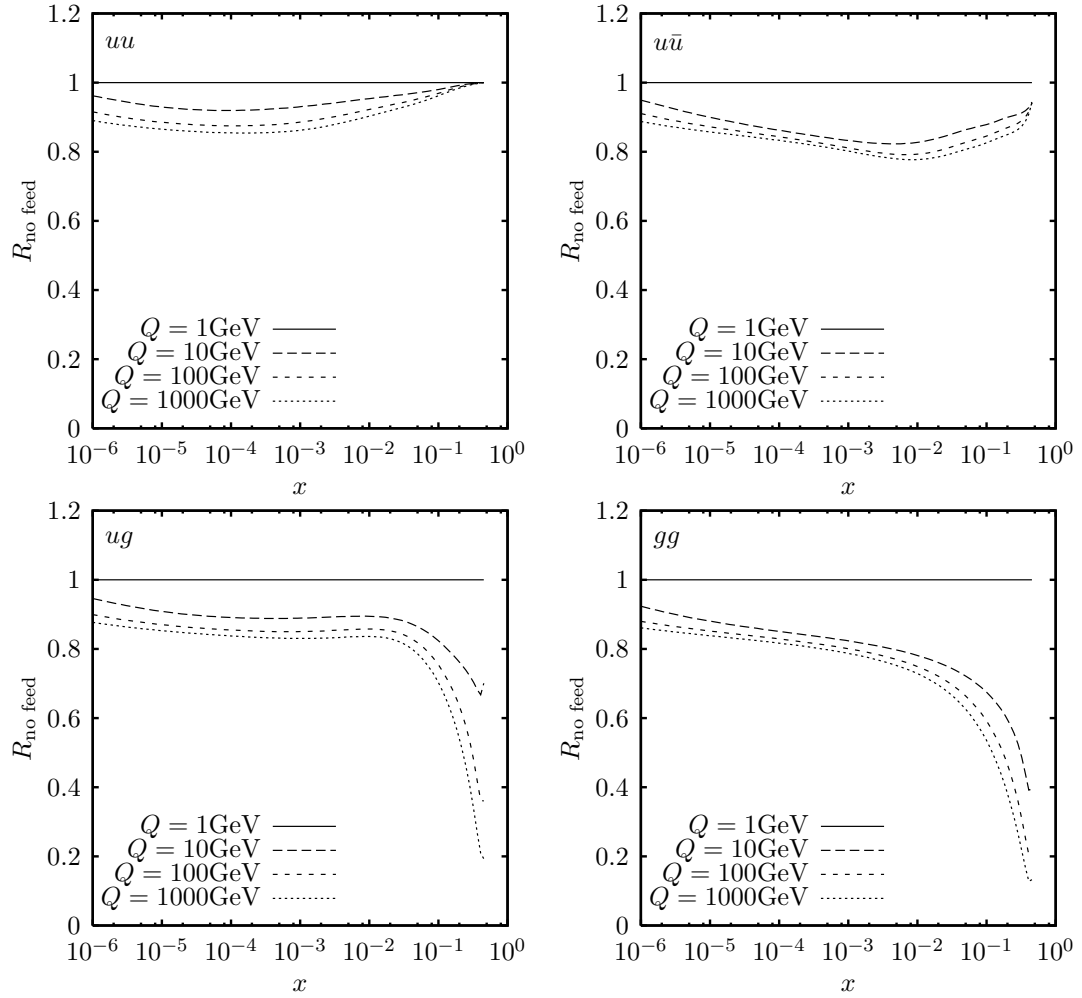


Figure 2.11: Plots of the ratio $R_{\text{no feed}}^{ij}$ defined in equation (2.39) for $Q = 1, 10, 100$ and 1000 GeV and the parton combinations ij discussed in the text.

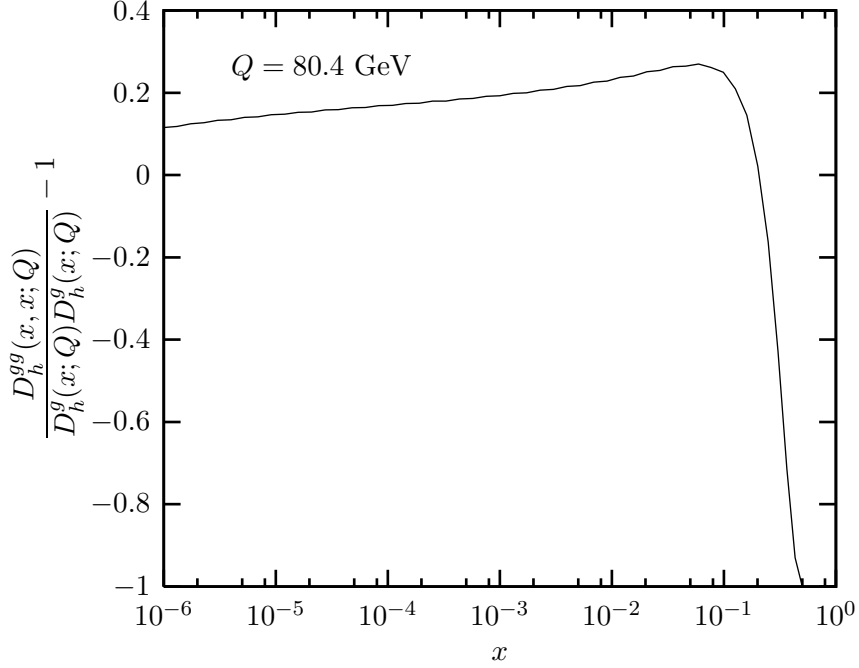


Figure 2.12: gg correlation ratio R^{gg} at $Q = 80.4$ GeV obtained using MSTW2008LO factorised inputs.

more slowly, whilst the ug and gg ratios plunge towards zero, the gg more rapidly than the ug . This implies that at large x , the sPDF feed contributions are more important to the gg than they are to the ug , and that they are more important to the ug than they are to the $u\bar{u}$. We can explain this ordering using a fact we have previously mentioned – namely, that the ‘pull’ on a gluon PDF towards lower x values during evolution is stronger than that on a quark type PDF. The gg distribution at large x is pulled strongly towards lower x values in two directions, and is very much smaller if it is not continuously fed by an sPDF. By contrast, the ‘pull’ on the large x $u\bar{u}$ distribution is smaller in both directions, and so the contribution of similar sPDF feed terms is proportionately smaller. The ug distribution has one gluon flavour index and one quark, so the importance of the sPDF feed on this distribution at large x is intermediate.

We have not been able to exactly reproduce the results of either of the extant numerical investigations into the correlations induced by evolution – [48] and [49]. However, we do agree with [49] that the accumulated sPDF feed contribution to the gg between ~ 1 GeV and 100 GeV accounts for about 10% of the $Q = 100$ GeV gg distribution at small x . In

Fig. 2.12, we plot the following ratio for $Q = 80.4$ GeV:

$$R^{gg}(x; Q) \equiv \frac{D_p^{gg}(x, x; Q) |_{\text{factorised inputs}} - D_p^g(x; Q) D_p^g(x; Q)}{D_p^g(x; Q) D_p^g(x; Q)} \quad (2.40)$$

This figure corresponds to the solid curve in Fig. 1 of [48], with MSTW2008LO inputs replacing the MRS99 inputs used there. We expect that the ratio R^{gg} should tend to -1 as x approaches 0.5 for any Q sufficiently larger than the input scale. This is because evolution will very quickly cause D_p^{gg} to become much smaller than the factorised value near the kinematic bound. Our curve exhibits this property, but it seems unlikely that the solid curve plotted in Fig. 1 of [48] will, especially if it reaches 0.6 for higher x values as is stated in [48].

Finally, we compare our full treatment (improved inputs plus full dDGLAP evolution) with the approximation that simply uses factorised inputs $\times (1 - x_1 - x_2)^p$ ($p = 0, 1$ or 2) at the scale Q . This approximation is frequently used in phenomenological studies of double parton scattering processes. In Fig. 2.13, we plot the following ratio along the line $x_1 = x_2 = x$ for our sample dPDFs and for $p = 0, 1$ and 2 :

$$R_{\Delta^{final}}^{ij}(x_1, x_2; Q) \equiv \frac{D_p^i(x_1; Q) D_p^j(x_2; Q) (1 - x_1 - x_2)^p}{D_p^{ij}(x_1, x_2; Q) |_{\text{our improved inputs}}} \quad (2.41)$$

The plots reveal that even a $(1 - x_1 - x_2)^2$ phase space factor multiplying a factorised form at Q underestimates the large x falloff in the dPDFs along $x_1 = x_2 = x$. For very small x , the ratios are all slightly less than 1 due to the fact that one misses the sPDF feed contributions if one uses a factorised form at Q (note that the ratio appears smallest at very low x for the $u\bar{u}$, due to the fact that the sPDF feed for the $u\bar{u}$ is particularly important around $x = 10^{-2}$ – see Fig. 2.11). One also notices the imprint of omitting the valence number effect and $j\bar{j}$ correlation terms in the ratios – the uu ratio rises above the others at $x \sim 0.05$, whilst the $u\bar{u}$ dips at this x value.

It is interesting to consider the behaviour of $R_{\Delta^{final}}^{ij}(x_1, x_2; Q)$ away from the line $x_1 = x_2 = x$. In Fig. 2.14, we plot the $p = 0$ ratio for the gg flavour combination along several lines emanating from the point $x_1 = 10^{-6}, x_2 = 10^{-6}$. The figure shows that the deviation of this ratio from 1 is maximal along $x_1 = x_2$ (in fact, this statement holds for any combination of parton indices). We observe that a $p = 0$ factorised form is a fairly good approximation to our gg dPDF close to the x_1 axis, except when x_1 is very large ($x_1 > 0.8$). This is to be expected, given our use of input dPDFs which essentially reduce

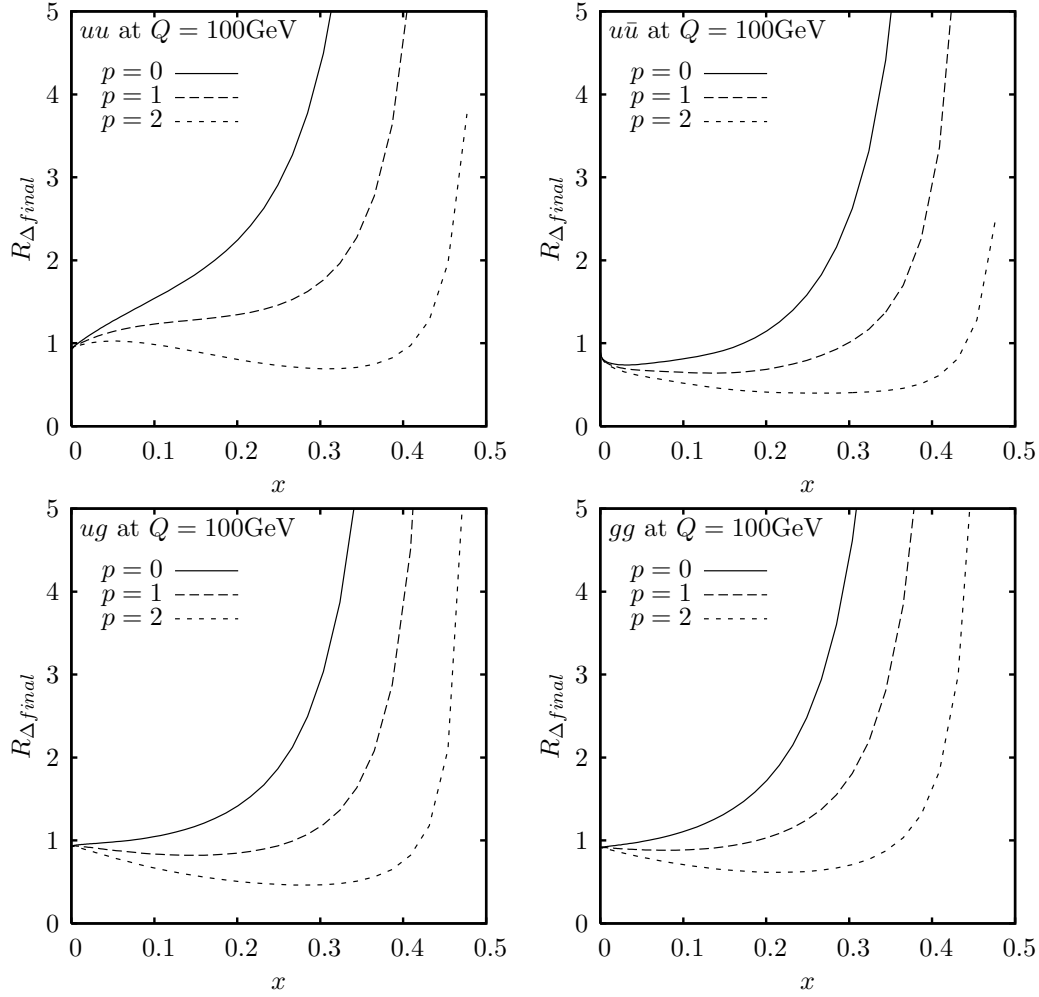


Figure 2.13: Plots of the ratio $R_{\Delta final}^{ij}$ defined in equation (2.41) at $Q = 100 \text{ GeV}$ and along the line $x_1 = x_2 = x$. The ratio is plotted for $p = 0, 1$ and 2 and for each of the parton combinations ij discussed in the text.

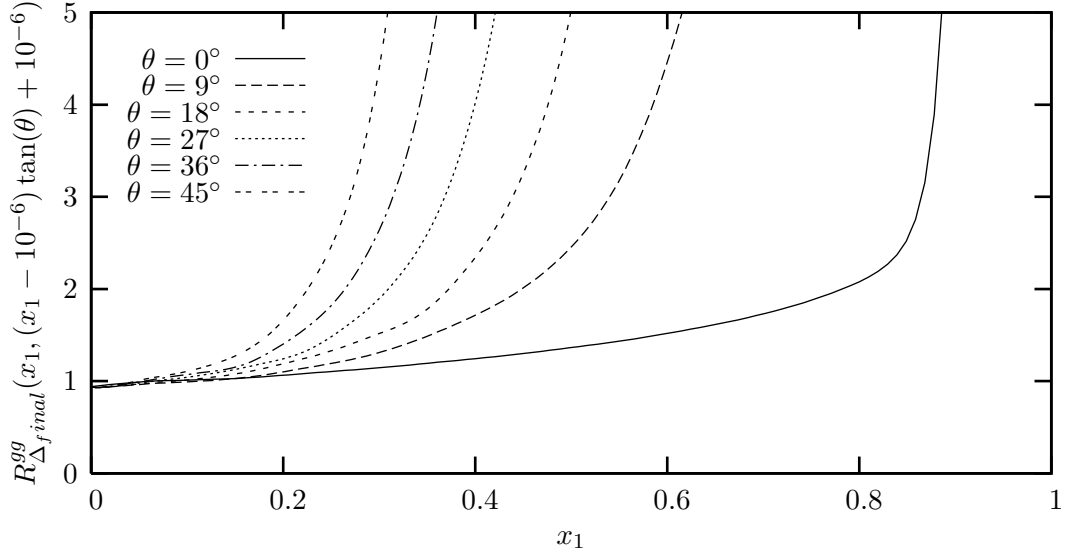


Figure 2.14: The ratio $R_{\Delta_{final}}^{gg}$ plotted along various lines of the form $x_2 = (x_1 - 10^{-6}) \tan(\theta) + 10^{-6}$ at $Q = 100$ GeV.

to $p = 0$ factorised forms near the lines $x_1 = 0$ and $x_2 = 0$. One can infer from the plot that use of a factorised form multiplied by either $(1 - x_1 - x_2)$ or $(1 - x_1 - x_2)^2$ will result in one overestimating the falloff in the dPDFs in the $x_1 \sim 0, x_2 \lesssim 0.8$ and $x_1 \lesssim 0.8, x_2 \sim 0$ regions.

2.6 Effects of using GS09 dPDFs on same-sign WW DPS signal

It is interesting to ask how the inclusion of pQCD evolution effects and sum rule constraints in GS09 affects experimentally measurable DPS signals. In [47], we compared the same-sign WW DPS signal produced using GS09 with that arising from simple factorised forms. The factorised forms used were simple products of MSTW2008LO dPDFs multiplied by $(1 - x_1 - x_2)^n$, $n = 0, 1, 2$ (the ‘MSTW_n’ dPDFs). Same-sign WW production was chosen as the DPS process because it has been traditionally considered as a clean channel for observation of DPS. The cross section for same-sign WW production via SPS is suppressed to the same order of magnitude as the DPS cross section due to the large number of vertices required in the Feynman diagrams. What is more, this SPS background must always produce two jets in addition to the WW pair – so it can be efficiently removed via a jet veto. In this section we present a brief summary of our study [47], referring the

	σ_{GS09}	σ_{MSTW_0}	σ_{MSTW_1}	σ_{MSTW_2}
W^+W^-	0.546	0.496	0.409	0.348
W^+W^+	0.321	0.338	0.269	0.223
W^-W^-	0.182	0.182	0.156	0.136

Table 2.2: DPS WW total cross sections (in pb) for pp collisions at $\sqrt{s} = 14$ TeV evaluated using different dPDF sets.

reader to [47] for further and more technical details.

Primarily we were interested in the experimentally clean same-sign dilepton (SSDL) plus missing transverse energy (\cancel{E}_T) signal generated when both of the W s decay leptonically. The DPS signals for the different dPDF sets were generated using the ‘dPDF framework’ formula (1.76), with $A = B = W^\pm$, $Q_A^2 = Q_B^2 = M_W^2$, and $m = 1$. The value of σ_{eff} used in our study was the one extracted from the CDF study of $\gamma + 3j$ [39], 14.5 mb. Parton level cross sections were calculated to leading order accuracy using MADGRAPH [73, 74], to be consistent with the order of the dPDFs. Note that such leading order calculations of the DPS process predict that the W bosons always emerge with zero transverse momentum p_T , which is not realistic. Therefore in cases where the W p_T s were important (e.g. when we were cutting on lepton p_T to reduce SPS backgrounds – see later), we redistributed the p_T of each W independently according to the resummed next-to-leading logarithmic p_T distribution of a W produced via SPS. The NLL p_T distribution was calculated with NLO MSTW2008 sPDFs, using the code of [75, 76] and the non-perturbative parameterisation of [77].

In Table 2.2, we compare the predictions of the different dPDFs for the total W^+W^+ and W^-W^- DPS cross sections (i.e. including all decay modes of the W s) at the LHC design energy of $\sqrt{s} = 14$ TeV. The W^+W^- DPS cross sections are also included in this table for comparison. It is observed that the predictions of the GS09 and MSTW₀ sets are rather similar, with those of the MSTW₁ and MSTW₂ sets lying rather lower owing to the suppression of these dPDFs by $(1 - x_1 - x_2)^n$ factors (we recall from section 2.3.2 that such suppression is excessive close to the lines $x_1 = 0$ and $x_2 = 0$).

In figures (2.15(a)) and (2.15(b)) we plot the pseudorapidity distributions of leptons arising from W^+W^+ and W^-W^- DPS processes respectively, for the different choices of dPDF. We observe that the distributions become more central for the MSTW _{n} dPDFs as n increases, since the higher n dPDFs are skewed more towards lower x_1, x_2 values by the $(1 - x_1 - x_2)^n$ factors. In this case, the GS09 prediction is matched most closely by MSTW₁ – there is a certain amount of suppression of large x_1, x_2 values in the GS09 set

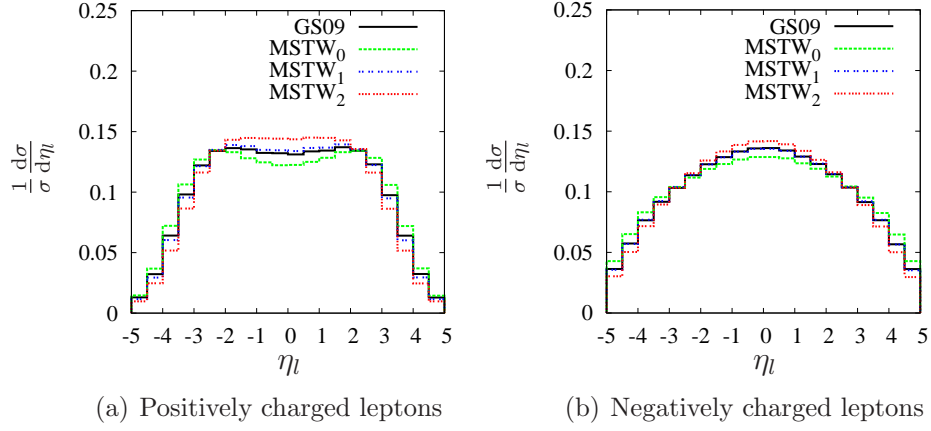


Figure 2.15: Normalised lepton pseudorapidity distributions for pp collisions at $\sqrt{s} = 14$ TeV evaluated using different dPDFs. No cuts are applied.

in the implementation of the valence number and momentum sum rule constraints.

We see that there is no hope of distinguishing the GS09 dPDFs from the simpler MSTW_n via simple observables such as the total cross section or lepton pseudorapidity distribution. One requires an observable that is sensitive to correlations in rapidity between the leptons, and therefore is sensitive at a basic level to longitudinal correlations in the dPDFs. A suitable variable is the lepton pseudorapidity asymmetry a_{η_l} , defined according to:

$$a_{\eta_l} = \frac{\sigma(\eta_{l_1} \times \eta_{l_2} < 0) - \sigma(\eta_{l_1} \times \eta_{l_2} > 0)}{\sigma(\eta_{l_1} \times \eta_{l_2} < 0) + \sigma(\eta_{l_1} \times \eta_{l_2} > 0)} \quad (2.42)$$

where η_{l_1} is the pseudorapidity of one lepton produced in a same-sign WW event, and η_{l_2} is the pseudorapidity of the other.

This quantity is plotted as a function of the minimum rapidity cut η_l^{\min} on the detector hemispheres in figure 2.16. In this case, the GS09 predictions are clearly distinguishable from the MSTW_n predictions, being significantly larger especially at large η_l^{\min} . The reason why the a_{η_l} predictions from GS09 are larger at large η_l^{\min} is because the probability of a proton providing two large x (valence) quarks is reduced under GS09 (since the GS09 dPDFs correctly take account of the fact that finding a valence quark in the proton dramatically reduces the chances to find another, whereas the MSTW_n sets do not). This causes the cross section for two leptons to be produced with large rapidity in the same

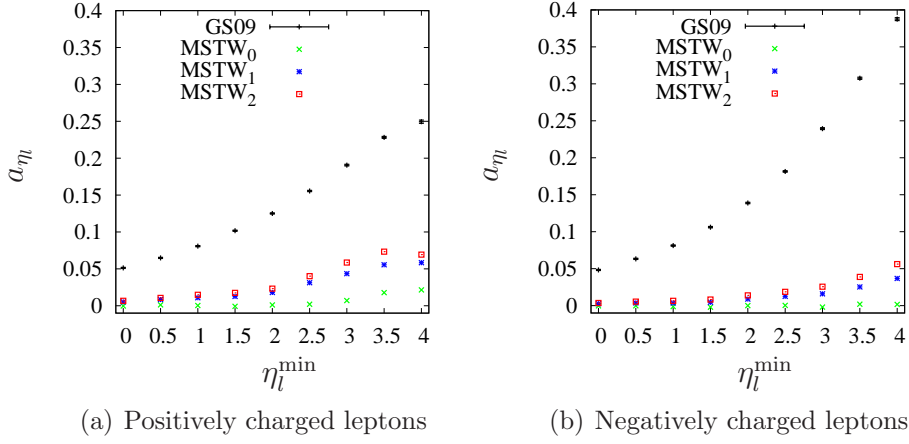


Figure 2.16: Pseudorapidity asymmetry a_η for pp collisions at $\sqrt{s} = 14$ TeV evaluated using different dPDFs. No cuts are applied.

hemisphere to fall under GS09, and therefore a_η to rise.

In addition to comparing the same-sign WW DPS signal obtained using GS09 to that obtained using simple factorised forms, in [47] we also conducted a detailed investigation into the SPS backgrounds to the process. We found that there are a number of SPS processes that can give rise to the same-sign dilepton + missing E_T signal in the detectors, aside from the canonical $WWjj$ background. In the following we discuss only the SPS backgrounds to l^+l^+ production – those for l^-l^- production are related to these by charge conjugation.

The first type of background process is associated with intermediate gauge boson pairs other than $WW - W^+Z(\gamma^*)$ and $Z(\gamma^*)Z(\gamma^*)$. Where these processes give rise to an l^+l^+ lepton pair, they also give rise to one or more ‘wrong sign’ leptons l^- :

$$q\bar{q}' \rightarrow W^+Z(\gamma^*) \rightarrow l^+l^+\nu + l^- \quad (2.43)$$

$$q\bar{q} \rightarrow Z(\gamma^*)Z(\gamma^*) \rightarrow l^+l^+ + l^-l^- \quad (2.44)$$

The wrong sign leptons must either be too forward or too soft to be identified in order for such processes to constitute a background to the SSDL DPS signal. In the context of our investigation this meant that they had to satisfy $|\eta_l| > \eta_{id}$ or $p_T < p_T^{id}$, with $\eta_{id} = 2.5$ and $p_T^{id} = 10$ GeV.

A further source of background lies in processes with intermediate heavy quarks. The

production of a $b\bar{b}$ pair can give rise to a SSDL pair if a neutral B-meson is present and undergoes $B^0 - \bar{B}^0$ mixing, and then both B mesons decay semi-leptonically:

$$\begin{aligned} gg &\rightarrow b\bar{b} \rightarrow B\bar{B} + \dots, \\ B &\rightarrow l^+ \nu X, \\ \bar{B}^0 &\rightarrow B^0 \rightarrow l^+ \nu \tilde{X} \end{aligned} \quad (2.45)$$

Production of $t\bar{t}$ pairs can also give rise to a SSDL pair, if one top and the bottom from the other top decays semi-leptonically:

$$\begin{aligned} gg &\rightarrow t\bar{t} \\ t &\rightarrow W^+ b \rightarrow l^+ \nu b, \\ \bar{t} &\rightarrow W^- \bar{b} \rightarrow q\bar{q}' l^+ \nu \bar{c} \end{aligned} \quad (2.46)$$

The $W^+Z(\gamma^*)$, $Z(\gamma^*)Z(\gamma^*)$, and $t\bar{t}$ processes give lepton p_T distributions that are harder than that of the signal, so these may be reduced using a maximum lepton p_T cut. On the other hand a minimum lepton p_T cut and minimum \cancel{E}_T cut is effective in reducing the (large) $b\bar{b}$ background, since this process tends to produce small lepton p_T s and missing energy. The $b\bar{b}$ and $t\bar{t}$ backgrounds will tend to give rise to leptons surrounded by hadronic junk, so these may be further reduced by imposing tight isolation cuts on the leptons. A wrong sign lepton veto in the central region is helpful in cutting down the Z contribution to the electroweak boson pair background, whilst looking for the presence of a low invariant mass system of an isolated charged track and a nearby identified lepton [78] is helpful in suppressing the γ^* contribution. Finally, we see from (2.46) that the $t\bar{t}$ background contains a lot of jet activity, so like the canonical $WWjj$ background, it may be effectively cut down using a central jet veto. In fact, a central jet veto (when combined with all other cuts) is so effective at suppressing the $WWjj$ and $t\bar{t}$ backgrounds that we do not need to consider these backgrounds further.

Following the above guidelines, we developed the following basic set of cuts to enhance the signal over background ratio for the same-sign WW DPS signal:

- Both leptons in the like sign lepton pair must have pseudorapidity $|\eta| < 2.5$. [This is not really a cut – we include it to model the limited rapidity range of the detector for tracking and identifying leptons].
- Both leptons are required to be isolated: $E_{\text{iso}}^l \leq E_{\text{iso}}^{\text{min}} = 10 \text{ GeV}$, where E_{iso}^l is the

hadronic transverse energy in a cone of $R = 0.4$ surrounding each of the like-sign leptons.

- The transverse momenta of both leptons, p_T^l , must satisfy $20 \leq p_T^l \leq 60$ GeV.
- An event is rejected whenever a third, opposite-signed, lepton is identified. A lepton is assumed to be identified with 100% efficiency when $p_T^l \geq p_T^{\text{id}}$ and $|\eta| < \eta^{\text{id}}$, where $p_T^{\text{id}} = 10$ GeV and $\eta^{\text{id}} = 2.5$.
- The missing transverse energy \cancel{E}_T of an event must satisfy $\cancel{E}_T \geq 20$ GeV.
- Reject an event if a charged (lepton) track with $p_T^{\text{id}} \geq p_T \geq 1$ GeV forms an invariant mass < 1 GeV with one of the same-sign leptons.
- Reject an event if it contains a jet with $p_T > 20$ GeV.

In Table 2.3, we present cross section results for the DPS signal and important backgrounds following our cuts, for $\sqrt{s} = 14$ GeV and in the case in which the final state leptons are muons. The diboson background was calculated at leading order using MADGRAPH [73,74] for the matrix elements and VEGAS [79] for the phase space integration. HERWIG6.510 [80] was used to generate the $b\bar{b}$ background, with various adjustments made to make the simulation manageable (these were a parton level cut on the p_T of the bs , $p_T^b \geq 20$ GeV, forced semi-leptonic B decays and forced $B^0 - \bar{B}^0$ mixing of one neutral B meson when at least one of these is produced in the event). We see from the table that our cuts are effective at suppressing the $b\bar{b}$ background (even though the cross section for this process starts off orders of magnitude larger than the signal). On the other hand, the $W^+Z(\gamma^*)$ background remains a factor of a few larger than the signal even following cuts. It is unlikely that further simple physics cuts will improve this situation, as many basic kinematic distributions are similar between the signal and this SPS background. Given such a large SPS background on top of a small DPS signal, it seems unlikely that we will be able to discriminate between GS09 and simple factorised forms in the near future by analysing LHC data for the SSDL + \cancel{E}_T process.

On the positive side, one can identify some features that distinguish the DPS signal from the $W^+Z(\gamma^*)$ background, and could prove useful as further experimental handles to extract the signal. The value of the lepton pseudorapidity asymmetry a_{η_l} is small and positive for the DPS signal, but it is negative for the $W^+Z(\gamma^*)$ background (see the left panel of figure 2.17). The negative a_{η_l} for the $W^+Z(\gamma^*)$ background reflects the fact that

	$\sigma_{\mu^+\mu^+}$ (fb)	$\sigma_{\mu^-\mu^-}$ (fb)
$W^\pm W^\pm$ (DPS)	0.82	0.46
$W^\pm Z(\gamma^*)$	5.1	3.6
$Z(\gamma^*)Z(\gamma^*)$	0.84	0.67
$b\bar{b}$ ($p_T^b \geq 20$ GeV)	0.43	0.43

Table 2.3: Cross sections (in fb) of the processes simulated after cuts, including branching ratios corresponding to same-sign dimuon production.

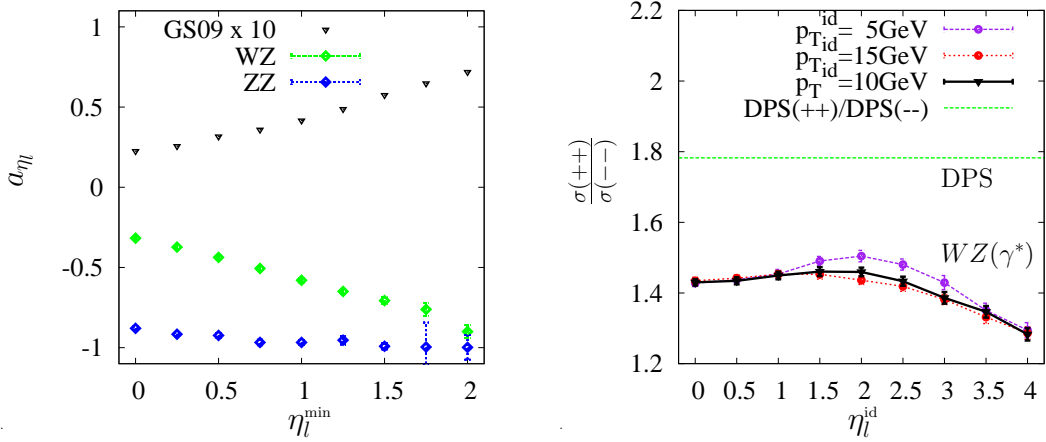


Figure 2.17: Left: pseudorapidity asymmetry a_{η_l} for the positive SSDL+ \cancel{E}_T DPS signal and selected SPS background, after imposing cuts described in the text. Right: charge asymmetry ratio $(++)/(- -)$ as a function of lepton identification criteria for different processes.

this process prefers the leptons to lie close in pseudorapidity space such that the CM energy of the system is smaller. Also, the ratio of positively charged $(++)$ to negatively charged $(--)$ SSDL events (which we shall call the charge asymmetry ratio) is larger for the DPS signal than for the $W^+Z(\gamma^*)$ background (see the right pane of 2.17), and appears to be stable against cuts.

2.7 Summary

At the start of this chapter we defined the double PDF $D_p^{ij}(x_1, x_2; t_A, t_B)$ ($t_{A,B} = \log(\mu_{A,B}^2)$) as the integral of the 2pGPD over \mathbf{b} , UV regulated in an appropriate way using a factorisation scale μ_A for the first parton, and μ_B for the second parton. It has been stated in the past [6], and appears intuitively reasonable, that the 2pGPD can be approximately

factorised into longitudinal and transverse pieces, where we denote the latter quantity by $F(\mathbf{b})$. Then, if we normalise the integral of $F(\mathbf{b})$ to 1, we can identify the longitudinal piece of the 2pGPD with the dPDF, and describe the proton-proton DPS cross section in terms of the dPDFs and $\sigma_{eff} \equiv 1/\int d^2\mathbf{b}F^2(\mathbf{b})$ (we call this the dPDF framework for describing pp DPS). The evolution equation for the equal scale dPDFs $D_p^{ij}(x_1, x_2; t)$, which we refer to as the dDGLAP equation, was derived long ago in [4].

In this chapter we have shown that the equal scale dPDFs are subject to momentum and valence number sum rule constraints analogous to the relations (1.65) and (1.66), and given the form of these constraints. We have also suggested how the unequal scale dPDFs might be obtained from the equal scale dPDFs. The main body of the chapter, however, has focussed on the development of a set of LO equal scale dPDFs – the GS09 dPDFs. There were two steps in this process – the first was the construction of a sensible set of nonperturbative ‘input’ dPDFs at a scale of $\mu_0 = 1$ GeV, and the second was the development of an algorithm to evolve the inputs to higher scales via the LO dDGLAP equation.

The inputs used were based on factorised products of MSTW2008LO sPDFs (in accordance with intuitive arguments and the limited evidence from CDF), with a number of physically-motivated adjustments added in order that the dPDF inputs should satisfy the newly-established sum rules. With the adjustments, the input dPDFs were found to satisfy all sum rules to better than 25% precision in the ‘double human’ basis, for $x < 0.8$. To evolve the inputs to higher scales, we decided to write a program that uses a direct x space method. The accuracy of the program is good for small x_1, x_2 – an evolution from 1 GeV to 100 GeV using a grid with only 150 points in each x direction and 10 points in the t direction produces dPDF values with numerical errors of less than 1% for $x_1 < 0.3, x_2 < 0.3$. We have produced a set of publicly available dPDF grids spanning the ranges $10^{-6} < x_1 < 1, 10^{-6} < x_2 < 1, 1 < Q^2 < 10^9 \text{GeV}^2$ by applying the evolution algorithm to our modified inputs, and the grid can be found along with interpolation code at [50]. To produce the grids, 600 points were used in each x direction, and 120 in the t , ensuring an accuracy much better than 1% for small x .

We summarised the results of a phenomenological investigation of DPS in same-sign W production [47]. In this study the DPS signal obtained using GS09 dPDFs was compared with that obtained using crude products of MSTW2008 PDFs multiplied by $(1 - x_1 - x_2)^n$ factors (‘MSTW $_n$ ’ dPDFs), and all possible SPS backgrounds to the process were carefully considered. We identified an observable that is especially sensitive to the longitudinal

correlations implemented in GS09 – this is the lepton pseudorapidity asymmetry a_η . This is larger with GS09 dPDFs than MSTW_n dPDFs since the former set takes account of the fact that finding a large x valence quark in the proton significantly reduces the chance to find another. In the study of SPS backgrounds to the process, we established that aside from the ‘canonical’ $W^\pm W^\pm jj$ background, there are di-boson and heavy flavour backgrounds that should also be considered. Although the $W^\pm W^\pm jj$ background can be efficiently removed via a central jet veto, the diboson background remains larger than the DPS signal by a factor of $\sim 7-9$ even following basic cuts to enhance S/B . The presence of such large SPS backgrounds on top of a small DPS $W^\pm W^\pm$ signal implies that detailed studies of DPS via this channel may be difficult with the statistics obtainable in the near future.

In the next section we will find out that in fact there are theoretical problems in describing pp DPS in terms of dPDFs. However, we should like to point out at this stage that there is still value in the work of this Chapter despite the flaws in the dPDF framework. The momentum and valence number constraints implemented in GS09 must also be present at some level in the true description of DPS, so use of GS09 to predict DPS signals represents an improvement on the approaches used previously involving products of single PDFs. It is very possible that the qualitative distinguishing features of the GS09 same-sign WW signal that we discovered, that are caused by very elementary valence number conservation considerations, should be present in the true DPS signal. Finally, as we will discuss in the next section, although proton-proton DPS turns out not to directly involve the dPDFs, there is a process which does – the two-nucleon contribution to proton-heavy nucleus DPS. The GS09 dPDFs can be used in the cross section predictions for this process.

Chapter 3

Flaws in the double PDF Framework

This chapter is based on the original research paper [81] and the conference proceedings [82]. The work for these was performed in collaboration with James Stirling.

3.1 Introduction

In this chapter we discover two ways in which the dPDF framework for describing the proton-proton DPS cross section, introduced in the previous section, is deficient. In section 3.2 we point out using simple arguments that there can be contributions to proton-proton DPS associated with interference and correlation effects in spin, colour, flavour and parton type (i.e. quark, antiquark or gluon), even when the colliding protons are unpolarised. We will see, however, that the 2pGPDs associated with colour correlation and interference, and parton type interference, are suppressed by Sudakov factors. Such interference and correlated parton contributions are omitted in the treatment of DPS presented in the previous section, which effectively only takes account of the diagonal unpolarised contribution in spin, colour, and flavour space. Then, in section 3.3, we conduct a detailed study of a particular Landau singularity in one-loop integrals known as the ‘double parton scattering’ singularity. The results of this study are used to show that there are theoretical problems in the way that the dPDF framework treats so-called ‘double perturbative splitting’ or ‘1v1’ diagrams. The study in section 3.3 is not only of interest to those studying DPS – it also answers some unresolved questions raised by the NLO multileg community in recent years.

The notion that spin and colour correlations might contribute to the proton-proton DPS cross section, as well as interference effects in colour, spin and parton type, was

actually put forward long ago by Mekhfi [83]. It was also pointed out long ago by Artru and Mekhfi [84] that the colour correlation and interference distributions, as well as the parton type interference distributions, are Sudakov suppressed. These issues were revisited recently by Diehl, Ostermeier and Schafer [36, 37] and Manohar and Waalewijn [33], with the former set of authors also demonstrating that the correlation and interference contributions may be sizeable, and pointing out that there can be interference effects in flavour space. The material in section 3.2 is therefore not new – rather it is a pedagogical summary of existing ideas (which is perhaps easier to follow than the more technical discussion in [33, 36, 37, 83, 84], and so is hopefully of use to those less familiar with the subject). On the other hand, it was only established recently that there are theoretical problems in the dPDF treatment of ‘double perturbative splitting’/‘1v1’ diagrams, in our paper [81] and in the paper [36] written slightly earlier by Diehl and Schafer (see also [37]). The approaches of the two papers [81] and [36] are complementary – in section 3.3 we show how our results fit together with those of Diehl and Schafer.

3.2 Interference and Correlation Effects in DPS

3.2.1 Why are Interference and Correlation Effects Allowed for DPS?

In this section we explain in simple terms why there can be interference and correlated parton contributions to the unpolarised p-p DPS cross section, where there are no such contributions to the corresponding SPS cross section. These interference and correlated parton contributions have the same power behaviour as the ‘conventional’ unpolarised diagonal contribution (i.e. $\mathcal{O}(\Lambda^2/Q^2)$ in the cross section). We hope that this explanation may be of aid to those less familiar with the subject, and refer the reader to [33, 36, 37, 83] for more details.

We recall that the cross section for leading power single parton scattering processes is calculated from ‘cut diagrams’ with the structure of figure 3.1(a). For definiteness we have taken the SPS process to be Drell-Yan in the figure, but the details of the final state are not important for our discussion. Now, if we consider the parton ‘returning’ to (say) the bottom proton on the right hand side of the diagram, then we see that it must have exactly the same flavour and colour as it ‘left’ with on the left hand side. This must be the case otherwise it cannot ‘reform’ the original proton when it combines with the spectators

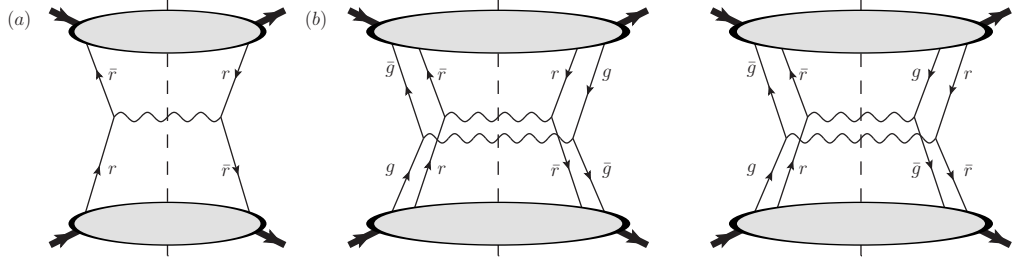


Figure 3.1: (a) Leading power diagram for single Drell-Yan (as an example process) in proton-proton collisions. (b) A diagonal in colour (left) and colour interference (right) diagram contributing to the double Drell-Yan DPS process.

on the right hand side. So there can be no flavour and colour interference contributions to p-p SPS. When the colliding protons are unpolarised, symmetry forbids any contribution to the SPS cross section associated with helicity or transversity polarisation effects. For similar reasons, there cannot be any contribution to the SPS cross section associated with the analogous effects in colour space. The only PDFs that contribute to the unpolarised SPS cross section are therefore the unpolarised diagonal colour-summed PDFs.

The cross section for DPS processes is calculated from cut diagrams with the structure of figure 3.1(b) in which two partons ‘leave’ each proton on the left, interact, and then ‘return’ on the right. In this case, the fact that the proton must be reformed at the end only imposes constraints on the overall quantum numbers of the diparton system. This allows for the possibility for non-diagonal diagrams to contribute to the DPS cross section in which some or all of the quantum numbers of the diparton system are distributed in different ways on the left and right hand sides of the cut. We have actually already seen that this can occur for the transverse momentum of the partons – see section 1.4 and figure 1.5 – but there are other possibilities for the quantum number that could be redistributed, including colour, angular momentum, and flavour.

The situation is perhaps simplest in the case of colour – in this case the allowed interference diagrams simply involve the colours of the active parton legs being swapped over in going from the left to the right hand side of the diagram. To conserve colour there must be swaps in both the upper and lower halves of the diagram, and these must be ‘in the opposite direction’. An example of a colour interference diagram that contributes to double Drell-Yan is given on the right hand side of figure 3.1(b).

In the case of spin matters appear to be more complicated, since the diparton system can have an orbital angular momentum (for nonzero \mathbf{b}), and this can potentially differ between the left and right hand sides of the diagram. If one neglects this issue and

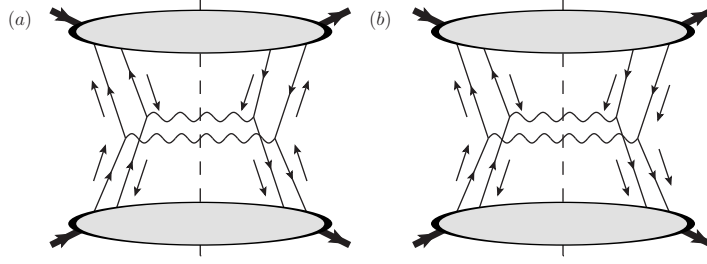


Figure 3.2: Spin interference diagrams that can potentially contribute to the DPS cross section.

simply conserves overall helicity of the diparton systems, then the only kind of interference diagrams that are allowed are ones like figure 3.2(a), in which the spins are swapped between the active partons in going from the left to the right hand side of the figure, and all spins flip direction in going from amplitude to conjugate. The 2pGPDs that are probed in diagrams such as figure 3.2(a) are the ‘double transversity’ distributions (e.g. $\delta q \delta q$). On the other hand if one takes orbital angular momentum into account one can have a contribution from diagrams such as figure 3.2(b) in which only one spin flips direction between amplitude and conjugate – such diagrams probe ‘single transversity’ distributions (e.g. $q \delta q$). The fact that single transversity distributions can be nonzero for finite \mathbf{b} was first noticed in [37] – in [83] it was stated that the (leading part of) such distributions should be zero, but this was based on an argument taken from [85] that only holds for zero transverse parton separation.

On the other hand, explicit calculations performed for the example process of double Drell-Yan [86] indicate that, for this process at least, once one assembles the partonic cross section and 2pGPD factors together and integrates over \mathbf{b} to generate the total cross section, the dependence on single transversity distributions drops out [86]. Furthermore, the contribution to the (differential) cross section associated with double transversity distributions depends on the angle between the plane defined by the leptons emerging from hard process A , and that defined by the leptons emerging from hard process B , in such a way that when one integrates over this angle to obtain the contribution to the total cross section, one obtains zero.

All of the discussion in this section has been in the context of the total DPS cross section and collinear 2pGPDs. If one considers the DPS cross section differential in \mathbf{q}_A and \mathbf{q}_B , and the associated transverse momentum dependent 2pGPDs (as one may in practice need to in order to make predictions that can readily be compared with experiment – see section 1.4), then the situation with regards to spin becomes somewhat more complex.

This is because each TMD 2pGPD contains two additional transverse vectors aside from \mathbf{b} (the average transverse parton momenta \mathbf{k}_1 and \mathbf{k}_2), and we can have additional distributions (or new parts of existing distributions) that quantify the degree to which the spins of the partons are correlated with these, or alternatively combinations of these. An example of a 2pGPD that is only nonzero in the TMD case is the $q\Delta q$ distribution – in the TMD case this measures the correlation between the helicity of one of the partons and the cross product of two of the transverse momentum vectors (note that the three possible cross products one can form from the transverse vectors are linearly dependent, so it suffices to consider only one of them) [37]. Note that the phenomenon of additional distributions appearing when one goes from collinear distributions to TMDs is not limited to the DPS case – it also occurs in the simple SPS case. To give an example, the transversity (single) TMD is nonzero even in an unpolarised proton, and measures the extent to which the parton’s transverse spin is correlated with its transverse momentum [87–90].

3.2.2 Sudakov Suppression of Colour Interference Distributions

Even though there are contributions to the total DPS cross section associated with colour correlations and colour interference effects, it has been shown in [83] (and later also in [33,37]) that the 2pGPDs associated with these effects are suppressed by Sudakov factors. Our intention in this section is to demonstrate this result in a simple and pedagogical fashion, using a method that is rather similar in spirit to the one we used in section 1.3.3.

For simplicity, let us consider the DIS process, so that we only have to concern ourselves with one proton and its constituent partons. Of course, DIS is somewhat different from DPS, but what we need to study in order to prove the result of this section is the behaviour of individual parton ladders when the upright sections are in various colour configurations, and it is easiest to do this within the context of DIS. In DPS, each proton of course provides two parton ladders (after any $1 \rightarrow 2$ ladder splittings). We work in axial gauge in this section so that the leading graphs have the simple ladder structure. Also we suppress parton indices – in the equations below the appropriate parton index should be clear from the context.

Let us start with the parton model picture of DIS, in which a parton-level cross section $\hat{\sigma}$ is convolved with a ‘nonperturbative PDF’ $f(x, \Lambda^2)$ that incorporates all partonic interactions with scales below Λ^2 – this is drawn on the left hand side of figure 3.3. Now let us say that we begin to reconstruct the full QCD picture with the running PDF $f(x, Q^2)$ at leading logarithmic order by adding the perturbative interactions back in. In the axial

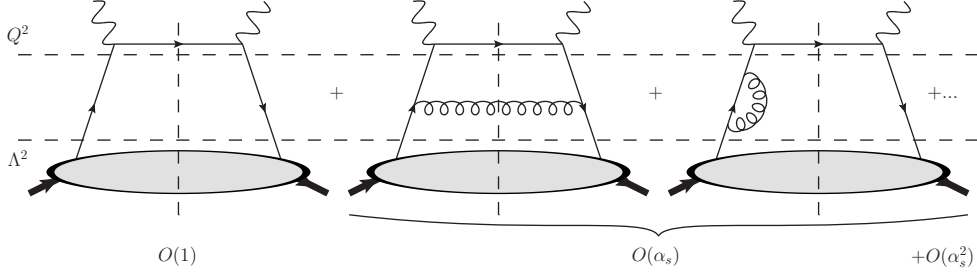


Figure 3.3: Parton model diagram for DIS (left diagram) and $O(\alpha_s)$ perturbative corrections to this picture that are associated with a leading logarithm (two diagrams on the right). Note that we have omitted one diagram that is just the mirror image of the final diagram above.

gauge, the leading $O(\alpha_s)$ corrections (i.e. the ones that also contain a large transverse momentum logarithm) are associated with the two diagrams on the right of figure 3.3. Computing the leading logarithmic parts of these diagrams, we obtain:

$$\sigma = \hat{\sigma}(x) \otimes \left[f(x, \Lambda^2) + \frac{\alpha_s}{2\pi} C_R \int_{\Lambda^2}^{Q^2} \frac{dk^2}{k^2} \int_x^{1-k^2/Q^2} \frac{dx'}{x'} \frac{1+x'^2}{1-x'} f\left(\frac{x}{x'}, \Lambda^2\right) \right. \\ \left. - \frac{\alpha_s}{2\pi} C_V \int_{\Lambda^2}^{Q^2} \frac{dk^2}{k^2} f(x, \Lambda^2) \int_0^{1-k^2/Q^2} dx' \frac{1+x'^2}{1-x'} + O(\alpha_s^2) \right] \quad (3.1)$$

The second term in (3.1) corresponds to the real emission diagram in figure 3.3, whilst the third corresponds to the virtual loop diagram(s). Since we are going to want to investigate what happens with different colour configurations in the ladder, we do not specify the colour factors for the diagrams C_R and C_V at present. Note that we have added an upper cutoff $1 - k^2/Q^2$ to the (divergent) integrals over x' in the second and third terms – we do this because x' values above this cutoff correspond to transverse momenta of the emitted quark (or scales) smaller than Λ , and this region of phase space has already been accounted for in $f(x, \Lambda^2)$ [23,91]. One notices the appearance of the real splitting part of $P_{qq}(x')$, i.e. $(1+x'^2)/(1-x')$, in both the real emission and virtual loop terms.

One could continue to carry out this procedure to all orders, and absorbing all leading logarithmic corrections into a parton distribution $f(x, Q^2)$ we would obtain the LL QCD picture of DIS, with a parton distribution that changes with scale according to the LO DGLAP equation (1.58) (provided that the uprights of the parton ladder are in a colour singlet configuration, as is required in the physical DIS process – see later). However, for the purposes of demonstrating the Sudakov suppression of colour interference ladders

in DPS we are not concerned with the leading logarithmic behaviour of the perturbative corrections, but rather the leading *double logarithmic* behaviour of these corrections. In the second or third term of (3.1), this corresponds to the part of the term where we get one logarithm $\ln(Q^2/\Lambda^2)$ from the transverse momentum integration, and a further logarithm $\ln(Q^2/\Lambda^2)$ from the integration over x' . This part of the term corresponds to the gluon in the accompanying diagram being collinear *and soft*.

Taking only the leading double logarithm parts of the corrections in (3.1), we obtain:

$$\begin{aligned} \sigma = \hat{\sigma}(x) \otimes & \left[f(x, \Lambda^2) + \frac{\alpha_s}{2\pi} C_R \ln^2 \left(\frac{Q^2}{\Lambda^2} \right) f(x, \Lambda^2) \right. \\ & \left. - \frac{\alpha_s}{2\pi} C_V \ln^2 \left(\frac{Q^2}{\Lambda^2} \right) f(x, \Lambda^2) + O(\alpha_s^2) \right] \end{aligned} \quad (3.2)$$

Note that the nonperturbative PDF now appears with the original x value even in the real emission term, since the double logarithmic part of this term corresponds to the emission of a soft gluon that cannot carry away any x .

Summing up the leading logarithmic parts of arbitrarily complex perturbative emission graphs, one obtains the exponential of the $\mathcal{O}(\alpha_s)$ prefactor of $f(x, \Lambda^2)$ in (3.2), multiplied by $f(x, \Lambda^2)$ (for details of the derivation of this exponential factor in the context of QED, see section 6.5 of [17] and references therein):

$$\sigma = \hat{\sigma}(x) \otimes f(x, \Lambda^2) \exp \left[\frac{\alpha_s}{2\pi} (C_R - C_V) \ln^2 \left(\frac{Q^2}{\Lambda^2} \right) \right] \quad (3.3)$$

Let us now consider what happens to the exponential factor when the quark legs forming the uprights of the parton ladder are put into different colour configurations. We start by considering the colour singlet configuration (that in practice is the only configuration allowed for DIS, for reasons discussed in section 3.2.1). The colour flow diagrams for the real and virtual emission processes under this colour configuration are given in figure 3.4(a) – from these diagrams it is clear that the colour factors C_R and C_V are identical and equal to $N/2 - 1/(2N) \equiv C_F$. Then the exponential factor in (3.3) reduces to unity and the expression for σ reduces to the parton model prediction $\sigma = \hat{\sigma}(x) \otimes f(x, \Lambda^2)$. This is exactly what one would expect – in DIS, the scaling predicted by the parton model is only broken by *single* logarithms.

Next we turn to the important case in which the quark legs are in a colour octet configuration – of course this is in practice forbidden in physical DIS, but can occur in

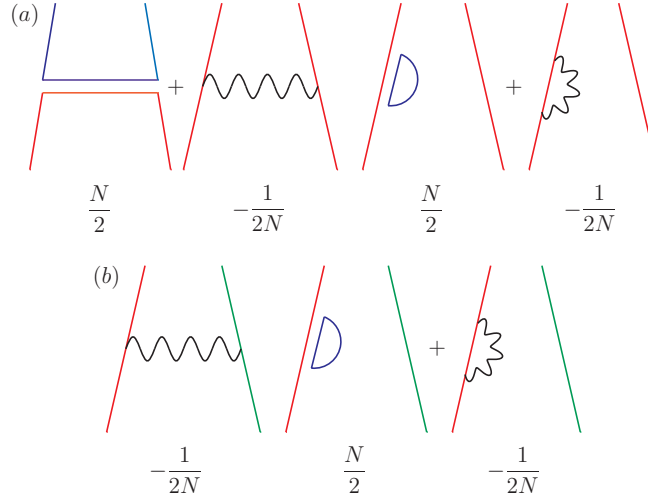


Figure 3.4: Colour flow diagrams and accompanying colour factors for the real gluon emission and virtual gluon loop processes in a quark ladder, when the two quarks are in (a) a colour singlet state, and (b) a colour octet state. The diagrams that just contain coloured lines are the only ones present in a $U(N)$ theory – when going to the $SU(N)$ theory we have to add a $U(1)$ ghost field, represented in the diagrams by a wavy black line, to cancel out the extra $U(1)$ gauge boson from the $U(N)$ theory [92].

DPS ladders for reasons discussed in section 3.2.1, and is associated with colour interference/correlated distributions. The relevant colour flow diagrams in this case are given in figure 3.4(b) – the important point to note is that the virtual diagrams remain more or less unchanged from the colour singlet case (since they only involve one of the quark legs), whilst in the real emission diagrams there is now no longer an analogous diagram to the first real emission diagram in figure 3.4(a). This means that whilst C_V remains the same as in the colour singlet case ($= C_F$), C_R is now negative and equal to $-1/(2N)$. The exponent in (3.3) becomes negative, and suppresses the contribution to the cross section associated with the colour octet ladder (or associated colour interference/correlation distribution) – this is precisely the Sudakov factor that we were looking for.

In physical terms, the Sudakov suppression of colour correlation/interference contributions occurs because such contributions involve a movement of colour by the large transverse distance \mathbf{b} in the hadron between amplitude and conjugate [33]. In our heuristic derivation of the Sudakov factor the low scale cut-off in the factor was Λ^2 – however, it has been argued in [84] that a more appropriate choice for the low scale cut-off should in fact be $1/\mathbf{b}^2$. This makes sense – the Sudakov factor is associated with soft gluons with wavelengths that are nevertheless short enough to resolve the transfer of colour between

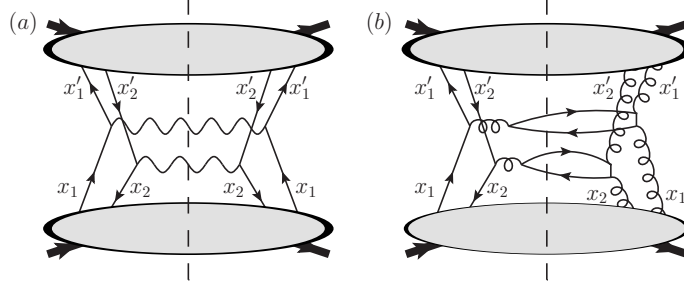


Figure 3.5: Some example diagrams contributing to the DPS cross section in which parton type changes between the amplitude and conjugate.

amplitude and conjugate – therefore for gluon wavelengths longer than $|\mathbf{b}|$, or equivalently scales smaller than $1/\mathbf{b}^2$, the Sudakov suppression should not apply.

Note that in this section we have effectively only shown that the quark colour correlation/interference distributions are Sudakov suppressed. An analogous argument can be used to show that the gluon colour correlation/interference distributions are similarly suppressed, although in the gluon case there is more than one such distribution. To give an example – for the colour octet distribution (either symmetric or antisymmetric) one finds for the real and virtual colour factors $C_V = N$ and $C_R = N/2$ [37]¹, so $C_R - C_V < 0$ once again and this distribution is Sudakov suppressed.

One class of interference diagrams that we did not discuss explicitly in section 3.2.1 but which can nevertheless contribute to the DPS cross section involves the partons with identical x fractions changing type as you go from the left to the right hand side of the diagram. When we say a ‘change in type’ here, we mean the parton changing from one out of the categories (quark, antiquark, gluon) to another choice out of these categories. This is distinct from a simple change in flavour, since the representation of SU(3) colour under which the parton is charged changes between the left and right hand sides of the diagram. Two example ‘type interference’ diagrams are given in figure 3.5 – in figure 3.5(a) the quarks on the left hand side become antiquarks on the right hand side and vice versa (such diagrams were discussed in [33, 36]), whilst in figure 3.5(b) quarks and antiquarks on the left hand side become gluons on the right hand side (such diagrams were discussed in [84]). Such diagrams must also experience a Sudakov suppression – since the partons with corresponding x values are not even in the same colour representation between the left and right hand sides of the diagram, there must be a movement of colour in these diagrams in going from amplitude to conjugate, and an associated Sudakov suppression.

¹Note that in [84] it is incorrectly written that $C_R = -N/2$ in this case.

3.2.3 Conclusions

In this section we demonstrated that there can potentially be contributions to the total DPS cross section associated with interference and correlation effects in colour, spin, flavour and parton type (where by parton type we mean either quark, antiquark or gluon). On the other hand it has been shown for double Drell-Yan [86] that there cannot be a contribution to the DPS cross section associated with single transversity distributions $q\delta q$, and double transversity distributions only contribute to the DPS cross section when one does not integrate over the azimuthal angle between the decay planes associated with the two vector bosons. Furthermore, we found in section 3.2.2 that the contributions to DPS associated with colour correlations or interference are Sudakov suppressed. The same is true for the contributions associated with parton type interference. Note that this section is a pedagogical review of results obtained previously in [33, 36, 37, 83, 84, 86].

Despite it being pointed out long ago in [83] that pp DPS may be affected by interference and correlated parton effects, such effects are rarely considered in phenomenological analyses of the process, and in particular are not taken account of in the dPDF framework of the previous section. Diehl and Schafer have shown using a simple SU(6) three-quark wavefunction that interference and correlation effects are expected to be quite large at large x where valence quarks dominate [36]. ‘Single parton feed’ $1 \rightarrow 2$ perturbative splitting processes give rise to parton pairs with correlated spins and colours (for example, in the $g \rightarrow q\bar{q}$ splitting process, the \bar{q} always has the opposite helicity and the anti-colour of the q), so one expects such processes to increase the importance of correlations. On the other hand, one expects ‘independent branching’ of parton pairs to ‘wash out’ the correlations between the pair. The general expectation appears to be that the interference and correlated parton effects are small at small x [34, 93].

It would be interesting to study this issue in more detail, and obtain some quantitative estimates of the size of the interference and correlated parton contributions. In order to make such estimates one would require some low-scale inputs for the interference and correlated parton two-parton distributions, along with the appropriate evolution framework for these objects. Very approximate forms for the nonperturbative inputs could perhaps be extracted from proton models (see e.g. [94, 95]). Such forms would of course not be reliable at low x owing to the fact that one cannot fit parton densities at low x even at low Q^2 without including a number of ‘nonperturbative’ gluons and sea quarks [96], and proton models typically only include the lowest few Fock states. An alternative approach for obtaining ‘first guess’ inputs for some of the distributions via single-parton GPDs is

given in [36]. We will not pursue the issue of quantitative estimates of interference and correlated parton contributions to DPS further in this thesis, as there are more pressing and fundamental issues at hand (in particular, we will see in the next section that the dPDF framework does not treat even the diagonal unpolarised contribution to DPS correctly, and therefore the question arises as to what the correct theoretical framework to describe DPS is). However, we would like to return to this issue in further work.

3.3 Double Parton Scattering Singularity in One-Loop Integrals

3.3.1 Introduction

A necessary part of any one-loop calculation is the loop integration over the undetermined four-momentum k in each diagram contributing to the process considered. A loop integration will become singular if the 4-dimensional real hypercontour over which the integration is performed becomes pinched by two (or more) poles associated with the denominator factors in the integrand. Such singularities are known as Landau singularities, and they have been studied for some time [97].

The denominator of a one-loop integral is equal to the product of propagator denominators in the associated Feynman diagram, which is independent of the nature of the particles in the diagram (i.e. whether they are spin 0 particles, spin 1/2 particles, spin 1 particles, etc. or a mixture of such particles). Thus, the locations of the Landau singularities in a particular Feynman diagram are independent of the nature of the particles in it. The behaviour of the integral at a singular point can however be affected by the nature of the particles in the diagram, which determines the numerator of the loop integral. If the numerator vanishes at the singular point, then the integral could be less singular than expected there, or even finite.

A relevant example of a one-loop calculation in which Landau singularities are encountered is $gg \rightarrow ZZ$ via massless quark boxes. Three of the six box topologies contributing to this process are sketched in figure 3.6 – the other three only differ by the direction of the arrow in the closed quark loop, and give the same contributions as the boxes drawn.

Apart from mundane threshold singularities, the loops in figure 3.6 contain Landau singularities that are associated with the initial state and loop particles being massless. In fact, all of the diagrams in figure 3.6 contain at least one of these singularities for arbitrary

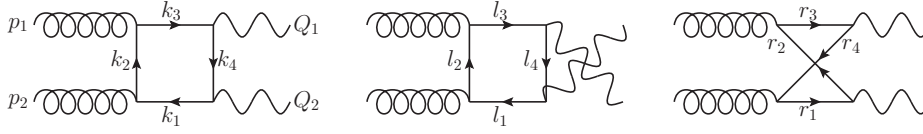


Figure 3.6: Box topologies contributing to $gg \rightarrow ZZ$.

values of the external invariants. Every loop integral contains a collinear singularity (to be more precise, two collinear singularities), which is so named because it is associated with a quark-antiquark pair attached to one of the external gluons becoming on-shell and collinear to that gluon. The first and second loops in figure 3.6 also contain a soft singularity, which is associated with the four-momentum k_2 or l_2 shrinking to zero.

We shall refer to the final box topology in figure 3.6 as the crossed box due to its appearance when drawn with initial states on the left and final states on the right (although, for reasons of clarity, we will not draw it in this way elsewhere in this section – see figure 3.8 for example). This contains a singularity which is not shared with the other two box topologies, and which only appears when the transverse momenta of the final states in the centre of momentum frame, Q_1 and Q_2 , are zero. This singularity is known as the double parton scattering (DPS) singularity [98], and it is associated with all of the loop particles becoming on-shell and collinear with the initial state gluons. The reason why the singularity is known as such is that it corresponds to the physical process in which two gluons each split to produce an on-shell, collinear quark-antiquark pair, and then the four resultant partons interact to produce two Z bosons. The four partons interact in pairs from different gluons in two separate annihilation interactions, which is essentially the definition of a double parton scattering.

None of these singularities are restricted to the box diagrams. The conditions to have a collinear or soft singularity in a one-loop diagram are well-documented [99, 100]. The double parton scattering singularity will occur for any one-loop diagram which satisfies the following criteria. First, the two initial state particles must be massless, and each of these initial state particles should be connected to two loop particles which are also massless. Then, the four massless loop particles should interact in two separate pairs, with particles from different initial state particles interacting. There is no restriction on the final state from each interaction, only that it should have total invariant mass squared which is timelike. Such diagrams will also generically contain collinear singularities.

What is the nature of the DPS singularity in Standard Model loops? The answer to this

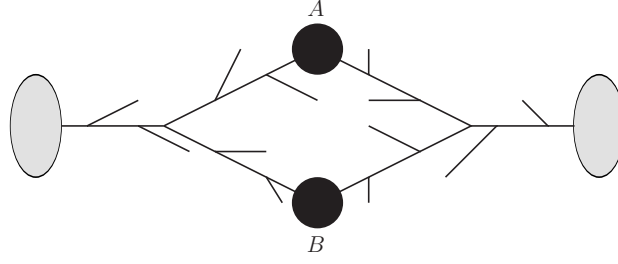


Figure 3.7: A diagram that apparently contributes to the leading order DPS cross section according to the ‘dPDF framework’ (see text). The black circles are hard processes, the grey blobs are protons, and the lines are partons.

question is relevant to the analysis of the dPDF framework that is the topic of this chapter because the dPDF framework anticipates that there should be a $[\log(Q^2/\Lambda^2)]^n/\sigma_{eff}$ structure in the DPS singular part of one-loop diagrams of a particular structure (Λ is a nonperturbative IR cutoff, and Q is the scale of the ‘hard processes’ in the loop – see below). By studying DPS singularities in one loop integrals we can ultimately see whether such a structure is present in the one-loop diagrams, and test the validity of the dPDF framework. In the next few paragraphs we will give the explicit form of the one-loop diagrams that are predicted by the dPDF framework to contain a $[\log(Q^2/\Lambda^2)]^n/\sigma_{eff}$ structure, explain why the dPDF framework predicts that these graphs contain such a structure, and define the value of n for a given graph. Before moving on, however, we note that an understanding of the nature of the DPS singularity in Standard Model loops is also of importance to the NLO multileg community, who need to know where the singularities are in a loop integral, and how bad they are, to ensure (for example) accurate numerical evaluation of the loop integral [98, 101, 102].

Let us consider the calculation of the cross section for a DPS process for which $Q_A = Q_B$ ($A = W^\pm, B = W^\pm$, for example). Then, if we use the dPDF framework to perform the calculation, then the result for the cross section will contain a term which contains the accumulated sPDF feed parts of two dPDFs being multiplied together (the accumulated sPDF feed part of a dPDF is that part generated by perturbative $1 \rightarrow 2$ splittings – it is the part $D_{p(corr)}^{j_1 j_2}$ in the expression (2.11)). Pictorially, the term corresponds to a sum of graphs with the structure of figure 3.7. We shall refer to these graphs as ‘double perturbative splitting’ or ‘1v1’ graphs (where the description ‘1v1’ refers to the fact that the graph is initiated by only one nonperturbative parton per proton).

Since the dPDF framework includes figure 3.7 in the LO DPS cross section, this

framework predicts that the loop process of figure 3.7 should contain a piece which is proportional to $[\alpha_S \log(Q^2/\Lambda^2)]^n/\sigma_{eff}$ at the cross section level (where n is the sum total of branchings that occur on either side of the two hard processes A and B). For such a piece to exist, every branching in the diagram has to be associated with a transverse momentum integration $\int d\mathbf{k}^2/\mathbf{k}^2$ at the cross section level – even the two ‘ $1 \rightarrow 2$ ’ branchings in the diagram that can be distinguished from the others by the fact that they only produce internal particles. The leading log part of the cross section is then associated with the region in which the transverse momenta are strictly ordered along the branchings on either side of the diagram². We naturally expect the $[\alpha_S \log(Q^2/\Lambda^2)]^n/\sigma_{eff}$ piece to be contained within the DPS singular part of the loop, where the transverse momenta and virtualities of the particles emerging from the ‘ $1 \rightarrow 2$ ’ branchings are small.

Looking at results that have been previously obtained for four- and six-point loops within the Standard Model [103–107], it is not clear that such logarithmic structures exist within the cross section expressions for these loops. The impression one gets from these papers is that the DPS singularity in any Standard Model one-loop diagram is in fact entirely cancelled.

In this section, we present a detailed and general study of the DPS singularity in one-loop integrals. To begin with, we only focus on the four-point diagram that can contain a DPS singularity – i.e. the crossed box. In subsection 3.3.2, we present results for the DPS singular parts of certain crossed box diagrams, including several Standard Model diagrams containing an internal fermion loop. Some of these have been extracted from the available literature, whilst others are derived by us – but all are (or have been) obtained using traditional loop integral techniques. We find that in some of the SM crossed box fermionic loop diagrams, the DPS singularity is not completely cancelled, but is instead relegated to an integrable logarithm.

Two questions then immediately arise, the first of which is why the fermionic loop SM boxes have a DPS singularity that is at most a logarithm of Q_2 , and the second of which is whether this behaviour extends to more general SM boxes. It is not efficient to try to answer these questions using traditional loop integral techniques, since such techniques involve calculating the full box integral, whilst we are only interested in the DPS singular

²Note that this prediction is analogous to the (correct) prediction of the single scattering framework that in a single scattering diagram with n initial state parton emissions distributed between the incoming legs, there is a piece of the diagram that is proportional to $[\alpha_S \log(Q^2/\Lambda^2)]^n$ at the cross section level. This piece is associated with the parton emissions on both incoming legs being strongly ordered in transverse momentum, and gets absorbed into the leading order PDFs. We saw this explicitly for the case of a single parton emission in section 1.3.3.

part. Further, we can gain little insight from these techniques as to why a particular box integral has a DPS divergence of a given nature. In subsection 3.3.3 we derive a framework for evaluating the DPS singular part of a crossed box diagram which only requires the calculation of simple leading order light-cone wavefunctions and tree-level matrix elements. Using this framework, we reproduce and provide physical explanations for all of the crossed box results found in subsection 3.3.2. We also give the conditions on a SM crossed box for it to contain a logarithmic DPS singularity (at most).

The framework that we derive for calculating the DPS divergence of a crossed box has the advantage that it is very easily generalised to loops with arbitrary numbers of external particles. In subsection 3.3.4, we use the generalised framework to check and generalise the results of [106,107] for the DPS divergence in six-photon helicity amplitudes. We also use it to determine the structure of the DPS singularity in figure 3.7, and compare the result with the predictions of the dPDF framework. Based on the outcome of this comparison, we make some comments regarding the theoretical validity of the dPDF framework. We also show how our work ties together with the study of the theory of proton-proton DPS performed by Diehl and Schafer [36].

3.3.2 Singularities in the Crossed Box

We consider a generic crossed box diagram with the particle names, momenta and helicities labelled as in figure 3.8 (note that any or all of the helicities could be zero in general). For the moment, we do not specify the nature of the external and loop particles. We do however impose the conditions that are necessary for the crossed box to contain a DPS singularity – namely, that the incoming particles (with momenta p_1 and p_2) should be on-shell and massless, whilst the outgoing particles (with momenta Q_1 and Q_2) should either be on-shell and massive, or off-shell such that Q_1^2 and $Q_2^2 > 0$. For the purposes of calculational simplicity, the squared four momenta of Q_1 and Q_2 shall be taken to be equal in all of the boxes studied. The common four momentum squared $Q_1^2 = Q_2^2$ will be denoted by M^2 . Further, we work at all times in the centre of momentum frame, and choose the z axis to be aligned with the spatial part of p_1 . We define:

$$s \equiv (p_1 + p_2)^2 \quad t \equiv (p_1 - Q_1)^2 \quad u \equiv (p_1 - Q_2)^2 \quad (3.4)$$

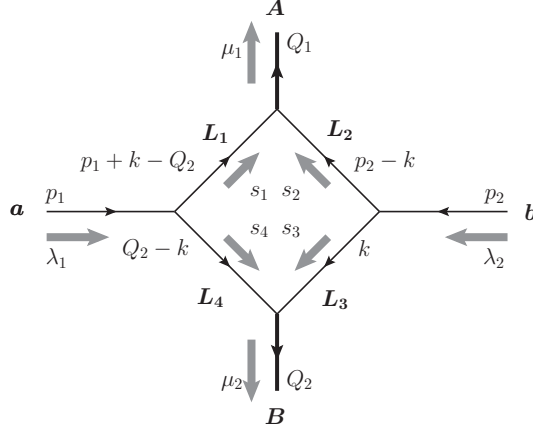


Figure 3.8: The crossed box topology, with annotations that demonstrate our labelling conventions for the particle names, helicity and momenta. The particle names are written in bold in this figure, whilst the helicity labels are accompanied by grey arrows. The arrows on the lines merely indicate the direction of momentum flow, and do not necessarily signify a fermion line. The thin lines represent massless particles, whereas the thick lines represent particles with invariant mass squared equal to M^2 .

The d dimensional loop integral associated with the crossed box has the following generic form:

$$L = \int d^d k \frac{\mathcal{N}}{[k^2 + i\epsilon][(k - Q_2)^2 + i\epsilon][(p_1 + k - Q_2)^2 + i\epsilon][(p_2 - k)^2 + i\epsilon]} \quad (3.5)$$

The nature of the external and loop particles determines the numerator factor \mathcal{N} , but not the denominator. L is defined such that \mathcal{N} only includes the trace structure of the crossed box amplitude, and does not include overall factors such as coupling constants and colour factors. For future reference, we write here the numerator factors for each of the specific crossed boxes that we will consider as examples in this section, and which are drawn in figure 3.9:

$$\mathcal{N} = \begin{cases} \text{Tr}[\not{\epsilon}_{\mu_2}^* \not{k} \not{\epsilon}_{\lambda_1} (\not{p}_2 - \not{k}) \not{\epsilon}_{\mu_1}^* (\not{p}_1 + \not{k} - \not{Q}_2) \not{\epsilon}_{\lambda_2} (\not{Q}_2 - \not{k})] & \text{for Fig 3.9(a)} \\ \text{Tr}[\not{k} \not{\epsilon}_{\lambda_1} (\not{p}_2 - \not{k}) (\not{p}_1 + \not{k} - \not{Q}_2) \not{\epsilon}_{\lambda_2} (\not{Q}_2 - \not{k})] & \text{for Fig 3.9(b)} \\ \text{Tr}[\not{k} (\not{p}_2 - \not{k}) (\not{p}_1 + \not{k} - \not{Q}_2) (\not{Q}_2 - \not{k})] & \text{for Fig 3.9(c)} \\ 1 & \text{for Fig 3.9(d)} \end{cases} \quad (3.6)$$

where ϵ_λ is the polarisation vector corresponding to helicity λ ($\lambda = \pm 1$ for gluons, and

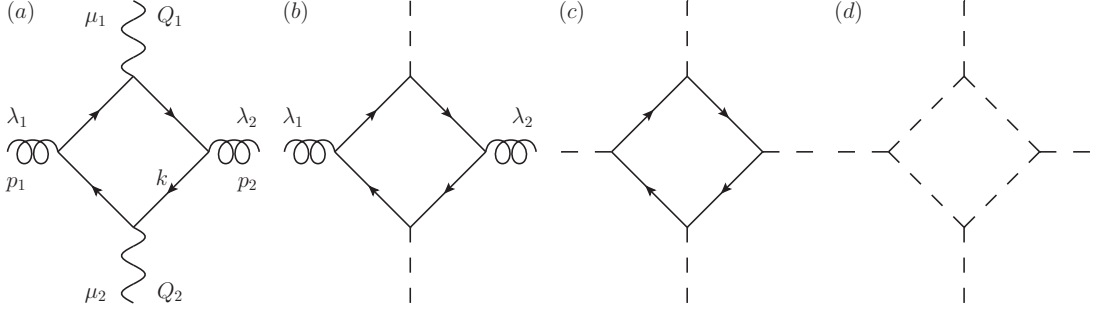


Figure 3.9: The crossed boxes that we shall consider as examples in this section. The helical lines represent gluons, the wavy lines Z bosons, the dashed lines scalars, and the lines with arrows represent fermions.

$\pm 1, 0$ for Z bosons). The numerator factor for figure 3.9(a) written above is of course not the initial expression you would write down, which would contain factors of $v_q + a_q \gamma^5$ before $\not{\epsilon}_{\mu_1}^*$ and $\not{\epsilon}_{\mu_2}^*$ (where we use the notation of [104] – v_q (a_q) is the vector (axial) coupling of the quarks in the loop to Z bosons). However, the terms in this initial expression proportional to $v_q a_q$ cannot contribute to the loop integral according to charge conjugation invariance [104], whilst the terms proportional to v_q^2 and a_q^2 can both be shown to have the trace structure written above (some anticommutation of the γ^5 matrices plus use of $(\gamma^5)^2 = 1$ is required in the latter case). Thus, the numerator of the $gg \rightarrow ZZ$ loop integral is equal to the above trace structure, times some overall coupling constant which we drop.

We recall that a crossed box contains collinear and double parton scattering Landau singularities. In the case of ϕ^3 theory in four dimensions, these nominal singularities both correspond to actual infinite values of the integral. We may calculate the most divergent part of the crossed box in this theory (drawn in figure 3.9(d)) using the elegant method presented in [100], which we briefly reiterate here.

We begin by introducing Feynman parameters and integrating over k in (3.5), giving:

$$L_{\phi,4D} = \Gamma(4 - D/2) \pi^{D/2} i \int_0^\infty dx_1 \cdots dx_N \frac{\delta(\sum_{i=1}^N x_i - 1)}{\Delta^{4-D/2}} \quad (3.7)$$

where:

$$\Delta = \begin{pmatrix} & & & \\ x_1 & x_2 & x_3 & x_4 \end{pmatrix} \begin{pmatrix} 0 & 0 & -t & -M^2 \\ 0 & 0 & -M^2 & -u \\ -t & -M^2 & 0 & 0 \\ -M^2 & -u & 0 & 0 \end{pmatrix} \begin{pmatrix} x_1 \\ x_2 \\ x_3 \\ x_4 \end{pmatrix} - i\epsilon \quad (3.8)$$

Note that we take the number of dimensions D to be equal to $4+2\varepsilon$ ($\varepsilon > 0$) to regulate the collinear divergence which appears for arbitrary values of the kinematic invariants. We now perform the following nonlinear change of variables:

$$x_1 = \sigma\alpha, \quad x_2 = \sigma(1-\alpha), \quad x_3 = \tau\beta, \quad x_4 = \tau(1-\beta). \quad (3.9)$$

The range of the variables is $0 \leq \sigma, \tau < \infty$, $0 \leq \alpha, \beta \leq 1$, and the Jacobian for the transformation is $\sigma\tau$. Under the change of variables (3.9), equation (3.7) factorises:

$$\begin{aligned} L_{\phi,4D} &= \pi^2 i \int_0^\infty d\sigma d\tau \frac{\delta(\sigma + \tau - 1)}{(\sigma\tau)^{1-\varepsilon}} \\ &\times \int_0^1 d\alpha d\beta \frac{1}{[s\alpha\beta + (u - M^2)(\alpha + \beta) - u - i\epsilon]^{2-\varepsilon}} + \dots \end{aligned} \quad (3.10)$$

In the above expression (and in further equations below) we will drop less singular terms which do not contribute to the DPS singularity, and denote them using an ellipsis. The first integral in (3.10) is just the Beta function $B(\varepsilon, \varepsilon)$ producing a collinear divergence. We use:

$$B(\varepsilon, \varepsilon) = \frac{\Gamma(\varepsilon)\Gamma(\varepsilon)}{\Gamma(2\varepsilon)} = \frac{2}{\varepsilon} + \mathcal{O}(\varepsilon) \quad (3.11)$$

to get

$$\begin{aligned} L_{\phi,4D} &= \frac{2\pi^2 i}{\varepsilon} \int_0^1 d\alpha d\beta \frac{1}{[s\alpha\beta + (u - M^2)(\alpha + \beta) - u - i\epsilon]^2} + \dots \\ &= -\frac{2\pi^2 i}{\varepsilon(M^2 - t)(M^2 - u)} \int_0^1 d\alpha \frac{1}{(\alpha - w)(\alpha - a)} + \dots \end{aligned} \quad (3.12)$$

where:

$$\begin{aligned} a &= \frac{M^2}{M^2 - t} + i\epsilon_a, & \epsilon_a &= \frac{\epsilon}{M^2 - t}, \\ w &= \frac{-u}{M^2 - u} - i\epsilon_w, & \epsilon_w &= \frac{\epsilon}{M^2 - u}. \end{aligned} \quad (3.13)$$

Here we have corrected the signs of the imaginary parts of a and w – in equation (4.99) of [100] they are incorrect (which leads to their result for the DPS singular part of the loop integral having the wrong sign). The integral on the second line of (3.12) is straightforwardly done using standard techniques. Only the imaginary part of this integral is divergent in the limit $\mathbf{Q}_2 \rightarrow \mathbf{0}$ (where \mathbf{Q}_2^2 is the transverse momentum squared of the second massive particle), so retaining only this piece, we obtain the following for the DPS singularity in the 4D scalar box:

$$\begin{aligned} L_{DPS,\phi,4D} &= \frac{2\pi^2 i}{\epsilon} \frac{2\pi i}{ut - M^4} \\ &= -\frac{4\pi^3}{s\mathbf{Q}_2^2 \epsilon} \end{aligned} \quad (3.14)$$

In the second line of (3.14) we have made use of the relation $ut - M^4 = s\mathbf{Q}_2^2 (= s\mathbf{Q}_1^2)$. One observes the appearance of a factor $1/\epsilon$ in the expression (3.14) which corresponds to the collinear singularity and is infinite in the limit $\epsilon \rightarrow 0$, and a factor $1/\mathbf{Q}_2^2$ which corresponds to the DPS singularity and is infinite in the limit $\mathbf{Q}_2 \rightarrow 0$. A critical point to note is that the DPS singular part of the 4D scalar crossed box is not integrable – that is, if one takes its modulus squared and integrates it over the final state phase space, then one obtains an infinite contribution to the cross section (the result is proportional to $d\mathbf{Q}_2^2/\mathbf{Q}_2^4$).

In more complex four dimensional theories, there exists the possibility that the collinear and DPS singularities in crossed box integrals may exhibit less singular behaviour, due to the fact that there is now a nontrivial numerator factor \mathcal{N} which may vanish at the singular points. Indeed, this appears to be the case for Standard Model crossed boxes containing a fermionic loop and obeying the appropriate conditions (i.e. $p_1^2 = p_2^2 = 0$, massless particles in the loop, and Q_1^2 and $Q_2^2 > 0$). In such boxes, the collinear divergence vanishes, and the DPS singularity is relegated to a logarithm of \mathbf{Q}_2^2 at most.

Let us give some examples of the logarithmic behaviour of DPS singularities in fermionic loop SM crossed boxes drawing from the established literature. The first example we shall

consider is $gg \rightarrow HH$ via a massless quark loop. Glover and van der Bij have calculated the crossed box integral for this process [103]. However, they only present results for the helicity matrix elements calculated using a general quark mass m_q in the loop. The helicity matrix elements are equal to the sum over loop integrals for the six different loop topologies contributing to $gg \rightarrow HH$, all multiplied by various factors (coupling constants, colour factors). We can nevertheless extract the leading low Q_2 behaviour of a single $gg \rightarrow HH$ crossed box from these results as follows. First, we strip the multiplying factors from the helicity matrix elements to obtain expressions for the loop integrals summed over topologies. This turns out to require extreme care since the authors of [103] have chosen to factor some constants out of their matrix elements and into their expression for $d\sigma/dt$. Then, we take the expansions for the scalar loop integrals in the low m_q limit (found in Appendix B of [104]), insert them into these expressions, and take $m_q \rightarrow 0$ to obtain the sums over loop topologies for the massless quark case³. Such a limit is perfectly well defined since the loop integrals do not contain collinear singularities. Finally, we isolate any low Q_2 divergences in the resulting expressions – these can be equated to twice the leading low Q_2 behaviour of the relevant crossed boxes. The reason for this is that only the crossed box loop integral can contain a DPS singularity, and there are two crossed box topologies that contribute equally to $gg \rightarrow HH$.

Performing this procedure, we find that there are two helicity configurations for which the crossed box diverges as $Q_2 \rightarrow 0$ – these are the $++$ and $--$ configurations. The corresponding leading low Q_2 behaviour of the crossed box integral with either of these helicity configurations is:

$$L_{DPS}(++) = L_{DPS}(--) = -\frac{8M_H^2\pi^3\log(Q_2^2)}{s} \quad (3.15)$$

This result may be directly checked by decomposing the $gg \rightarrow HH$ crossed box loop integral to scalar integrals using `FeynCalc` [109], before inserting the low m_q expansions of the scalar integrals and taking $m_q \rightarrow 0$. We obtain the same expression using this method.

Another example of a crossed box satisfying the appropriate conditions is $gg \rightarrow ZZ$, again via a massless quark loop. Glover and van der Bij have calculated the loop integrals

³An alternative approach would be to insert the dimensionally regulated scalar loop integrals with massless internal lines found in [99]. One has to exercise some care in analytically continuing the results of [99] to the region of present interest however – see the detailed discussion in [108]. Of course, either method gives the same result.

for this process as well [104]. As in the $gg \rightarrow HH$ case, they only present amplitudes summed over all box topologies and for the case of general quark mass – however we can extract the leading low \mathbf{Q}_2 behaviour of the $m_q = 0$ $gg \rightarrow ZZ$ crossed boxes from these results using the same technique as was applied in the $gg \rightarrow HH$ case.

We denote the helicity configuration in a crossed box integral by $\lambda_1 \lambda_2 \mu_1 \mu_2$ where λ_1 and λ_2 correspond to the helicities of gluons 1 and 2, and μ_1 and μ_2 correspond to the helicities of Z bosons 1 and 2. Then only the $++++, -- --, ++ --$ and $-- ++$ integrals are divergent in the limit $\mathbf{Q}_2 \rightarrow 0$:

$$L_{DPS}(++++)=L_{DPS}(----)=\frac{4\pi^3\left[s-2M_Z^2+s\sqrt{1-4M_Z^2/s}\right]\log(\mathbf{Q}_2^2)}{s}\quad(3.16)$$

$$L_{DPS}(++--)=L_{DPS}(--++)=\frac{4\pi^3\left[s-2M_Z^2-s\sqrt{1-4M_Z^2/s}\right]\log(\mathbf{Q}_2^2)}{s}\quad(3.17)$$

Unfortunately we cannot check this result using `FeynCalc` as it requires the Passarino-Veltman reduction [110] of tensor integrals of index 4, which `FeynCalc` cannot handle. We remark in passing that the same results for L_{DPS} are obtained if the final state Z bosons are replaced by off-shell photons (with $Q_1^2 = Q_2^2 = M^2$) or W bosons, except that M_Z in (3.16) and (3.17) should be replaced by M or M_W . The coupling constant factor that multiplies L_{DPS} in the full expression for the amplitude is $(v_q^2 + a_q^2)g_Z^2 g_s^2$ in the $gg \rightarrow ZZ$ case. The coupling constant factor for $gg \rightarrow \gamma^* \gamma^*$ may be obtained from this by setting $v_q = Q_q, a_q = 0$ and replacing g_Z by e , whilst that for $gg \rightarrow W^+ W^-$ is obtained by setting $v_q = -a_q = 1$ and replacing g_Z by $g_w/(2\sqrt{2})$.

Despite assertions to the contrary that exist in the literature [105], some of the fermionic loop SM crossed box loop integrals are divergent in the limit $\mathbf{Q}_2 \rightarrow 0$. They are, however, not sufficiently divergent to cause the cross section for $gg \rightarrow ZZ$ or $gg \rightarrow HH$ to diverge ($\int d\mathbf{Q}_2^2 \log^2(\mathbf{Q}_2^2) = \text{finite}$).

It is interesting to ask whether the phenomenon by which the numerator of the crossed box integral vanishes at the singular point such that the DPS singularity is integrable can only occur in the crossed boxes of gauge theories (such as the Standard Model). To investigate this question, we examined the crossed box loop integral associated with the process $g_s g_s \rightarrow g_s^* g_s^*$ in scalar gluon theory (also known as massless Yukawa theory), where the final state scalars are off-shell by the same timelike amount. The Feynman diagram

corresponding to the integral is figure 3.9(c).

To calculate the leading low \mathbf{Q}_2 behaviour of the $g_s g_s \rightarrow g_s^* g_s^*$ crossed box loop integral, we use two methods. First, we perform the Passarino-Veltman reduction of the integral ‘by hand’ in **Maple** [111], before inserting the expansions of the scalar integrals for small loop particle mass found in [104], and then taking the limit of zero loop particle mass. The other approach involves using **FeynCalc** to perform the Passarino-Veltman reduction. Both approaches return the same result:

$$L_{DPS} = 4\pi^3 \log(\mathbf{Q}_2^2) \quad (3.18)$$

We see that the singular behaviour of this box is exactly the same as the SM fermionic loop boxes – i.e. the DPS singularity becomes an integrable logarithm (and the collinear singularity disappears). This example indicates that we cannot uniquely associate a logarithmic DPS singularity with gauge theories.

Although the scalar crossed box integral in four dimensions has a very different singular behaviour to the SM fermionic loop and Yukawa boxes, the same integral in *six* dimensions (corresponding to 6D ϕ^3 theory) has exactly the same singular behaviour as the 4D SM fermionic loop and Yukawa boxes. We can calculate the most singular part of the 6D scalar box by applying the method found in section 4.6.2 of [100] to $D = 6$. In this case, we do not need to deform the number of dimensions to $D = 6 + 2\epsilon$ since there are no collinear singularities in the integral.

Repeating the steps (4.95)-(4.97) of [100] with $D = 6$, we obtain:

$$L_{DPS,\phi,6D} = \pi^3 i \int_0^1 \frac{d\alpha d\beta}{[s\alpha + u - M^2 - i\epsilon]\beta + [(u - M^2)\alpha - u - i\epsilon]} \quad (3.19)$$

where α and β are Feynman parameters. It is simple to perform the integration over β , which gives:

$$L_{DPS,\phi,6D} = \pi^3 i \int_0^1 \frac{d\alpha}{s\alpha + u - M^2 - i\epsilon} [\ln(s\alpha - M^2 + (u - M^2)\alpha - i\epsilon) - \ln((u - M^2)\alpha - u - i\epsilon)] \quad (3.20)$$

The real part of this integral is finite as $\mathbf{Q}_2 \rightarrow 0$, and so for the purposes of extracting

the leading low Q_2 singularity we can ignore it:

$$\begin{aligned}
 L_{DPS,\phi,6D} &\simeq \pi^3 i \int_0^1 \frac{d\alpha}{s\alpha + u - M^2} [-i\pi\Theta(M^2 - s\alpha - (u - M^2)\alpha) + i\pi\Theta(u - (u - M^2)\alpha)] \\
 &= \frac{2\pi^4 \log(Q_2^2)}{s}
 \end{aligned} \tag{3.21}$$

As asserted, the 6D scalar box has a logarithmic DPS singularity in its crossed box.

There must exist some characteristic that is common to the 6D scalar boxes, 4D scalar gluon boxes, and the SM fermionic loop boxes that ensures that the leading DPS singularity in these boxes is converted from a single inverse power of Q_2^2 to a logarithm (and that the collinear singularity vanishes). Using traditional techniques for handling loops, it is exceedingly difficult to elucidate the mechanism by which this occurs, and to investigate whether more general SM boxes share the same characteristics. The reason for this is that we lose contact with the original structure of the loop integral when we start introducing Feynman parameters (and, in the Yukawa and SM cases, even before this when we perform the Passarino-Veltman reduction). In the next section, we shall introduce a technique for directly calculating the portion of a crossed box loop integral which contains the DPS singular point when $Q_2 = 0$ (i.e. the point at which all of the internal lines go on shell). As the evaluation of the portion of the integral is direct, neither Passarino-Veltman reduction nor introduction of Feynman parameters needs to be performed. By use of this method, we will discover the physical origin of the logarithmic DPS singularity in 6D scalar boxes, 4D scalar gluon boxes, and SM fermionic loop boxes, and give the conditions on a general SM box for it to have a logarithmic DPS singularity (at most).

3.3.3 Physical Investigation of the Crossed Box

We would like to investigate the nature and origin of the part of the amplitude L which is most singular as the transverse momenta of the produced particles go to zero. This part of the amplitude is associated with the region of the loop integration in which the transverse part of the loop variable, \mathbf{k} , is small (i.e. much less than \sqrt{s} and masses of produced particles). The reason for this is that, when the transverse momenta of the produced particles are zero, the small \mathbf{k} region contains the point in which all four of the loop particles go on shell simultaneously.

Therefore we study the contribution to L coming from the small \mathbf{k} region in the case

in which the transverse momenta of the produced particles are also small. The method we use is similar to that described in section V of [112], although we fix some errors and address some subtleties of which the author of [112] did not seem to be aware.

To begin, we apply the lightcone decomposition described in equation A.6 to all of the vectors in (3.5). That is, we define lightlike vectors n and p as follows:

$$p = \frac{1}{\sqrt{2}}(1, 0, 0, 1) \quad n = \frac{1}{\sqrt{2}}(1, 0, 0, -1) \quad (3.22)$$

An arbitrary four vector V may be written in terms of these vectors plus a transverse part \mathbf{V} (which only has x and y components) as follows:

$$V = V^+ p + V^- n + \mathbf{V} \quad (3.23)$$

Writing out all of the four momenta in (3.5) in terms of n , p , and a transverse part, (3.5) becomes:

$$L = \int d^{d-2} \mathbf{k} dk^+ dk^- \frac{\mathcal{N}}{(2k^+ k^- - \mathbf{k}^2 + i\epsilon)[2(k^+ - Q_2^+)(k^- - Q_2^-) - (\mathbf{k} - \mathbf{Q}_2)^2 + i\epsilon]} \times \frac{1}{[2(k^+ + Q_1^+)(k^- - Q_2^-) - (\mathbf{k} - \mathbf{Q}_2)^2 + i\epsilon][2k^+(k^- - Q_1^- - Q_2^-) - \mathbf{k}^2 + i\epsilon]} \quad (3.24)$$

In deriving (3.24), we have used the fact that, in our chosen reference frame for which $p_1 \propto p$, $p_2 \propto n$, conservation of four momentum implies:

$$p_1 = (Q_1^+ + Q_2^+)p \quad p_2 = (Q_1^- + Q_2^-)n \quad (3.25)$$

In the following discussion, an important point to bear in mind is that Q_i^+ and Q_i^- are always positive (provided the masses of the produced particles are not zero).

The part of L that we are interested in is the low \mathbf{k} portion of the integral, which we shall denote as L_{DPS} . Our strategy to evaluate L_{DPS} will be to perform the k^- , k^+ and \mathbf{k} integrals in that order, making copious use of the fact that \mathbf{k} in the integration is small.

The k^- integration is straightforward. When $0 < k^+ < Q_2^+$, only the second k^- pole in the denominator lies on the upper half complex plane, so we close the contour on the upper half plane and pick up the pole at:

$$k_2^- = Q_2^- + \frac{(\mathbf{k} - \mathbf{Q})^2}{2(k^+ - Q_2^+)} \quad (3.26)$$

When $-Q_1^+ < k^+ < 0$, only the third k^- pole in the denominator is located in the lower half complex plane, so in this case we close the contour on the lower half plane and pick up the pole at:

$$k_3^- = Q_2^- + \frac{(\mathbf{k} - \mathbf{Q}_2)^2}{2(k^+ + Q_1^+)} \quad (3.27)$$

Finally, when $k^+ < -Q_1^+$ or $k^+ > Q_2^+$, all of the poles lie on one side of the real axis, so we close the contour on the other side and get zero for the value of the integral. Putting it all together, we find that the result of the k^- integration is the following:

$$\begin{aligned} L_{DPS} = & -2\pi i \int_{|\mathbf{k}| \ll Q_i^+, Q_i^-} d^{d-2} \mathbf{k} \int_{-Q_1^+}^0 dk^+ \frac{\mathcal{N}|_{k^-=k_3^-}}{\left(2k^+ Q_2^- + \frac{k^+(\mathbf{k}-\mathbf{Q}_2)^2}{(k^++Q_1^+)} - \mathbf{k}^2 + i\epsilon\right)} \\ & \times \frac{1}{2(-Q_1^+ - Q_2^+)(\mathbf{k} - \mathbf{Q}_2)^2 \left(-2k^+ Q_1^- + \frac{k^+(\mathbf{k}-\mathbf{Q}_2)^2}{(k^++Q_1^+)} - \mathbf{k}^2 + i\epsilon\right)} \\ & + 2\pi i \int_{|\mathbf{k}| \ll Q_i^+, Q_i^-} d^{d-2} \mathbf{k} \int_0^{Q_2^+} dk^+ \frac{\mathcal{N}|_{k^-=k_2^-}}{\left(2k^+ Q_2^- + \frac{k^+(\mathbf{k}-\mathbf{Q}_2)^2}{(k^+-Q_2^+)} - \mathbf{k}^2 + i\epsilon\right)} \\ & \times \frac{1}{2(Q_1^+ + Q_2^+)(\mathbf{k} - \mathbf{Q}_2)^2 \left(-2k^+ Q_1^- + \frac{k^+(\mathbf{k}-\mathbf{Q}_2)^2}{(k^+-Q_2^+)} - \mathbf{k}^2 + i\epsilon\right)} \end{aligned} \quad (3.28)$$

We note that the terms $k^+(\mathbf{k} - \mathbf{Q}_2)^2/(k^+ + Q_1^+)$ and $k^+(\mathbf{k} - \mathbf{Q}_2)^2/(k^+ - Q_2^+)$ appear in some of the denominator factors. These terms are negligible except where $k^+ \sim -Q_1^+$ or $k^+ = Q_2^+$. However, the region of k^+ which is relevant to the leading \mathbf{Q}_2 singularity in L is $|\mathbf{k}| \ll Q_i^+, Q_i^-$. This is because, when \mathbf{Q}_2 vanishes, the configuration in which all of the loop particles are on shell corresponds to $k = Q_2^- n$ (i.e. $k^+ = 0$). Therefore, for the purposes of finding the leading singularity in L , we can drop the $k^+(\mathbf{k} - \mathbf{Q}_2)^2/(k^+ + Q_1^+)$ and $k^+(\mathbf{k} - \mathbf{Q}_2)^2/(k^+ - Q_2^+)$ terms in the denominator. For similar reasons, we can replace k_2^- and k_3^- by Q_2^- and set $k^+ = 0$ in the numerator. Then, L_{DPS} becomes:

$$\begin{aligned} L_{DPS} \simeq & \frac{2\pi i}{2(Q_1^+ + Q_2^+)} \int_{|\mathbf{k}| \ll Q_i^+, Q_i^-} \frac{d^{d-2} \mathbf{k}}{(\mathbf{k} - \mathbf{Q}_2)^2} \\ & \times \int_{-Q_1^+}^{Q_2^+} dk^+ \frac{\mathcal{N}|_{k^-=Q_2^-, k^+=0}}{(2k^+ Q_2^- - \mathbf{k}^2 + i\epsilon)(-2k^+ Q_1^- - \mathbf{k}^2 + i\epsilon)} \end{aligned} \quad (3.29)$$

Given that $|\mathbf{k}| \ll Q_i^+, Q_i^-$, the integrand of the k^+ integration in (3.29) is strongly peaked near the origin, and falls off rapidly before either of the two endpoints of integration are reached. We can replace the limits of the integration by $\pm\infty$ without affecting the

leading singularity in the integral. This allows us to perform the k^+ integral using contour integration, closing in the lower half plane and picking up the pole at $k^+ = \mathbf{k}^2/(2Q_2^-)$:

$$L_{DPS} \simeq \frac{(2\pi i)^2}{4(Q_1^+ + Q_2^+)(Q_1^- + Q_2^-)} \int_{|\mathbf{k}| \ll Q_i^+, Q_i^-} \frac{d^{d-2} \mathbf{k} \mathcal{N} |_{k^- = Q_2^-, k^+ = 0}}{(\mathbf{k} - \mathbf{Q}_2)^2 \mathbf{k}^2} \quad (3.30)$$

Noticing that $4(Q_1^+ + Q_2^+)(Q_1^- + Q_2^-)$ is simply equal to $2s$, we obtain a compact expression for the leading \mathbf{Q}_2 singularity in L :

$$L_{DPS} \simeq \frac{(2\pi i)^2}{2s} \int_{|\mathbf{k}| \ll Q_i^+, Q_i^-} \frac{d^{d-2} \mathbf{k} \mathcal{N} |_{k^- = Q_2^-, k^+ = 0}}{(\mathbf{k} - \mathbf{Q}_2)^2 \mathbf{k}^2} \quad (3.31)$$

The same result may be obtained by closing the k^+ integration in the upper half plane.

Using (3.31), we can reproduce the leading low \mathbf{Q}_2 behaviour of all of the DPS boxes described in the previous section. To obtain the 4D scalar box result (3.14), we set $\mathcal{N} = 1$ and $d = 4 + 2\epsilon$ (note that, just as in section 3.3.2, we must perform the calculation here in slightly more than 4 dimensions to regulate the collinear divergence in the loop integral):

$$\begin{aligned} L_{DPS, \phi, 4D} &= \frac{(2\pi i)^2}{2s} \int_{|\mathbf{k}| \ll Q_i^+, Q_i^-} \frac{d^{2+2\epsilon} \mathbf{k}}{(\mathbf{k} - \mathbf{Q}_2)^2 \mathbf{k}^2} \\ &\simeq \frac{(2\pi i)^2}{2s} \int \frac{d^{2+2\epsilon} \mathbf{k}}{(\mathbf{k} - \mathbf{Q}_2)^2 \mathbf{k}^2} \\ &= -\frac{4\pi^3}{s\epsilon \mathbf{Q}_2^2} \end{aligned} \quad (3.32)$$

We can expand the domain of integration to infinity because the integrand is strongly peaked at $\mathbf{k} = \mathbf{0}$ when \mathbf{Q}_2 is small. The usual method of Feynman parameters has been used to arrive at the final result.

The form of the integrand in (3.32) makes particularly clear the interplay between the collinear and DPS divergences in the 4D scalar box integral, and their origins. When $\mathbf{Q}_2 \neq 0$, there are effectively two distinct poles in the \mathbf{k} integration, producing an overall logarithmic divergence in the integral. One of these is associated with the loop particles on the right hand side of figure 3.8 becoming collinear ($\mathbf{k} = 0$) whilst the other is associated with the particles on the left hand side becoming collinear ($\mathbf{k} - \mathbf{Q}_2 = 0$). As \mathbf{Q}_2 is reduced to zero, the two poles merge to form a double pole and the divergence in the integral becomes stronger (single inverse power rather than logarithmic). The double pole is now associated with all of the particles in the loop becoming collinear, and the

stronger divergence in the integral is precisely the DPS divergence.

Let us next consider the 6D scalar box:

$$L_{DPS,\phi,6D} = \frac{(2\pi i)^2}{2s} \int_{|\mathbf{k}| \ll Q_i^+, Q_i^-} \frac{d^4 \mathbf{k}}{(\mathbf{k} - \mathbf{Q}_2)^2 \mathbf{k}^2} \quad (3.33)$$

From this expression, we can clearly see that the 6D scalar box does not possess any collinear divergences.

In the 6D case, we cannot straightforwardly apply the method of extending the integration region to infinity that we used in the 4D case. The reason for this is that the integrand no longer falls away sufficiently quickly as $|\mathbf{k}| \rightarrow \infty$, and we would get infinity if we extended the integration region.

We could evaluate the integral (3.33) by imposing a sharp cutoff Λ on the integration over $|\mathbf{k}|$, where $|\mathbf{Q}_2| \ll \Lambda \ll Q_i^+, Q_i^-$. However, in practical terms it is simpler to use dimensional regularisation to extract the leading low \mathbf{Q}_2 behaviour in $L_{DPS,\phi,6D}$. We evaluate the integral in $6 - 2\varepsilon$ dimensions – this allows us to extend the integration region to infinity without getting an infinite result. The previously infinite contribution from the high \mathbf{k} end of the integral now manifests itself as a term containing a single pole in $1/\varepsilon$. This can simply be dropped, since we only want the contribution from the low \mathbf{k} end of the integral. Indeed, we discard every term except for the most singular term in \mathbf{Q}_2 . As is typical, the dimensional regularisation approach is conceptually more difficult to handle – but it produces the same result as the sharp cut-off for the leading singularity in \mathbf{Q}_2 .

Applying the method, we obtain a result which agrees with (3.21):

$$L_{DPS,\phi,6D} = \frac{(2\pi i)^2}{2s} \int \frac{d^{4-2\varepsilon} \mathbf{k}}{(\mathbf{k} - \mathbf{Q}_2)^2 \mathbf{k}^2} - \text{UV pole} \simeq \frac{2\pi^4 \log(\mathbf{Q}_2^2)}{s} \quad (3.34)$$

It turns out that we must use the dimensional regularisation method to evaluate the integral (3.31) for the Yukawa $g_s g_s \rightarrow g_s^* g_s^*$, SM $gg \rightarrow HH$ and SM $gg \rightarrow ZZ$ cases as well. We evaluated the numerator factors for these integrals using FORM [113]. The results of the calculations are listed below – for the $gg \rightarrow HH$ and $gg \rightarrow ZZ$ cases, we only list results for the helicity amplitudes which give a nonzero result for L_{DPS} (i.e. are divergent in the limit $\mathbf{Q}_2 \rightarrow 0$):

Yukawa $g_s g_s \rightarrow g_s^* g_s^*$:

$$L_{DPS} = \frac{(2\pi i)^2}{2s} \int \frac{d^{2-2\epsilon} \mathbf{k} \text{Tr}[(Q_2^- \gamma^+ - \not{\mathbf{k}})(Q_1^- \gamma^+ + \not{\mathbf{k}})(Q_1^+ \gamma^- - \not{\mathbf{k}} + \not{Q}_2)(Q_2^+ \gamma^- + \not{\mathbf{k}} - \not{Q}_2)]}{(\mathbf{k} - \mathbf{Q}_2)^2 k^2} \quad (3.35)$$

– UV pole

$$\simeq 4\pi^3 \log(\mathbf{Q}_2^2)$$

SM $gg \rightarrow HH$:

$$L_{DPS}(++) = L_{DPS}(--) \simeq - \frac{8M_H^2 \pi^3 \log(\mathbf{Q}_2^2)}{s} \quad (3.36)$$

SM $gg \rightarrow ZZ$:

$$L_{DPS}(++++) = L_{DPS}(----) = \frac{4\pi^3 \left[s - 2M_Z^2 + s\sqrt{1 - 4M_Z^2/s} \right] \log(\mathbf{Q}_2^2)}{s} \quad (3.37)$$

$$L_{DPS}(++--) = L_{DPS}(--++) = \frac{4\pi^3 \left[s - 2M_Z^2 - s\sqrt{1 - 4M_Z^2/s} \right] \log(\mathbf{Q}_2^2)}{s}$$

The results (3.35)-(3.37) agree with those presented in section 3.3.2, both in terms of dependence on kinematical variables, and in terms of the numerical prefactors.

In the numerator factor of each of these box integrals, the terms with the smallest number of powers of \mathbf{k} and/or $\mathbf{k} - \mathbf{Q}_2$ are proportional to $\mathbf{k} \cdot (\mathbf{k} - \mathbf{Q}_2)$ – the coefficients of the terms with lower powers of \mathbf{k} and/or $\mathbf{k} - \mathbf{Q}_2$ are all zero. A consequence of the numerators having this structure is that the leading \mathbf{Q}_2 singularity in each amplitude is demoted from a single inverse power of \mathbf{Q}_2 to a logarithm. A further consequence is that the amplitudes are free from collinear singularities.

Let us consider the broad features of the method that we have just introduced for isolating the low \mathbf{Q}_2 singularity of a box. It consists of performing two sequential integrations over the full real axis, picking up the contribution from exactly one pole each time, and then performing the integration over \mathbf{k} . Picking up the contribution for a particular pole is equivalent to replacing the denominator factor corresponding to the pole by a delta function ($\times 2\pi i$). Essentially, our method is equivalent to replacing the k^2 and $(k - Q_2)^2$ factors in the denominator by $2\pi i \delta(k^2)$ and $2\pi i \delta[(k - Q_2)^2]$ respectively, before

multiplying by -1 . We then neglect all the numerator terms during the \mathbf{k} integration other than the ones with the lowest powers of \mathbf{k} and/or $\mathbf{k} - \mathbf{Q}_2$, such that we pick up the leading singularity in \mathbf{Q}_2 . It is not hard to show the equivalence explicitly:

$$\begin{aligned}
& - (2\pi i)^2 \int d^d k \frac{\mathcal{N}}{[(p_1 + k - Q_2)^2 + i\epsilon][(p_2 - k)^2 + i\epsilon]} \delta(k^2) \delta((k - Q_2)^2) \\
&= - (2\pi i)^2 \int d^{d-2} \mathbf{k} dk^+ dk^- \frac{\mathcal{N}}{[(p_1 + k - Q_2)^2 + i\epsilon][(p_2 - k)^2 + i\epsilon]} \\
&\quad \times \frac{1}{2k^-} \delta\left(k^+ = \frac{\mathbf{k}^2}{2k^-}\right) \frac{1}{2[(k^+ - Q_2^+) - (k^- - Q_2^-)k^+/k^-]} \delta\left(k^- = Q_2^- + \frac{(\mathbf{k} - \mathbf{Q}_2)^2}{2(k^+ - Q_2^+)}\right) \\
&= (2\pi i)^2 \int d^{d-2} \mathbf{k} dk^+ dk^- \frac{\mathcal{N}}{2s\mathbf{k}^2(\mathbf{k} - \mathbf{Q}_2)^2} \delta\left(k^+ = \frac{\mathbf{k}^2}{2k^-}\right) \delta\left(k^- = Q_2^- + \frac{(\mathbf{k} - \mathbf{Q}_2)^2}{2(k^+ - Q_2^+)}\right) \\
&\quad + \text{higher order in } \mathbf{Q}_2 \\
&= \frac{(2\pi i)^2}{2s} \int d^{d-2} \mathbf{k} \frac{\mathcal{N}_{k^+=0, k^-=Q_2^-}}{\mathbf{k}^2(\mathbf{k} - \mathbf{Q}_2)^2} + \text{higher order in } \mathbf{Q}_2
\end{aligned} \tag{3.38}$$

It should not be a surprise that the leading \mathbf{Q}_2 singularity of a box can be obtained by replacing the k^2 and $(k - Q_2)^2$ denominator factors by delta functions. Notice that the leading \mathbf{Q}_2 singularity always appears in the real part of L . This corresponds to the imaginary part of a box amplitude \mathcal{M} since L is always multiplied by $-i$ (along with vertex factors etc.) to make an amplitude. But we can obtain the imaginary part of an amplitude by using the Cutkosky rules [114, 115]. Thus, twice the real part of L is given by minus the sum over all cuts for which the cut propagators may be put on shell (the minus comes from the fact that $\mathcal{M} \propto -iL$). There are two such cuts for the box diagram, which we have drawn in figure 3.10. They give equivalent contributions in the small \mathbf{k} and $\mathbf{k} - \mathbf{Q}_2$ limit, with both contributions being equal to minus (3.38). Putting everything together, we see that the Cutkosky rules predict that the leading \mathbf{Q}_2 singularity in the real part of L (= the leading singularity in L) is given by (3.38).

Inserting the values for d and \mathcal{N} for the 6D scalar, 4D Yukawa, and 4D Standard Model crossed boxes into (3.38), one might get the impression that the real parts of the loop integrals L for these boxes are all ultraviolet divergent. It is well-known that an ultraviolet divergence exists in the 4D Yukawa and Standard Model crossed boxes – however, this occurs in the imaginary part, as can be verified by examining the loop integral expressions in the large k limit, and remembering that a factor of i appears during Wick rotation. What we have not written down explicitly in (3.38), but is easy to show, is that for large \mathbf{k} both delta functions cannot be satisfied simultaneously. Therefore the

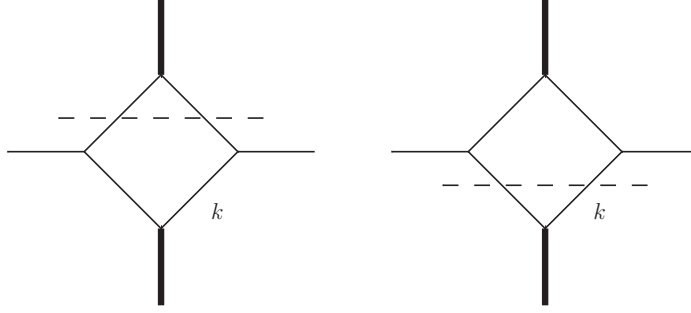


Figure 3.10: The two cuts of the crossed box that can give rise to on-shell particles.

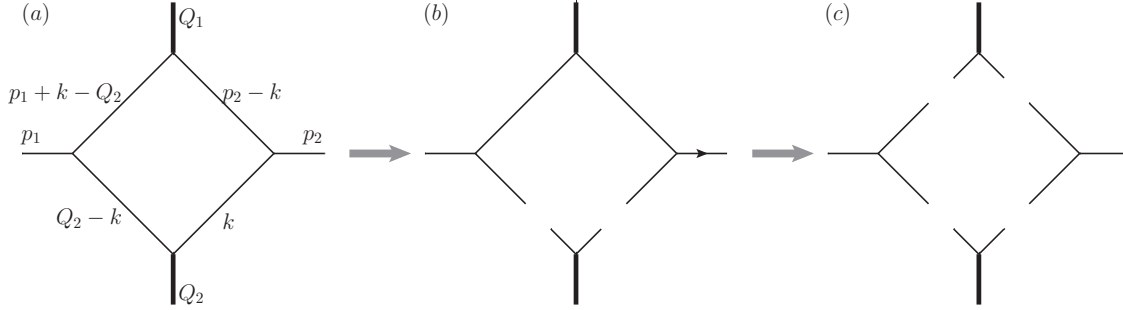


Figure 3.11: Decomposition of the box integrand.

integral is effectively cut off at large \mathbf{k} and the real part of L for any crossed box is UV finite. The appropriate integration region in \mathbf{k} space for the real part of L is an ellipse with the foci at $\mathbf{0}$ and \mathbf{Q}_2 and semi-minor axis length $M/2$. This approximates to a circle of radius $M/2$ centred at the origin when \mathbf{Q}_2 is small.

In the presence of the two delta functions, the remainder of the integrand in (3.38) can be decomposed into two factors, corresponding to the two Feynman diagrams of figure 3.11(b). Given that the lines with momentum $p_1 + k - Q_2$ and $p_2 - k$ are almost on shell when \mathbf{k} and $\mathbf{k} - \mathbf{Q}_2$ are small, we can use completeness relations to further decompose the upper diagram of figure 3.11(b) into three smaller diagrams (divided by two propagator factors) – see figure 3.11(c). This procedure is very similar to, say, the textbook decomposition of the matrix element for $e^- X \rightarrow \gamma Y$ into $e^- \rightarrow \gamma e^-$, $e^- X \rightarrow Y$ (divided by a propagator factor) in the collinear limit (see Chapter 17 of [17]).

Applying the decomposition of figure 3.11, the leading low \mathbf{Q}_2 divergence of a general crossed box may be written as follows (recall that our labelling conventions are given in

figure 3.8):

$$\begin{aligned}
L_{DPS}(\lambda_1 \lambda_2 \mu_1 \mu_2) = & \sum_{s_i, L_i} \int d^d k \delta(k^2) \delta((k - Q_2)^2) \Phi_{b \rightarrow L_2 L_3}^{\lambda_2 \rightarrow s_2 s_3}(p_2; p_2 - k, k) \\
& \times \Phi_{a \rightarrow L_1 L_4}^{\lambda_1 \rightarrow s_1 s_4}(p_1; p_1 + k - Q_2, Q_2 - k) \mathcal{M}_{L_3 L_4 \rightarrow B}^{s_3 s_4 \rightarrow \mu_2}(k, Q_2 - k; Q_2) \\
& \times \mathcal{M}_{L_1 L_2 \rightarrow A}^{s_1 s_2 \rightarrow \mu_1}(p_1 + k - Q_2, p_2 - k; Q_1)
\end{aligned} \tag{3.39}$$

$\Phi_{a \rightarrow bc}^{\lambda \rightarrow s_1 s_2}$ is essentially the light-cone wavefunction to find the pair bc with helicities $s_1 s_2$ inside the particle a with helicity λ [116]. Each of these functions in (3.39) is composed from three ingredients – the matrix element from the relevant Feynman diagram in figure 3.11(c), the denominator of the propagator factor nearest to this diagram in figure 3.11(b), and one further factor R . The last factor is equal to the square rooted ratio of the collinear momentum fractions of the upper and lower outgoing particles in the relevant Feynman diagram. In the spirit of [17], the matrix elements in the Φ factors of (3.39) should be evaluated using the following approximate expressions for the loop vectors:

$$\begin{aligned}
k &= Q_2^- n + \mathbf{k}; & Q_2 - k &= Q_2^+ p - (\mathbf{k} - \mathbf{Q}_2) \\
p_1 + k - Q_2 &= Q_1^+ p + (\mathbf{k} - \mathbf{Q}_2); & p_2 - k &= Q_1^- n - \mathbf{k}
\end{aligned} \tag{3.40}$$

$\mathcal{M}_{L_3 L_4 \rightarrow B}^{s_3 s_4 \rightarrow \mu_2}$ is the matrix element for the ‘hard process’ in which the pair $L_3 L_4$ with helicities $s_3 s_4$ interact to make particle B with helicity μ_2 . Given that we are only interested in extracting the leading \mathbf{Q}_2 singularity of L_{DPS} , it is actually acceptable to evaluate this ingredient of (3.39) with all transverse momenta set to zero.

It should be pointed out that the formula (3.39) only strictly applies when the masses of A and B are equal. The reason for this is that to introduce the R factors which are a part of the Φ functions into the box integrand, we have used the fact that R for the left hand Φ is the reciprocal of the R for the right hand Φ . Then we can introduce the R functions via $1 = R_{left} R_{right}$. This relation only actually holds when $M_A = M_B$. In the more general case in which M_A is not necessarily equal to M_B , there will be a prefactor equal to M_B/M_A in front of (3.39).

From our experience of the QCD light cone wavefunction, we can say that $\Phi_{a \rightarrow bc}^{\lambda \rightarrow s_1 s_2}$ will in general factorise into two parts, one of which is only dependent on the transverse momentum of b relative to a , and the other of which is only dependent on the collinear

fraction of the momentum of a that is carried by b . So, for $\Phi_{a \rightarrow L_1 L_4}$ for example:

$$\Phi_{a \rightarrow L_1 L_4}^{\lambda_1 \rightarrow s_1 s_4}(p_1; p_1 + k - Q_2, Q_2 - k) = X_{a \rightarrow L_1 L_4}^{\lambda_1 \rightarrow s_1 s_4} \left(\frac{Q_1^+}{Q_1^+ + Q_2^+} \right) K_{a \rightarrow L_1 L_4}^{\lambda_1 \rightarrow s_1 s_4}(\mathbf{k} - \mathbf{Q}_2) \quad (3.41)$$

The factor X in (3.41) can be interpreted as the square root of the real splitting part of a helicity dependent splitting function. In scalar field theory, the function $K_{\phi \rightarrow \phi\phi}(\mathbf{k})$ is simply the $1/\mathbf{k}^2$ coming from the propagator denominator since the splitting matrix element is proportional to 1 in this theory. On the other hand, the K functions for QCD, QED and scalar gluon theory only diverge like $1/\mathbf{k}$ for small \mathbf{k} when all of the external particles are physically polarised (this is always the case for scalar gluon theory). The reason for this is that all of the $1 \rightarrow 2$ splittings with physically polarised external particles in these theories are forbidden in the absolute collinear limit, due to nonconservation of J_z . This means that the splitting matrix elements must all be proportional to \mathbf{k} , which goes together with the $1/\mathbf{k}^2$ from the propagator denominator to produce a $1/\mathbf{k}$ dependence for $K(\mathbf{k})^4$. In QED/QCD, J_z is not conserved for the $g/\gamma \rightarrow q\bar{q}$ collinear splitting because the initial state must have helicity ± 1 , and the vector nature of the theory forces the quark and antiquark in the final state to have opposite helicities (i.e. total $J_z = 0$). In scalar gluon theory, J_z is not conserved for the $g_s \rightarrow q\bar{q}$ collinear splitting because the initial state has helicity 0, and the structure of the theory in this case forces the outgoing fermions to both have the same helicity (i.e. total $J_z = \pm 1$).

Recall that we can consider \mathcal{M} as being independent of \mathbf{k} , since we can calculate it in the limit in which \mathbf{k} is zero. Thus, ignoring \mathcal{M} and the X parts of Φ in (3.39), which will only contribute to the prefactor of the leading \mathbf{Q}_2 divergence in L_{DPS} , we can write L_{DPS} schematically as:

$$L_{DPS}(\lambda_1 \lambda_2 \mu_1 \mu_2) \sim \sum_{s_i} \int d^{d-2} \mathbf{k} K_{a \rightarrow L_1 L_4}^{\lambda_1 \rightarrow s_1 s_4}(\mathbf{k} - \mathbf{Q}_2) K_{b \rightarrow L_2 L_3}^{\lambda_2 \rightarrow s_2 s_3}(-\mathbf{k}) \quad (3.42)$$

It is clear from this equation that if $K(\mathbf{k})$ is proportional to $1/\mathbf{k}^2$, then the DPS singularity in L can at most be proportional to $1/\mathbf{Q}_2^2$ in four dimensions (or a logarithm of \mathbf{Q}_2^2 in six dimensions), whilst if $K(\mathbf{k})$ is proportional to $1/\mathbf{k}$, the DPS singularity cannot be stronger than a logarithm of \mathbf{Q}_2^2 . We can use this statement along with the

⁴Note that this behaviour of $K(\mathbf{k})$ when the external particles are physically polarised is intimately related with the fact that QCD, QED and scalar gluon theory ‘parton distributions’ experience logarithmic scaling violations [17, 116].

behaviour of $K(\mathbf{k})$ in various theories above to explain why the DPS singularity in the 4D scalar crossed box $\propto 1/Q_2^2$, whilst the DPS singularities in the 6D crossed box, 4D scalar gluon box, and SM fermionic loop boxes cannot be stronger than a logarithm of Q_2^2 . We can also use it to make the important statement that any SM crossed box in which the initial-state and loop particles are restricted to have physical polarisations cannot have a DPS singularity that is stronger than a logarithm of Q_2^2 . In practice this corresponds to a physical gauge choice for any massless gauge fields appearing in the loop.

For the process $g \rightarrow q\bar{q}$, we present below explicit expressions for the functions Φ for all possible helicity configurations. Overall numerical prefactors are omitted in these expressions – we give only the dependence on the transverse momentum of the quark \mathbf{k} and the collinear fraction of the gluon's momentum that goes to the quark x :

$$\begin{aligned}\Phi_{g \rightarrow q\bar{q}}^{+\rightarrow+-}(x, \mathbf{k}) &\propto x(\epsilon^+ \cdot \mathbf{k})/\mathbf{k}^2 & \Phi_{g \rightarrow q\bar{q}}^{+\rightarrow-+}(x, \mathbf{k}) &\propto (1-x)(\epsilon^+ \cdot \mathbf{k})/\mathbf{k}^2 \\ \Phi_{g \rightarrow q\bar{q}}^{-\rightarrow-+}(x, \mathbf{k}) &\propto x(\epsilon^- \cdot \mathbf{k})/\mathbf{k}^2 & \Phi_{g \rightarrow q\bar{q}}^{-\rightarrow+-}(x, \mathbf{k}) &\propto (1-x)(\epsilon^- \cdot \mathbf{k})/\mathbf{k}^2\end{aligned}\quad (3.43)$$

ϵ^+ (ϵ^-) is the transverse part of the polarisation vector with positive (negative) helicity along the gluon direction.

The unpolarised and polarised $g \rightarrow q$ splitting functions divided by \mathbf{k}^2 are formed from appropriate linear combinations of the mod squares of these Φ functions:

$$\sum_{\lambda, s_1, s_2} |\Phi_{g \rightarrow q\bar{q}}^{\lambda \rightarrow s_1 s_2}|^2 \propto \frac{x^2 + (1-x)^2}{\mathbf{k}^2} \propto \frac{P_{qg}(x)}{\mathbf{k}^2} \quad (3.44)$$

$$\sum_{\lambda, s_1, s_2} \lambda \frac{s_1}{|s_1|} |\Phi_{g \rightarrow q\bar{q}}^{\lambda \rightarrow s_1 s_2}|^2 \propto \frac{x^2 - (1-x)^2}{\mathbf{k}^2} \propto \frac{\Delta P_{qg}(x)}{\mathbf{k}^2} \quad (3.45)$$

Let us consider the box integral (3.39) for the process $gg \rightarrow AB$ via a massless quark loop (with A and B arbitrary final states) and ignore the \mathcal{M} and X functions in (3.39) which do not depend on \mathbf{k} . If the two initial state gluons have the same helicity, then in the limit $Q_2 = 0$ this integral looks like $\int d^2\mathbf{k}(\epsilon^{+z} \cdot \mathbf{k})(\epsilon^{-z} \cdot \mathbf{k})/\mathbf{k}^4$ ($\epsilon^{+z} = (1, i)$ and $\epsilon^{-z} = (1, -i)$). This is logarithmically divergent. On the other hand, when the gluon helicities are opposite, we get $\int d^2\mathbf{k}(\epsilon^{\pm z} \cdot \mathbf{k})(\epsilon^{\pm z} \cdot \mathbf{k})/\mathbf{k}^4$ which evaluates to zero. Thus, the $gg \rightarrow AB$ fermionic loop crossed box will not contain a logarithmic DPS singularity if the initial state gluons have opposite helicities. It is important to emphasise that this statement is totally independent of the final states AB . Note that this general rule is

obeyed for the case of the $gg \rightarrow ZZ$ and $gg \rightarrow HH$ crossed boxes – see (3.36) and (3.37).

The physical explanation for this phenomenon is as follows. The vector nature of the QCD theory forces the $q\bar{q}q\bar{q}$ intermediate state in the crossed box process $gg \rightarrow q\bar{q}q\bar{q} \rightarrow AB$ (which is essentially real in the collinear limit) to have total $J_z = 0$ in the collinear limit. Then, if the initial state gluons have opposing helicities $J_z = \pm 2$, there is an issue with total J_z nonconservation aside from local J_z nonconservation at each $g \rightarrow q\bar{q}$ vertex. This manifests itself as a further suppression of the $gg \rightarrow AB$ box integral numerator in the limit $\mathbf{k}, \mathbf{Q}_2 \rightarrow 0$, which makes the integral convergent.

If the final state particles AB have spin, then there is one further way in which a $gg \rightarrow AB$ fermionic loop crossed box can become convergent in the limit $\mathbf{Q}_2 = 0$ contrary to naive expectations. If the helicities of A and B are such that there is no assignment of helicities to the internal lines which simultaneously conserves helicity at the $g \rightarrow q\bar{q}$ vertices, and conserves J_z at the $q\bar{q} \rightarrow A$ and $q\bar{q} \rightarrow B$ vertices in the collinear limit, then the crossed box integral will not contain a DPS singularity. The extra numerator suppression in the limit $\mathbf{k}, \mathbf{Q}_2 \rightarrow 0$ comes from one or both of the factors \mathcal{M} in this case. This rule can be seen to hold in the case $gg \rightarrow ZZ$.

We can make some sense of the prefactors in (3.35) - (3.37) in terms of products of square roots of helicity dependent splitting functions using our decomposition (3.39). Where the factors \mathcal{M} are nonzero, they can only be proportional to M regardless of the final state. We also find $\int d^4k \delta(k^2) \delta((k - Q_2)^2) \propto \int d^2\mathbf{k} / M^2$ for small \mathbf{k}, \mathbf{Q}_2 . Taking $d = 4$ in L_{DPS} :

$$L_{DPS}(\lambda_1 \lambda_2 \mu_1 \mu_2) \propto \sum_{s_i, L_i} X_{g \rightarrow L_1 L_4}^{\lambda_1 \rightarrow s_1 s_4}(x) X_{g \rightarrow L_2 L_3}^{\lambda_2 \rightarrow s_2 s_3}(1-y) \delta_{L_1 L_2 \rightarrow A}^{s_1 s_2 \rightarrow \mu_1} \delta_{L_3 L_4 \rightarrow B}^{s_3 s_4 \rightarrow \mu_2} \quad (3.46)$$

$$\times \int d^2\mathbf{k} K_{g \rightarrow L_1 L_4}^{\lambda_1 \rightarrow s_1 s_4}(\mathbf{k} - \mathbf{Q}_2) K_{g \rightarrow L_2 L_3}^{\lambda_2 \rightarrow s_2 s_3}(-\mathbf{k})$$

where $\delta_{L_1 L_2 \rightarrow A}^{s_1 s_2 \rightarrow \mu_1}$ is simply a function that is equal to 1 if J_z is conserved in the ‘hard process’ producing final state A , and zero otherwise. Here x is defined to be equal to $Q_1^+ / (Q_1^+ + Q_2^+)$ and $y = Q_2^- / (Q_1^- + Q_2^-)$. Since we have taken the masses of A and B equal and work in the centre of mass frame, $Q_1^+ = Q_2^-$, $Q_1^- = Q_2^+$, and $y = x$.

It is clear that the second line of (3.46) provides the factor of $\log(\mathbf{Q}_2^2)$, whilst the first line provides the prefactor that depends on M and s . Without loss of generality, let us take $Q_1^+ > Q_1^-$, $Q_2^- > Q_2^+$ – i.e. we take A to be the final state particle that travels along the $+z$ axis in the collinear limit.

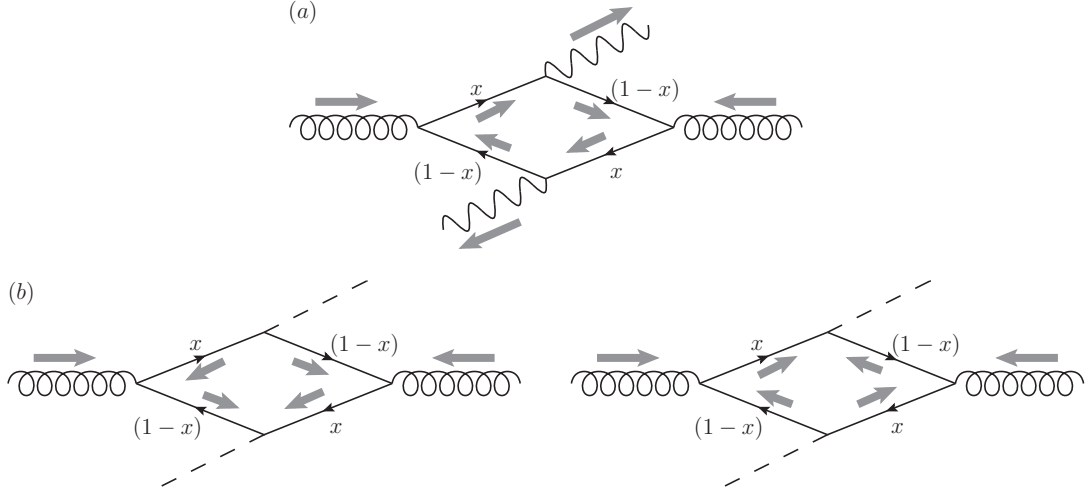


Figure 3.12: Possible configurations of internal helicity for the $gg \rightarrow AB$ crossed box in the collinear limit, where we have taken $Q_1^+ > Q_1^-, Q_2^- > Q_2^+$, both initial state gluons have positive helicity, and the final state is (a) a pair of Z bosons with positive helicity (b) a pair of Higgs bosons. Note that the permitted internal helicity configurations would be the same for both (a) and (b) if the helicities of the gluons were both negative instead.

Consider the $++++$ helicity configuration for the $gg \rightarrow ZZ$ box. In the collinear limit there is only one possible assignment of helicities to the internal lines which is permitted by the structure of the theory and conserves J_z at the hard processes. This is presented in figure 3.12(a). In this diagram, the internal lines with positive helicity both have collinear momentum fraction of parent equal to x . Bearing this in mind, and using the formulae (3.43), we see that the prefactor of the $++++$ crossed box must be proportional to x^2 , which in turn is proportional to $(s - 2M_Z^2 + s\sqrt{1 - 4M_Z^2/s})/s$.

This process can be repeated for all other processes and helicity configurations. The internal helicity configuration is the same for the $gg \rightarrow ZZ -- ++$ process – looking at (3.43) we can then clearly see that the prefactor must be proportional to $(1-x)^2 \propto (s - 2M_Z^2 - s\sqrt{1 - 4M_Z^2/s})/s$. For the $gg \rightarrow HH$ diagram, the two possible arrangements of internal helicities are always the same regardless of the gluon helicities (figure 3.12(b)). For both of these arrangements, the internal lines with the same helicity always have complementary momentum fractions (this is different from the $gg \rightarrow ZZ$ case, in which internal lines with the same helicity always have the same momentum fraction). As a result of this, the prefactor for the $gg \rightarrow HH$ process is proportional to $x(1-x) \propto M_H^2/s$. Finally, the $g_s \rightarrow q\bar{q}$ light cone wavefunctions do not contain any dependence on x (a consequence of this being that P_{qg_s} does not depend on x [117]), so the prefactor of the

$g_s g_s \rightarrow g_s^* g_s^*$ crossed box does not contain any dependence on s or M .

Actually, we can also justify the prefactor for the 6D scalar box (3.34) using the framework of (3.39). For the 6D scalar case \mathcal{M} is now independent of M , so the equivalent expression to (3.46) in this case has a prefactor of $1/M^2$, besides having $d^2 \mathbf{k}$ replaced by $d^4 \mathbf{k}$ and all helicity labels removed. As there are no complications involving spin for 6D scalar theory, we can straightforwardly associate the function $X_{\phi \rightarrow \phi \phi}(x)$ with the square root of the real splitting part of the $\phi \rightarrow \phi$ splitting function in 6D ϕ^3 theory, which is given by $P_{\phi \phi}(x) \propto x(1-x)$ [55]. Putting everything together, we find that the prefactor for the crossed box in 6D ϕ^3 theory is proportional to $x(1-x)/M^2 = 1/s$.

It is not hard to show that equation (3.46) continues to hold even when the masses of A and B are not equal, although one has to bear in mind that x is not necessarily equal to y in general. It is easy to use this expression (or the scalar 4D/6D equivalent) to generalise the results (3.32) - (3.37) to arbitrary masses for A and B . We only write down one of these generalisations here – $gg \rightarrow AB$, where A and B are scalars – and leave the others as exercises for the reader. The $\log \mathbf{Q}_2^2$ prefactors of the DPS divergent graphs in this case ($++$ and $--$) are identical and proportional to $x(1-y) + y(1-x) \propto (M_A^2 + M_B^2)/s$. The two terms in this result are associated with the two diagrams of figure 3.12(b).

Let us consider the part of the $pp \rightarrow AB + X$ cross section associated with two gluons splitting almost collinearly into quark and antiquark pairs, and then these pairs interacting to form A and B . Suppressing helicity and colour indices:

$$\sigma_{pp \rightarrow gg \rightarrow AB+X, DPS}(s) = \int dX d\bar{X} f_g(X) f_g(\bar{X}) \hat{\sigma}_{gg \rightarrow AB, DPS}(\hat{s} = sX\bar{X}) \quad (3.47)$$

$$\begin{aligned} \hat{\sigma}_{gg \rightarrow AB, DPS}(s) &\propto \frac{1}{s} \int d^4 q_1 d^4 q_2 \delta(q_1^2 - M^2) \delta(q_2^2 - M^2) \delta^{(4)}(q_1 + q_2 - p_1 - p_2) \\ &\times |L_{DPS, gg \rightarrow AB}|^2 \end{aligned} \quad (3.48)$$

By decomposing L_{DPS} according to (3.39) and (3.41), and then making a few substitutions for the integration variables in (3.47), (3.48), one finds that one can bring (3.47) into the form of a double parton scattering cross section expressed in terms of the two-parton

GPDs Γ of [36]:

$$\begin{aligned} \sigma_{pp \rightarrow gg \rightarrow AB+X, DPS} &\propto \int \prod_{i=1}^2 dx_i d\bar{x}_i \hat{\sigma}_{q\bar{q} \rightarrow A}(\hat{s} = x_1 \bar{x}_1 s) \hat{\sigma}_{q\bar{q} \rightarrow B}(\hat{s} = x_2 \bar{x}_2 s) \\ &\times \int \frac{d^2 \mathbf{r}}{(2\pi)^2} \Gamma_{q\bar{q}|g \rightarrow q\bar{q}}(x_1, x_2, \mathbf{r}) \Gamma_{q\bar{q}|g \rightarrow q\bar{q}}(\bar{x}_1, \bar{x}_2, -\mathbf{r}) \end{aligned} \quad (3.49)$$

The Γ factors in (3.49) are ‘perturbative splitting’ \mathbf{r} -space $g \rightarrow q\bar{q}$ two-parton GPDs, as defined in section 12 of [36]. Equation (3.49) is somewhat schematic, in that our full result (and the full expression for $\sigma_{pp \rightarrow gg \rightarrow AB+X, DPS}$ in [36]) is actually a sum over terms containing helicity- and colour-dependent cross sections and helicity- and colour-dependent two-parton GPDs in which the 2pGPDs are either both diagonal or both off-diagonal in helicity and colour space. We have such a sum of terms because, from the point of view of the quarks, there is a diagonal ‘unpolarised’ contribution in helicity and colour space, plus polarised and interference contributions (essentially for reasons that are summarised in section 3.2.1). The same formula (3.49) is obtained for the close-to-collinear part of the $pp \rightarrow gg \rightarrow AB + X$ cross section if the masses of A and B are not equal.

Thus, we have shown that the expression obtained by Diehl and Schafer for the $pp \rightarrow gg \rightarrow AB + X$ crossed box process, which they obtained using a pure DPS viewpoint, can also be obtained starting from the conventional ‘Feynman rules’ expression for the $gg \rightarrow AB$ box, and the standard expression for the SPS cross section. In the process we have demonstrated to what part of the full $pp \rightarrow gg \rightarrow AB + X$ one-loop cross section the Diehl-Schafer expression corresponds (i.e. the DPS singular part of the crossed box).

Let us consider the part of the integral (3.49) that is associated with the magnitude of the imbalance \mathbf{r} being smaller than some small cut-off Λ that is of the order of Λ_{QCD} . The contribution to the cross section from this portion contains a $\log^2(M^2/\Lambda^2)$ factor multiplied by Λ^2 (which can be thought of as an effective ‘ $1/\sigma_{eff}$ ’ factor for this contribution). The majority of this contribution comes from the region in which the transverse momenta and virtualities of the quarks and antiquarks in the $gg \rightarrow AB$ loop are much smaller in magnitude than M (i.e. the region in which the assumptions used to derive (3.49) apply), which is a necessary feature of a contribution to be able to regard it as a DPS-type contribution. By making a specific choice of Λ (let us call this Λ_S), one could obtain an expression which is exactly in accord with the expectations of the dPDF framework – that is, a product of two large DGLAP logarithms multiplied by the same $1/\sigma_{eff}$

factor that appears in ‘2v2’ diagrams in which the parton pair from neither proton has arisen as a result of one parton perturbatively splitting into two. The $1/\sigma_{eff}$ factor for the 2v2 diagrams presumably has a natural value of the order of $1/R_p^2$ that is set by the nonperturbative dynamics (R_p = proton radius).

The fact that we have to make a somewhat arbitrary choice for Λ in order to arrive at the result anticipated by the dPDF framework is concerning. There is nothing in the calculation of the $gg \rightarrow AB$ crossed box to indicate that we should take the region of it with $|\mathbf{r}| < \Lambda_S$ as the ‘DPS part’ – the scale Λ_S does not naturally appear at any stage of the calculation. There is no more justification for taking the part of the box with $|\mathbf{r}| < \Lambda_S$ to be the DPS part than there is for, say, taking the piece with $|\mathbf{r}| < 2\Lambda_S$, or that with $|\mathbf{r}| < \Lambda_S/2$, to be the DPS part. We have had to artificially introduce the cut-off Λ_S in figure 3.7 in order to obtain a power-suppressed DPS part because there is no scale in the graph apart from Q^2 , so in order to obtain a term proportional to $1/Q^2$, a second scale has to be introduced ‘by hand’⁵.

There therefore appear to be some unsatisfactory features of the dPDF framework with regards to its treatment of the crossed box. Since no natural scale of order Λ_{QCD} appears in the crossed box calculation which one could use to separate out a natural DPS part, it is perhaps the case that we should not regard any of the box as DPS. Treating the box in this way has the advantage that we do not perform any double counting between DPS and SPS – the $gg \rightarrow AB$ box is of course already included in the SPS $pp \rightarrow AB$ cross section.

One can gain some insight into the source of the problems in the framework of [6] by looking at the \mathbf{b} -space 2pGPD corresponding to $\Gamma_{q\bar{q}}|_{g \rightarrow q\bar{q}}(x_1, x_2, \mathbf{r})$. This comes out as being proportional to $1/\mathbf{b}^2$ – this behaviour (which was first spotted in [36]) can be traced to the fact that the $g \rightarrow q\bar{q}$ light cone wavefunction in \mathbf{b} space (like any light cone wavefunction corresponding to a QCD perturbative splitting with physically polarised external particles) is proportional to $1/\mathbf{b}$, and $\Gamma(\mathbf{b}) \sim \Phi(\mathbf{b})^2$. Note that this behaviour is very different from the \mathbf{b} -dependence of all 2pGPDs that is anticipated by the dPDF framework (i.e. smooth function of size R_p). There is no natural feature in the product of two ‘perturbative splitting’ 2pGPDs that has transverse radius $\sim R_p$ and can be naturally identified as DPS. A key error then in the formulation of the dPDF framework is the assumption (1.75) that all 2pGPDs can be approximately factorised into dPDFs and smooth transverse functions of size R_p .

⁵This is related to the fact that in massless perturbation theory, there are no power corrections.

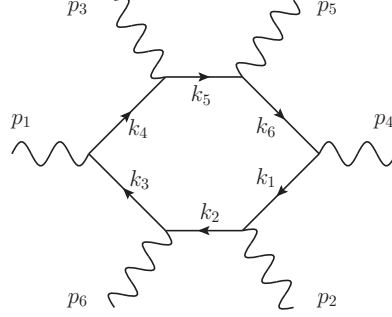


Figure 3.13: The six-photon loop diagram.

3.3.4 DPS singularity in Loops with More Than Four Legs

An example of a loop diagram with more than four legs which contains a DPS singularity is the six-photon amplitude displayed in figure 3.13. For the diagram to contain a DPS singularity, we must take the initial state particles to be the photons with momenta p_1 and p_4 , whilst the remaining particles are in the final state. All of the external particles are taken to be on-shell (i.e. $p_i^2 = 0$). The DPS singularity occurs when the total transverse momentum \mathbf{P}_Σ of photons 3 and 5 (or equivalently 2 and 6) becomes zero. It is associated with the point in the loop integration at which k_1 and k_6 become collinear with p_4 , whilst k_3 and k_4 become collinear with p_1 .

The first result for a six-photon helicity amplitude, summed over loop topologies, was obtained by Mahlon [118] for the MHV helicity configuration. Since then, numerical techniques have been developed for performing the loop integration for arbitrary values of the external momentum and helicity [98, 101, 102] and analytical expressions for all of the six photon helicity amplitudes have been obtained in [119, 120]. In [106, 107], the behaviour of an MHV and an NMHV helicity amplitude (in particular the latter) close to a DPS singular point is investigated. The helicity configuration in the MHV amplitude is $- + + - + +$, whilst that for the NMHV amplitude is $- - - + + +$ (the ordering of the helicities here corresponds to the numbering of the external momenta, and all helicities are defined relative to incoming external momenta). Detailed plots are presented in [106, 107] illustrating the approach of the NMHV amplitude to the following phase space point satisfying $\mathbf{P}_\Sigma = 0$:

$$\begin{aligned} \vec{p}_2 &= (-33.5, -15.9, -25.0) & \vec{p}_3 &= (-12.5, 15.3, 22.0) \\ \vec{p}_5 &= (12.5, -15.3, -0.3) & \vec{p}_6 &= (33.5, 15.9, 3.3) \end{aligned} \quad (3.50)$$

The values given above for each photon are the (x, y, z) components of the four momentum – the remaining t component is fixed by the on shellness condition. The momenta \vec{p}_1 and \vec{p}_4 are taken to be along the positive and negative z axis respectively.

The conclusion drawn from the plots is that the NMHV amplitude is finite at the DPS singular point, at least for the configuration of external momenta (3.50). It is also inferred that the MHV amplitude is finite at the singular point, from the fact that the amplitude does not contain any sharp structure when the Nagy-Soper final state momentum configuration [98] is rotated around the y axis (with some rotation angles corresponding to quite a close approach to the DPS singular point). It is implied in [107] that this behaviour is somewhat surprising, given that simple power counting arguments indicate that the amplitude should diverge at the DPS singular point as $1/\mathbf{P}_\Sigma^2$ (similar to (3.14)).

The loop decomposition technique developed in the last section can be very straightforwardly applied to the present situation, to check the results of [106,107] and investigate in more generality the low \mathbf{P}_Σ behaviour of the six-photon amplitude. One thing we can say straight away, bearing in mind our experience with the fermionic loop box integrals and noting that the loops under consideration are of the same character (only with initial-state gluons replaced with photons, which in the present context behave in exactly the same way), is that the DPS divergence in the six-photon amplitude can be no worse than a logarithm of \mathbf{P}_Σ . Thus there is certainly no danger of the $2\gamma \rightarrow 4\gamma$ cross section being infinite.

We can actually reproduce the results of [106,107] without doing any further calculations. The DPS singularity in a particular $-++-++$ MHV diagram will cancel when we add on all other loop topologies which have their DPS singularity in the same place. The reason for this is that when we decompose all of these topologies according to (3.39), and then add all of the decomposed integrals together, then one finds that one can extract two factors from the result which are equal to the full tree-level matrix element for $q\bar{q} \rightarrow \gamma\gamma$ (i.e. the sum of both possible Feynman diagrams). This is, of course, not unexpected. For the MHV helicity configuration considered the helicity of both final state photons in these matrix elements will be the same. But it is well known that the amplitude for a quark and an antiquark to produce two photons with the same helicity is zero (see for example [121]). So the leading DPS singularity in the $-++-++$ MHV diagram goes to zero – i.e. the amplitude is convergent.

The $---++$ NMHV amplitude cannot contain a DPS singularity simply because

the J_z of the initial state is not equal to zero. We showed in the last section that a crossed box loop integral with two gluons in the initial state does not contain a DPS singularity unless the total J_z of the gluons is equal to zero. This result obviously generalises to any one-loop fermionic loop integral that can potentially contain a DPS singularity, and still applies when the initial state gluons are swapped for photons. Thus, the DPS singularity in the NMHV amplitude vanishes on a diagram by diagram basis.

Note that these results serve as a generalisation of the results of [106, 107] to the case of arbitrary initial and final state momenta. Aside from using our loop decomposition framework to do this, we can also use it to make some interesting statements about the singular behaviour of the other NMHV and MHV amplitudes. First, we can say that no NMHV six-photon amplitude can ever contain a logarithmic DPS singularity. The reason for this is that, however one distributes the helicities, one always ends up either with the initial state photons having opposite helicities, or with one of the pairs of the final state photons having the same helicity. On the other hand, there are MHV amplitudes that do have logarithmic DPS singularities – for example, the $+- - + ++$ configuration.

We saw in section 3.3.1 that the dPDF framework predicts that there should be a portion of the arbitrary ‘double perturbative splitting’ graph in figure 3.7 which is proportional to $[\alpha_s \log(Q^2/\Lambda^2)]^n$ at the cross section level, where n is the sum total of branchings in the diagram. To be more precise, it predicts that there is a part of this diagram which at the cross section level is proportional to $1/\sigma_{eff} \times [\alpha_s \log(Q^2/\Lambda^2)]^n$, where σ_{eff} is the ‘universal’ σ_{eff} of (1.76) that is supposedly shared between diagrams in which neither parton pair is generated perturbatively, diagrams where only one is, and diagrams where both are.

Applying the loop decomposition technique of section 3.3.3 to this arbitrary loop, and using a physical gauge for the gluons in the loop for simplicity, one finds that there does exist a portion of the cross section integral for this diagram which has the required structure. This portion corresponds to the region of integration in which the transverse momentum imbalance between the loop momentum in the amplitude and that in the conjugate, \mathbf{r} , satisfies $|\mathbf{r}| < \Lambda_S$ (Λ_S is defined at the end of section 3.3.3), and the transverse momenta of branchings on either side of the diagram are strongly ordered.

Just as we found for the simple crossed box, so too is it true for a general loop that there is no natural reason why one should demarcate precisely the region of the cross section integration with $|\mathbf{r}| < \Lambda_S$ as DPS. That is, there appear to be unsatisfactory features in the dPDF framework treatment of very general diagrams of the structure of

figure 3.7. Since there is no part of a general ‘double perturbative splitting’ graph that can be naturally identified as a DPS part, it is perhaps appropriate to remove such diagrams from the DPS cross section entirely, and consider them as pure SPS. Just as in the simple box case, this choice has the advantage that we do not perform any double counting between DPS and SPS – the graph of figure 3.7 is in principle also included in the SPS $pp \rightarrow AB$ cross section (albeit as a very high order correction that will not be included in practical low order calculations, if the number of QCD emissions from inside the loop of the graph is large).

Very similar conclusions may be reached if one uses a covariant gauge such as the Feynman gauge for the gluon fields in figure 3.7, although these conclusions are perhaps not obtained so readily. In a covariant gauge, gluons with unphysical ‘scalar’ polarisation can exist in loop diagrams. Such scalar-polarised gluons can give rise to power-law DPS divergences rather than logarithmic ones, and additional ‘super-leading’ contributions to the AB production process (in terms of powers of Q) – the two phenomena are related. On the other hand one generally expects the ‘super-leading’ contribution to cancel in a suitable sum over graphs (as in [122]), which effectively leaves one with the same logarithmic DPS divergences that are encountered in a physical gauge.

It is worth pointing out in passing that there is a double scattering process that appears to directly involve the dPDF of the proton. This is the contribution to proton-heavy nucleus DPS associated with partons from two separate nucleons interacting with two partons from the proton. The reason why this probes the dPDF is that in this case the ‘probe’ parton pair coming from the nucleus has a (roughly) flat distribution in \mathbf{b} , such that in the cross section formula the proton 2pGPD is uniformly integrated over \mathbf{b} to give the dPDF. For more details and a discussion of how the two-nucleon contribution to proton-heavy nucleus DPS might be extracted experimentally, see [123, 124].

3.3.5 Conclusions

In this section, we have demonstrated that the DPS singular part of any one-loop diagram of the appropriate structure may be simply expressed in terms of the transverse momentum integral of two light cone wavefunctions and two hard matrix elements. An explicit derivation of this expression was given for the four-point case, but it is clear that such an expression will continue to be applicable for larger numbers of external particles.

A naive treatment of Standard Model one-loop diagrams initiated by QED/QCD vertices connected to massless particles indicates that the DPS singularities in these diagrams

should be of the same strength as those in the corresponding diagrams with scalars – i.e. $1/\mathbf{p}_T^2$, where \mathbf{p}_T is the transverse momentum sum of all of the final state particles on one of the loop lines extending between the initial state particles. Using our expression for the DPS singularity, we have shown that SM loops cannot have a DPS singularity that is stronger than a logarithm of \mathbf{p}_T^2 provided that the initial-state particles and loop particles emerging from them are restricted to have physical polarisations. In practice this corresponds to a physical gauge choice for any of these loop particles that are massless gauge fields. There is clearly a suppression of the numerator in such loops at the DPS singular point which causes their DPS singularity to go from $1/\mathbf{p}_T^2$ to $\log(\mathbf{p}_T^2)$. This is associated with J_z nonconservation in, and therefore suppression of, any SM $1 \rightarrow 2$ massless particle splitting in which the external particles are physically polarised.

We exploited our framework to show that an arbitrary one-loop diagram initiated by gluons/photons with fermions running around the loop does not contain a DPS singularity if the total J_z of the initial state is not zero. The physical reason for this is that the total J_z of the $f\bar{f}f\bar{f}$ intermediate state in the loop, which becomes real at the DPS singular point, is constrained to have $J_z = 0$ at the DPS singular point by the vector nature of QED/QCD. If initial $J_z \neq 0$ there is then an issue of total J_z nonconservation (aside from local J_z nonconservation at each vertex), which suppresses the loop numerator further at the DPS singular point and completely removes the DPS singularity. The DPS singularity in a given diagram in which the initial state particles and loop particles emerging from them are restricted to have physical polarisations will also disappear if one or both of the hard matrix elements happen to vanish in the limit of collinear, on-shell initial state particles.

These general principles were applied to explain why the $gg \rightarrow ZZ$ and $gg \rightarrow HH$ box integrals only contain logarithmic DPS divergences for certain configurations of the external helicity. In both cases, a necessary condition for the box to have a DPS divergence is that the gluons should have the same helicity (ensuring total $J_z = 0$). In the $gg \rightarrow ZZ$ case, the Z bosons must have the same helicity otherwise there is no configuration of internal helicity which ensures J_z conservation at both $q\bar{q} \rightarrow Z$ vertices in the collinear limit, and the DPS singularity vanishes. It was shown that the prefactors of $\log(Q^2)$ in the diagrams with DPS divergences could be rationalised as the products of square rooted helicity dependent splitting functions (the prefactors of the scalar gluon and 6D ϕ^3 boxes could also be understood in this way).

We also applied our general rules to explain why the particular MHV and NMHV

six-photon amplitudes discussed in [106, 107] contain no DPS divergence. The MHV amplitude does not contain a DPS divergence since its hard matrix elements correspond to diagrams in which a $q\bar{q}$ pair go to two photons of the same helicity, which are zero according to the MHV rules for QED. There is no DPS divergence in the NMHV amplitude because the total J_z of the initial state is not zero. We pointed out that no NMHV six-photon diagram can ever contain a DPS divergence, whilst there are MHV helicity amplitudes that do contain a DPS divergence.

The ‘dPDF framework’ for describing proton-proton DPS anticipates that there should be a natural part of the ‘double perturbative splitting’/‘1v1’ diagram in figure 3.7 that is proportional to $\log(Q^2/\Lambda^2)^n/R_p^2$, where n is the total number of QCD branching vertices in the diagram, and R_p is the proton radius. This part should be associated with the transverse momenta inside the loop being strongly ordered on either side of the diagram. By using our method to investigate the DPS singular structure of figure 3.7, we established that there is no natural part of the graph that has this structure (in fact, most of the contribution to the total cross section expression for the graph comes from the region of integration in which the transverse momenta of particles inside the loop are of $\mathcal{O}(\sqrt{Q^2})$). The dPDF framework therefore appears to be unsatisfactory, at least with regards to its treatment of 1v1 diagrams. Based on our findings, we suggested that no part of the 1v1 graphs should be included in the pp DPS cross section – rather they should be entirely considered as SPS. The root of the problem in the dPDF framework is its assumption that any 2pGPD can be approximately factorised into a longitudinal piece and a smooth transverse function with a width of order R_p , which is not valid.

Chapter 4

The Double Parton Scattering Cross Section

The contents of this chapter are based on the original research paper [125].

4.1 Introduction

In the previous chapter, we carefully examined ‘double perturbative splitting’/‘1v1’ graphs – diagrams with the structure of figure 4.1(c). We argued that no part of these diagrams should be included as part of the leading order proton-proton (pp) DPS cross section, contrary to the prescription of a long-established framework for calculating the pp DPS cross section [4–6].

In light of this discovery, a careful re-analysis of other classes of graph that can potentially contribute to the LO DPS cross section would seem appropriate. In this chapter we will pay particular attention to graphs in which there is only a single $1 \rightarrow 2$ perturbative ladder branching, such as that drawn in figure 4.1(b) (we’ll also discuss to a certain extent ‘2v2’ graphs such as 4.1(a) in which there are no perturbative $1 \rightarrow 2$ ladder branchings, although it should be reasonably clear that these should be included in the LO DPS cross section). We’ll refer to graphs in which there is only a single perturbative splitting as ‘2v1’ graphs.

In section 4.2, we will begin to address the issue of whether contributions from the 2v1 graphs should be included in the LO DPS cross section, and what form these contributions should take. We’ll do this using a similar strategy as we employed for the 1v1 graphs in the previous chapter. That is, we’ll take a 2v1 graph with the simplest possible structure

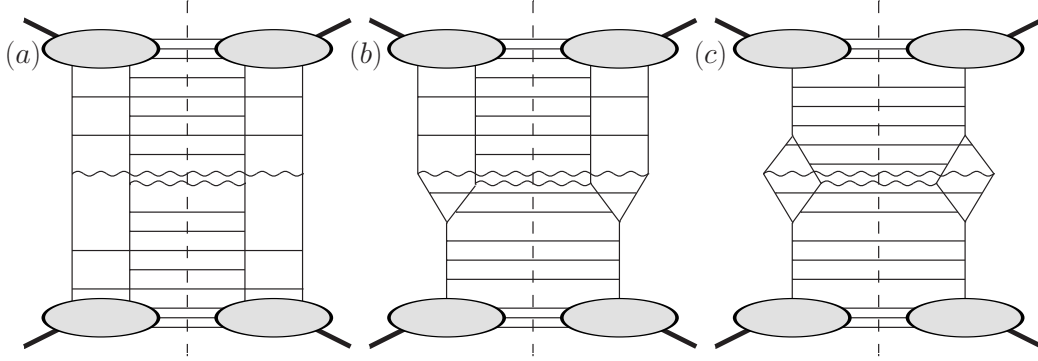


Figure 4.1: Some types of graph that can potentially contribute to the DPS cross section. The partons emerging from the grey proton blobs are nonperturbatively generated partons – i.e. ones existing at a low scale $\sim \Lambda_{QCD}$.

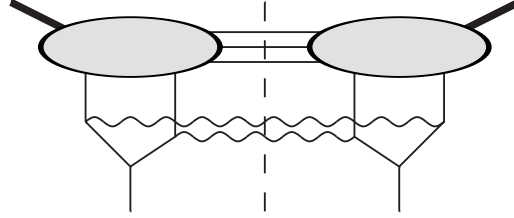


Figure 4.2: The simplest structure possible for the 2v1 graph.

(i.e. the structure of figure 4.2) and see whether there is a ‘natural’ part of the cross section expression for it that is proportional to $1/R_p^2$, and also contains a large logarithm associated with the $1 \rightarrow 2$ splitting. The large logarithm should be associated with transverse momenta of the partons emerging from the $1 \rightarrow 2$ splitting being $\ll Q^2$ (where we take $Q_A^2 = Q_B^2 \equiv Q^2$ for simplicity). If there is such a structure in the 2v1 graph, then this part of this graph should be included in the LO DPS cross section. Furthermore, if there is a $\log(Q^2/\Lambda^2)/R_p^2$ structure in the simplest 2v1 diagram, then we expect there to be a $\log(Q^2/\Lambda^2)^n/R_p^2$ piece in the more general 2v1 diagram of figure 4.1(b) that should also be included in the LO DPS cross section. This will be associated with the branchings in the diagram being strongly ordered in transverse momentum. From the structure of the contribution to the LO DPS cross section coming from the simplest 2v1 diagram, we’ll be able to write down a resummed expression for the contribution to the LO DPS cross section coming from 2v1 diagrams with the structure of figure 4.1(b).

The results that we obtain in section 4.2 have in fact already been written down in the papers [35, 126], and one can view the content of that section as a more detailed re-derivation of some of the results in those papers. In section 4.3, we will however

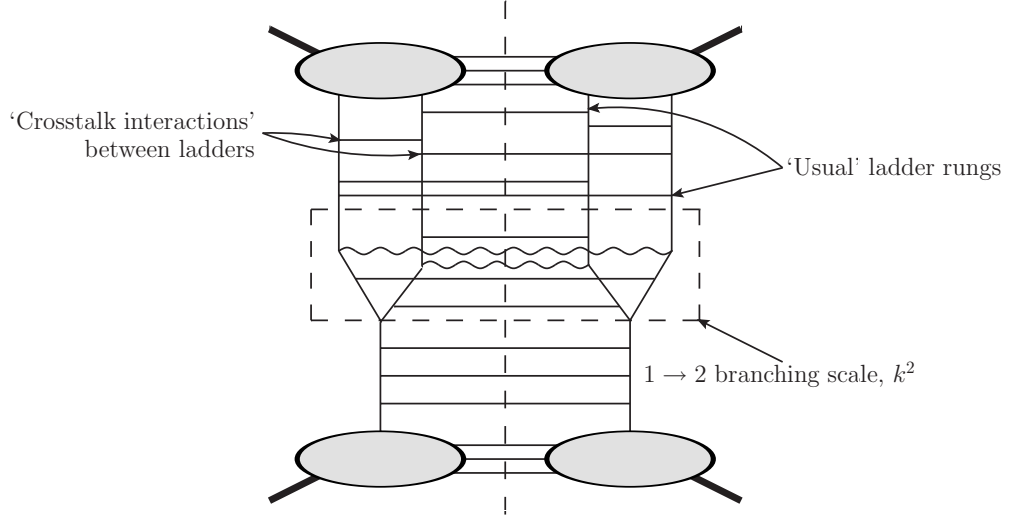


Figure 4.3: Generic 2v1 diagram including ‘crosstalk’ that we argue contributes to the 2v1 DPS cross section at the leading logarithmic level.

establish a further result with regard to the contribution of 2v1 graphs to the LO DPS cross section. We will discover that the final formula that we obtained in section 4.2 is incomplete, and that there are further diagrams of the 2v1 type that contribute to the LO DPS cross section. These diagrams involve non-diagonal crosstalk interactions between the two nonperturbatively generated parton ladders, at scales lower than the perturbative $1 \rightarrow 2$ ladder branching on the other side – an example diagram of this type is sketched in figure 4.3 (note that there are no such crosstalk interactions in figure 4.1(b)). This result is again established by analysis of the simplest Feynman graphs of the appropriate type.

In section 4.4 the results of our analyses of the different types of graph that can potentially contribute to the DPS cross section are combined, to give a suggested expression for the LO cross section for DPS. Recently, three other groups have proposed expressions for the LO DPS cross section, in [126], [35] and [33, 127]. The expressions proposed in these papers do not agree with one another, nor do they agree with our formula. We make some comments on the discrepancies in section 4.4.

4.2 ‘Two versus One’ Contributions to the DPS Cross Section

In this section, we show explicitly that for a 2v1 diagram with the structure of figure 4.2, there is a part of the cross section expression that contains a DGLAP-type large

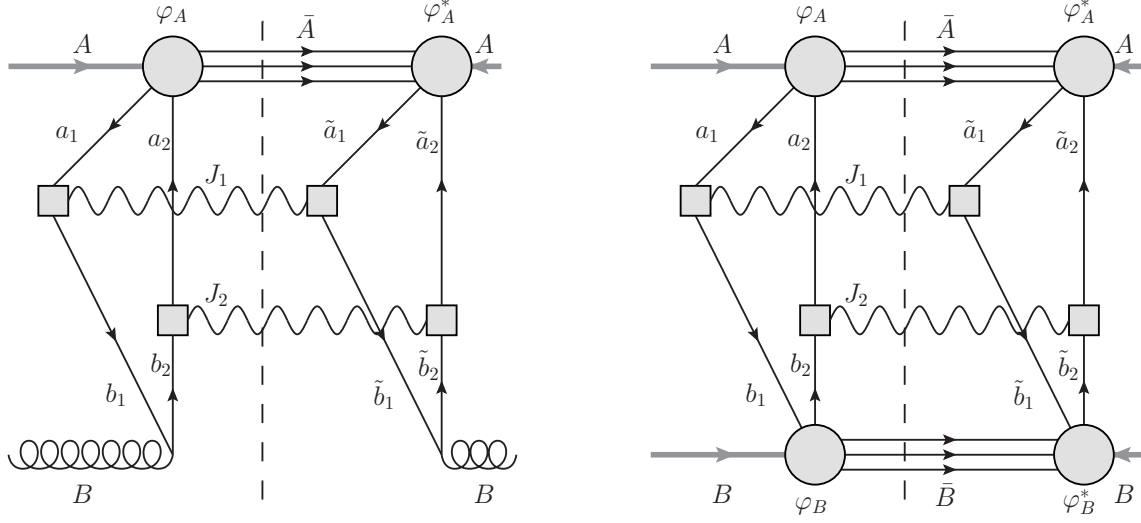


Figure 4.4: (a) An example of a ‘2v1’ DPS-type scattering diagram. (b) An example of a ‘2v2’ DPS-type scattering diagram. The thick grey lines are protons, whilst the grey circles are proton vertices. The labels on the lines correspond to the four momenta of those lines.

logarithm and a factor of order $1/R_p^2$, which should be considered as part of the LO DPS cross section. We present details of the calculation only for the particular flavour-diagonal contribution to the $gp \rightarrow gq\bar{q} + X \rightarrow \gamma^*\gamma^* + X$ process presented in figure 4.4(a), where the two off-shell photons both have a positive invariant mass. However, the general method outlined below can be applied to any diagram of the appropriate structure, and will always give a large logarithm provided that the corresponding process is allowed in the collinear limit (apart from issues of J_z nonconservation at the splitting vertex).

In the calculation of the cross section for figure 4.4(a), we will have to include a wavefunction factor or hadronic amplitude φ to find two nonperturbatively generated partons in the proton, at the amplitude level in the calculation. This factor takes account of the fact that the two partons at the top of figure 4.4(a) are tied together in the same proton [35]. The use of proton wavefunctions or hadronic amplitudes in the calculation of DPS-type graphs was discussed long ago in [128], and has been discussed more recently in [35, 37]. We utilise the approach and notation of [128] in our work. That is, we assign a wavefunction factor φ to the $p \rightarrow q\bar{q}X$ vertex that is assumed to be strongly damped for values of the parton transverse momentum and virtuality larger than the hadronic scale $\Lambda \sim 1/R_p$. In our case the factor φ is a matrix in spinor space, and also carries a label χ that describes the spins of all of the particles in X .

In the following we will take a number of steps to simplify the calculation as much as possible. First, we will largely ignore considerations of colour, and will suppress colour indices, factors and sums where they appear, in order to avoid the proliferation of too many indices. Second, we will take the four-momenta squared of the two off-shell photons to be the same, and refer to this common four-momentum squared as Q^2 . Finally, we will take the protons involved to be unpolarised, as is the case for the colliding protons at the LHC.

We apply the lightcone decomposition described in equation (A.6) to all four-vectors used, just as we did in section 3.3.3.

Rather than proceeding to calculate the cross section contribution from figure 4.4(a) directly, we instead begin by calculating the cross section contribution σ_{2v2} associated with the Feynman diagram in figure 4.4(b). In this diagram, two nonperturbatively generated quark-antiquark pairs produced by colliding protons interact via two separate $q\bar{q} \rightarrow \gamma^*$ hard processes. We should be able to express the cross section of this process in terms of ‘nonperturbatively generated parton pair’ \mathbf{r} -space 2pGPDs $\Gamma(x_1, x_2; \mathbf{\Delta})$ and hard subprocess cross sections $\hat{\sigma}$ as follows:

$$\begin{aligned} \sigma_{2v2}(s) = & \int dx_1 dx_2 dy_1 dy_2 \hat{\sigma}_{q\bar{q} \rightarrow \gamma^*}(\hat{s} = x_1 y_1 s) \hat{\sigma}_{q\bar{q} \rightarrow \gamma^*}(\hat{s} = x_2 y_2 s) \\ & \times \int \frac{d^2 \mathbf{\Delta}}{(2\pi)^2} \Gamma_p(x_1, x_2; \mathbf{\Delta}) \Gamma_p(y_1, y_2; -\mathbf{\Delta}) \end{aligned} \quad (4.1)$$

Helicity labels are omitted in the above schematic expression, but they will be included in the full calculation below. By using the fact that the expression for the cross section must end up in this form, we can establish the connection between the vertex factor φ and the ‘nonperturbatively generated parton pair’ \mathbf{r} -space 2pGPD Γ . We shall need to make use of this relationship when we come to study figure 4.4(a).

Note that a calculation of σ_{2v2} has already been performed by Paver and Treleani in [128] for the case of spinless partons, and by Mekhfi [129] and Diehl, Ostermeier and Schafer [36, 37] for the case of partons with spin. We follow closely the approach of Paver and Treleani, and our calculation of σ_{2v2} can be considered as a brief review of the method in [128].

We will neglect the proton mass with respect to the total centre of mass energy \sqrt{s} and work in a frame in which A is proportional to p , whilst B is proportional to n , $A = A^+ p, B = B^- n$. One can directly write down the following expression for the cross

section contribution from figure 4.4(b), $\sigma_{2v2}(s)$:

$$\begin{aligned} \sigma_{2v2}(s) = & \frac{1}{2(2\pi)^{10}s} \sum_{\chi\gamma} \int d^4\bar{A} d^4\bar{B} d^4J_1 d^4J_2 \delta^{(4)}(\bar{A} + \bar{B} + J_1 + J_2 - A - B) \delta(J_1^2 - Q^2) \\ & \times \delta(J_2^2 - Q^2) \mathcal{M}^{\chi\gamma\mu_1\mu_2}(A, B; \bar{A}, \bar{B}, J_1, J_2) \mathcal{M}^{\chi\gamma\mu_1\mu_2}(A, B; \bar{A}, \bar{B}, J_1, J_2)^* \end{aligned} \quad (4.2)$$

where:

$$\mathcal{M}^{\chi\gamma\mu_1\mu_2}(A, B; \bar{A}, \bar{B}, J_1, J_2) \quad (4.3)$$

$$\equiv \int \frac{d^4a_1}{(2\pi)^4} \frac{\text{Tr} [T^{\mu_1}(J_1) \not{a}_1 \varphi_p^\chi(a_1, a_2, \bar{A}) \not{a}_2 T^{\mu_2}(J_2) \not{b}_2 \varphi_p^\gamma(b_2, b_1, \bar{B}) \not{b}_1]}{D(a_1)D(a_2)D(b_1)D(b_2)},$$

$$D(a) \equiv a^2 + i\epsilon, \quad T^{\mu_1}(J_1) \equiv ieQ_q \not{a}_{\mu_1}^*(J_1) \quad (4.4)$$

$$a_2 \equiv A - \bar{A} - a_1 \quad b_1 \equiv J_1 - a_1 \quad b_2 \equiv B - \bar{B} + a_1 - J_1 \quad (4.5)$$

The vertex factors φ ensure that the quark and antiquark lines with momenta a_i and b_i have small virtuality. Given that this is the case, we can rewrite the slashed vectors in (4.3) as sums over outer products of particle or antiparticle spinors (as appropriate), using the completeness relations. Then we have:

$$\mathcal{M}^{\chi\gamma\mu_1\mu_2}(A, B; \bar{A}, \bar{B}, J_1, J_2) \quad (4.6)$$

$$\begin{aligned} & \simeq \int \frac{d^4a_1}{(2\pi)^4} \sum_{s_i t_i} \mathcal{M}_{q\bar{q} \rightarrow \gamma^*}^{s_1 t_1; \mu_1}(a_1 b_1 \rightarrow J_1) \mathcal{M}_{\bar{q}q \rightarrow \gamma^*}^{s_2 t_2; \mu_2}(a_2 b_2 \rightarrow J_2) \\ & \times \left[\frac{\bar{u}^{s_1}(a_1) \varphi_p^\chi(a_1, a_2, \bar{A}) v^{s_2}(a_2)}{D(a_1)D(a_2)} \right] \left[\frac{\bar{u}^{t_2}(b_2) \varphi_p^\gamma(b_2, b_1, \bar{B}) v^{t_1}(b_1)}{D(b_1)D(b_2)} \right] \end{aligned}$$

The s_i and t_i are quark or antiquark helicity labels, and the $\mathcal{M}_{q\bar{q} \rightarrow \gamma^*}$ factors are ‘hard’ $q\bar{q} \rightarrow \gamma^*$ matrix elements. The hard matrix elements should be evaluated with initial state partons having small (i.e. hadron scale) transverse momenta and off-shellness – however, we make the approximation in the matrix elements that the initial-state partons are on-shell and collinear, which only corresponds to a small relative error $\mathcal{O}(\Lambda^2/Q^2) \ll 1$.

Consider now the integrations over the longitudinal parts of a_1 – i.e. a_1^+ and a_1^- . It is not hard to show that the integration over a_1^- is restricted to values of order Λ^2/Q by

the vertex factor $\varphi(a_1, a_2, \bar{A})$, whilst $\varphi(b_1, b_2, \bar{B})$, $D(b_i)$, and the $\mathcal{M}_{q\bar{q} \rightarrow \gamma^*}$ are practically constant in this range (and approximately equal to their values with a_1^- set to zero). Similarly, the integration over a_1^+ is restricted to values differing from J_1^+ by $\sim \Lambda^2/Q$ by the vertex factor $\varphi(b_1, b_2, \bar{B})$, with $\varphi(a_1, a_2, \bar{A})$, $D(a_i)$ and the $\mathcal{M}_{q\bar{q} \rightarrow \gamma^*}$ being approximately constant and equal to their values at $a_1^+ = J_1^+$ in this range. This allows us to write:

$$\begin{aligned} \mathcal{M}^{\chi\gamma\mu_1\mu_2}(A, B; \bar{A}, \bar{B}, J_1, J_2) &\simeq \sum_{s_i t_i} \mathcal{M}_{q\bar{q} \rightarrow \gamma^*}^{s_1 t_1; \mu_1}(J_1^+ p, J_1^- n \rightarrow J_1) \\ &\times \mathcal{M}_{q\bar{q} \rightarrow \gamma^*}^{s_2 t_2; \mu_2}(J_2^+ p, J_2^- n \rightarrow J_2) \int \frac{d^2 \mathbf{a}_1}{(2\pi)^2} \left[\int \frac{da_1^-}{2\pi} \frac{\bar{u}^{s_1}(a_1) \varphi_p^\chi(a_1, a_2, \bar{A}) v^{s_2}(a_2)}{D(a_1) D(a_2)} \right]_{a_1^+ = J_1^+} \\ &\times \left[\int \frac{db_1^+}{2\pi} \frac{\bar{u}^{t_2}(b_2) \varphi_p^\gamma(b_2, b_1, \bar{B}) v^{t_1}(b_1)}{D(b_1) D(b_2)} \right]_{b_1^- = J_1^-} \end{aligned} \quad (4.7)$$

Define:

$$\psi_{p; q\bar{q}}^{s_1 s_2 \chi}(a_1^+, a_2^+, \mathbf{a}_1, \mathbf{a}_2, \bar{A}^-) \equiv - \int \frac{da_1^-}{2\pi} \frac{\bar{u}^{s_1}(a_1) \varphi_p^\chi(a_1, a_2, \bar{A}) v^{s_2}(a_2)}{D(a_1) D(a_2)} \quad (4.8)$$

Then we can write $\mathcal{M}^{\chi\gamma\mu_1\mu_2}(A, B; \bar{A}, \bar{B}, J_1, J_2)$ in a more compact form:

$$\begin{aligned} \mathcal{M}^{\chi\gamma\mu_1\mu_2}(A, B; \bar{A}, \bar{B}, J_1, J_2) &\simeq \sum_{s_i t_i} \mathcal{M}_{q\bar{q} \rightarrow \gamma^*}^{s_1 t_1; \mu_1}(J_1^+ p, J_1^- n \rightarrow J_1) \mathcal{M}_{q\bar{q} \rightarrow \gamma^*}^{s_2 t_2; \mu_2}(J_2^+ p, J_2^- n \rightarrow J_2) \\ &\times \int \frac{d^2 \mathbf{a}_1}{(2\pi)^2} \psi_{p; q\bar{q}}^{s_1 s_2 \chi}(J_1^+, J_2^+, \mathbf{a}_1, \mathbf{a}_2, \bar{A}^-) \psi_{p; q\bar{q}}^{t_2 t_1 \gamma}(J_2^-, J_1^-, \mathbf{b}_2, \mathbf{b}_1, \bar{B}^+) \end{aligned} \quad (4.9)$$

We now insert (4.9) into (4.2), and make use of the following relation in the resulting expression:

$$\begin{aligned} \mathcal{M}_{q\bar{q} \rightarrow \gamma^*}^{s_1 t_1; \mu_1}(J_1^+ p, J_1^- n \rightarrow J_1) \mathcal{M}_{q\bar{q} \rightarrow \gamma^*}^{* \tilde{s}_1 \tilde{t}_1; \mu_1}(J_1^+ p, J_1^- n \rightarrow J_1) (2\pi) \delta(J_1^2 - Q^2) \\ = \hat{\sigma}_{q\bar{q} \rightarrow \gamma^*}^{s_1, t_1; \tilde{s}_1, \tilde{t}_1; \mu_1}(\hat{s} = 2J_1^+ J_1^-) 4J_1^+ J_1^- \end{aligned} \quad (4.10)$$

$\hat{\sigma}_{q\bar{q} \rightarrow \gamma^*}^{s_1, t_1; \tilde{s}_1, \tilde{t}_1; \mu_1}$ is the $q\bar{q} \rightarrow \gamma^*$ ‘cross section’ with q, \bar{q}, γ^* helicities s_1, t_1, μ_1 in the matrix element, and $\tilde{s}_1, \tilde{t}_1, \mu_1$ in the conjugate matrix element (note that if $s_1 \neq \tilde{s}_1$ and/or $t_1 \neq \tilde{t}_1$ this is not a cross section in the strict sense). $\hat{\sigma}_{q\bar{q} \rightarrow \gamma^*}^{s_1, t_1; \tilde{s}_1, \tilde{t}_1; \mu_1}$ is related to the spin-averaged

$q\bar{q} \rightarrow \gamma^*$ cross section $\hat{\sigma}_{q\bar{q} \rightarrow \gamma^*}$ by:

$$\hat{\sigma}_{q\bar{q} \rightarrow \gamma^*}^{s_1, t_1; \tilde{s}_1, \tilde{t}_1; \mu_1} = 2\hat{\sigma}_{q\bar{q} \rightarrow \gamma^*} \delta_{s_1, -t_1} \delta_{\tilde{s}_1, -\tilde{t}_1} \delta_{s_1, \tilde{s}_1} \quad (4.11)$$

where on the right hand side there is no summation over repeated indices.

The result of inserting (4.9) into (4.2) is:

$$\begin{aligned} \sigma_{2v2}(s) &= \frac{1}{2(2\pi)^{12}s} \sum_{s_i t_i \tilde{s}_i, \tilde{t}_i \chi \gamma} \int d^4 \bar{A} d^4 \bar{B} d^4 J_1 \hat{\sigma}_{q\bar{q} \rightarrow \gamma^*}^{s_1, t_1; \tilde{s}_1, \tilde{t}_1; \mu_1} (\hat{s} = 2J_1^+ J_1^-) 4J_1^+ J_1^- \\ &\quad \times \hat{\sigma}_{q\bar{q} \rightarrow \gamma^*}^{s_2, t_2; \tilde{s}_2, \tilde{t}_2; \mu_2} (\hat{s} = 2J_2^+ J_2^-) 4J_2^+ J_2^- \int \frac{d^2 \mathbf{a}_1}{(2\pi)^2} \frac{d^2 \tilde{\mathbf{a}}_1}{(2\pi)^2} \psi_{p; q\bar{q}}^{s_1 s_2 \chi}(J_1^+, J_2^+, \mathbf{a}_1, \mathbf{a}_2, \bar{A}^-) \\ &\quad \times \psi_{p; q\bar{q}}^{t_2 t_1 \gamma}(J_2^-, J_1^-, \mathbf{b}_2, \mathbf{b}_1, \bar{B}^+) \psi_{p; q\bar{q}}^{* \tilde{s}_1 \tilde{s}_2 \chi}(J_1^+, J_2^+, \tilde{\mathbf{a}}_1, \tilde{\mathbf{a}}_2, \bar{A}^-) \psi_{p; q\bar{q}}^{* \tilde{t}_2 \tilde{t}_1 \gamma}(J_2^-, J_1^-, \tilde{\mathbf{b}}_2, \tilde{\mathbf{b}}_1, \bar{B}^+) \\ &= \frac{1}{4(2\pi)^{16} A^{+2} B^{-2}} \sum_{s_i t_i s'_i t'_i} \int d\bar{A}^+ d\bar{B}^- dJ_1^+ dJ_1^- \hat{\sigma}_{q\bar{q} \rightarrow \gamma^*}^{s_1, t_1; \tilde{s}_1, \tilde{t}_1; \mu_1} (\hat{s} = 2J_1^+ J_1^-) \\ &\quad \times \hat{\sigma}_{q\bar{q} \rightarrow \gamma^*}^{s_2, t_2; \tilde{s}_2, \tilde{t}_2; \mu_2} (\hat{s} = 2J_2^+ J_2^-) \int d^2 \mathbf{a}_1 d^2 \mathbf{b}_1 d^2 \Delta d^2 \bar{A} d\bar{A}^- d^2 \bar{B} d\bar{B}^+ \\ &\quad \times \sum_{\chi} \psi_{p; q\bar{q}}^{s_1 s_2 \chi}(J_1^+, J_2^+, \mathbf{a}_1, \mathbf{a}_2, \bar{A}^-) \psi_{p; q\bar{q}}^{* \tilde{s}_1 \tilde{s}_2 \chi}(J_1^+, J_2^+, \mathbf{a}_1 + \Delta, \mathbf{a}_2 - \Delta, \bar{A}^-) 4J_1^+ J_2^+ A^+ \\ &\quad \times \sum_{\gamma} \psi_{p; q\bar{q}}^{t_2 t_1 \gamma}(J_2^-, J_1^-, \mathbf{b}_2, \mathbf{b}_1, \bar{B}^+) \psi_{p; q\bar{q}}^{* \tilde{t}_2 \tilde{t}_1 \gamma}(J_2^-, J_1^-, \mathbf{b}_2 + \Delta, \mathbf{b}_1 - \Delta, \bar{B}^+) 4J_1^- J_2^- B^- \end{aligned} \quad (4.12)$$

In the second line of (4.12), we have changed integration variables from $\tilde{\mathbf{a}}_1$ to Δ , where Δ is the transverse momentum imbalance in the loop between amplitude and conjugate, defined by $\Delta = \tilde{\mathbf{a}}_1 - \mathbf{a}_1$ (and denoted in previous chapters as \mathbf{r}). We have also converted the integral over \mathbf{J}_1 to an integral over \mathbf{b}_1 using $\mathbf{a}_1 + \mathbf{b}_1 = \mathbf{J}_1$, and made use of the fact that $s = 2A^+ B^-$. Let us define the ‘nonperturbatively generated parton pair’ \mathbf{r} -space 2pGPD according to:

$$\begin{aligned} \Gamma_{p; q\bar{q}}^{s_1 s_2, \tilde{s}_1 \tilde{s}_2} \left(\frac{J_1^+}{A^+}, \frac{J_2^+}{A^+}; \Delta \right) &\equiv \frac{2}{(2\pi)^7} \sum_{\chi} \int d\bar{A}^- d^2 \bar{A} d^2 \mathbf{a}_1 \psi_{p; q\bar{q}}^{s_1 s_2 \chi}(J_1^+, J_2^+, \mathbf{a}_1, \mathbf{a}_2, \bar{A}^-, \bar{A}) \\ &\quad \times \psi_{p; q\bar{q}}^{* \tilde{s}_1 \tilde{s}_2 \chi}(J_1^+, J_2^+, \mathbf{a}_1 + \Delta, \mathbf{a}_2 - \Delta, \bar{A}^-, \bar{A}) J_1^+ J_2^+ A^+ \end{aligned} \quad (4.13)$$

We also introduce the following scaling variables:

$$x_1 \equiv J_1^+ / A^+ \quad x_2 \equiv J_2^+ / A^+ \quad y_1 \equiv J_1^- / B^- \quad y_2 \equiv J_2^- / B^- \quad (4.14)$$

Changing variables in (4.12) to the scaling variables, replacing appropriate combinations of ψ s by Γ s according to (4.13), and using the obvious relation $\Gamma_{p;\bar{q}q}^{s_1 s_2, \tilde{s}_1 \tilde{s}_2}(x_1, x_2; \Delta) = \Gamma_{p;\bar{q}q}^{s_2 s_1, \tilde{s}_2 \tilde{s}_1}(x_2, x_1; -\Delta)$, we finally obtain:

$$\begin{aligned} \sigma_{2v2}(s) &= \sum_{s_i t_i \tilde{s}_i \tilde{t}_i} \int dx_1 dx_2 dy_1 dy_2 \hat{\sigma}_{q\bar{q} \rightarrow \gamma^*}^{s_1, t_1; \tilde{s}_1, \tilde{t}_1; \mu_1}(\hat{s} = x_1 y_1 s) \hat{\sigma}_{q\bar{q} \rightarrow \gamma^*}^{s_2, t_2; \tilde{s}_2, \tilde{t}_2; \mu_2}(\hat{s} = x_2 y_2 s) \quad (4.15) \\ &\times \int \frac{d^2 \Delta}{(2\pi)^2} \Gamma_{p;\bar{q}q}^{s_1 s_2, \tilde{s}_1 \tilde{s}_2}(x_1, x_2; \Delta) \Gamma_{p;\bar{q}q}^{t_1 t_2, \tilde{t}_1 \tilde{t}_2}(y_1, y_2; -\Delta) \end{aligned}$$

The cross section is of the anticipated form (4.1). The most important result of this preliminary calculation is the definition of the ‘nonperturbatively generated parton pair’ \mathbf{r} -space 2pGPD (4.13), which we shall make use of later.

The calculation of the cross section contribution associated with figure 4.4(a), $\sigma_{2v1}(s)$, proceeds in a very similar manner to the calculation of $\sigma_{2v2}(s)$. Once again we work in a frame in which $A = A^+ p$ and $B = B^+ n$. We can directly write down the following expression for the cross section:

$$\begin{aligned} \sigma_{2v1}(s) &= \frac{1}{2(2\pi)^6 s} \sum_{\chi} \int d^4 \bar{A} d^4 J_1 d^4 J_2 \delta(J_1^2 - Q^2) \delta(J_2^2 - Q^2) \delta^{(4)}(\bar{A} + J_1 + J_2 - A - B) \quad (4.16) \\ &\times \mathcal{M}^{\lambda; \chi \mu_1 \mu_2}(A, B; \bar{A}, J_1, J_2) \mathcal{M}^{\lambda; \chi \mu_1 \mu_2}(A, B; \bar{A}, J_1, J_2)^* \end{aligned}$$

where:

$$\begin{aligned} \mathcal{M}^{\lambda; \chi \mu_1 \mu_2}(A, B; \bar{A}, J_1, J_2) &\quad (4.17) \\ &\equiv \int \frac{d^4 a_1}{(2\pi)^4} i^2 \text{Tr}(\not{a}_1 \varphi_p^\chi(a_1, a_2, \bar{A}) \not{a}_2 T^{\lambda; \mu_1 \mu_2}(a_2 a_1 B \rightarrow J_1 J_2)) / [D(a_1) D(a_2)], \end{aligned}$$

$$T^{\lambda; \mu_1 \mu_2}(a_2 a_1 B \rightarrow J_1 J_2) \equiv i^5 (e Q_q)^2 g_s \frac{\not{\epsilon}_{\mu_2}^*(J_2) \not{b}_2 \not{\epsilon}_\lambda(B) \not{b}_1 \not{\epsilon}_{\mu_1}^*(J_1)}{D(b_1) D(b_2)} \quad (4.18)$$

The lines with momentum a_1 are restricted to small virtuality by φ_A , so we can decompose the slashed a_i vectors in (4.17) into outer products of particle or antiparticle

spinors:

$$\begin{aligned} \mathcal{M}^{\lambda;\chi\mu_1\mu_2}(A, B; \bar{A}, J_1, J_2) \\ \simeq \sum_{s_i} \int \frac{d^4 a_1}{(2\pi)^4} \left[-\frac{\bar{u}^{s_1}(a_1) \varphi_p^\chi(a_1, a_2, \bar{A}) v^{s_2}(a_2)}{D(a_1) D(a_2)} \right] \mathcal{M}^{s_2 s_1 \lambda; \mu_1 \mu_2}(a_2 a_1 B \rightarrow J_1 J_2) \end{aligned} \quad (4.19)$$

$\mathcal{M}^{s_2 s_1 \lambda; \mu_1 \mu_2}(a_2 a_1 B \rightarrow J_1 J_2)$ is the matrix element for $q\bar{q}g \rightarrow \gamma^* \gamma^*$ with initial quark and antiquark having small transverse momentum and virtuality.

For reasons similar to those leading to equation (4.7), we can move the a_1^- integration such that it only acts on the part of (4.19) in square brackets, and set $a_1^- = 0$ in the rest of the integrand. Provided that $\mathbf{J}_1^2 \gg \Lambda^2$, we can perform an analogous operation for the \mathbf{a}_1 integration. The reason for this is that when $\mathbf{J}_1^2 \gg \Lambda^2$, the transverse momenta of the a_i lines (constrained to be of order Λ by φ_A) are negligible compared to the transverse momenta of the b_i and J_i lines in $\mathcal{M}^{s_2 s_1 \lambda; \mu_1 \mu_2}(a_2 a_1 B \rightarrow J_1 J_2)$, so we make only a small error by setting \mathbf{a}_i to zero in this factor provided $\mathbf{J}_1^2 \gg \Lambda^2$. Applying these approximations:

$$\begin{aligned} \mathcal{M}^{\lambda;\chi\mu_1\mu_2}(A, B; \bar{A}, J_1, J_2) \\ \simeq \sum_{s_i} \int \frac{da_1^+}{2\pi} \mathcal{M}^{s_2 s_1 \lambda; \mu_1 \mu_2}(a_2 a_1 B \rightarrow J_1 J_2)|_{a_1^-=0, \mathbf{a}_1=0} \\ \times - \int \frac{d^2 \mathbf{a}_1}{(2\pi)^2} \frac{da_1^-}{2\pi} \frac{[\bar{u}^{s_1}(a_1) \varphi_p^\chi(a_1, a_2, \bar{A}) v^{s_2}(a_2)]}{D(a_1) D(a_2)} \end{aligned} \quad (4.20)$$

We identify the final factor in (4.20) as the integral of ψ_p over \mathbf{a}_1 . Writing out the denominator factors in $\mathcal{M}^{s_2 s_1 \lambda; \mu_1 \mu_2}(a_2 a_1 B \rightarrow J_1 J_2)$ explicitly we have:

$$\begin{aligned} \mathcal{M}^{\lambda;\chi\mu_1\mu_2}(A, B; \bar{A}, J_1, J_2) \\ \simeq \sum_{s_i} \int \frac{da_1^+}{2\pi} \left[\int d^2 \mathbf{a}_1 / (2\pi)^2 \psi_p^{s_1 s_2 \chi}(a_1^+, a_2^+, \mathbf{a}_1, \mathbf{a}_2, \bar{A}^-) \right] \\ \times \frac{\mathcal{T}^{s_2 s_1 \lambda; \mu_1 \mu_2}(a_2 a_1 B \rightarrow J_1 J_2)|_{a_1^-=0, \mathbf{a}_1=0}}{[2(J_1^+ - a_1^+)J_1^- - \mathbf{J}_1^2 + i\epsilon][2(a_1^+ - J_1^+)J_2^- - \mathbf{J}_1^2 + i\epsilon]} \end{aligned} \quad (4.21)$$

where:

$$\mathcal{T}^{s_2 s_1 \lambda; \mu_1 \mu_2}(a_2 a_1 B \rightarrow J_1 J_2) \equiv i^5 g_s (eQ_q)^2 \bar{v}^{s_2}(a_2) \not{\epsilon}_{\mu_2}^* (J_2) \not{b}_2 \not{\epsilon}_\lambda (B) \not{b}_1 \not{\epsilon}_{\mu_1}^* (J_1) u^{s_1}(a_1) \quad (4.22)$$

Examination of the denominator factors in (4.20) reveals that the majority of the

contribution to the a_1^+ integration comes from the region $a_1^+ \sim J_1^+$. For this reason we can set $a_1^+ = J_1^+$ in the numerator before evaluating the a_1^+ integral using contour integration:

$$\begin{aligned} \mathcal{M}^{\lambda; \chi \mu_1 \mu_2}(A, B; \bar{A}, J_1, J_2) \\ \simeq \sum_{s_i} i \left[\int d^2 \mathbf{a}_1 / (2\pi)^2 \psi_p^{s_1 s_2 \chi}(J_1^+, J_2^+, \mathbf{a}_1, \mathbf{a}_2, \bar{A}^-) \right] \\ \times \frac{\mathcal{T}^{s_2 s_1 \lambda; \mu_1 \mu_2}(a_2 a_1 B \rightarrow J_1 J_2)|_{a_1^- = 0, \mathbf{a}_1 = 0, a_1^+ = J_1^+}}{2(J_1^- + J_2^-) \mathbf{J}_1^2} \end{aligned} \quad (4.23)$$

We are interested in the behaviour of $\mathcal{M}^{\lambda; \chi \mu_1 \mu_2}(A, B; \bar{A}, J_1, J_2)$ when $\mathbf{J}_1^2 \ll Q^2$ (but still $\gg \Lambda^2$) such that all of the internal particles have transverse momenta and virtualities much less than Q . In this limit we can use spinor completeness relations to split \mathcal{T} up into two $q\bar{q} \rightarrow \gamma^*$ matrix elements and one $g \rightarrow q\bar{q}$ matrix element, with the quark and antiquark having small transverse momenta and virtuality $\mathcal{O}(|\mathbf{J}_1|)$ in each matrix element. The quark and antiquark transverse momenta and virtualities can be set to zero in the ‘hard’ $q\bar{q} \rightarrow \gamma^*$ matrix elements with only a small accompanying error $\mathcal{O}(\mathbf{J}_1^2/Q^2)^1$, but we must keep the term proportional to \mathbf{J}_1 in the $g \rightarrow q\bar{q}$ matrix element as this vanishes in the limit $\mathbf{J}_1 \rightarrow 0$:

$$\begin{aligned} \mathcal{M}^{\lambda; \chi \mu_1 \mu_2}(A, B; \bar{A}, J_1, J_2) \\ \simeq \sum_{s_i t_i} \frac{-i \left[\int d^2 \mathbf{a}_1 / (2\pi)^2 \psi_p^{s_1 s_2 \chi}(a_1^+, a_2^+, \mathbf{a}_1, \mathbf{a}_2, \bar{A}^-) \right] \mathcal{M}_{g \rightarrow q\bar{q}}^{\lambda \rightarrow t_1 t_2}(B; J_1^- n + \mathbf{J}_1, J_2^- n + \mathbf{J}_2)}{2(J_1^- + J_2^-) \mathbf{J}_1^2} \\ \times \mathcal{M}_{q\bar{q} \rightarrow \gamma^*}^{t_1 s_1 \rightarrow \mu_1}(J_1^- n, J_1^+ p; J_1^- n + J_1^+ p) \mathcal{M}_{q\bar{q} \rightarrow \gamma^*}^{t_2 s_2 \rightarrow \mu_2}(J_2^- n, J_2^+ p; J_2^- n + J_2^+ p) \end{aligned} \quad (4.24)$$

Having inserted (4.24) into (4.16), we use (4.10) and the following connection between

¹We eventually integrate \mathbf{J}_1^2 all the way up to Q^2 , so one might worry that the terms that we have neglected here are not small. The important point is that the terms we have dropped do not contribute to the large DGLAP logarithm that we are looking for in this section and will eventually find in equation (4.28). In other words, the terms that we have dropped give a small contribution to the integral over \mathbf{J}_1^2 in comparison with the terms we have kept.

$\mathcal{M}_{g \rightarrow \bar{q}q}$ and helicity-dependent unregularised splitting functions in the result [17]:

$$\begin{aligned} & \frac{J_1^- J_2^-}{(J_1^- + J_2^-)^2} \mathcal{M}_{g \rightarrow \bar{q}q}^{\lambda \rightarrow t_1 t_2}(B; J_1^- n + \mathbf{J}_1, J_2^- n + \mathbf{J}_2) \mathcal{M}_{g \rightarrow \bar{q}q}^{*\lambda \rightarrow \tilde{t}_1 \tilde{t}_2}(B; J_1^- n + \mathbf{J}_1, J_2^- n + \mathbf{J}_2) \quad (4.25) \\ & = 2g_s^2 P_{g \rightarrow q\bar{q}}^{\lambda \rightarrow t_2 t_1, \tilde{t}_2 \tilde{t}_1} \left(\frac{J_2^-}{J_1^- + J_2^-} \right) \mathbf{J}_1^2 \end{aligned}$$

This yields:

$$\begin{aligned} \sigma_{2v1}(s) &= \sum_{s_i \tilde{s}_i t_i \tilde{t}_i} \frac{4}{(2\pi)^{12} s} \int d^4 \bar{A} d^4 J_1 \hat{\sigma}_{\bar{q}q \rightarrow \gamma^*}^{s_1, t_1; \tilde{s}_1, \tilde{t}_1; \mu_1}(\hat{s} = 2J_1^+ J_1^-) J_1^+ \hat{\sigma}_{q\bar{q} \rightarrow \gamma^*}^{s_2, t_2; \tilde{s}_2, \tilde{t}_2; \mu_2}(\hat{s} = 2J_2^+ J_2^-) J_2^+ \\ & \times \left[\int d^2 \mathbf{a}_1 \psi_p^{s_1 s_2 \chi}(J_1^+, J_2^+, \mathbf{a}_1, \mathbf{a}_2, \bar{A}^-) \right] \quad (4.26) \end{aligned}$$

$$\begin{aligned} & \times \left[\int d^2 \mathbf{a}'_1 \psi_p^{*s_1 \tilde{s}_2 \chi}(J_1^+, J_2^+, \tilde{\mathbf{a}}_1, \tilde{\mathbf{a}}_2, \bar{A}^-) \right] g_s^2 P_{g \rightarrow q\bar{q}}^{\lambda \rightarrow t_2 t_1, \tilde{t}_2 \tilde{t}_1} \left(\frac{J_2^-}{J_1^- + J_2^-} \right) \frac{1}{\mathbf{J}_1^2} \\ & = \sum_{s_i \tilde{s}_i t_i \tilde{t}_i} \frac{1}{(2\pi)^3 A^{+2} B^-} \int d^4 J_1 d\bar{A}^+ \hat{\sigma}_{\bar{q}q \rightarrow \gamma^*}^{s_1, t_1; \tilde{s}_1, \tilde{t}_1; \mu_1}(\hat{s} = 2J_1^+ J_1^-) \hat{\sigma}_{q\bar{q} \rightarrow \gamma^*}^{s_2, t_2; \tilde{s}_2, \tilde{t}_2; \mu_2}(\hat{s} = 2J_2^+ J_2^-) \\ & \times \left[\frac{2}{(2\pi)^7} \sum_{\chi} \int \frac{d^2 \Delta}{(2\pi)^2} d^2 \bar{A} d\bar{A}^- d^2 \mathbf{a}_1 \psi_p^{s_1 s_2 \chi}(J_1^+, J_2^+, \mathbf{a}_1, \mathbf{a}_2, \bar{A}^-) \right. \quad (4.27) \\ & \left. \times \psi_p^{*s_1 \tilde{s}_2 \chi}(J_1^+, J_2^+, \mathbf{a}_1 + \Delta, \mathbf{a}_2 - \Delta, \bar{A}^-) J_1^+ J_2^+ A^+ \right] g_s^2 P_{g \rightarrow q\bar{q}}^{\lambda \rightarrow t_2 t_1, \tilde{t}_2 \tilde{t}_1} \left(\frac{J_2^-}{J_1^- + J_2^-} \right) \frac{1}{\mathbf{J}_1^2} \end{aligned}$$

In (4.27) we have once again introduced the transverse variable Δ via the same relation as in the $2v2$ case. We recognise the object in square brackets in (4.27) as the integral of the nonperturbatively generated parton pair \mathbf{r} -space 2pGPD over Δ . If we make a change of longitudinal integration variables in (4.27) to the scaling variables (4.14), then we finally obtain:

$$\begin{aligned} \sigma_{2v1}(s) &= \sum_{s_i \tilde{s}_i t_i \tilde{t}_i} \int dx_1 dx_2 dy_1 dy_2 \hat{\sigma}_{\bar{q}q \rightarrow \gamma^*}^{s_1, t_1; \tilde{s}_1, \tilde{t}_1; \mu_1}(\hat{s} = x_1 y_1 s) \hat{\sigma}_{q\bar{q} \rightarrow \gamma^*}^{s_2, t_2; \tilde{s}_2, \tilde{t}_2; \mu_2}(\hat{s} = x_2 y_2 s) \quad (4.28) \\ & \times \left[\int \frac{d^2 \Delta}{(2\pi)^2} \Gamma_{p; q\bar{q}}^{s_1 s_2, \tilde{s}_1 \tilde{s}_2}(x_1, x_2; \Delta) \right] \left[\frac{\alpha_s}{2\pi} P_{g \rightarrow q\bar{q}}^{\lambda \rightarrow t_2 t_1, \tilde{t}_2 \tilde{t}_1}(y_2) \delta(1 - y_1 - y_2) \int_{\Lambda^2}^{Q^2} \frac{d\mathbf{J}_1^2}{\mathbf{J}_1^2} \right] \end{aligned}$$

We have restricted our integration over \mathbf{J}_1^2 to the range $\Lambda^2 < \mathbf{J}_1^2 < Q^2$, which corresponds to the range over which our approximate expression for the matrix element (4.24) is valid. The contributions to σ_{2v1} coming from \mathbf{J}_1^2 values outside this range do not have the same $1/\mathbf{J}_1^2$ structure.

The integral over \mathbf{J}_1 in (4.28) gives rise to a large transverse momentum logarithm $\log(Q^2/\Lambda^2)$, whilst the integral over Δ gives a prefactor of order $\Lambda^2 \sim 1/R_p^2$ (since the nonperturbatively generated parton pair \mathbf{r} -space 2pGPD only has support for transverse momenta, and therefore transverse momentum imbalances \mathbf{r} , of order Λ_{QCD}). Thus, as we asserted at the beginning of this section, there is a part of the cross section expression for figure 4.4(a) that is proportional to $\log(Q^2/\Lambda^2)/R_p^2$ and should be included in the LO DPS cross section.

Note that the quantity $\int d^2\Delta \Gamma_p^{s_1 s_2, \tilde{s}_1 \tilde{s}_2}(x_1, x_2; \Delta) / (2\pi)^2$ is equal to the \mathbf{b} -space nonperturbatively generated parton pair 2pGPD evaluated at zero transverse separation, $\Gamma_p^{s_1 s_2, \tilde{s}_1 \tilde{s}_2}(x_1, x_2; \mathbf{b} = \mathbf{0})$. This appears to indicate that the 2v1 contribution to DPS probes nonperturbatively generated parton pair 2pGPDs at zero parton separation. In fact, the result (4.28) actually corresponds to a broad logarithmic integral over values of \mathbf{b}^2 that are $\ll R_p^2$ but $\gg 1/Q^2$. The \mathbf{b} -space 2pGPD evaluated at $\mathbf{b} = \mathbf{0}$ appears in (4.28) because the \mathbf{r} -space nonperturbatively generated parton pair 2pGPD dies off rapidly for $\Delta^2 \gg \Lambda^2$, which is equivalent to the \mathbf{b} -space nonperturbatively generated parton pair 2pGPD not containing any fluctuations with length scales $\ll R_p$. Then we can approximate $\Gamma_p(\mathbf{b})$ for the relevant values of \mathbf{b} in (4.28) by $\Gamma_p(\mathbf{b} = \mathbf{0})$.

If one assumes that diagrams of the form of figure 4.1(b) are the only diagrams of the ‘2v1’ type that contribute to the DPS cross section at leading logarithmic order, then a generalisation of the result in (4.28) yields the expression below for the contribution of 2v1 graphs to the LO DPS cross section²:

$$\begin{aligned} \sigma_{(A,B)}^{D,2v1}(s) = & 2 \times \frac{m}{2} \sum_{liji'i'_i j'_i} \int_{\Lambda^2}^{Q^2} dk^2 \frac{\alpha_s(k^2)}{2\pi k^2} \int dx_1 dx_2 dy_1 dy_2 \frac{dx'_1}{x'_1} \frac{dx'_2}{x'_2} \frac{dy'_1}{y'_1} \frac{dy'_2}{y'_2} \\ & \times \hat{\sigma}_{i_1 j_1 \rightarrow A}(\hat{s} = x_1 y_1 s) \hat{\sigma}_{i_2 j_2 \rightarrow B}(\hat{s} = x_2 y_2 s) \\ & \times \frac{D_p^l(y'_1 + y'_2, k^2)}{y'_1 + y'_2} P_{l \rightarrow j'_1 j'_2} \left(\frac{y'_1}{y'_1 + y'_2} \right) D_{j'_1}^{j_1} \left(\frac{y_1}{y'_1}; Q^2, k^2 \right) D_{j'_2}^{j_2} \left(\frac{y_2}{y'_2}; Q^2, k^2 \right) \\ & \times D_{i'_1}^{i_1} \left(\frac{x_1}{x'_1}; Q^2, \Lambda^2 \right) D_{i'_2}^{i_2} \left(\frac{x_2}{x'_2}; Q^2, \Lambda^2 \right) \Gamma_{p, indep}^{i'_1 i'_2}(x'_1, x'_2, \mathbf{b} = \mathbf{0}; \Lambda^2) \end{aligned} \quad (4.29)$$

²Note that here and in the rest of this section we will take the scales associated with the two hard scales to be equal, $Q_A^2 = Q_B^2 = Q^2$. We will comment in section 4.4 on the generalisation of the results of this section to the case of unequal scales. Note also that we only write down the unpolarised diagonal contribution in colour, flavour and spin space here. The contributions associated with spin polarisation (either longitudinal or transverse) and flavour interference are expected to have a similar structure. On the other hand, it is known that the colour correlation/interference and parton type interference contributions will be suppressed by Sudakov factors, as is discussed in section 3.2.2.

$D_i^j(x; Q^2, k^2)$ are the Green's functions of the DGLAP equations, defined immediately under equation (2.12). $\Gamma_{p, indep}^{i'_1 i'_2}(x'_1, x'_2; \mathbf{b} = \mathbf{0}, \Lambda^2)$ represents a nonperturbative initial condition for the two independent ladders in figure 4.1(b). In (4.29) we have re-inserted the symmetry factor $m/2$ that has been omitted in earlier discussion in this section ($m = 1$ if the two hard processes are identical, and $m = 2$ otherwise). There is an additional prefactor of 2 in (4.29) because there are two sets of 2v1 graphs that give equivalent contributions – in one set the nonperturbatively generated parton pair emerges from the ‘left’ proton, whilst in the other it emerges from the ‘right’ proton.

Equation (4.29) can be written in a more compact fashion as:

$$\begin{aligned} \sigma_{(A,B)}^{D,2v1}(s) &= 2 \times \frac{m}{2} \sum_{i_i j_i} \int dx_1 dx_2 dy_1 dy_2 \hat{\sigma}_{i_1 j_1 \rightarrow A}(\hat{s} = x_1 y_1 s) \hat{\sigma}_{i_2 j_2 \rightarrow B}(\hat{s} = x_2 y_2 s) \quad (4.30) \\ &\quad \times \check{D}_p^{j_1 j_2}(y_1, y_2; Q^2) \int \frac{d^2 \Delta}{(2\pi)^2} \Gamma_{p, indep}^{i_1 i_2}(x_1, x_2, \Delta; Q^2) \\ &= 2 \times \frac{m}{2} \sum_{i_i j_i} \int dx_1 dx_2 dy_1 dy_2 \hat{\sigma}_{i_1 j_1 \rightarrow A}(\hat{s} = x_1 y_1 s) \hat{\sigma}_{i_2 j_2 \rightarrow B}(\hat{s} = x_2 y_2 s) \\ &\quad \times \check{D}_p^{j_1 j_2}(y_1, y_2; Q^2) \Gamma_{p, indep}^{i_1 i_2}(x_1, x_2, \mathbf{b} = \mathbf{0}; Q^2) \end{aligned}$$

where:

$$\Gamma_{p, indep}^{i_1 i_2}(x_1, x_2, \mathbf{b}; Q^2) \equiv \sum_{i'_i} \int \frac{dx'_1}{x'_1} \frac{dx'_2}{x'_2} D_{i'_1}^{i_1} \left(\frac{x_1}{x'_1}; \Lambda^2, Q^2 \right) D_{i'_2}^{i_2} \left(\frac{x_2}{x'_2}; \Lambda^2, Q^2 \right) \quad (4.31)$$

$$\begin{aligned} \check{D}_p^{j_1 j_2}(y_1, y_2; Q^2) &\equiv \sum_{l j'_i} \int_{\Lambda^2}^{Q^2} dk^2 \frac{\alpha_s(k^2)}{2\pi k^2} \frac{dy'_1}{y'_1} \frac{dy'_2}{y'_2} \frac{D_p^l(y'_1 + y'_2, k^2)}{y'_1 + y'_2} \quad (4.32) \\ &\quad \times P_{l \rightarrow j'_1 j'_2} \left(\frac{y'_1}{y'_1 + y'_2} \right) D_{j'_1}^{j_1} \left(\frac{y_1}{y'_1}; k^2, Q^2 \right) D_{j'_2}^{j_2} \left(\frac{y_2}{y'_2}; k^2, Q^2 \right) \end{aligned}$$

As mentioned in section 4.1, and as will be explored in detail in section 4.3, there are additional diagrams of the ‘2v1’ type that contribute at leading logarithmic order to the DPS cross section, aside from those represented by figure 4.1(b). These involve crosstalk interactions between the two nonperturbatively generated ladders. Equation (4.29) (or (4.30)) therefore represents only part of the 2v1 contribution to the LO DPS cross section. For the moment, however, we’ll limit our discussion to just this part.

A necessary requirement for (4.29) (or (4.30)) to be valid (at least as an incomplete

part of a contribution to the DPS cross section) is that the independent two-ladder 2pGPD $\Gamma_{p, indep}^{i_1 i_2}(x_1, x_2; \mathbf{b}, Q^2)$ should be smooth on distance scales $\ll R_p \sim 1/\Lambda$ (or equivalently that the corresponding distribution in terms of the transverse momentum imbalance Δ is cut off at values of order Λ). This appears to be a somewhat reasonable requirement – at the scale Λ there is only this scale available to set the size of the Δ profile for $\Gamma_{p, indep}^{i_1 i_2}(x_1, x_2; \Delta, \Lambda^2)$, and the evolution equation for the independent two-ladder 2pGPD (which is just the double DGLAP equation (2.2) with the sPDF feed terms removed) preserves the transverse profile. In any case, such behaviour for $\Gamma_{p, indep}^{i_1 i_2}(x_1, x_2; \Delta, Q^2)$ would appear to be required in order to get the necessary prefactor of order $1/R_p^2$ in the 2v2 contribution to DPS, which is calculated according to the following expression (for the diagonal unpolarised contribution):

$$\begin{aligned} \sigma_{(A,B)}^{D,2v2}(s) &= \frac{m}{2} \sum_{i_i j_i} \int dx_1 dx_2 dy_1 dy_2 \hat{\sigma}_{i_1 j_1 \rightarrow A}(\hat{s} = x_1 y_1 s) \hat{\sigma}_{i_2 j_2 \rightarrow B}(\hat{s} = x_2 y_2 s) \\ &\quad \times \int \frac{d^2 \Delta}{(2\pi)^2} \Gamma_{p, indep}^{i_1 i_2}(x_1, x_2, \Delta; Q^2) \Gamma_{p, indep}^{j_1 j_2}(y_1, y_2, -\Delta; Q^2) \\ &= \frac{m}{2} \sum_{i_i j_i} \int dx_1 dx_2 dy_1 dy_2 \hat{\sigma}_{i_1 j_1 \rightarrow A}(\hat{s} = x_1 y_1 s) \hat{\sigma}_{i_2 j_2 \rightarrow B}(\hat{s} = x_2 y_2 s) \\ &\quad \times \int d^2 \mathbf{b} \Gamma_{p, indep}^{i_1 i_2}(x_1, x_2, \mathbf{b}; Q^2) \Gamma_{p, indep}^{j_1 j_2}(y_1, y_2, \mathbf{b}; Q^2) \end{aligned} \quad (4.33)$$

If one assumes that $\Gamma_{p, indep}^{ij}(x_1, x_2; \mathbf{b}, Q^2)$ can be factorised into a longitudinal piece $\tilde{D}_{p, indep}^{ij}(x_1, x_2; Q^2)$ and a flavour-independent transverse piece $F(\mathbf{b})$, where $F(\mathbf{b})$ is a smooth function of radius R_p normalised to 1, then (4.29) and (4.33) become:

$$\begin{aligned} \sigma_{(A,B)}^{D,2v2}(s) &= \frac{m}{2} \sum_{i_i j_i} \frac{1}{\sigma_{eff,2v2}} \int dx_1 dx_2 dy_1 dy_2 \hat{\sigma}_{i_1 j_1 \rightarrow A}(\hat{s} = x_1 y_1 s) \\ &\quad \times \hat{\sigma}_{i_2 j_2 \rightarrow B}(\hat{s} = x_2 y_2 s) \tilde{D}_{p, indep}^{i_1 i_2}(x_1, x_2; Q^2) \tilde{D}_{p, indep}^{j_1 j_2}(y_1, y_2; Q^2) \end{aligned} \quad (4.34)$$

$$\begin{aligned} \sigma_{(A,B)}^{D,2v1}(s) &= 2 \times \frac{m}{2} \sum_{i_i j_i} \frac{1}{\sigma_{eff,2v1}} \int dx_1 dx_2 dy_1 dy_2 \hat{\sigma}_{i_1 j_1 \rightarrow A}(\hat{s} = x_1 y_1 s) \\ &\quad \times \hat{\sigma}_{i_2 j_2 \rightarrow B}(\hat{s} = x_2 y_2 s) \check{D}_p^{j_1 j_2}(y_1, y_2; Q^2) \tilde{D}_{p, indep}^{i_1 i_2}(x_1, x_2; Q^2) \end{aligned} \quad (4.35)$$

where:

$$\frac{1}{\sigma_{eff,2v2}} \equiv \int d^2 \mathbf{b} [F(\mathbf{b})]^2 = \int \frac{d^2 \Delta}{(2\pi)^2} [F(\Delta)]^2 \quad (4.36)$$

$$\frac{1}{\sigma_{eff,2v1}} \equiv F(\mathbf{b} = \mathbf{0}) = \int \frac{d^2\Delta}{(2\pi)^2} [F(\Delta)] \quad (4.37)$$

$F(\Delta)$ is the Fourier transform of $F(\mathbf{b})$. We see that the geometrical prefactors for the two different contributions to the DPS cross section are different in general, $\sigma_{eff,2v2} \neq \sigma_{eff,2v1}$. If one assumes that two nonperturbatively generated ladders are to some degree uncorrelated in transverse space, $F(\mathbf{b})$ is given by a convolution of an azimuthally symmetric transverse parton density in the proton $\rho(\mathbf{r})$ with itself, where $\rho(\mathbf{r})$ must be normalised to 1 in order to ensure the appropriate normalisation of $F(\mathbf{b})$:

$$F(\mathbf{b}) = \int d^2\mathbf{r} \rho(\mathbf{r}) \rho(\mathbf{b} - \mathbf{r}) \quad (4.38)$$

Then, if one takes the Gaussian form $\exp[-r^2/(2R^2)]/(\pi R^2)$ for ρ (with R a constant parameter), one finds that $\sigma_{eff,2v1} = \sigma_{eff,2v2}/2$ – that is, the 2v1 contribution receives a factor of 2 enhancement over the 2v2 contribution from the geometrical prefactor alone (in the next section, we'll discover that the 2v1 contribution is further enhanced at low x as a result of the crosstalk interactions on the two-ladder side that are allowed for this contribution). The ratio $\sigma_{eff,2v2}/\sigma_{eff,2v1}$ does not depend much on the precise shape of ρ – for example, one obtains 2.18 if ρ is a top hat $\frac{1}{\pi R^2}\Theta(R-r)$, 2.32 if ρ is the projection of an exponential $\int dz \frac{1}{8\pi R^3} \exp(-\sqrt{r^2+z^2}/R)$, and 1.94 if ρ is the projection of a hard sphere $\frac{3}{2\pi R^2}(1-r^2/R^2)^{1/2}\Theta(R-r)$ (with R once again a constant parameter in these expressions). It is important to bear in mind, however, that in order to obtain an enhancement that is roughly a factor of 2 we have had to make a number of assumptions whose validity is somewhat uncertain (this is particularly the case for the assumption (4.38)). There could be some ‘clustering’ of the nonperturbative partons in transverse space, which would tend to increase $\sigma_{eff,2v2}/\sigma_{eff,2v1}$. Alternatively it is not inconceivable that the probability to find two nonperturbative partons separated by small distances $\ll R_p$ could be smaller than the probability to find them separated by distances of order R_p – in this scenario $\sigma_{eff,2v2}/\sigma_{eff,2v1}$ would be reduced.

4.3 Crosstalk between Ladders in the 2v1 Contribution

In the previous section we demonstrated that there is a leading logarithmic contribution to the DPS cross section associated with diagrams in which a single parton ladder from one proton splits into two, and then the two daughter ladders interact with two independent ladders from the other proton (that are only connected to one another via low-scale nonperturbative interactions). It is suggested in a number of works [35, 126, 130] that these diagrams are the only ones involving a single $1 \rightarrow 2$ ladder branching that give rise to a leading logarithmic contribution to DPS. Here, we show that there is also a leading logarithmic contribution to the DPS cross section associated with diagrams such as those in figure 4.3 in which the two nonperturbatively generated ladders talk to one another by exchanging partons, provided that the crosstalk occurs at a lower scale than the scale of the $1 \rightarrow 2$ ladder branching. There are two types of crosstalk that are possible, which are illustrated in the simple diagrams in figure 4.5(a) and (b) - we'll call these off-diagonal real emission and virtual exchange processes respectively. As in the previous section, we'll demonstrate that there is a leading logarithmic contribution from diagrams such as figure 4.3 by examining one of the simplest possible diagrams of the appropriate type - namely, that of figure 4.5(a). We will find that there is a large DGLAP logarithm associated with both the $1 \rightarrow 2$ splitting and the off-diagonal real emission ('crosstalk') processes in the figure, and that this is associated exclusively with the region of integration in which the partonic products of the off-diagonal real emission have much smaller transverse momentum than the products of the $1 \rightarrow 2$ splitting (and all of these transverse momenta are $\gg \Lambda^2$ but $\ll Q^2$).

In our calculation, we'll ignore considerations of colour for simplicity, just as we did in section 4.2. However, the colour structure of crosstalk processes is quite nontrivial, and is important when considering the size of such contributions to cross sections. The colour structure of crosstalk processes has been considered previously in the context of twist-4 contributions to DIS in [131–134], and in the context of DPS in [33, 127, 135]. We will make some comments with regards to the colour structure of the crosstalk processes at the end of this section.

As in section 4.2, we work in a frame in which $A = A^+p$, $B = B^-n$. The cross section

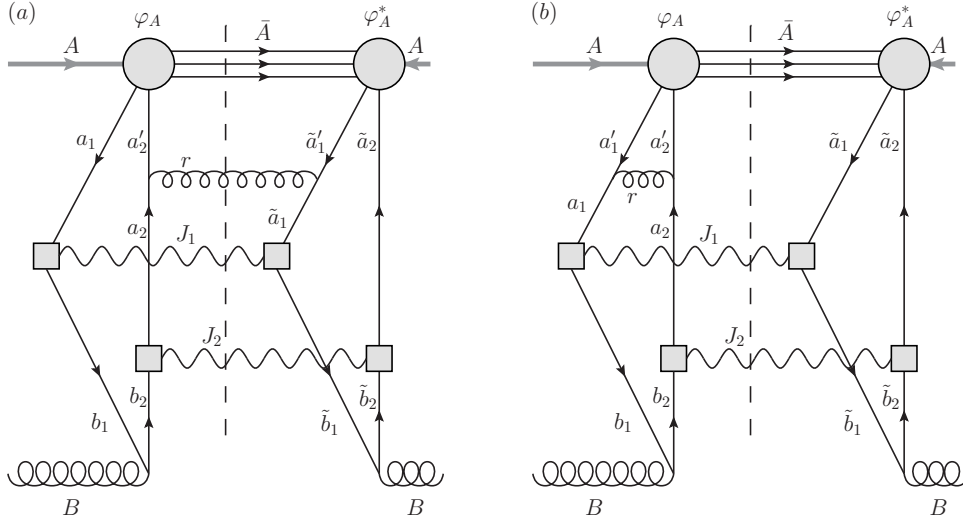


Figure 4.5: (a) Simple 2v1 diagram including an ‘off-diagonal real emission’ process. (b) Simple 2v1 diagram including a ‘virtual exchange’ process.

expression associated with figure 4.5(a) is:

$$\sigma_{XT}(s) = \frac{1}{2(2\pi)^{10}s} \int d^4\bar{A} d^4r d^4J_1 d^4J_2 \delta(J_1^2 - Q^2) \delta(J_2^2 - Q^2) \delta(r^2) \quad (4.39)$$

$$\delta^{(4)}(A + B - \bar{A} - r - J_1 - J_2) \mathcal{M}_L^{\lambda_1; \mu_1 \mu_2 \mu_3 \chi}(A, B; J_1, J_2, r, \bar{A})$$

$$\mathcal{M}_R^{\lambda_1; \mu_1 \mu_2 \mu_3 \chi}(A, B; J_1, J_2, r, \bar{A})^*$$

where:

$$\mathcal{M}_L^{\lambda_1; \mu_1 \mu_2 \mu_3 \chi}(A, B; J_1, J_2, r, \bar{A}) \quad (4.40)$$

$$= i^9 g_s^2 (eQ_q)^2 \int \frac{d^4 a_1}{(2\pi)^4} \frac{\text{Tr} \left[\not{\epsilon}_\lambda(B) \not{b}_1 \not{\epsilon}_{\mu_1}^*(J_1) \not{a}_1 \not{\epsilon}_p^\chi(a_1, a_2, \bar{A}) \not{a}_2' \not{\epsilon}_{\mu_3}^*(r) \not{a}_2 \not{\epsilon}_{\mu_2}^*(J_2) \not{b}_2 \right]}{D(a_1) D(b_1) D(a_2') D(b_2) D(a_2)}$$

$$\mathcal{M}_R^{\lambda_1; \mu_1 \mu_2 \mu_3 \chi}(A, B; J_1, J_2, r, \bar{A}) \quad (4.41)$$

$$= i^9 g_s^2 (eQ_q)^2 \int \frac{d^4 \tilde{a}_1}{(2\pi)^4} \frac{\text{Tr} \left[\not{\epsilon}_{\lambda_1}(B) \not{\tilde{b}}_1 \not{\epsilon}_{\mu_1}^*(J_1) \not{\tilde{a}}_1 \not{\epsilon}_{\mu_3}^*(r) \not{\tilde{a}}_1' \not{\epsilon}_p^\chi(\tilde{a}_1, \tilde{a}_2, \bar{A}) \not{\tilde{a}}_2 \not{\epsilon}_{\mu_2}^*(J_2) \not{\tilde{b}}_2 \right]}{D(\tilde{a}_1) D(\tilde{b}_1) D(\tilde{a}_1') D(\tilde{b}_2) D(\tilde{a}_2)}$$

Following a procedure that is similar to that leading to equation (4.21), and is valid in the region of transverse momentum integration in which $\mathbf{J}_1^2, \mathbf{J}_2^2, \mathbf{r}^2 \gg \Lambda^2$ (or equivalently

$\mathbf{a}_2^2, \mathbf{b}_1^2, \mathbf{b}_2^2 \gg \Lambda^2$), we can write down the following approximate expression for \mathcal{M}_L :

$$\begin{aligned} \mathcal{M}_L^{\lambda; \mu_1 \mu_2 \mu_3 \chi}(A, B; J_1, J_2, r, \bar{A}) & \\ \simeq \sum_{s_1 s'_2} \int \frac{da_1^+}{2\pi} \left[\int d^2 \mathbf{a}_1 / (2\pi)^2 \psi_p^{s_1 s'_2 \chi}(a_1^+, a_2^+, \mathbf{a}_1, \mathbf{a}'_2, \bar{A}^-) \right] & (4.42) \\ \times \frac{\mathcal{T}_L^{s'_2 s_1 \lambda; \mu_1 \mu_2 \mu_3}(a'_2 a_1 B \rightarrow J_1 J_2 r)|_{a_1^- = 0, \mathbf{a}_1 = 0}}{[2(J_1^+ - a_1^+)J_1^- - \mathbf{J}_1^2 + i\epsilon][2(a_1^+ - J_1^+)(B^- - J_1^-) - \mathbf{J}_1^2 + i\epsilon]} \\ \times \frac{1}{[2(J_1^+ + J_2^+ - a_1^+)(-r^-) - \mathbf{r}^2 + i\epsilon]} \end{aligned}$$

where $\mathcal{T}_L(a_2 a_1 B \rightarrow J_1 J_2 r)$ includes all of the numerator structure of the $\mathcal{M}_L(a_2 a_1 B \rightarrow J_1 J_2 r)$ matrix element.

Performing the a_1^+ integral using contour methods, and making use of the fact that the overall integrand is strongly peaked near $a_1^+ = J_1^+$ whilst the numerator factor \mathcal{T}_L is a relatively smooth function in this region, we obtain:

$$\begin{aligned} \mathcal{M}_L^{\lambda; \mu_1 \mu_2 \mu_3 \chi}(A, B; J_1, J_2, r, \bar{A}) & \\ \simeq \sum_{s_1 s'_2} \frac{-ir^+}{2} \left[\int d^2 \mathbf{a}_1 / (2\pi)^2 \psi_p^{s_1 s'_2 \chi}(J_1^+, a_2^+, \mathbf{a}_1, \mathbf{a}'_2, \bar{A}^-) \right] & (4.43) \\ \times \frac{\mathcal{T}_L^{s'_2 s_1 \lambda; \mu_1 \mu_2 \mu_3}(a'_2 a_1 B \rightarrow J_1 J_2 r)|_{a_1^+ = J_1^+, a_1^- = 0, \mathbf{a}_1 = 0}}{\mathbf{J}_1^2 \mathbf{r}^2 [J_2^+ + \frac{\mathbf{J}_1^2}{2J_1^-} + r^+]} \end{aligned}$$

In the region of integration in which $\mathbf{J}_1^2 \ll Q^2$, we can drop the second term in the denominator factor $[J_2^+ + \frac{\mathbf{J}_1^2}{2J_1^-} + r^+]$. Also, when $\mathbf{J}_1^2, \mathbf{J}_2^2, \mathbf{r}^2 \ll Q^2$, we can approximately decompose \mathcal{T}_L as follows:

$$\begin{aligned} \mathcal{T}_L^{s'_2 s_1 \lambda; \mu_1 \mu_2 \mu_3}(a'_2 a_1 B \rightarrow J_1 J_2 r)|_{a_1^- = 0, \mathbf{a}_1 = 0} & \simeq \mathcal{M}_{q\bar{q} \rightarrow \gamma^*}^{s_1 t_1; \mu_1}(J_1^+ p, J_1^- n \rightarrow J_1) \\ \times \mathcal{M}_{q\bar{q} \rightarrow \gamma^*}^{s_2 t_2; \mu_2}(J_2^+ p, J_2^- n \rightarrow J_2) & \mathcal{M}_{\bar{q} \rightarrow qg}^{s'_2 \rightarrow s_2 \mu_3}(a_2^+ p, a_2^+ p - \mathbf{r}, (a_2^+ - a_2^+)p + \mathbf{r}) \\ \times \mathcal{M}_{g \rightarrow \bar{q}q}^{\lambda \rightarrow t_1 t_2}(B; J_1^- n + \mathbf{J}_1, J_2^- n - \mathbf{J}_1) & \end{aligned} \quad (4.44)$$

Performing a similar sequence of operations for \mathcal{M}_R , we obtain the expression below

that is valid for $\Lambda^2 \ll \tilde{\mathbf{a}}_1^2, \tilde{\mathbf{b}}_1^2, \tilde{\mathbf{b}}_2^2 \ll Q^2$, or equivalently $\Lambda^2 \ll \mathbf{J}_1^2, \mathbf{J}_2^2, \mathbf{r}^2 \ll Q^2$:

$$\begin{aligned}
& \mathcal{M}_R^{\lambda; \mu_1 \mu_2 \mu_3 \chi}(A, B; J_1, J_2, r, \bar{A}) \\
& \simeq \sum_{s_i} \frac{-ir^+}{2} \left[\int d^2 \tilde{\mathbf{a}}'_1 / (2\pi)^2 \psi_p^{\tilde{s}'_1 \tilde{s}_2 \chi}(\tilde{a}'_1, J_2^+, \tilde{\mathbf{a}}'_1, \tilde{\mathbf{a}}_2, \bar{A}^-) \right] \\
& \quad \times \frac{\mathcal{M}_{q \rightarrow qg}^{\tilde{s}'_1 \rightarrow \tilde{s}_1 \mu_3}(\tilde{a}'_1 p, a_1^+ p - \mathbf{r}, (\tilde{a}'_1 - a_1^+)p + \mathbf{r})}{\mathbf{J}_2^2 \mathbf{r}^2 [J_1^+ + \frac{\mathbf{J}_2^2}{2J_2^-} + r^+]} \\
& \quad \times \mathcal{M}_{q\bar{q} \rightarrow \gamma^*}^{\tilde{s}_1 \tilde{t}_1; \mu_1}(J_1^+ p, J_1^- n \rightarrow J_1) \mathcal{M}_{q\bar{q} \rightarrow \gamma^*}^{\tilde{s}_2 \tilde{t}_2; \mu_2}(J_2^+ p, J_2^- n \rightarrow J_2) \\
& \quad \times \mathcal{M}_{g \rightarrow \bar{q}q}^{\lambda \rightarrow \tilde{t}_1 \tilde{t}_2}(B; J_1^- n - \mathbf{J}_2, J_2^- n + \mathbf{J}_2)
\end{aligned} \tag{4.45}$$

Given that the transverse momenta of the partons emerging from the $g \rightarrow q\bar{q}$ branching process are different on the left and right hand sides of the cut in figure 4.5(a) ($\pm \mathbf{J}_1$ and $\mp \mathbf{J}_2$ respectively), we will require a generalised version of the relation (4.25), which reads:

$$\begin{aligned}
& \frac{J_1^- J_2^-}{(J_1^- + J_2^-)^2} \mathcal{M}_{g \rightarrow \bar{q}q}^{\lambda \rightarrow t_1 t_2}(B; J_1^- n + \mathbf{J}_1, J_2^- n - \mathbf{J}_1) \mathcal{M}_{g \rightarrow \bar{q}q}^{*\lambda \rightarrow \tilde{t}_1 \tilde{t}_2}(B; J_1^- n - \mathbf{J}_2, J_2^- n + \mathbf{J}_2) \\
& = -4g_s^2 P_{g \rightarrow \bar{q}q}^{\lambda \rightarrow t_2 t_1, \tilde{t}_2 \tilde{t}_1} \left(\frac{J_2^-}{J_1^- + J_2^-} \right) \epsilon_\lambda \cdot \mathbf{J}_1 \epsilon_\lambda^* \cdot \mathbf{J}_2
\end{aligned} \tag{4.46}$$

Note that in the off-diagonal emission process, the partons emitting the gluon in the amplitude and conjugate do not in general have the same plus momentum (and indeed are not of the same type). This means that the product of $\mathcal{M}_{\bar{q} \rightarrow qg}$ and $\mathcal{M}_{q \rightarrow qg}^*$ from the left and right hand sides of the diagram does not give rise to a conventional splitting function multiplied by the appropriate transverse momentum squared, as occurred in (4.25). Instead, one obtains:

$$\begin{aligned}
& \frac{r^+ A^+}{\tilde{a}_1^+ a_2^+} \sqrt{\frac{a_1^+ a_2^+}{\tilde{a}_1^+ a_2^+}} \mathcal{M}_{\bar{q} \rightarrow qg}^{s'_2 \rightarrow s_2 \mu_3}(\tilde{a}_2^+ p, a_2^+ p - \mathbf{r}, (\tilde{a}_2^+ - a_2^+)p + \mathbf{r}) \\
& \quad \times \mathcal{M}_{q \rightarrow qg}^{*\tilde{s}'_1 \rightarrow \tilde{s}_1 \mu_3}(\tilde{a}_1^+ p, a_1^+ p - \mathbf{r}, (\tilde{a}_1^+ - a_1^+)p + \mathbf{r}) \\
& \quad \equiv 2g_s^2 V_{I, q \rightarrow q}^{\tilde{s}'_1 s'_2 \rightarrow \tilde{s}_1 s_2; \mu_3} \left(\frac{a_1^+}{A^+}, \frac{\tilde{a}_1^+}{A^+}, \frac{a_2^+}{A^+} \right) \mathbf{r}^2
\end{aligned} \tag{4.47}$$

where $V_{I, q \rightarrow q}^{\tilde{s}'_1 s'_2 \rightarrow \tilde{s}_1 s_2; \mu_3} \left(\frac{a_1^+}{A^+}, \frac{\tilde{a}_1^+}{A^+}, \frac{a_2^+}{A^+} \right)$ represents some kind of generalised splitting function,

that satisfies the following relation:

$$V_{I,q \rightarrow q}^{\bar{s}_1' s_2' \rightarrow \bar{s}_1 s_2; \mu_3} \left(\frac{a^+}{A^+}, \frac{a'^+}{A^+}, \frac{a'^+}{A^+} \right) = \frac{A^+}{a'^+} P_{q\bar{q}}^{\bar{s}_1' s_2' \rightarrow \bar{s}_1 s_2; \mu_3} \left(\frac{a^+}{a'^+} \right) \quad (4.48)$$

Furthermore, since the partons emerging from the hadronic blob in figure 4.5(a) do not in general carry the same momentum on the left and right hand sides of the diagram, the process in figure 4.5(a) probes a two-parton PDF that is not diagonal in x . It is defined according to:

$$\begin{aligned} \Gamma_{p;q\bar{q}}^{s_1 s_2, \bar{s}_1 \bar{s}_2} \left(\frac{a_1^+}{A^+}, \frac{a_2'^+}{A^+}, \frac{\tilde{a}_1'^+}{A^+} \right) &\equiv \frac{2}{(2\pi)^9} \sum_x \int d\bar{A}^- d^2 \bar{\mathbf{A}} d^2 \mathbf{a}_1 d^2 \tilde{\mathbf{a}}_1' \sqrt{a_1^+ a_2'^+ \tilde{a}_1'^+ \tilde{a}_2'^+} A^+ \\ &\times \psi_{p;q\bar{q}}^{s_1 s_2 \chi}(a_1^+, a_2'^+, \mathbf{a}_1, \mathbf{a}_2', \bar{A}^-, \bar{\mathbf{A}}) \psi_{p;q\bar{q}}^{*s_1' s_2' \chi}(\tilde{a}_1'^+, \tilde{a}_2'^+, \tilde{\mathbf{a}}_1', \tilde{\mathbf{a}}_2', \bar{A}^-, \bar{\mathbf{A}}) \end{aligned} \quad (4.49)$$

Note that this distribution is somewhat similar to the four-quark matrix element that is probed in the twist-four contribution to Drell-Yan, and that is defined in [32,85,136,137]. Here, however, we do not absorb two powers of the strong coupling constant g_s into the four quark matrix element, as is done (and makes sense) in the context of the twist-four contribution to Drell-Yan.

Inserting (4.43), (4.44), and (4.45) into (4.39), and making use of (4.46), (4.47) and (4.49), we find that the contribution to σ_{XT} coming from the region of transverse momentum integration with $\Lambda^2 \ll \mathbf{r}^2, \mathbf{J}_1^2, \mathbf{J}_2^2 \ll Q^2$ is:

$$\begin{aligned} \sigma_{XT}(s) &= \sum_{s_i \bar{s}_i t_i \bar{t}_i s_1' s_2'} \int dx_1 dx_2 dy_1 dy_2 \hat{\sigma}_{q\bar{q} \rightarrow \gamma^*}^{s_1, t_1; \bar{s}_1, \bar{t}_1; \mu_1}(\hat{s} = x_1 y_1 s) \hat{\sigma}_{q\bar{q} \rightarrow \gamma^*}^{s_2, t_2; \bar{s}_2, \bar{t}_2; \mu_2}(\hat{s} = x_2 y_2 s) \\ &\left[\frac{\alpha_s}{2\pi} \int_{x_1}^{1-x_2} d\tilde{x}_1' V_{I,q \rightarrow q}^{\bar{s}_1' s_2' \rightarrow \bar{s}_1 s_2; \mu_3}(x_1, \tilde{x}_1', x_2') \Gamma_{p;q\bar{q}}^{s_1 s_2, \bar{s}_1' \bar{s}_2'}(x_1, x_2', \tilde{x}_1') \right] \\ &\left[\frac{\alpha_s}{2\pi} P_{g \rightarrow q\bar{q}}^{\lambda \rightarrow t_2 t_1, \bar{t}_2 \bar{t}_1}(y_2) \delta(1 - y_1 - y_2) \right] \int d\mathbf{J}_1^2 d\mathbf{r}^2 \frac{2\epsilon_\lambda \cdot \mathbf{J}_1 \epsilon_\lambda^* \cdot (\mathbf{J}_1 + \mathbf{r})}{\mathbf{r}^2 \mathbf{J}_1^2 (\mathbf{J}_1 + \mathbf{r})^2} \end{aligned} \quad (4.50)$$

In the region of transverse momentum integration in which $\mathbf{r}^2 \ll \mathbf{J}_1^2, \mathbf{J}_2^2$, the transverse momentum integrand simplifies as below, and we obtain two large DGLAP logarithms from this region:

$$\int d\mathbf{J}_1^2 d\mathbf{r}^2 \frac{2\epsilon_\lambda \cdot \mathbf{J}_1 \epsilon_\lambda^* \cdot (\mathbf{J}_1 + \mathbf{r})}{\mathbf{r}^2 \mathbf{J}_1^2 (\mathbf{J}_1 + \mathbf{r})^2} \xrightarrow{\mathbf{J}_1^2 \gg \mathbf{r}^2} \int_{\Lambda^2}^{Q^2} \frac{d\mathbf{J}_1^2}{\mathbf{J}_1^2} \int_{\Lambda^2}^{\mathbf{J}_1^2} \frac{d\mathbf{r}^2}{\mathbf{r}^2} = \log^2 \left(\frac{Q^2}{\Lambda^2} \right) \quad (4.51)$$

Two large DGLAP logarithms implies a leading logarithmic contribution, since there are two powers of α_s in (4.50). Thus, there is a leading logarithmic contribution to the DPS cross section coming from the region of figure 4.5(a) in which $\mathbf{r}^2 \ll \mathbf{J}_1^2$ (i.e. in which the scale of the off-diagonal real emission process is strictly smaller than the scale of the $1 \rightarrow 2$ branching process). Note that it is only this region of transverse momentum integration that gives rise to a leading double logarithm – other regions only give rise to either a single logarithm, or no logarithm at all. The single DGLAP logarithm is essentially associated with a logarithmic integral over \mathbf{r} only, and this should be absorbed into the four-quark matrix element in the ‘conventional’ twist-4 contribution to double Drell-Yan.

Aside from the process in figure 4.5(a) involving an off-diagonal real emission, the process in figure 4.5(b) involving a virtual exchange also gives rise to a leading double logarithm, provided once again that the virtual exchange process occurs at a lower scale than the $1 \rightarrow 2$ branching. This is straightforward to show using a procedure similar to the one we have used above. Generalising these results, we find that in the most general 2v1 DPS diagram, all possible types of parton exchange are allowed inside the two ladders emerging from one of the protons at leading logarithmic order, provided that they occur at a lower scale than the $1 \rightarrow 2$ ladder branching occurring in the other proton. Schematically, the LO (diagonal unpolarised) cross section expression for the 2v1 contribution to DPS is:

$$\begin{aligned} \sigma_{(A,B)}^{D,2v1}(s) = & 2 \times \frac{m}{2} \sum_{liji'i'j'_i} \int_{\Lambda^2}^{Q^2} dk^2 \frac{\alpha_s(k^2)}{2\pi k^2} \int dx_1 dx_2 dy_1 dy_2 \frac{dx'_1}{x'_1} \frac{dx'_2}{x'_2} \frac{dy'_1}{y'_1} \frac{dy'_2}{y'_2} \\ & \times \hat{\sigma}_{i_1 j_1 \rightarrow A}(\hat{s} = x_1 y_1 s) \hat{\sigma}_{i_2 j_2 \rightarrow B}(\hat{s} = x_2 y_2 s) \\ & \times \frac{D_h^l(y'_1 + y'_2, k^2)}{y'_1 + y'_2} P_{l \rightarrow j'_1 j'_2} \left(\frac{y'_1}{y'_1 + y'_2} \right) D_{j'_1}^{j_1} \left(\frac{y_1}{y'_1}; Q^2, k^2 \right) D_{j'_2}^{j_2} \left(\frac{y_2}{y'_2}; Q^2, k^2 \right) \\ & \times D_{i'_1}^{i_1} \left(\frac{x_1}{x'_1}; Q^2, k^2 \right) D_{i'_2}^{i_2} \left(\frac{x_2}{x'_2}; Q^2, k^2 \right) \Gamma_h^{i'_1 i'_2}(x'_1, x'_2; x'_1, k^2) \end{aligned} \quad (4.52)$$

$\Gamma_h^{i'_1 i'_2}(x_1, x_2; \tilde{x}_1, \mu^2)$ is a four-parton matrix element whose evolution involves all possible exchanges between these partons in an axial gauge³ [138].

Note that at the next-to-leading logarithmic (or NLO) level, one needs to append an

³In a covariant gauge, such as Feynman gauge, there are further diagrams that contribute to the evolution due to the presence of a nontrivial Wilson line in the definition of the operator. These diagrams involve gluon connections to the Wilson line.

extra term to (4.52) that is of the following form:

$$\int dx_1 dx_2 d\tilde{x}_1 dy D_h^k(y, Q^2) \Gamma_h^{ij}(x_1, x_2; \tilde{x}_1, Q^2) \hat{\sigma}_{ijk \rightarrow AB}(x_1, x_2, \tilde{x}_1, y) \quad (4.53)$$

This is essentially the ‘conventional’ twist-4 contribution to the $pp \rightarrow AB + X$ production cross section. At the level of total cross sections, the DPS contribution to the production of AB cannot be distinguished from the conventional twist-4 contribution, and the two should really just be considered together as components of the $\mathcal{O}(\Lambda^2/Q^2)$ correction to the $pp \rightarrow AB + X$ cross section.

Let us now discuss the issue of colour in the evolution of the four-parton (twist-4) matrix element $\Gamma_h^{i'_1 i'_2}(x_1, x_2; \tilde{x}_1, \mu^2)$. We recall that, for the 2pGPD with finite \mathbf{b} , every distribution that does not have the partons with the same light-cone momentum fractions on either side of the cut paired up into colour singlets is suppressed by a Sudakov factor – see section 3.2.2 and references therein. This factor arises in axial gauge because there is an incomplete cancellation of the soft gluon region between (diagonal) real emission diagrams and virtual self-energy corrections in the colour interference/correlation distributions [84]. In physical terms, it occurs because such distributions involve a movement of colour by the large transverse distance \mathbf{b} in the hadron [33].

In the twist-4 matrix element $\Gamma_h^{i'_1 i'_2}(x_1, x_2; \tilde{x}_1, \mu^2)$ there is no such Sudakov suppression of colour interference/correlation distributions. The extra diagrams that are allowed in the evolution of this distribution (i.e. the off-diagonal emission and virtual exchange diagrams in axial gauge) provide extra soft-gluon divergences that cancel any remaining divergence from adding the diagonal real emission and virtual self-energy diagrams together. The soft divergence in both real emission diagrams (diagonal and off-diagonal) is positive, whilst that in both virtual diagrams (self-energy and exchange) is negative, and in the sum the positive and negative contributions always cancel each other out. We can see why this cancellation occurs physically as follows. In the operator definition of the twist-4 matrix element, the four operators corresponding to the partons all lie on the same lightlike line, with no transverse separation between any of them. Note that this does not correspond exactly to the physical situation – in (4.52) the transverse separation of the partons in $\Gamma_h^{i'_1 i'_2}(x'_1, x'_2; x'_1, k^2)$ is in fact more like $1/|\mathbf{k}|$ – but for the purposes of obtaining $\Gamma_h^{i'_1 i'_2}(x'_1, x'_2; x'_1, k^2)$ by solving the evolution equation at scales $\mu^2 < k^2$, the distinction is unimportant. The fact that the four operators/partons in $\Gamma_h^{i'_1 i'_2}(x_1, x_2; \tilde{x}_1, \mu^2)$ are on top of (or at least very close to) one another in transverse space means that soft longwave

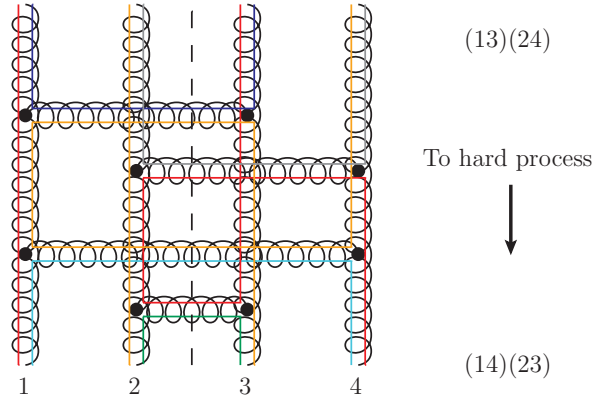


Figure 4.6: A process that can bring about a colour recombination in the four gluon state. On the diagram we have indicated the colour flow in the large N_C limit.

gluons can only resolve the total colour of all of them. But the summed colour of the four partons must be zero, since the proton is a colour singlet object – therefore the effects of soft gluons must cancel, as is indeed observed in practical calculations. The cancellation of soft gluon divergences in the twist-4 matrix elements has been discussed before, in [131, 139, 140] (for example).

Let us now focus our attention on the region of small x (which is perhaps the most relevant region of x for DPS processes at the LHC). It is well known that in this region the gluons dominate, so we will only consider these partons in what follows. We have seen that the colour correlated/interference twist-4 distributions are not Sudakov suppressed – however, in the low x region, the distributions in which two pairs of gluons are in colour singlet configurations tend to win out. This is because the colour factors in the anomalous dimensions for these distributions are larger (see section 3.2 of [131] or section 5.1.3 of [37]). Bear in mind that in figure 4.3 at scale k^2 the nonperturbatively generated partons with identical x fractions must be in a colour singlet state if one wants to avoid any Sudakov suppression. By combining two off-diagonal real emission processes put together with two diagonal real emission processes as in figure 4.6, it is possible to achieve a ‘colour recombination’ on the two ladder side at scales lower than k^2 , and alter the way in which the parton legs are grouped into two sets of colour singlets. For example, in figure 4.6 the grouping is changed from (14)(23) afterwards to (13)(24) before, using the leg labelling conventions from the figure. Such a colour recombination is not disfavoured from the point of view of evolution before and after the process – however, it is itself suppressed by a colour factor equal to $1/(N_C^2 - 1)$ [131–135]. This colour factor suppression is associated

with the fact that the recombination process is non-planar.

Based on these observations, one might expect that crosstalk processes and colour recombinations actually make very little numerical impact on the 2v1 DPS cross section at small x . On the other hand, in an investigation of the four-gluon matrix element in the context of shadowing corrections to DIS [134], it has been shown that despite the $1/(N_C^2 - 1)$ suppression of the ‘recombination vertex’, the inclusion of recombination effects in the evolution of the four-gluon matrix element leads to an increase in this matrix element by approximately 70%, for values of x and an ‘evolution length’ $t = \ln(Q^2/Q_0^2)$ relevant to the HERA experiment ($x \simeq 10^{-3}$, $t \simeq 3$). According to equation (23) in [134] this correction should become even larger for smaller values of x and longer evolution lengths, such as those that will be relevant in DPS at the LHC. Therefore, we cannot simply ignore the effect of the recombination processes in the 2v1 DPS cross section purely because of their colour suppression – they must be carefully taken into account.

From the point of view of low x physics, there is an important distinction between the two crosstalk processes that we have discussed in this section – i.e. the off-diagonal real emission and virtual exchange processes. The off-diagonal real emission process can significantly reduce the magnitudes of the lightcone momentum fractions of the two active parton legs involved in the process, since it is a real emission process. On the other hand, the same is not true for the virtual exchange process. Here, the sum of the lightcone momentum fractions of the two parton legs involved must be conserved, and since the two legs are forced to have positive lightcone momentum fractions by the kinematics of the process, the magnitudes of both x s cannot simultaneously decrease – one must increase to compensate the decrease of the other. This means that, taking all partons involved to be gluons as is appropriate at low x , the virtual exchange splitting function is not enhanced at small x in the same way that the off-diagonal exchange (and indeed diagonal exchange) splitting functions are. In particular, the virtual exchange diagrams do not contribute at double leading logarithmic order to the evolution of the four-gluon matrix element. This result has been known for some time – see [131, 141–145]. This is the reason why we drew the colour recombination process in figure 4.6 using two off-diagonal real emission processes – it would be also possible to engineer a colour recombination using two virtual exchange processes instead, but such a process would not be as strongly enhanced at low x .

The statement that the ‘ $\mathbf{b} = \mathbf{0}$ ’ twist-4 distributions probed in the 2v1 contribution to DPS evolve differently from the 2pGPDs with finite \mathbf{b} has been made recently in Appendix

A of [127]. However, in this paper it is claimed that only the evolution of the colour correlation/interference distributions changes at $\mathbf{b} = \mathbf{0}$ – we contend that the evolution of the colour diagonal/singlet distribution is also affected in an important way. In equation (A1) of [127], an evolution equation for the colour octet twist-4 $q\bar{q}$ distribution diagonal in x fractions is proposed. However, the equation they propose involves only similar distributions diagonal in x fractions on the right hand side – in fact the correct evolution equation should contain more general distributions nondiagonal in x on the right hand side, since the crosstalk processes that are allowed for $\mathbf{b} = \mathbf{0}$ will necessarily disrupt a diagonal/symmetric pattern of x values⁴.

4.4 Total Cross Section for Double Parton Scattering

In this chapter and the last we have examined several different types of diagram that can potentially contribute to the LO pp DPS cross section – the ‘1v1’ graph of figure 3.7 (or figure 4.1(c)), the ‘2v1’ graphs of figures 4.1(b) and 4.3, and (briefly) the ‘2v2’ graphs of figure 4.1(a). In the previous chapter, we suggested that the ‘1v1’ diagrams should not be included at all in the LO pp DPS cross section. In this chapter we have seen some indication that the ‘2v1’ diagrams should be included, with crosstalk effects incorporated on the ‘two-ladder’ side (up to the scale of the $1 \rightarrow 2$ branching on the other side), and with a different geometrical prefactor to the one appearing in the ‘2v2’ contribution. We therefore tentatively suggest the following expression for the total pp DPS cross section:

$$\sigma_{(A,B)}^D(s) = \sigma_{(A,B)}^{D,2v2}(s) + \sigma_{(A,B)}^{D,2v1}(s) \quad (4.54)$$

with $\sigma_{(A,B)}^{D,2v2}(s)$ and $\sigma_{(A,B)}^{D,2v1}(s)$ being given by the expressions (4.33) and (4.52) respectively⁵.

Three other groups have produced papers containing explicit formulae for the total LO

⁴After the work [125] was completed we learned of the published version of ‘What is Double Parton Scattering?’ by Manohar and Waalewijn [146] in which were corrected the errors of the arXiv version [127] discussed here. The discussion in that paper now appears to be in alignment with our own findings.

⁵Note that this is really our prediction for the unpolarised diagonal contribution to the total DPS cross section when the scales of the two hard interactions are the same, $Q_A^2 = Q_B^2 = Q^2$. To generalise this result to unequal scales, one needs to change Q^2 to Q_A^2 in all Green’s functions in (4.52) involving a ‘1’ index, change Q^2 to Q_B^2 in all Green’s functions in (4.52) involving a ‘2’ index, change the upper limit of the k^2 integration to $\min(Q_A^2, Q_B^2)$, and perform a similar operation for the ‘2v2’ contribution. As mentioned previously, the contributions associated with spin polarisation (either longitudinal or transverse) and flavour interference are expected to have a similar structure to (4.54), whilst the colour correlation/interference and parton type interference contributions should be suppressed by Sudakov factors, as is discussed in section 3.2.2.

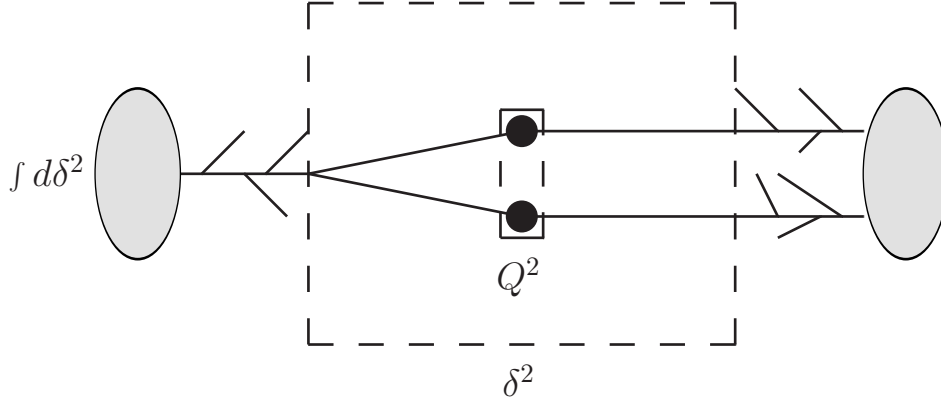


Figure 4.7: Schematic depiction of the extra ‘2v1’ contribution to the total LO DPS cross section included in section VI of [35].

pp DPS cross section in QCD – Snigirev and Ryskin [126], Blok et al. [35], and Manohar and Waalewijn [33, 127]. The results given in these papers differ from (4.54) and from each other. In this section we will comment on the discrepancies between our result for the DPS cross section (4.54) and those presented in [33, 35, 126, 127].

In none of the papers [33, 35, 126, 127] are the crosstalk effects in the 2v1 graphs taken into account correctly. In [35, 126] they appear to have been overlooked, whilst in [33, 127] they are included in an incorrect fashion, as we have already mentioned at the end of section 4.3. In fact, the only difference between the formula proposed in [33, 127] and our equation (4.54) is in the treatment of crosstalk effects in the 2v1 contribution⁶.

In the paper of Blok et al. [35], it is suggested in section VI that there is an additional ‘2v1’ contribution to the total DPS cross section which is not included in our formula (4.54) (and is distinct from the additional crosstalk contribution that we identified in section 4.3). This extra contribution is contained in equation (32c) of that paper. Here we will attempt to represent this expression visually, in figure 4.7, and in words. The extra contribution included by Blok et al. is associated with graphs in which one proton provides two partons at a low scale, and the other only one. The two partons from one side and the one from the other are both allowed to emit partons up to a common scale δ . At this point the single parton splits into two, and all further parton emissions from the resulting four partons are vetoed up to the scale Q .

At this point it is essential to recognise that graphs of this exact character are already

⁶In the published version of ‘What is Double Parton Scattering?’ by Manohar and Waalewijn [146] the discussion of crosstalk effects has been revised such that their equation for the DPS cross section appears to agree with our own.

included in the part of the cross section formula in section VI of [35] that is equivalent to the ‘no crosstalk’ part of (4.54). The ‘no crosstalk’ 2v1 parts of (4.54) correspond to graphs in which a parton from one proton splits into two and the two daughters interact with two partons from the other proton, with any number of (diagonal) parton emissions on either side along the way (this includes the case in which there are no emissions between certain scales on either/both sides, and/or no emissions on certain legs). In our view, the additional contribution to the DPS cross section presented in equation 32(c) arises from double counting and so should not be included.

To get an idea of how such double counting could have occurred, let us examine the process by which equations (32a-c) were derived. Following [81] let us define the total transverse momentum of the products of one hard scattering in the DPS process as \mathbf{Q}_1 , and the transverse momentum of the products of the other as \mathbf{Q}_2 . In [35], expressions for the differential DPS cross section are obtained in the limit $\mathbf{Q}_1^2, \mathbf{Q}_2^2 \ll Q^2$ and also in the limit $(\mathbf{Q}_1 + \mathbf{Q}_2)^2 \ll \mathbf{Q}_1^2, \mathbf{Q}_2^2 \ll Q^2$. The expressions in the two limits were integrated over transverse momenta and then added to get the total DPS cross section. But the two regions $\mathbf{Q}_1^2, \mathbf{Q}_2^2 \ll Q^2$ and $(\mathbf{Q}_1 + \mathbf{Q}_2)^2 \ll \mathbf{Q}_1^2, \mathbf{Q}_2^2 \ll Q^2$ are not mutually exclusive – in fact the latter is contained within the former. Therefore on integrating and adding the two expressions one will make a double counting error.

It is perhaps worth pointing out in passing that the additional contribution of equation (32c) in [35] would probably make very little numerical difference to the DPS cross section even if it was included. There are so many constraints on the emission allowed in the additional 2v1 contribution compared to the 2v1 contribution of (4.54) that it is likely the former is highly suppressed compared to the latter.

Snigirev and Ryskin include a contribution from the 1v1 graphs in their formula for the LO DPS cross section [126], where we (and the authors of [33,35,127]) do not include such a contribution. The contribution that Snigirev and Ryskin include essentially corresponds to our expression for the ‘DPS singular’ (or small transverse momentum and virtuality) part of a Standard Model crossed box, with strongly ordered parton emissions being added onto the initial and internal legs of the box and summed over. A cutoff Λ_{RS} on the loop transverse momentum imbalance between amplitude and conjugate Δ (denoted in [126] as q) has to be added ‘by hand’ in this expression to avoid a divergent result – the scale chosen for the cutoff Λ_{RS} is the hard scale $\sqrt{Q^2}$. It is argued that the inclusion of such a 1v1 term is valid for small x values in the hard scattering subprocesses. In this regime, there is strong pressure on either side of the 1v1 diagram for most of the evolution in x

and transverse momentum to occur after the $1 \rightarrow 2$ perturbative splitting. This is because there are two legs emitting partons after the $1 \rightarrow 2$ splitting rather than one – then, if one has most of the evolution after the $1 \rightarrow 2$ splitting one effectively maximises the number of splittings and accompanying large logarithms of $1/x$. It is suggested in [126] that this pressure forces most of the contribution to their 1v1 expression to come from the region in which Δ and the transverse momenta of all partons in the graph $\ll \sqrt{Q^2}$ (as is required for a contribution to the DPS cross section). The sensitivity of the result to the ad-hoc cut-off Λ_{RS} in the low x regime is then supposed to be minimal.

We can be certain that the Ryskin-Snigirev 1v1 expression cannot continue to be included in the DPS cross section at moderate to large x values. At such x values, the integrals over transverse momenta inside the 1v1 loops in the Ryskin-Snigirev expression become dominated by values of order $\sqrt{Q^2}$, and the 1v1 graphs should rather be included as part of the SPS cross section. Note that the Ryskin-Snigirev 1v1 expression is a very poor approximation to the contribution from the 1v1 graphs in this x regime, since the expression inside the integral has been derived in the limit in which all transverse momenta and virtualities inside the loop are $\ll \sqrt{Q^2}$, whereas the dominant contribution to the integral comes from transverse momenta and virtualities of $\mathcal{O}(\sqrt{Q^2})$. An explicit indicator of the inadequacy of the Ryskin-Snigirev 1v1 expression in the moderate to large x region is a strong dependence of the expression on Λ_{RS} in this region. These points are echoed in the recent paper [130]. This paper also presents some numerical investigations performed under the double leading logarithm approximation, that give some indication of how small the x values need to be (and how large Q needs to be) before it is appropriate to use the DPS cross section expression of [126] (although one should recall that the crosstalk interactions in the 2v1 contribution are erroneously neglected in this paper).

We would like to point out at this stage that there are two features in the equation (4.54) that are potentially concerning, and that might indicate that modifications to it may be required in order to correctly describe the DPS cross section.

The first issue is that we were originally expecting to obtain an expression for the DPS cross section looking something like (1.72) (or (1.73)), with the 2pGPDs in these formulae each having an interpretation in terms of hadronic operator matrix elements. Our proposed expression (4.54) deviates somewhat in structure from these expectations. An important consequence of this is that in (4.54) we no longer have the concept of a cleanly defined 2pGPD with an associated evolution equation.

The second issue is that there is a rather sharp distinction in (4.54) between pertur-

batively and nonperturbatively generated parton pairs, with the 2pGPD for the latter having a natural width in \mathbf{r} space of order Λ (as was discussed in section 4.2). Does there exist some scale at which we can (approximately) regard all parton pairs in the proton as being ‘nonperturbatively generated’ in this sense (as is assumed in (4.54))? If so, what is the appropriate value for the scale (presumably it should be rather close to Λ_{QCD})?

These issues are related in an essential way to the fact that we have cut the contribution from ‘1v1’ graphs out of the DPS cross section entirely. It may therefore not be correct to entirely remove these graphs from the DPS cross section in this way. On the other hand, at present we do not have a suitable alternative prescription for handling these graphs, and leave finding the appropriate way of including the 1v1 graphs to future work.

4.5 Conclusions

In this section we have closely examined the contribution to the LO p-p DPS cross section from graphs in which two ‘nonperturbatively generated’ ladders interact with two ladders that have been generated via a perturbative $1 \rightarrow 2$ branching process – ‘2v1’ graphs. We have presented a detailed calculation demonstrating that 2v1 graphs in which the two nonperturbatively generated ladders do not interact with one another contribute to the LO p-p DPS cross section in the way originally written down by Ryskin and Snigirev [126], and then later by Blok et al. [35] and Manohar and Waalewijn [33, 127]. We have also shown that 2v1 graphs in which the ‘nonperturbatively generated’ ladders exchange partons with one another contribute to the LO p-p DPS cross section, provided that this ‘crosstalk’ occurs at a lower scale than the $1 \rightarrow 2$ branching on the other side of the graph. We have proposed a formula for the contribution from 2v1 graphs to the LO DPS cross section, equation (4.52).

Crosstalk interactions between the two nonperturbatively generated ladders are suppressed by colour effects, as has been noted in past studies of these interactions in the context of the twist 4 contribution to DIS. The most likely type of crosstalk interaction at low x is a ‘colour recombination’, in which the grouping of the four parton legs into two colour singlet ladders is altered – this is preferred because it maintains the overall system as two colour singlet ladders, and the anomalous dimension is largest for this configuration. For such a recombination, the colour factor associated with the vertex is $1/(N_C^2 - 1)$. However, this suppression of the vertex does not necessarily mean that the effects of colour recombinations can be neglected – it was discovered in [134] that crosstalk

effects significantly affected the size of the four-gluon twist-4 operator for x values $\simeq 10^{-3}$ and an evolution length $\ln(Q^2/Q_0^2) \simeq 3$, so it is plausible that they could have an important impact in the context of DPS at the LHC. Clearly, more detailed investigations are required in order to assess the precise numerical contribution of colour recombinations on the DPS cross section.

We combined our formula for the 2v1 contribution to the DPS cross section (4.52) with the suggestion that we made in section 3.3 that 1v1 graphs should be completely removed from the DPS cross section to suggest a formula for the DPS cross section, equation (4.54). This proposed formula was compared with those found in [33, 35, 126, 127]. Two potentially concerning features were identified in (4.54), and the existence of these might indicate that completely removing the 1v1 graphs from the DPS cross section is not quite the correct prescription. The determination of the appropriate manner of treating the 1v1 graphs is left to future work.

Chapter 5

Conclusions

Protons are composite objects, made up of point-like quark and gluon constituents (collectively, partons). This means that when two protons collide, such as occurs in the Large Hadron Collider at CERN in Geneva, there is the possibility to have more than one hard parton-parton interaction in the proton-proton collision process. Multiple hard interactions are typically rare compared to single hard interactions, and are often neglected in phenomenological calculations. However, double parton scattering (as the most probable multiple hard interaction process) can give rise to important backgrounds to rare single scattering processes, and is also an interesting signal process in its own right, as it sheds light on the correlations between partons in the proton. DPS is expected to be more important relative to SPS at the LHC than at any previous hadron-hadron collider, owing to the higher energy of this machine. In this thesis we have studied the theoretical description of double parton scattering.

In Chapter 2 we described the double PDF (dPDF) framework for describing proton-proton DPS that was introduced in the series of papers [4–6] by Snigirev *et al.* We showed that the equal-scale dPDF objects of [4, 5] are subject to momentum and number sum rule constraints, and used these constraints to guide the construction of a sensible set of nonperturbative LO dPDF inputs at the scale $Q_0 = 1$ GeV, corresponding to the MSTW 2008 LO single PDF inputs. The inputs were evolved to higher scales using the LO ‘double DGLAP’ equation of [4, 5], generating an explicit set of equal-scale dPDFs (the ‘GS09’ dPDFs), that incorporated pQCD effects as well as number and momentum sum rule constraints, and which could be used for phenomenology. We investigated how the leptonic same-sign WW DPS signal generated using GS09 dPDFs differed from that obtained using simple products of MSTW 2008 LO sPDFs multiplied by $(1 - x_1 - x_2)^n$

factors as the dPDFs. It was found that the GS09 prediction for the lepton pseudorapidity asymmetry a_{ν_ℓ} differed significantly from that obtained using the simple ‘MSTW_n’ dPDFs. It was found to be larger owing to the fact that the GS09 dPDFs correctly take account of the fact that finding a large x valence quark in the proton significantly reduces the chance to find another (since the number of valence quarks in the proton is small). A detailed study of the single scattering (SPS) backgrounds to the leptonic same-sign WW signal revealed that these backgrounds were large and difficult to suppress using kinematic cuts – this fact coupled with the small signal cross section means that observation of the distinguishing features of the GS09 DPS signal is unlikely in the near future.

In Chapter 3 we established two ways in which the dPDF framework for describing proton-proton DPS is deficient. We showed using simple arguments that there can be contributions to the DPS cross section associated with correlation and interference effects in flavour, spin, colour and parton type (i.e. quark, antiquark or gluon), although we also found that the contributions associated with colour correlation and interference, and parton type interference, are Sudakov suppressed. These facts were established long ago [83,84] and revisited recently [33,36,37], but the correlation and interference distributions have received rather little phenomenological attention, and are neglected by the dPDF framework. After this, we presented a detailed study of a particular Landau singularity in one-loop integrals known as the double parton scattering singularity, and derived a compact analytic expression for the DPS singular part of an arbitrary one loop integral. Using the results of this study we established that the treatment of so-called ‘double perturbative splitting’ or ‘1v1’ graphs by the dPDF framework is unsatisfactory. We suggested that such graphs should not be included in the LO DPS cross section, and instead should be regarded as a contribution to the SPS cross section. Our study of the DPS singularity in one-loop graphs was not only relevant to the topic of DPS – it also answered some unresolved questions posed by the NLO multileg community in recent years.

Even though we discovered in Chapter 3 that the dPDF framework for describing proton-proton DPS contains flaws, there is still value in the content of Chapter 2. The momentum and valence number constraints implemented in GS09 must also be present at some level in the true description of DPS, so use of GS09 to predict DPS signals represents an improvement on the approaches used previously involving products of single PDFs. It is very possible that the qualitative distinguishing features of the GS09 same-sign WW signal that we discovered, caused by very elementary valence number conservation

considerations, should be present in the true DPS signal. Finally, as we discussed in Chapter 3, although proton-proton DPS turns out not to directly involve the dPDFs, there is a process which does – the two-nucleon contribution to proton-heavy nucleus DPS. The GS09 dPDFs can be used in the cross section predictions for this process.

Chapter 4 was dedicated to a detailed study of a further class of graph that can potentially contribute to the LO pp DPS cross section – ‘2v1’ graphs in which two non-perturbatively generated ladders interact with one ladder that has split perturbatively into two. We discovered that graphs of the 2v1 type contribute to the LO DPS cross section, that crosstalk between the ‘nonperturbatively generated’ ladders is permissible at leading logarithmic order provided that it occurs at a lower scale than the $1 \rightarrow 2$ branching, and that the geometrical prefactor for these graphs is different in general from that for the ‘2v2’ graphs. These results were combined with our suggestion for handling the ‘1v1’ graphs made in Chapter 3 to obtain an expression for the total DPS cross section at LO, and our suggested expression was compared with those found in [33, 35, 126, 127]. We pointed out that there were two potentially concerning features in our equation, and the existence of these might indicate that completely removing the 1v1 graphs from the DPS cross section is not quite the correct prescription.

There is still a considerable amount of work left to do in the field of double parton scattering theory. One important issue that in our view has not yet been resolved in a satisfactory manner is one that we have just touched upon – namely, the appropriate way of treating the 1v1 graphs. There is also a need to go beyond the simple ‘leading logarithmic approach’ we have taken here, and derive (if possible) all-order factorisation formulae for the total DPS cross section and cross section differential in final state momentum, in terms of parton level cross sections and operator matrix elements (of which two should be hadronic). Important progress towards these goals has been made by Diehl, Ostermeier and Schafer in [36, 37], but a number of important theoretical issues remain which need to be addressed. Once the theoretical framework for describing DPS is firmly established, a number of further avenues for further work open up. In particular, it would be interesting to perform a detailed phenomenological study of the interference and correlated parton contributions to DPS for different DPS processes and hard scales in the double scattering, and attempt to estimate their size relative to the ‘diagonal unpolarised’ contribution that is usually the only one considered. It would also be interesting to investigate the precise numerical impact of the crosstalk effects in the 2v1 contribution to DPS that we discovered in section 4.3. We intend to pursue these avenues of investigation in the future.

Appendix A

Conventions and Notation

In this thesis, we follow the conventions used by Peskin and Schroeder [17], although some of our notation is slightly different. We briefly outline our notation and conventions here.

As is normal in studies of high energy physics, we choose to use ‘natural units’, a set of units in which:

$$\hbar = c = 1 \tag{A.1}$$

The metric tensor is defined as follows:

$$g_{\mu\nu} = g^{\mu\nu} = \begin{pmatrix} 1 & 0 & 0 & 0 \\ 0 & -1 & 0 & 0 \\ 0 & 0 & -1 & 0 \\ 0 & 0 & 0 & -1 \end{pmatrix} \tag{A.2}$$

with the Greek indices running over $0, 1, 2, 3$ or t, x, y, z . We denote four-vectors using ordinary italicised letters, whilst spatial three-vectors are denoted using a right-facing arrow over the letter. So, for example, we have:

$$V^\mu = (V^0, \vec{V}) \quad V_\mu = (V^0, -\vec{V}) \tag{A.3}$$

$$V \cdot W = V^0 W^0 - \vec{V} \cdot \vec{W} \tag{A.4}$$

We often make use of a light-cone coordinate system, or equivalently a lightcone decomposition (or Sudakov decomposition) of four-vectors in the problem. Our conventions

for such a decomposition are as follows. First we define vectors p and n as follows:

$$p = \frac{1}{\sqrt{2}}(1, 0, 0, 1) \quad n = \frac{1}{\sqrt{2}}(1, 0, 0, -1) \quad (\text{A.5})$$

Then we write an arbitrary four vector V in terms of p , n and $\mathbf{V} \equiv (V^1, V^2)$ as follows:

$$V^\mu = V^+ p + V^- n + \mathbf{V} \quad (\text{A.6})$$

Note that we always use a bold letter to denote a two-component transverse vector, rather than a three-component spatial vector. Occasionally we will write a four-vector V in terms of the light-cone components:

$$V = (V^+, V^-, \mathbf{V}) \quad (\text{A.7})$$

The ‘plus’ and ‘minus’ components of V are related to the ‘0’ and ‘3’ components according to:

$$V^\pm = \frac{1}{\sqrt{2}}(V^0 \pm V^3) \quad (\text{A.8})$$

The dot product of two four-vectors V and W written in terms of their light-cone components is:

$$V \cdot W = V^+ W^- + V^- W^+ - \mathbf{V} \cdot \mathbf{W} \quad (\text{A.9})$$

We define the four-momentum operator acting on a single-particle wavefunction according to the usual conventions:

$$p^\mu = i\partial^\mu \quad (\text{A.10})$$

For the Dirac (or gamma) matrices, we use a chiral basis:

$$\gamma^0 = \begin{pmatrix} 0 & \mathbb{1} \\ \mathbb{1} & 0 \end{pmatrix} \quad \gamma^i = \begin{pmatrix} 0 & \sigma^i \\ -\sigma^i & 0 \end{pmatrix} \quad (\text{A.11})$$

where the σ^i are the Pauli matrices:

$$\sigma^1 = \begin{pmatrix} 0 & 1 \\ 1 & 0 \end{pmatrix} \quad \sigma^2 = \begin{pmatrix} 0 & -i \\ i & 0 \end{pmatrix} \quad \sigma^3 = \begin{pmatrix} 1 & 0 \\ 0 & -1 \end{pmatrix} \quad (\text{A.12})$$

The matrices (A.11) satisfy the required relation for gamma matrices:

$$\{\gamma^\mu, \gamma^\nu\} = 2g^{\mu\nu} \quad (\text{A.13})$$

where the brackets $\{\dots\}$ denote the anticommutator. We define the chirality matrix γ^5 according to $\gamma^5 \equiv i\gamma^0\gamma^1\gamma^2\gamma^3$ – in our chiral basis it has the explicit form:

$$\gamma^5 = \begin{pmatrix} -\mathbb{1} & 0 \\ 0 & \mathbb{1} \end{pmatrix} \quad (\text{A.14})$$

We often make use of the helicity eigenstates for the particle and antiparticle spinors u and v . For a particle with 3-momentum $\vec{p} = (p \sin(\theta) \cos(\phi), p \sin(\theta) \sin(\phi), p \cos(\theta))$ and energy $E = \sqrt{p^2 + m^2}$, these are defined in our chiral basis as follows:

$$\begin{aligned} u_\uparrow(p) &= \begin{pmatrix} \frac{m}{E+p} \cos\left(\frac{\theta}{2}\right) \\ \frac{m}{E+p} e^{i\phi} \sin\left(\frac{\theta}{2}\right) \\ \cos\left(\frac{\theta}{2}\right) \\ e^{i\phi} \sin\left(\frac{\theta}{2}\right) \end{pmatrix} & u_\downarrow(p) &= \begin{pmatrix} -\sin\left(\frac{\theta}{2}\right) \\ e^{i\phi} \cos\left(\frac{\theta}{2}\right) \\ -\frac{m}{E+p} \sin\left(\frac{\theta}{2}\right) \\ \frac{m}{E+p} e^{i\phi} \cos\left(\frac{\theta}{2}\right) \end{pmatrix} \\ v_\uparrow(p) &= \begin{pmatrix} -\sin\left(\frac{\theta}{2}\right) \\ e^{i\phi} \cos\left(\frac{\theta}{2}\right) \\ \frac{m}{E+p} \sin\left(\frac{\theta}{2}\right) \\ -\frac{m}{E+p} e^{i\phi} \cos\left(\frac{\theta}{2}\right) \end{pmatrix} & v_\downarrow(p) &= \begin{pmatrix} \frac{m}{E+p} \cos\left(\frac{\theta}{2}\right) \\ \frac{m}{E+p} e^{i\phi} \sin\left(\frac{\theta}{2}\right) \\ -\cos\left(\frac{\theta}{2}\right) \\ -e^{i\phi} \sin\left(\frac{\theta}{2}\right) \end{pmatrix} \end{aligned} \quad (\text{A.15})$$

These spinors are normalised according to:

$$u_r^\dagger(p) u_s(p) = 2E \delta_{rs} \quad v_r^\dagger(p) v_s(p) = 2E \delta_{rs} \quad (\text{A.16})$$

They obey the Dirac equation in the form:

$$\begin{aligned} 0 &= (\not{p} - m) u_s(p) = \bar{u}_s(p) (\not{p} - m) \\ &(\not{p} + m) v_s(p) = \bar{v}_s(p) (\not{p} + m) \end{aligned} \quad (\text{A.17})$$

where:

$$\not{p} \equiv p_\mu \gamma^\mu \tag{A.18}$$

$$\bar{u} \equiv u^\dagger \gamma^0 \tag{A.19}$$

Appendix B

Numerical techniques for evaluating dDGLAP integrals

Let us consider the integrals which have to be numerically approximated using the (x_1, x_2) grid. All of these integrals are of the following schematic form:

$$I(y) = \int_x^{1-y} \frac{dz}{z} D(z, y) P\left(\frac{x}{z}\right) \quad (\text{B.1})$$

The splitting function $P(x)$ may in general consist of three terms. The first of these is a regular term $A(x)$ and the second is a term proportional to a delta function $K\delta(1-x)$. The final term consists of a product of two factors. The first of these is a simple regular function $R(x)$, whilst the second is a function $S(x)$ containing a singular factor $1/(1-x)$ which is regularised by the plus prescription:

$$P(x) = A(x) + K\delta(1-x) + R(x)[S(x)]_+. \quad (\text{B.2})$$

Inserting the form (B.2) into (B.1), we find that the integrals which have to be approximated using the grid have the following general form:

$$I(y) = I_1(y) + I_2(y) + I_3(y) \text{ with} \quad (\text{B.3})$$

$$I_1(y) \equiv \int_x^{1-y} \frac{dz}{z} D(z, y) A\left(\frac{x}{z}\right) \quad (\text{B.4})$$

$$I_2(y) \equiv K D(x, y) \quad (\text{B.5})$$

$$\begin{aligned}
I_3(y) \equiv & \int_x^{1-y} \frac{dz}{z} S\left(\frac{x}{z}\right) \left[D(z, y) R\left(\frac{x}{z}\right) - \frac{x}{z} D(x, y) R(1) \right] \\
& - R(1) D(x, y) \int_0^{x/(1-y)} dz S(z).
\end{aligned} \tag{B.6}$$

The integral in the last term of (B.6) can be done analytically for each splitting function. The integrals in (B.4) and the first term of (B.6) are the ones that must be performed on the grid. We note that the integrand in the first term of (B.6) has the property that it is undefined for $z = x$ (due to the fact that $S(x/z)$ contains a factor $1/(1 - x/z)$). It nevertheless tends to a finite limit as $z \rightarrow x$ (due to the fact that the divergence in $S(x/z)$ is compensated for by the other factor in the integrand going to zero as $z \rightarrow x$). This suggests the use of a method for performing the numerical integrations which effectively estimates the integrand between $z = x$ and the grid point with next highest z by extrapolating from integrand values on nearby grid points (with higher z).

A method which uses an open Newton-Cotes rule of degree n for the first n integration intervals, and then switches to a closed Newton-Cotes rule to perform the integration over the remaining intervals, has this property. If the number of integration intervals is greater than 3, we use Simpson's rule as the closed rule, combined with an open rule of degree 4 when the number of integration intervals is even, and an open rule of degree 5 otherwise. Open rules of the appropriate degree are used on their own when the number of intervals is 3 or fewer. This ensures an overall integration method which for most integrals has an error of $O(n\Delta u^5 \frac{df^{(4)}(\xi)}{du^4})$. In this formula, n is the number of intervals used, Δu is the (even) grid spacing in $u = \ln(\frac{x}{1-x})$, f is the integrand taking into account the Jacobian on the transformation into u space, and ξ is the value of u that maximises $df^{(4)}/du^4$.

With the numerical method described, the integral (B.1) is approximated by:

$$\begin{aligned}
I(y) \approx & \sum_{j=i+1}^k D(z_j, y) \left[A\left(\frac{z_i}{z_j}\right) + R\left(\frac{z_i}{z_j}\right) S\left(\frac{z_i}{z_j}\right) \right] w_{ijk} \frac{J(z_j)}{z_j} \Delta u \\
& + D(z_i, y) \left[K - R(1) \int_0^{x/(1-y)} dz S(z) \right. \\
& \left. - \sum_{j=i+1}^k S\left(\frac{z_i}{z_j}\right) \frac{z_i}{z_j} R(1) w_{ijk} \frac{J(z_j)}{z_j} \Delta u \right].
\end{aligned} \tag{B.7}$$

The indices $\{i, j, k\}$ represent grid points, with i corresponding to the grid point with z value equal to x ($z_i \equiv x$) and k corresponding to the point with z value equal to $1 - y$

($z_k \equiv 1 - y$). The w_{ijk} are Newton-Cotes type integration weights whose values are dictated by the prescription described above. Note that the weight at grid point j under this prescription depends on the start and end points of the integration – hence w depends on the indices i and k . The function $J(x)$ is the Jacobian, $J(x) \equiv dx/du = x(1 - x)$.

We may rewrite (B.7) as:

$$I(y) \approx \sum_{j=i}^k P_{ijk} D(x_j, y), \quad (\text{B.8})$$

where

$$P_{ijk} = \begin{cases} \left[A\left(\frac{z_i}{z_j}\right) + R\left(\frac{z_i}{z_j}\right) S\left(\frac{z_i}{z_j}\right) \right] w_{ijk} \frac{J(z_j)}{z_j} \Delta u & \text{if } i < j \leq k \\ K - R(1) \int_0^{x/(1-y)} dz S(z) \\ - \sum_{j=i+1}^k S\left(\frac{z_i}{z_j}\right) \frac{z_i}{z_j} R(1) w_{ijk} \frac{J(z_j)}{z_j} \Delta u & \text{if } j = i, i < k \\ 0 & \text{otherwise.} \end{cases} \quad (\text{B.9})$$

The three-dimensional array P_{ijk} only depends on the splitting function $P(x)$, Jacobian $J(x)$ and weights w_{ijk} . None of these vary during an evolution, with the possible exception of P_{gg} (this contains a term proportional to n_f in the $K\delta(1-x)$ piece and so may vary in a variable flavour number scheme – see Section 2.4.2). We therefore precalculate and store the elements of P_{ijk} during program initialisation, to increase efficiency. The possible variation of the contributions to P_{ijk} from the term in P_{gg} proportional to n_f is handled by postponing the calculation of these contributions such that they are calculated and reintroduced at each evolution step (using the value of n_f appropriate to that step).

Appendix C

Sum Rules using Light Cone Wavefunction Representations

In this section we will use the light-cone coordinate system defined in equations (A.5)-(A.8).

If one performs quantisation of QCD on the light cone $x^+ = 0$ (see, for example, [15, 147–149]), then one arrives at a set of (bare) creation and annihilation operators which are related to the Fourier transforms of the so-called ‘good’ components of the quark and gluon fields. Let us write the creation operators as $b_{\alpha_f}^\dagger(k)$ (creation operator for quark with discrete quantum numbers α_f and momentum $k = (k^+, \mathbf{k})$), $d_{\alpha_f}^\dagger(k)$ (creation operator for antiquark) and $a_{\alpha_g}^\dagger(k)$ (creation operator for gluon with discrete quantum numbers α_g and momentum $k = (k^+, \mathbf{k})$). We can construct a complete set of basis states by applying these bare operators to the true vacuum $|0\rangle$ – let us write a typical basis state as follows:

$$|N : \{\beta_i, k_i^+, \mathbf{k}_i\}\rangle \quad (\text{C.1})$$

This is a Fock state containing N particles (i.e. N creation operators acting on the vacuum). The i th label $\beta_i, k_i^+, \mathbf{k}_i$ on the basis state describes the discrete quantum numbers and momentum of the i th creation operator in that basis state operating on the vacuum (where the discrete quantum number descriptor β_i now also describes whether the creation operator is for a quark, antiquark or gluon, as well as its helicity, colour and flavour).

Given that the basis (C.1) is a complete basis, we can decompose the hadron state

$|P, \mu_P\rangle$ with momentum $P = P^+p$ and helicity μ_P as follows:

$$|P, \mu_P\rangle = \sum_{N, \{\beta_i\}} \int d[\{x, \mathbf{k}\}]_N |N : \{\beta_i, x_i P^+, \mathbf{k}_i\}\rangle \Phi_N(\{\beta_i, x_i, \mathbf{k}_i\}) \quad (\text{C.2})$$

The sum in (C.2) is over distinguishable Fock states only, and is restricted to those states which reproduce the appropriate quantum numbers of the hadron (colourless, spin component along z direction = μ_P , etc.). Similarly, the integral is only over momenta that sum up to the total hadron momentum P^+p . $\Phi_N(\beta; \{x_i, \mathbf{k}_i\})$ is the bare light-cone amplitude (or wavefunction) to find the given arrangement of partons in the hadron. To some extent the definitions of $d[\{x, \mathbf{k}\}]_N$, $|N : \{\beta_i, x_i P^+, \mathbf{k}_i\}\rangle$ and $\Phi_N(\{\beta_i, x_i, \mathbf{k}_i\})$ are convention dependent, and one can shuffle factors amongst them (indeed, the definition almost always differs between papers by different authors). We shall adopt a definition that is based on the work by Harindranath, Zhang, and collaborators [116, 150–153], in which $|N : \{\beta_i, x_i P^+, \mathbf{k}_i\}\rangle$ is just a simple string of creation operators acting on the vacuum (with no extra factors), and:

$$d[\{x, \mathbf{k}\}]_N = \prod_i^N \left[\frac{dx_i d^2 \mathbf{k}_i}{\sqrt{2(2\pi)^3 x_i}} \right] \sqrt{2(2\pi)^3} \delta(1 - \sum_i^N x_i) \delta^{(2)}(\sum_i^N \mathbf{k}_i) \quad (\text{C.3})$$

In fact we will not actually make much reference to these precise definitions in what follows.

One may insert the Fock space expansion of the hadron state (C.2) into the operator definitions for the bare sPDF ((1.67) and (1.68)) and dPDF (2.1) to obtain expressions for these quantities in terms of bare light cone wavefunctions:

$$D_{h(0)}^p(x) = \sum_{N, \{\beta_i\}} \int [dx]_N [d^2 \mathbf{k}]_N |\Phi_N(\{\beta_i, x_i, \mathbf{k}_i\})|^2 \sum_i^N \delta(x - x_i) \delta_{pp_i} \quad (\text{C.4})$$

$$D_{h(0)}^{pp'}(x, y) = \sum_{N, \{\beta_i\}} \int [dx]_N [d^2 \mathbf{k}]_N |\Phi_N(\{\beta_i, x_i, \mathbf{k}_i\})|^2 \sum_i^N \sum_{j \neq i}^N \delta(x - x_i) \delta(y - y_j) \delta_{p_i p} \delta_{p_j p'} \quad (\text{C.5})$$

where:

$$[dx]_N \equiv \prod_{i=1}^N dx_i \delta \left(1 - \sum_i^N x_i \right) \quad (\text{C.6})$$

$$[d^2\mathbf{k}]_N \equiv \prod_{i=1}^N d^2\mathbf{k}_i \delta^{(2)}\left(\sum_i \mathbf{k}_i\right) \quad (\text{C.7})$$

p, p' and p_i are parton flavour indices.

In the next two sections we will show using the representations (C.4) and (C.5) that the bare dPDFs and sPDFs obey the dPDF momentum and number sum rules. According to an argument that is very similar to that presented in Section 8.6 of [15], this implies that the \overline{MS} renormalised dPDFs and sPDFs also obey the momentum and number sum rules.

C.1 Momentum sum rule

Let us write down the momentum sum rule integral of [46] for the bare dPDF, and then expand this dPDF in terms of light cone wavefunctions using (C.5):

$$\begin{aligned} \sum_p \int_0^{1-y} dx \, x \, D_{h(0)}^{pp'}(x, y) &= \sum_p \int_0^{1-y} dx \, x \sum_{N, \{\beta_i\}} \int \prod_i^N [dx]_N [d^2\mathbf{k}]_N |\Phi_N(\{\beta_i, x_i, \mathbf{k}_i\})|^2 \\ &\quad \times \sum_i^N \sum_{j \neq i}^N \delta(x - x_i) \delta(y - x_j) \delta_{p_i p} \delta_{p_j p'} \\ &= \sum_{N, \{\beta_i\}} \int \prod_i^N [dx]_N [d^2\mathbf{k}]_N |\Phi_N(\{\beta_i, x_i, \mathbf{k}_i\})|^2 \sum_i^N \sum_{j \neq i}^N x_i \delta(y - x_j) \delta_{p_j p'} \\ &= \sum_{N, \{\beta_i\}} \int \prod_i^N [dx]_N [d^2\mathbf{k}]_N |\Phi_N(\{\beta_i, x_i, \mathbf{k}_i\})|^2 \sum_j^N \delta(y - x_j) \delta_{p_j p'} \left[\sum_{i \neq j}^N x_i \right] \\ &= (1-y) \sum_{N, \{\beta_i\}} \int \prod_i^N [dx]_N [d^2\mathbf{k}]_N |\Phi_N(\{\beta_i, x_i, \mathbf{k}_i\})|^2 \sum_j^N \delta(y - x_j) \delta_{p_j p'} \end{aligned} \quad (\text{C.8})$$

To reach the last line, we have used the fact that $\sum_{i \neq j} x_i$ is always equal to $(1-y)$ in the presence of the constraints $\sum x_i = 1$ and $x_j = y$. The term multiplying $(1-y)$ on the last line of (C.8) is exactly equal to the bare sPDF $D_{h(0)}^{p'}(y)$ according to the definition (C.4). Thus the right hand side of the equation is equal to $(1-y) D_{h(0)}^{p'}(y)$ and we have demonstrated that the momentum sum rule holds for the bare PDFs.

C.2 Number sum rule

We begin by considering the quantity $\int_0^{1-y} dx D_{h(0)}^{pp'}(x, y)$, where p and p' are arbitrary human flavour basis parton indices. Substituting the definition (C.5) into this quantity we obtain:

$$\begin{aligned}
 \int_0^{1-y} dx D_{h(0)}^{pp'}(x, y) &= \int_0^{1-y} dx \sum_{N, \{\beta_i\}} \int \prod_i^N [dx_i] [d^2 \mathbf{k}_i] |\Phi_N(\{\beta_i, x_i, \mathbf{k}_i\})|^2 \\
 &\quad \times \sum_i^N \sum_{j \neq i}^N \delta(x - x_i) \delta(y - x_j) \delta_{p_i p} \delta_{p_j p'} \\
 &= \sum_{N, \{\beta_i\}} \int \prod_i^N [dx_i] [d^2 \mathbf{k}_i] |\Phi_N(\{\beta_i, x_i, \mathbf{k}_i\})|^2 \sum_i^N \sum_{j \neq i}^N \delta(y - x_j) \delta_{p_i p} \delta_{p_j p'} \\
 &= \sum_{N, \{\beta_i\}} \int \prod_i^N [dx_i] [d^2 \mathbf{k}_i] |\Phi_N(\{\beta_i, x_i, \mathbf{k}_i\})|^2 \sum_j^N \delta(y - x_j) \delta_{p_j p'} \left[\sum_{i \neq j}^N \delta_{p_i p} \right] \\
 &= \sum_{N, \{\beta_i\}} \mathcal{N}(p|p', \{\beta_i\}) D_{N, \{\beta_i\}(0)}^{p'}(y)
 \end{aligned} \tag{C.9}$$

$\mathcal{N}(p|p', \{\beta_i\})$ is equal to the number of p partons in the state which is defined by removing the p' parton from $\{\beta_i\}$:

$$\mathcal{N}(p|p', \{\beta_i\}) = N_p(\{\beta_i\}) - \delta_{pp'} \tag{C.10}$$

where $N_p(\{\beta_i\})$ is the number of p partons in the state $\{\beta_i\}$. $D_{N, \{\beta_i\}(0)}^{p'}(y)$ is the contribution of the state $\{\beta_i\}$ to the bare p' sPDF.

We apply (C.9) to the number sum rule integral:

$$\begin{aligned}
 \int_0^{1-y} dx D_{h(0)}^{pvp'}(x, y) &\equiv \int_0^{1-y} dx D_{h(0)}^{pp'}(x, y) - \int_0^{1-y} dx D_{h(0)}^{\bar{p}p'}(x, y) \\
 &= \sum_{N, \{\beta_i\}} [\mathcal{N}(p|p', \{\beta_i\}) - \mathcal{N}(\bar{p}|p', \{\beta_i\})] D_{N, \{\beta_i\}(0)}^{p'}(y) \\
 &= \sum_{N, \{\beta_i\}} [N_p(\{\beta_i\}) - N_{\bar{p}}(\{\beta_i\}) - \delta_{pp'} + \delta_{\bar{p}p'}] D_{N, \{\beta_i\}(0)}^{p'}(y)
 \end{aligned} \tag{C.11}$$

$$\begin{aligned}
&= \left\{ \sum_{N, \{\beta_i\}} [N_p(\{\beta_i\}) - N_{\bar{p}}(\{\beta_i\})] D_{N, \{\beta_i\}(0)}^{p'}(y) \right\} \\
&\quad + (-\delta_{pp'} + \delta_{\bar{p}p'}) D_{h(0)}^{p'}(y)
\end{aligned}$$

Now, we know that the difference between the number of p and \bar{p} partons is the same for every possible Fock state of the hadron h - let us denote this difference by N_{p_v} . Since this number is independent of $\{\beta_i\}$ we can pull it out of the sum, obtaining:

$$\int_0^{1-y} dx D_{h(0)}^{p_v p'}(x, y) = (N_{p_v} - \delta_{pp'} + \delta_{\bar{p}p'}) D_{h(0)}^{p'}(y) \quad (\text{C.12})$$

This is the dPDF number sum rule for the bare PDFs.

Bibliography

- [1] M. Gell-Mann, *A Schematic Model of Baryons and Mesons*, *Phys.Lett.* **8** (1964) 214–215.
- [2] G. Zweig, “An SU_3 model for strong interaction symmetry and its breaking; Part I.” CERN Report Number CERN-TH-401.
- [3] G. Zweig, “An SU_3 model for strong interaction symmetry and its breaking; Part II.” CERN Report Number CERN-TH-412.
- [4] V. P. Shelest, A. M. Snigirev, and G. M. Zinovjev, *Gazing into the multiparton distribution equations in QCD*, *Phys. Lett.* **B113** (1982) 325.
- [5] G. M. Zinovev, A. M. Snigirev, and V. P. Shelest, *Equations for many parton distributions in quantum chromodynamics*, *Theor. Math. Phys.* **51** (1982) 523–528.
- [6] A. M. Snigirev, *Double parton distributions in the leading logarithm approximation of perturbative QCD*, *Phys. Rev.* **D68** (2003) 114012, [[hep-ph/0304172](#)].
- [7] C. G. Callan and D. J. Gross, *High-energy electroproduction and the constitution of the electric current*, *Phys.Rev.Lett.* **22** (1969) 156–159.
- [8] R. P. Feynman, *Photon-hadron interactions*. Addison-Wesley, 1972. Reading 1972, 282p.
- [9] D. E. Soper, *Basics of QCD perturbation theory*, [hep-ph/0011256](#).
- [10] G. F. Sterman, *Partons, factorization and resummation*, *TASI 95*, [hep-ph/9606312](#).
- [11] S. Drell and T.-M. Yan, *Massive Lepton Pair Production in Hadron-Hadron Collisions at High-Energies*, *Phys.Rev.Lett.* **25** (1970) 316–320.

- [12] I. Kenyon, *The Drell-Yan Process*, *Rept.Prog.Phys.* **45** (1982) 1261.
- [13] H. D. Politzer, *Reliable perturbative results for strong interactions?*, *Phys. Rev. Lett.* **30** (1973) 1346–1349.
- [14] D. Gross and F. Wilczek, *Ultraviolet Behavior of Nonabelian Gauge Theories*, *Phys.Rev.Lett.* **30** (1973) 1343–1346.
- [15] J. Collins, *Foundations of perturbative QCD*. Cambridge monographs on particle physics, nuclear physics, and cosmology. Cambridge Univ. Press, New York, NY, 2011.
- [16] J. C. Collins, D. E. Soper, and G. F. Sterman, *Factorization of Hard Processes in QCD*, *Adv.Ser.Direct.High Energy Phys.* **5** (1988) 1–91, [[hep-ph/0409313](#)]. Publ. in 'Perturbative QCD' (A.H. Mueller, ed.) (World Scientific Publ., 1989).
- [17] M. E. Peskin and D. V. Schroeder, *An Introduction to quantum field theory*. Addison-Wesley Publishing Co., 1995.
- [18] J. C. Collins, F. Wilczek, and A. Zee, *Low-Energy Manifestations of Heavy Particles: Application to the Neutral Current*, *Phys.Rev.* **D18** (1978) 242.
- [19] M. Srednicki, *Quantum Field Theory. Part 1. Spin Zero*, [hep-th/0409035](#). This is a draft version of Part 1 of a three-part introductory textbook on quantum field theory.
- [20] M. H. Seymour, *Quantum ChromoDynamics*, [hep-ph/0505192](#).
- [21] H. Georgi and H. D. Politzer, *Electroproduction scaling in an asymptotically free theory of strong interactions*, *Phys.Rev.* **D9** (1974) 416–420.
- [22] D. Gross and F. Wilczek, *Asymptotically Free Gauge Theories. 2.*, *Phys.Rev.* **D9** (1974) 980–993.
- [23] R. K. Ellis, W. J. Stirling, and B. R. Webber, *QCD and Collider Physics*, vol. 8. Cambridge University Press, 1996.
- [24] J. C. Collins, D. E. Soper, and G. F. Sterman, *Soft Gluons and Factorization*, *Nucl.Phys.* **B308** (1988) 833.
- [25] <http://projects.hepforge.org/mstwpdf>.

- [26] A. Del Fabbro and D. Treleani, *A double parton scattering background to Higgs boson production at the LHC*, *Phys. Rev.* **D61** (2000) 077502, [[hep-ph/9911358](#)].
- [27] A. Kulesza and W. J. Stirling, *Like sign W boson production at the LHC as a probe of double parton scattering*, *Phys. Lett.* **B475** (2000) 168–175, [[hep-ph/9912232](#)].
- [28] A. Del Fabbro and D. Treleani, *Double parton scatterings in b -quark pairs production at the LHC*, *Phys. Rev.* **D66** (2002) 074012, [[hep-ph/0207311](#)].
- [29] M. Y. Hussein, *A double parton scattering background to associate WH and ZH production at the LHC*, *Nucl. Phys. Proc. Suppl.* **174** (2007) 55–58, [[hep-ph/0610207](#)].
- [30] M. Y. Hussein, *Double parton scattering in associate Higgs boson production with bottom quarks at hadron colliders*, [arXiv:0710.0203](#).
- [31] D. Bandurin, G. Golovanov, and N. Skachkov, *Double parton interactions as a background to associated HW production at the Tevatron*, *JHEP* **1104** (2011) 054, [[arXiv:1011.2186](#)].
- [32] J.-W. Qiu and G. F. Sterman, *Power corrections in hadronic scattering. 1. Leading $1/Q^2$ corrections to the Drell-Yan cross-section*, *Nucl.Phys.* **B353** (1991) 105–136.
- [33] A. V. Manohar and W. J. Waalewijn, *A QCD Analysis of Double Parton Scattering: Color Correlations, Interference Effects and Evolution*, *Phys.Rev.* **D85** (2012) 114009, [[arXiv:1202.3794](#)].
- [34] B. Blok, Y. Dokshitzer, L. Frankfurt, and M. Strikman, *The Four jet production at LHC and Tevatron in QCD*, *Phys.Rev.* **D83** (2011) 071501, [[arXiv:1009.2714](#)].
- [35] B. Blok, Y. Dokshitzer, L. Frankfurt, and M. Strikman, *p QCD physics of multiparton interactions*, *Eur.Phys.J.* **C72** (2012) 1963, [[arXiv:1106.5533](#)].
- [36] M. Diehl and A. Schafer, *Theoretical considerations on multiparton interactions in QCD*, *Phys.Lett.* **B698** (2011) 389–402, [[arXiv:1102.3081](#)].
- [37] M. Diehl, D. Ostermeier, and A. Schafer, *Elements of a theory for multiparton interactions in QCD*, *JHEP* **1203** (2012) 089, [[arXiv:1111.0910](#)].

- [38] **D0** Collaboration, V. M. Abazov *et. al.*, *Double parton interactions in photon+3 jet events in $p\bar{p}$ collisions $\sqrt{s}=1.96$ TeV*, *Phys. Rev.* **D81** (2010) 052012, [[arXiv:0912.5104](#)].
- [39] **CDF** Collaboration, F. Abe *et. al.*, *Double parton scattering in $\bar{p}p$ collisions at $\sqrt{s} = 1.8$ TeV*, *Phys. Rev.* **D56** (1997) 3811–3832.
- [40] **CDF** Collaboration, F. Abe *et. al.*, *Measurement of double parton scattering in $\bar{p}p$ collisions at $\sqrt{s} = 1.8$ TeV*, *Phys. Rev. Lett.* **79** (1997) 584–589.
- [41] **Axial Field Spectrometer** Collaboration, T. Akesson *et. al.*, *Double parton scattering in pp collisions at $\sqrt{s} = 63$ GeV*, *Z. Phys.* **C34** (1987) 163.
- [42] **UA2** Collaboration, J. Alitti *et. al.*, *A Study of multi - jet events at the CERN anti- p p collider and a search for double parton scattering*, *Phys.Lett.* **B268** (1991) 145–154.
- [43] **CDF** Collaboration, F. Abe *et. al.*, *Study of four jet events and evidence for double parton interactions in $p\bar{p}$ collisions at $\sqrt{s} = 1.8$ TeV*, *Phys.Rev.* **D47** (1993) 4857–4871.
- [44] *A measurement of hard double-partonic interactions in $W \rightarrow l\nu + 2$ jet events*, Tech. Rep. ATLAS-CONF-2011-160, CERN, Geneva, Dec, 2011.
- [45] C. Flensburg, G. Gustafson, L. Lonnblad, and A. Ster, *Correlations in double parton distributions at small x* , *JHEP* **1106** (2011) 066, [[arXiv:1103.4320](#)].
- [46] J. R. Gaunt and W. J. Stirling, *Double Parton Distributions Incorporating Perturbative QCD Evolution and Momentum and Quark Number Sum Rules*, *JHEP* **1003** (2010) 005, [[0910.4347](#)].
- [47] J. R. Gaunt, C.-H. Kom, A. Kulesza, and W. Stirling, *Same-sign W pair production as a probe of double parton scattering at the LHC*, *Eur.Phys.J.* **C69** (2010) 53–65, [[arXiv:1003.3953](#)].
- [48] E. Cattaruzza, A. Del Fabbro, and D. Treleani, *Fractional momentum correlations in multiple production of W bosons and of $b\bar{b}$ pairs in high energy pp collisions*, *Phys. Rev.* **D72** (2005) 034022, [[hep-ph/0507052](#)].

- [49] V. L. Korotkikh and A. M. Snigirev, *Double parton correlations versus factorized distributions*, *Phys. Lett.* **B594** (2004) 171–176, [[hep-ph/0404155](#)].
- [50] <http://projects.hepforge.org/gsdpdf>.
- [51] G. Altarelli and G. Parisi, *Asymptotic Freedom in Parton Language*, *Nucl. Phys.* **B126** (1977) 298.
- [52] F. A. Ceccopieri, *An update on the evolution of double parton distributions*, *Phys. Lett.* **B697** (2011) 482–487, [[arXiv:1011.6586](#)]. * Temporary entry *.
- [53] R. K. Ellis, W. J. Stirling, and B. R. Webber, *QCD and Collider Physics*. Cambridge University Press, 1996.
- [54] R. Kirschner, *Generalized Lipatov-Altarelli-Parisi equations and jet calculus rules*, *Phys. Lett.* **B84** (1979) 266.
- [55] K. Konishi, A. Ukawa, and G. Veneziano, *Jet Calculus: A Simple Algorithm for Resolving QCD Jets*, *Nucl. Phys.* **B157** (1979) 45–107.
- [56] C. Goebel, F. Halzen, and D. M. Scott, *Double Drell-Yan annihilations in hadron collisions: novel tests of the constituent picture*, *Phys. Rev.* **D22** (1980) 2789.
- [57] F. Halzen, P. Hoyer, and W. J. Stirling, *Evidence for multiple parton interactions from the observation of multi - muon events in Drell-Yan experiments*, *Phys. Lett.* **B188** (1987) 375–378.
- [58] A. D. Martin, W. J. Stirling, R. S. Thorne, and G. Watt, *Parton distributions for the LHC*, [arXiv:0901.0002](#).
- [59] B. Humpert, *Are there multi - quark interactions?*, *Phys. Lett.* **B131** (1983) 461.
- [60] B. Humpert and R. Odorico, *Multiparton scattering and QCD radiation as sources of four jet events*, *Phys. Lett.* **B154** (1985) 211.
- [61] K. P. Das and R. C. Hwa, *Quark - anti-Quark Recombination in the Fragmentation Region*, *Phys. Lett.* **B68** (1977) 459.
- [62] J. Kuti and V. F. Weisskopf, *Inelastic lepton - nucleon scattering and lepton pair production in the relativistic quark parton model*, *Phys. Rev.* **D4** (1971) 3418–3439.

- [63] S. A. Kulagin and R. Petti, *Global study of nuclear structure functions*, *Nucl.Phys.* **A765** (2006) 126–187, [[hep-ph/0412425](#)].
- [64] G. Parisi and R. Petronzio, *On the Breaking of Bjorken Scaling*, *Phys. Lett.* **B62** (1976) 331.
- [65] A. I. Vainshtein, V. I. Zakharov, V. A. Novikov, and M. A. Shifman, *Deep Inelastic Lepton Scattering on Hadrons and Gluon Bremsstrahlung*, *JETP Lett.* **24** (1976) 341.
- [66] V. A. Novikov, M. A. Shifman, A. I. Vainshtein, and V. I. Zakharov, *Naive Quark Model and Deep Inelastic Scattering*, *Ann. Phys.* **105** (1977) 276.
- [67] M. Gluck and E. Reya, *Dynamical Determination of Parton and Gluon Distributions in Quantum Chromodynamics*, *Nucl. Phys.* **B130** (1977) 76.
- [68] M. Gluck, R. M. Godbole, and E. Reya, *Dynamically generated parton distributions for high-energy collisions*, *Z. Phys.* **C41** (1989) 667.
- [69] M. Gluck, E. Reya, and A. Vogt, *Radiatively generated parton distributions for high-energy collisions*, *Z. Phys.* **C48** (1990) 471–482.
- [70] M. Botje, *QCDNUM: Fast QCD Evolution and Convolution*, *ZEUS Note 97-066* (2009). Available at <http://www.nikhef.nl/~h24/qcdnum/>.
- [71] G. P. Salam and J. Rojo, *A Higher Order Perturbative Parton Evolution Toolkit (HOPPET)*, *Comput. Phys. Commun.* **180** (2009) 120–156, [[arXiv:0804.3755](#)].
- [72] A. Vogt, *Efficient evolution of unpolarized and polarized parton distributions with QCD-PEGASUS*, *Comput. Phys. Commun.* **170** (2005) 65–92, [[hep-ph/0408244](#)].
- [73] T. Stelzer and W. F. Long, *Automatic generation of tree level helicity amplitudes*, *Comput. Phys. Commun.* **81** (1994) 357–371, [[hep-ph/9401258](#)].
- [74] F. Maltoni and T. Stelzer, *MadEvent: Automatic event generation with MadGraph*, *JHEP* **0302** (2003) 027, [[hep-ph/0208156](#)].
- [75] A. Kulesza and W. J. Stirling, *Sudakov logarithm resummation in transverse momentum space for electroweak boson production at hadron colliders*, *Nucl.Phys.* **B555** (1999) 279–305, [[hep-ph/9902234](#)].

- [76] A. Kulesza and W. J. Stirling, *Soft gluon resummation in transverse momentum space for electroweak boson production at hadron colliders*, *Eur.Phys.J.* **C20** (2001) 349–356, [[hep-ph/0103089](#)].
- [77] A. Kulesza and W. J. Stirling, *Nonperturbative effects and the resummed Higgs transverse momentum distribution at the LHC*, *JHEP* **0312** (2003) 056, [[hep-ph/0307208](#)].
- [78] M. S. Chanowitz and W. B. Kilgore, *W^+Z and $W^+\gamma^*$ backgrounds to strong W^+W^+ scattering at the LHC*, *Phys.Lett.* **B347** (1995) 387–393, [[hep-ph/9412275](#)].
- [79] G. P. Lepage, *A New Algorithm for Adaptive Multidimensional Integration*, *J. Comput. Phys.* **27** (1978) 192.
- [80] G. Corcella, I. Knowles, G. Marchesini, S. Moretti, K. Odagiri, *et. al.*, *HERWIG 6: An Event generator for hadron emission reactions with interfering gluons (including supersymmetric processes)*, *JHEP* **0101** (2001) 010, [[hep-ph/0011363](#)].
- [81] J. R. Gaunt and W. J. Stirling, *Double Parton Scattering Singularity in One-Loop Integrals*, *JHEP* **1106** (2011) 048, [[arXiv:1103.1888](#)].
- [82] J. R. Gaunt, *Double Parton Splitting Diagrams and Interference and Correlation Effects in Double Parton Scattering*, [arXiv:1110.1536](#). * Temporary entry *.
- [83] M. Mekhfi, *Correlations in color and spin in multiparton processes*, *Phys. Rev.* **D32** (1985) 2380.
- [84] M. Mekhfi and X. Artru, *Sudakov suppression of color correlations in multiparton scattering*, *Phys.Rev.* **D37** (1988) 2618–2622.
- [85] R. K. Ellis, W. Furmanski, and R. Petronzio, *Power Corrections to the Parton Model in QCD*, *Nucl.Phys.* **B207** (1982) 1.
- [86] T. Kasemets, “Talk at MPI@LHC 2011, DESY, Hamburg.”
<https://indico.desy.de/conferenceDisplay.py?confId=3241>, 2011.
- [87] D. Boer and P. Mulders, *Time reversal odd distribution functions in leptonproduction*, *Phys.Rev.* **D57** (1998) 5780–5786, [[hep-ph/9711485](#)].

-
- [88] D. Boer, *Investigating the origins of transverse spin asymmetries at RHIC*, *Phys.Rev.* **D60** (1999) 014012, [[hep-ph/9902255](#)].
- [89] D. Boer, S. J. Brodsky, and D. S. Hwang, *Initial state interactions in the unpolarized Drell-Yan process*, *Phys.Rev.* **D67** (2003) 054003, [[hep-ph/0211110](#)].
- [90] D. Boer, S. J. Brodsky, P. J. Mulders, and C. Pisano, *Direct Probes of Linearly Polarized Gluons inside Unpolarized Hadrons*, *Phys.Rev.Lett.* **106** (2011) 132001, [[arXiv:1011.4225](#)].
- [91] R. Field, *Applications Of Perturbative QCD*, vol. 77 of *Frontiers in Physics*. Westview Press, 1995.
- [92] A. V. Manohar, *Large N QCD*, [hep-ph/9802419](#).
- [93] M. Diehl, ‘*When protons collide: multi-parton interactions at the LHC*’ – Seminar at IPPP Durham, June, 2011.
- [94] M. Diehl, T. Feldmann, R. Jakob, and P. Kroll, *Linking parton distributions to form-factors and Compton scattering*, *Eur.Phys.J.* **C8** (1999) 409–434, [[hep-ph/9811253](#)].
- [95] V. M. Braun, T. Lautenschlager, A. N. Manashov, and B. Pirnay, *Higher twist parton distributions from light-cone wave functions*, *Phys. Rev.* **D83** (2011) 094023, [[arXiv:1103.1269](#)].
- [96] M. Gluck, P. Jimenez-Delgado, and E. Reya, *Dynamical parton distributions of the nucleon and very small- x physics*, *Eur. Phys. J.* **C53** (2008) 355–366, [[arXiv:0709.0614](#)].
- [97] R. J. Eden, P. V. Landshoff, D. I. Olive, and J. C. Polkinghorne, *The Analytic S Matrix*. Cambridge University Press, 1966.
- [98] Z. Nagy and D. E. Soper, *Numerical integration of one-loop Feynman diagrams for N -photon amplitudes*, *Phys.Rev.* **D74** (2006) 093006, [[hep-ph/0610028](#)].
- [99] R. Ellis and G. Zanderighi, *Scalar one-loop integrals for QCD*, *JHEP* **0802** (2008) 002, [[arXiv:0712.1851](#)].

- [100] L. D. Ninh, *One-Loop Yukawa Corrections to the Process $pp \rightarrow b\bar{b}H$ in the Standard Model at the LHC: Landau Singularities*, [arXiv:0810.4078](#).
- [101] G. Ossola, C. G. Papadopoulos, and R. Pittau, *Numerical evaluation of six-photon amplitudes*, *JHEP* **0707** (2007) 085, [[arXiv:0704.1271](#)].
- [102] W. Gong, Z. Nagy, and D. E. Soper, *Direct numerical integration of one-loop Feynman diagrams for N-photon amplitudes*, *Phys.Rev.* **D79** (2009) 033005, [[arXiv:0812.3686](#)].
- [103] E. Glover and J. van der Bij, *Higgs boson pair production via gluon fusion*, *Nucl.Phys.* **B309** (1988) 282.
- [104] E. Glover and J. van der Bij, *Z boson pair production via gluon fusion*, *Nucl.Phys.* **B321** (1989) 561.
- [105] T. Binoth, M. Ciccolini, N. Kauer, and M. Kramer, *Gluon-induced W-boson pair production at the LHC*, *JHEP* **0612** (2006) 046, [[hep-ph/0611170](#)].
- [106] C. Bernicot, *The six-photon amplitude*, [arXiv:0804.1315](#).
- [107] **NLO Multileg Working Group** Collaboration, Z. Bern *et. al.*, *The NLO multileg working group: Summary report*, [arXiv:0803.0494](#).
- [108] G. Duplancic and B. Nizic, *Dimensionally regulated one loop box scalar integrals with massless internal lines*, *Eur.Phys.J.* **C20** (2001) 357–370, [[hep-ph/0006249](#)].
- [109] R. Mertig and M. Böhm and A. Denner, *FeynCalc - Computer-algebraic calculation of Feynman amplitudes*, *Computer Physics Communications* **64** (1991), no. 3 345–359.
- [110] G. Passarino and M. Veltman, *One Loop Corrections for e^+e^- Annihilation Into $\mu^+\mu^-$ in the Weinberg Model*, *Nucl.Phys.* **B160** (1979) 151.
- [111] Maple 14. Maplesoft, a division of Waterloo Maple Inc., Waterloo, Ontario.
- [112] H. H. Liu, *Double parton scattering of hadron hadron interaction and its gluonic contribution*, [hep-ph/9704395](#).
- [113] J. A. M. Vermaseren, *New features of FORM*, [math-ph/0010025](#).

- [114] R. Cutkosky, *Singularities and discontinuities of Feynman amplitudes*, *J.Math.Phys.* **1** (1960) 429–433.
- [115] M. Veltman, *Diagrammatica : the path to Feynman rules*. Cambridge University Press, 1994.
- [116] A. Harindranath, R. Kundu, and W.-M. Zhang, *Deep inelastic structure functions in light front QCD: Radiative corrections*, *Phys.Rev.* **D59** (1999) 094013, [[hep-ph/9806221](#)].
- [117] Y. Tosa, *Masses in scalar dynamics*, *Nuovo Cim.* **A55** (1980) 485.
- [118] G. Mahlon, *Use of recursion relations to compute one loop helicity amplitudes*, [hep-ph/9412350](#).
- [119] T. Binoth, G. Heinrich, T. Gehrmann, and P. Mastrolia, *Six-Photon Amplitudes*, *Phys.Lett.* **B649** (2007) 422–426, [[hep-ph/0703311](#)].
- [120] C. Bernicot and J.-P. Guillet, *Six-Photon Amplitudes in Scalar QED*, *JHEP* **0801** (2008) 059, [[arXiv:0711.4713](#)].
- [121] K. J. Ozeren and W. J. Stirling, *MHV techniques for QED processes*, *JHEP* **11** (2005) 016, [[hep-th/0509063](#)].
- [122] J. Labastida and G. F. Sterman, *Inclusive Hadron - Hadron Scattering In The Feynman Gauge*, *Nucl.Phys.* **B254** (1985) 425.
- [123] M. Strikman and D. Treleani, *Measuring double parton distributions in nucleons at proton nucleus colliders*, *Phys.Rev.Lett.* **88** (2002) 031801, [[hep-ph/0111468](#)].
- [124] E. Cattaruzza, A. Del Fabbro, and D. Treleani, *Heavy-quark production in proton-nucleus collision at the CERN LHC*, *Phys.Rev.* **D70** (2004) 034022, [[hep-ph/0404177](#)].
- [125] J. R. Gaunt, *Single Perturbative Splitting Diagrams in Double Parton Scattering*, [arXiv:1207.0480](#).
- [126] M. Ryskin and A. Snigirev, *A Fresh look at double parton scattering*, *Phys.Rev.* **D83** (2011) 114047, [[arXiv:1103.3495](#)].

- [127] A. V. Manohar and W. J. Waalewijn, *What is Double Parton Scattering?*, [arXiv:1202.5034](#).
- [128] N. Paver and D. Treleani, *Multi-quark scattering and large p_T jet production in hadronic collisions*, *Nuovo Cim.* **A70** (1982) 215.
- [129] M. Mekhfi, *Multiparton processes: an application to double Drell- Yan*, *Phys. Rev.* **D32** (1985) 2371.
- [130] M. Ryskin and A. Snigirev, *Double parton scattering in double logarithm approximation of perturbative QCD*, [arXiv:1203.2330](#).
- [131] E. Levin, M. Ryskin, and A. Shuvaev, *Anomalous dimension of the twist four gluon operator and pomeron cuts in deep inelastic scattering*, *Nucl.Phys.* **B387** (1992) 589–616.
- [132] J. Bartels, *Unitarity corrections to the Lipatov pomeron and the small x region in deep inelastic scattering in QCD*, *Phys.Lett.* **B298** (1993) 204–210.
- [133] J. Bartels, *Unitarity corrections to the Lipatov pomeron and the four gluon operator in deep inelastic scattering in QCD*, *Z.Phys.* **C60** (1993) 471–488.
- [134] J. Bartels and M. Ryskin, *Absorptive corrections to structure functions at small x* , *Z.Phys.* **C60** (1993) 751–756.
- [135] J. Bartels and M. Ryskin, *Recombination within multi-chain contributions in pp scattering*, [arXiv:1105.1638](#).
- [136] R. K. Ellis, W. Furmanski, and R. Petronzio, *Unraveling Higher Twists*, *Nucl.Phys.* **B212** (1983) 29.
- [137] J.-W. Qiu, *Twist four contributions to the parton structure functions*, *Phys.Rev.* **D42** (1990) 30–44.
- [138] A. Bukhvostov, G. Frolov, L. Lipatov, and E. Kuraev, *Evolution Equations for Quasi-Partonic Operators*, *Nucl.Phys.* **B258** (1985) 601–646.
- [139] L. Gribov and M. Ryskin. LNPI-865 (1983).
- [140] L. Gribov, Y. Dokshitzer, S. Troyan, and V. Khoze *Sov. Phys. JETP* **88** (1988) 1303.

- [141] B. M. McCoy and T. T. Wu, *Mandelstam Diagrams Are Not Enough*, *Phys.Rev.* **D12** (1975) 546.
- [142] B. M. McCoy and T. T. Wu, *Three Particle Regge Pole in ϕ^3 Theory*, *Phys.Rev.* **D12** (1975) 578.
- [143] S. Matinyan and A. Sedrakyan *JETP Lett.* **23** (1976) 588.
- [144] S. Matinyan and A. Sedrakyan *JETP Lett.* **24** (1976) 240.
- [145] S. Matinyan and A. Sedrakyan *Sov. J. Nucl. Phys.* **24** (1976) 844.
- [146] A. V. Manohar and W. J. Waalewijn, *What is Double Parton Scattering?*, *Phys.Lett.* **B713** (2012) 196–201.
- [147] S. J. Brodsky, T. Huang, and G. Lepage, “Quantum chromodynamics and hadronic interactions at short distances.” SLAC-PUB-2857, 1981.
- [148] S. J. Brodsky, H.-C. Pauli, and S. S. Pinsky, *Quantum Chromodynamics and Other Field Theories on the Light Cone*, *Phys. Rept.* **301** (1998) 299–486, [[hep-ph/9705477](#)].
- [149] T. Heinzl, *Light-cone quantization: Foundations and applications*, *Lect. Notes Phys.* **572** (2001) 55–142, [[hep-th/0008096](#)].
- [150] W.-M. Zhang and A. Harindranath, *Light front QCD. 1: Role of longitudinal boundary integrals*, *Phys.Rev.* **D48** (1993) 4868–4880, [[hep-th/9302119](#)].
- [151] W.-M. Zhang and A. Harindranath, *Light front QCD. 2: Two component theory*, *Phys.Rev.* **D48** (1993) 4881–4902.
- [152] A. Harindranath and W.-M. Zhang, *Light front QCD. 3: Coupling constant renormalization*, *Phys.Rev.* **D48** (1993) 4903–4915.
- [153] A. Harindranath, R. Kundu, and W.-M. Zhang, *Nonperturbative description of deep inelastic structure functions in light front QCD*, *Phys.Rev.* **D59** (1999) 094012, [[hep-ph/9806220](#)].